Development of novel polyurethane foam supports for 13X adsorbent for respiratory protection applications

Green, James

Award date:
2021

Awarding institution:
University of Bath

Development of novel polyurethane foam supports for 13X adsorbent for respiratory protection applications

Green, James

Award date:
2021

Awarding institution:
University of Bath

Development of novel polyurethane foam supports for 13X adsorbent for respiratory protection applications

James Dennis Towland Green

A thesis submitted for the degree of Doctor of Philosophy

University of Bath

Department of Chemical Engineering

April 2020

Copyright Notice

Attention is drawn to the fact that copyright of this thesis/portfolio rests with the author and copyright of any previously published materials included may rest with third parties. A copy of this thesis/portfolio has been supplied on condition that anyone who consults it understands that they must not copy it or use material from it except as licenced, permitted by law or with the consent of the author or other copyright owners, as applicable.

Declaration of any previous submission of the work

The material presented here for examination for the award of a higher degree by research ~~has~~ / has not been incorporated into a submission for another degree.

…….

Candidate's signature

Declaration of authorship

I am the author of this thesis, and the work described therein was carried out by myself personally

…….

Candidate's signature

Abstract

The current state of the art in respiratory protection uses cartridges of packed adsorbent beads to provide protection from chemical respiratory hazards. These cartridges impose a significant pressure drop, which has a physiological impact on the user. This work seeks to reduce this impact by developing a new material to contain the adsorbent in the cartridge instead of packed beads. This material was a polymeric foam, using polymer to contain and support a chosen adsorbent powder within a foam matrix. Foams can offer lower pressure drop and the ability to mould the material into any desired shape.

Polyimide and polyurethane foam formulations were developed, which proved capable for the first time of containing significant amounts of 13X adsorbent powder. Polyimide formulations proved capable of containing 67 wt% 13X but were superseded by polyurethane formulations containing 75 wt% 13X. These polyurethane formulations were further modified with additional surfactant to give control over the density and pressure drop of the resulting foams, improving their adsorption density. A novel heat treatment technique was developed to improve the accessibility of the adsorbent in the foams and to increase the mass of adsorbent in the foam after production.

Polyurethane 13X foams were investigated by use of adsorption breakthrough testing with 1000ppm n-butane and isotherm measurements with cyclohexane using the Thomas model to extract mass transfer data from the breakthrough curves. True adsorbent mass loadings of the materials were measured via a thermogravimetric analysis technique developed during the research to dry the samples and burn off the polymer fraction. Pressure drop behaviour was investigated by use of flowing air through dry cylindrical foam samples. Scanning electron microscopy was used to measure bubble and window sizes of the foams produced and helium pycnometry to measure the void fraction of the foams.

Heat treated foams showed isotherm uptake of up to 11.5 wt% cyclohexane based on total composite weight, compared to 17.0 wt% for 13X powder and 20.6 wt% for commercial 13X beads. Kinetic accessibility of the foams was found to be up to -4.236×10^{-7} $ppm^{-1}s^{-1}$ compared to -5.11×10^{-7} $ppm^{-1}s^{-1}$ for the commercial beads, showing inferior adsorption performance. However this was balanced out with superior pressure drop characteristics with the PU-13X foams, with activated foams showing pressure drops as low at 7.59% of

the adsorbent beads. A literature model for pressure drop through the foams by Dietrich (2012) was modified to create a new model which was used to successfully predict pressure drop through the PU-13X foams. Void fraction of the foams was found to be the critical physical parameter governing pressure drop.

Combining pressure drop and adsorption data found that the superior pressure drop could compensate for the lower adsorption uptake offered by the foams compared to the commercial beads, as long as the foams had a high mass density. One PU-13X foam offered this required density, a sample which had used additional surfactant in the formulation in order to suppress foam formation to make a significantly more dense material. This work developed the techniques for creating a successful PU-13X adsorbent foam, including both their formulation and heat treatment. This work also identified the control variables for these processes, outlining the path for further adsorbent foam development.

Contents

Table of Figures

Nomenclature

Acronyms

BSI	British Standards Institution
CBRN	Chemical, biological, radiological, nuclear
CFR	Code of Federal Regulations
CPSI	Cells per square inch
DMF	N, N dimethyl formamide
FID	Flame ionisation detector
IUPAC	International Union of Pure and Applied Chemistry
MoD	Ministry of Defence
MOF	Metal organic framework
MRI	Magnetic resonance imaging
MTZ	Mass transfer zone
NMP	1-Methyl-2-pyrrolidinone
PEG	Polyethylene glycol
PI	Polyimide
PIM	Polymer of intrinsic microporosity
PMDA	Pyromelletic dianhydride
PMDI	Poly[(phenyl isocyanate)-co-formaldehyde]
PPI	Pores per inch
PSA	Pressure swing adsorption
PTFE	Polytetrafluoroethylene
PU	Polyurethane
RPUF	Rigid polyurethane foam
SEM	Scanning electron microscopy
TGA	Thermogravimetric analysis
WoB	Work of breathing
ZIF	Zeolitic imidazolate framework

List of symbols

A	Area
C	Concentration
c	Constant
d	Diameter
E	Ergun's constant
g	Acceleration due to gravity
K	Rate constant
L	Length
m	Mass
n	Scaling factor
P	Pressure
Q	Volumtric flowrate
q	Equilibrium uptake
R	Rate
Re	Reynolds number
r	Radius
S	Surface area
t	Time
u	Velocity
V	Volume
X	Unknown
α	Angle
β	Shape factor
σ	Shear stress
ε	Voidage
ρ	Density
μ	Viscosity
τ	Torque
ϕ	Bubble diameter
$\dot{\gamma}$	Shear rate
γ	Surface tension
ω	Angular velocity

List of subscripts and superscripts

Script	Meaning
b	Breakthrough
bub	Bubble
c	Chamber
eff	Effluent
g	Gas/gravity
h	Hydraulic
p	Particle
r	Reference
s	Skeletal
sam	Sample
sat	Saturation
sk	Skin
t	Time
Th	Thomas
tub	Tube
Yn	Young-Nelson
w	Window
0	Initial
50	50% Breakthrough
γ	Surface tension

Acknowledgements

I wish to thank Dstl and the University of Bath for providing funding for this project, as well as the particular support of Martin Smith and Joe Jackson of Dstl for their regular advice and feedback throughout the project from a user perspective on the material. Further thanks are also due to Martin Smith for his testing of samples on Dstl's adsorption isotherm measurement equipment, and to Corinne Stone of Dstl for guidance in the field of surface tension theory and assistance with equipment.

My thanks are also due to Dr Olivier Camus for his assistance during the project in training on gas breakthrough equipment and techniques, as well as tolerating large use of fume cupboard space during production periods. My thanks also go to Fernando Acosta for his help in training me to use the TGA equipment, as well as to Ursula Potter for her assistance with microscopy.

Special thanks go to my supervisors Professor Barry Crittenden & Professor Semali Perera for their support and encouragement throughout the PhD giving useful advice and feedback wherever necessary and helping make this project a reality.

1 Introduction

The importance of personal protection against respiratory hazards is well known throughout history, particularly in relation to mining activity dating back to antiquity (Riley 1855). Originally this took the form of a need for ventilation to prevent the build-up of hazardous gases within enclosed spaces. The recognition of the hazards present led to legislative action which mandated a safe atmosphere to work by provision of ventilation (Anna 2011). However the use of devices to remove toxic gases on a personal scale was not developed until the mid-19th century where the Industrial Revolution made possible devices which could be worn to remove hazardous gases. These improved on previous devices by using activated charcoal to remove hazards from the air the wearer breathed. The most significant developments in respiratory protection were in the First World War, where the first uses of chemical weapons led to research to develop countermeasures. In particular these countermeasures had to be personal, portable and as non-burdensome to use as possible to maximise their effectiveness as protection in a combat environment. These countermeasures are the foundation of modern respiratory protection.

The current typical respirator comprises of a face mask and canister filled with a bed of chemically impregnated activated carbon granules which remove hazardous chemicals, through which air is drawn by the user's breathing, with typical contact time of 0.27s between the air and the bed (Janvier *et al.* 2016). These beds impose a significant pressure drop which the wearer must overcome, which imposes a physical burden to wearing them, causing fatigue in the user which is detrimental to their performance. Research into other structures than packed beds has not been successful in creating a structure which is both low pressure drop and effective at removing respiratory hazards.

The aim of this research is to develop and produce adsorbent foam structures to replace the existing packed adsorbent beds in respiratory protection applications. These foams are made of a polymer in which an adsorbent powder is contained, chosen following a review of polymers and adsorbent materials, and offer higher porosities than the packed bed and thus the opportunity for lower pressure drops than comparable packed bed structures. The polymer foams can also be made in moulds which allow for the production of structures in a variety of shapes not limited to traditional canisters and avoids particle packing issues associated with packed beds. The adsorbent foams are also significantly less dense and therefore lighter than the granular canisters.

1.1 Aims and objectives of the research

The overall goal of the research is to develop highly adsorbent loaded novel polymeric adsorbent foam structures which can replace packed beds of adsorbent in respiratory protection applications suitable for one-shot use. These will be developed to remove toxic gases whilst being able to be reliably produced and physically resilient. Hence the specific objectives are:

1. Determine suitable polymers for use as the polymer support in the adsorbent foam materials.
2. Determine optimal choices of adsorbents for the removal of toxic gases which are compatible with the polymer foam reaction via literature review of adsorption isotherm data.
3. Adapt and optimise the foam formulation and production process to maximise the adsorbent loading of the adsorbent foams to at least 70 wt% to give effective adsorption without blinding from an inert support, as well as develop a technique for accurately determining the adsorbent mass fraction of the foams.
4. Develop techniques for improving the adsorption performance of the adsorbent foams via post-processing techniques to modify the bubble skin, such as heat treatment, controlling foam drying and surface solvent etching.
5. Model pressure drop for produced adsorbent foams using data collected, measure the bubble size, window size and porosity of the foams and identify which of these physical properties are responsible for the foam's pressure drop behaviour.
6. Measure adsorption isotherms and breakthrough data for the foams, as well as packed beds of similar adsorbents. Using this data develop techniques for comparing the overall performances of the adsorbent foams structure to packed beds of adsorbents, taking into account differences in pressure drop, packing density and adsorbent uptake.

1.2 Structure of this thesis

Chapter 1 introduces the research being performed, explaining the nature of the respiratory protection problem and the need for a lower pressure drop material to make such devices easier to wear. It also outlines the goals for the research, and the structure of this thesis.

Chapter 2 presents relevant information to the research including a literature review on respiratory protection and existing standards, adsorbents, structured adsorbents including existing adsorbent foams, polymer foams and current research on pressure drop in foam structures. It also includes a review of theory relevant to the research including adsorption, foam formation and structure, breakthrough curves, mass transfer and pressure drop.

Chapter 3 describes the development of a process to allow for the production of highly loaded adsorbent foam material beyond the existing limits of powder content in polymeric foams, using initial polyimide chemistry. The addition of extra solvent to ensure a liquid phase which bubble formation can occur in, as well as surfactant to control foaming behaviour, is investigated to develop a process which can reliably create adsorbent foams without foam collapse. Modifications of the chemistry to produce polyurethane adsorbent foams are also described, as well as the development of post-processing techniques to allow for the foams to be used in adsorbent applications after successful polymerisation, and improve adsorptive accessibility.

Chapter 4 contains the analysis into the physical properties of the produced polymeric adsorbent foams. It describes the scanning electron microscopy and image analysis techniques used to measure the bubble and window sizes of the produced polymeric adsorbent foams, the helium pycnometry for their void fractions and the apparatus used for pressure drops. This data is then used to model the pressure drop behaviour of the foams and compare to reference data from packed beds.

Chapter 5 presents the analysis of the adsorption behaviour of the polyurethane adsorbent foams. It describes the experimental techniques used to measure adsorbent mass loading in the foams, acquire adsorbent isotherms and breakthrough curves for the foams using cyclohexane and n-butane respectively. This data is used to analyse the adsorptive accessibility of the materials to determine the effectiveness of the polymeric foams as a

support structure. Further analysis is also performed to investigate the effects of the polyurethane bubble skin of the foams on their adsorption performance, and how this can be mitigated by thermal treatment of the polyurethane.

Chapter 6 gives an overall evaluation of the effectiveness of the polyurethane adsorbent foams at providing protection in a respiratory protection environment compared to reference packed beds. This takes into account the packing density of the adsorbent, the adsorption uptake and the pressure drop of the foams to determine if the produced foams can offer less pressure drop for the same amount of adsorption uptake. This data is also used to evaluate the effectiveness of post-production processing techniques developed in Chapter 3 at improving adsorbent uptake in the foams.

Chapter 7 presents the overall conclusions of the research, using the physical and adsorption data gathered in Chapters 4 and 5, as well as the combined evaluation of Chapter 6 to determine if the research has produced adsorbent foams capable of achieving the aims put forward in Chapter 1. It also highlights the successfully developed production process from Chapter 3 and how this can be used to produce effective adsorbent foams. Finally it describes areas in the research which have potential for further investigation and the basis for doing so. The benefits of further investigation into different support polymers both with higher thermal resistance and polymers of intrinsic microporosity are described and supported. The potential for further development of polyimide-13X foams, the post production heat treatment process and the use of metal organic frameworks as adsorbents in foams are also discussed.

2 Literature review & theoretical background

This literature review covers the various publications relevant to the development of a successful material for respiratory protection, according to the objectives outlined in Chapter 1 by considering the following areas:

Technical standards and regulations which govern respirators are reviewed to make the case for lower pressure drop materials being required and beneficial for respiratory protection, as well as to identify the typical threats that a respirator would be expected to defend against. The field of adsorption is introduced, explaining the features which make a successful adsorbent material, as well as introducing isotherms and adsorption breakthrough curves which are used to evaluate the effectiveness of an adsorbent. Both of these areas of literature are then used to review the available adsorbents for effectiveness in respiratory protection and guide the choice of adsorbent to be supported.

The theory behind adsorbent support structures and what makes a successful support is also reviewed, as well as modelling literature on adsorbent structures to select which shape would be most effective to make the support into, as well as choosing which material would be effective to make such a shape out of. Having selected a foam for further investigation, the Chapter outlines the theory of foam formation and existing work on the production of polymeric foam materials, in order to identify favourable avenues for investigation for the production of a suitable adsorbent support, and techniques which can be adapted and expanded upon for its development. The Chapter also reviews existing work in the literature in the production and use of adsorbents in foam support structures in order to identify areas of potential investigation and development which have been poorly covered in existing work.

Published work on the analysis of pressure drop through packed beds via the Ergun equation, as well as efforts to adapt this equation to foam materials, is reviewed and investigated in order to develop an understanding for analysis of pressure drop results of the produced materials in later sections. Finally, recommendations are drawn from the discussed literature as to areas which are suitable for investigation, and relevant expertise highlighted, which forms the basis for the beginning of practical investigative work into the production of adsorbent supports.

2.1 Respiratory protection

Respiratory protection is defined as the protection against respiratory hazards. These are hazards which can enter the body when a person breathes and include dusts, fumes, mists, gases, vapours and oxygen deficient atmospheres (Rajhans *et al.* 2002). This protection can take a variety of forms depending upon the environment and types of people which need to be protected, but for the purposes of this research the case of protection on a personal scale from an uncontrolled environment is being considered.

On a personal scale, the most common type of respiratory protection equipment used is a gas mask or respirator (Figure 1), which can take any one of a variety of forms, dependent upon the type of respiratory threat being encountered.

Figure 1: A soldier wearing the General Service Respirator (Ministry of Defence 2012) (Crown Copyright 2012).

These respirators can take various forms, but two distinct categories emerge which have very different types of configuration: Air supplying respirators and air purifying respirators (Rajhans *et al.* 2002). An air supplying respirator supplies air from a source which is known to be safe, which can either be from a tank carried by the user or via a pipeline from an external source. Air purifying respirators on the other hand take air from the surrounding hazardous environment and purify this for safe inhalation via the removal of the relevant hazards, using a relevant removal technique dependent upon the particular hazard.

Each different hazard category requires its own particular removal and purification method. Solids, suspended solid particles and suspended liquid droplets can all be removed by a variety of filtration papers and fabrics which are compact and use the effect of layered

strands to remove particles from the airflow (Mills 2004), whilst oxygen deficient atmospheres are unsuitable for the use of air purifying respirators. Relevant to this work on the other hand are the environments with chemical hazards: gases and vapours and the method by which these are removed from the inhaled airstream. Because they mix with and form part of the gas phase itself they cannot be removed by filtration techniques which separate on the basis of physical differences like filtration pads. These thus require a different separation process.

Toxic and hazardous gases are removed from the airstream in an air purifying respirator typically via use of adsorption, absorption or chemical reaction depending upon the specific threat being protected against. Most commonly, and in the case of this research, the relevant technique is adsorption, where the airstream has to pass through and contact the adsorbent material in order to enact a separation which removes the hazard from the airstream and provides the protection needed by the wearer. Either a single adsorbent or multiple adsorbents canisters may be used depending upon the threat or threats being protected against (Rousseau 1987; British Standards Institution 2004). The material is typically stored in the form of a canister which holds the material in a packed bed of granules which are comprised either of the adsorbent itself, or the adsorbent supported by some binder in the case of adsorbents which take the form of a powder to reach the required degree of physical resilience to be used. Canisters, or cartridges, can take a wide variety of potential form factors depending upon the device manufacturer and the intended application. A schematic of a typical canister as might be used in a respirator for a multi-threat environment is shown below in Figure 2.

The types of toxic gases that the material must defend against varies widely depending upon the environment, but standards literature narrows this down into categories A,B,E,K and X, each of which covers a variety of types of threatening compound. The model gases for these categories are cyclohexane (A), chlorine, hydrogen sulphide and hydrogen cyanide (B), sulphur dioxide (E), ammonia (K), and dimethyl ether and isobutane (X) (British Standards Institution 2004). These have to be removed from environments at a range of humidity and temperatures as well, with standards listing test conditions including humidity of up to 85% (National Institute for Occupational Safety and Health 2008). The type of adsorbent used depends on the threats chosen to be protected against from these model gases and is discussed in more detail later in this Chapter.

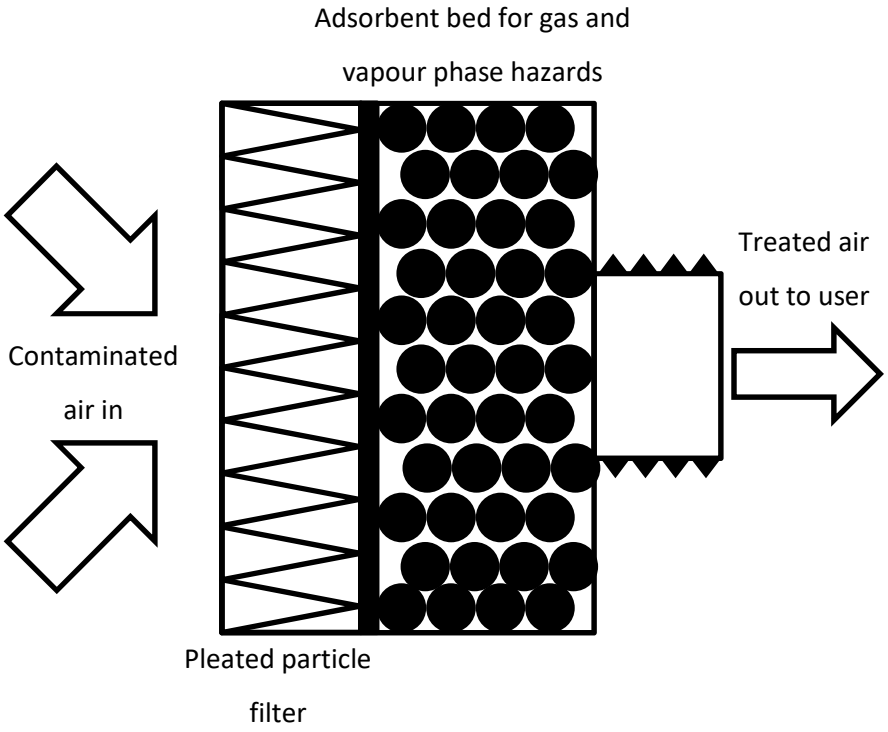

Figure 2: A schematic diagram of a combined respirator cartridge for particle and gas based hazards as might be seen in a multi-threat environment.

The power needed to move the airstream through this bed of granules in turn can be provided by one of two sources: A powered fan which forms part of the respirator or an unpowered device driven by the breathing effort of the wearer. For most air purifying respirators the unpowered version is typical and it is this type of respirator which is relevant for this project, and the specific properties this application requires of the adsorbent being used.

One of the key features in terms of wearability and comfort for respirator use in unpowered respirators is breathing resistance, typically divided into inhalation and exhalation resistances, which describes in terms of a pressure drop the added burden which the device places upon the wearer's respiratory system when worn. As this inhalation resistance increases, the physical burden of wearing the respirator increases also, degrading performance of the wearer, in particular under strenuous conditions (Caretti *et al.* 2006). As a result of this, there are significant benefits to a respirator which offers lower inhalation resistances in terms of user comfort and performance.

The work of breathing is defined as the work required to move air in and out of the lungs and comprises of several separate factors depending upon the nature of breathing being performed (Cabello *et al.* 2006). Divided into inhalation and exhalation resistances, under normal breathing this work is simply a factor of the volume of air being moved into the lungs and the effort expended in expanding and contracting the lungs. However, when wearing a respirator an additional resistance is added which the body must move air against, represented by the pressure drop of the device being worn on the air inlet.

In recognition of this undesirable property of respirators, various standards exist defining maximum allowable pressure drops of respirators depending upon the air flowrate and type of application the respirator is intended to protect against. These are summarised in Table 1. Both the British Standards Institution (BSI) and the American Code of Federal Regulations (CFR) set standards for allowable pressure drops, with the BSI specifying a wider range of applications and flowrates than the CFR but with similar allowable pressure drops where overlaps exist. However a common phrase from the standard literature is the following: "The resistance imposed by filter(s) to the flow of air shall be as low as possible" (British Standards Institution 2004). This is due to the detrimental effect any breathing resistance has on wearer comfort and performance shown in the literature as follows.

Caretti *et al.* (2006) describe in their work an investigation into the effects of varying breathing resistance of respirators on the performance of subjects performing strenuous work. During this they subjected a group of 11 test subjects to a standardised exercise regimen and measured the time until exhaustion for all subjects under a variety of different inhalation and exhalation respiratory resistances. They found a significant negative relationship between increasing inhalation resistance and maximum performance time in the exercise regimen, which strongly supports the claims made that a respirator with lower inhalation resistance would improve wearer performance under stressful conditions.

It is clear that the primary source of discomfort to the wearer for traditional respiratory devices is the resistance caused by the canister containing the adsorbent which provides protection from respiratory hazards. In order to improve the experience of the wearer over current devices, new methods of containing and structuring this adsorbent must therefore be developed to reduce pressure drop over the current state of the art. As a result, the fields of adsorption and pressure drop behaviour must now be considered in detail.

Table 1: A summary of various maximum allowable filter pressure drops for wearer powered respirators (negative pressure) as defined by standards literature.

Type of filter/application	Breathing flowrate (litres per minute)	Permissible pressure drop (mbar)	Source/Reference
Emergency response & CBRN contamination	30	1.6	(British Standards Institution 2006)
	95	6.0	
Fire escape hood	90 (equivalent) (British Standards Institution 2001)	8.0	(British Standards Institution 2004)
Respiratory protection devices, full face mask			(British Standards Institution 2004)
Low capacity (Organics, inorganics, acid gases and ammonia)	30	1.0	
	95	4.0	
Medium capacity (Organics, inorganics, acid gases and ammonia)	30	1.4	
	95	5.6	
High capacity (Organics, inorganics, acid gases and ammonia)	30	1.6	
	95	6.4	
Low boiling organics	30	1.4	
	95	5.6	
Other gases	30	1.4	
	95	5.6	
NOX with particle filter	30	2.6	
	95	9.8	
Mercury with particle filter	30	2.6	
	95	9.8	
Respiratory protection devices, half face mask			(British Standards Institution 1999)
Low capacity	30	1.0	
	95	4.0	
Medium capacity	30	1.4	
	95	5.6	
Low boiling organics	30	1.4	
	95	5.6	
Other gases	30	1.4	
	95	5.6	
Front mounted gas mask	85	6.0	(Code of Federal Regulations 2004)
Chin style gas mask	85	4.0	
Escape gas mask	85	6.0	

2.2 Adsorption

Adsorption is typically defined as “The enrichment of one or more phases in the vicinity of an interface” (Rouquerol *et al.* 2013), where an interface is the point at which two distinct phases come into contact and can be between gas-liquid, gas-solid, liquid-solid, liquid-liquid and solid-solid (Birdi 2009). In more practical terms this refers to the transfer of a compound, or adsorptive, from a fluid stream which can be either a liquid or gas, onto the solid surface of a material, known as an adsorbent, which said fluid stream comes into contact with during flow. Such uptake can either be physical or chemical in nature.

Adsorbents are chosen for having very high surface areas per unit mass to maximise the ability of the materials to adsorb adsorptive due to this surface binding process. Adsorbents typically used in commercial applications fall into the categories of activated carbons, zeolites, silica gel and activated alumina (Yang 2003), whilst more novel adsorbent materials include metal organic frameworks (MOFs) and polymers of intrinsic microporosity (PIMs).

Several types of adsorbent have crystalline structures, where the adsorbent sites are located within the crystal matrix. This requires the adsorptive molecules to diffuse through the solid structure in order for adsorption to occur, which is a relatively slow process. In order to allow for this to happen at practical speeds for adsorption to occur, they are employed practically in the form of finely divided crystalline powders, which reduces the distance between the surface of the crystal and the interior, and increases the surface area of the crystals to allow for mass transfer into the material. Whilst this form allows for an extremely high density of surface area per unit volume and a resulting high adsorption performance, it is impractical in practice due to the excessive pressure drop and flow difficulties in passing a fluid through such a densely packed material.

In order to overcome this difficulty it is common to mix these adsorbents with some form of binder in order to allow for them to be made into shapes and forms with more practical pressure drop characteristics, typically beads (Thomas *et al.* 1998), without the mass transfer difficulties of using large solid crystals or crystal aggregates. Various other binding structures exist, and the choice of structure will be considered in section 2.3.

The degree to which adsorption occurs, which is of particular importance when devising a material for respiratory protection which must remove a material or materials from an airstream to very high levels, is governed by both equilibrium and kinetic behaviour. Firstly interaction is required between the material and the adsorbent surface to cause the removal, which is described by an adsorption isotherm. It is also important that this active surface can be accessed from the fluid phase quickly due to the low contact times seen in respiratory protection, and this behaviour can be described in an adsorption breakthrough curve.

2.2.1 Adsorption isotherms

An adsorption isotherm, as the name suggests, is a description of how much of an adsorbate that an adsorbent can take up at a certain pressure for a constant temperature. In more useful terms it describes the maximum uptake of an adsorbent being used for a certain application.

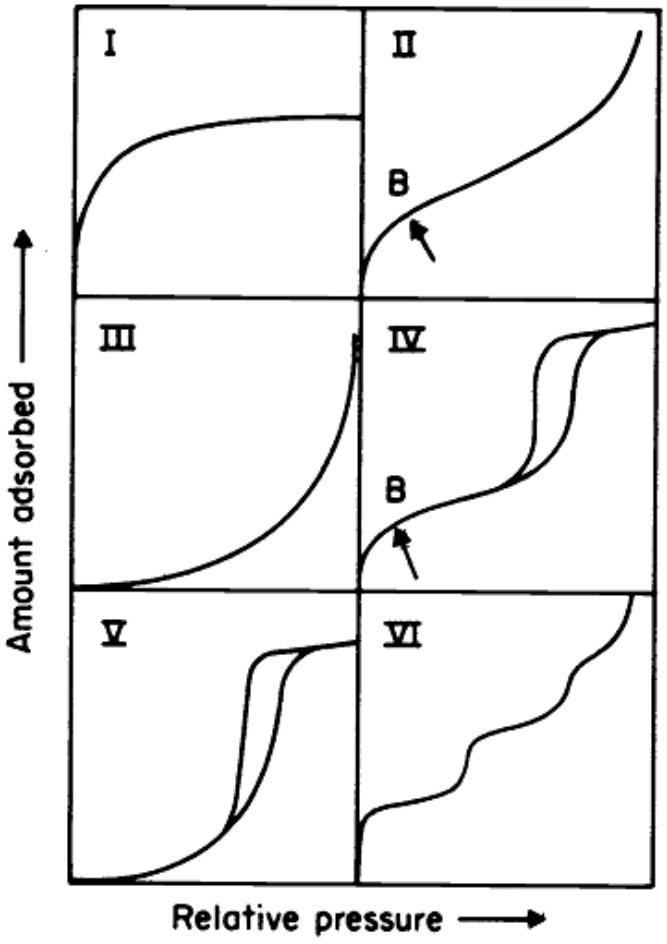

Figure 3: Types of physisorption isotherms (©1985 IUPAC (Sing 1985)).

Isotherms for physical uptake of a material onto an adsorbent surface can take various forms depending upon the adsorbent in question, as seen in Figure 3. A successful adsorbent for a respiratory protection application however should show good levels of uptake at low pressures as these show good performance at removing unwanted materials to low concentrations. Figure 4 shows an isotherm for 13X and water which displays this favourable Type 1 behaviour. Adsorbent uptake should also not be significantly affected by the choice of structure or support for optimal performance.

However isotherms do not provide any information about how fast it takes the adsorptive to enter and be taken up in the adsorbent. Also, as can be seen in Figure 4, the uptake of the adsorbent is a function of the adsorptive pressure. This means that as adsorptive is removed from the fluid phase, the ability of the adsorbent to remove this remaining adsorptive diminishes. As a result, the isotherm alone cannot fully describe the adsorption process and must be considered in conjunction with a second characteristic property of the adsorbent, its mass transfer zone, which is described by the adsorption breakthrough curve.

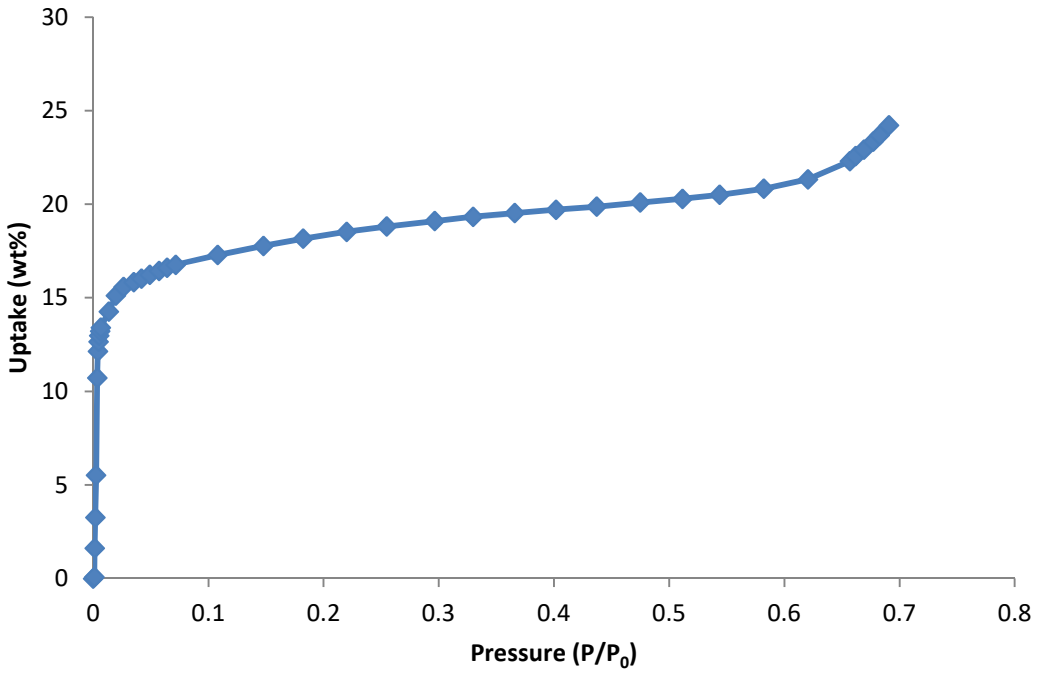

Figure 4: An adsorption isotherm for water on 13X zeolite (Kim *et al.* 2016).

2.2.2 Adsorption breakthrough curves

As opposed to an isotherm, which is measured when an adsorbent system reaches equilibrium, an adsorption breakthrough curve measures the amount of material retained within an outlet stream which has been passed through an adsorbent material being tested. The nature in which the outlet value returns to the inlet value and the speed at which it does so offers insight into the barriers between the active adsorbent surface and the fluid stream as show by Figure 5.

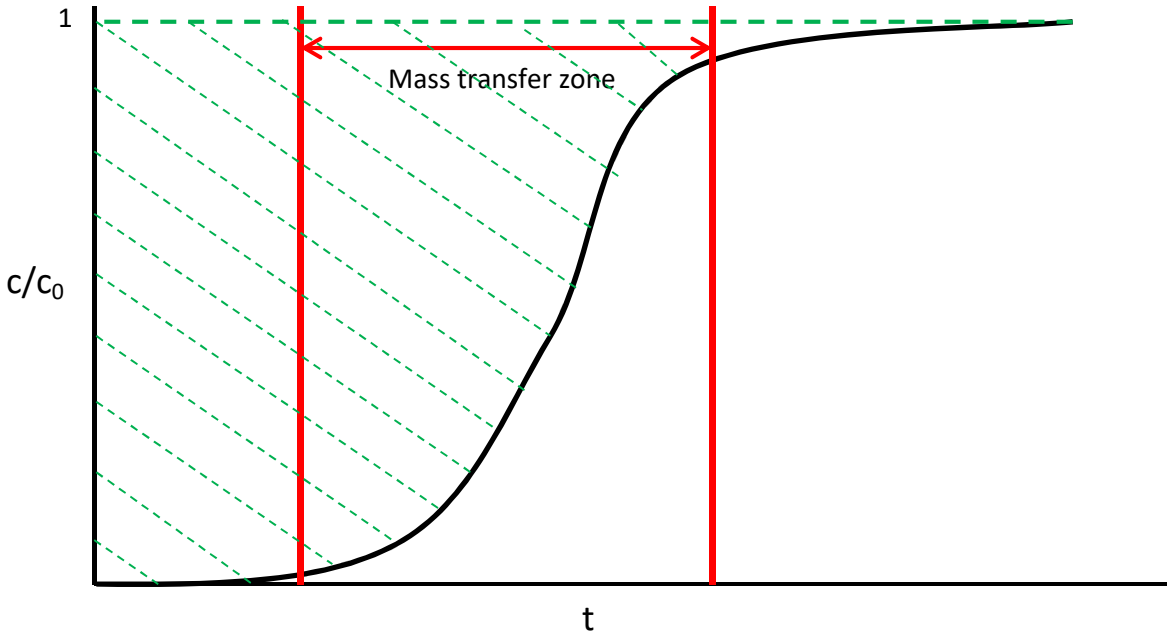

Figure 5: Example of an adsorption breakthrough curve which might be found experimentally.

In order for adsorption of an adsorptive to occur, the adsorptive molecule must pass from the bulk fluid phase passing through the adsorbent through the overall adsorbent structure to the solid surface. It is at this surface where the process of adsorption occurs and where the behaviour as described in the adsorbent isotherm applies. The mass transfer zone (MTZ) describes the zone within a packed bed in which this ongoing mass transfer occurs and is the section within the bed where adsorption is actively performed (Thomas *et al.* 1998).

On one side of the MTZ, the adsorbate concentration will be equal to that of the inlet concentration, whilst on the other side the adsorbate concentration will be as low as the isotherm behaviour of the adsorbent can achieve in terms of removing it from the bulk phase. The behaviour in between these extremes is described by a breakthrough curve.

Figure 6 shows an MTZ as it progresses down a packed bed over time as well as the breakthrough curve associated with the MTZ. The breakthrough curve shows the concentration of adsorbate in the outlet once the MTZ breaks through the bed and is directly linked to the shape and width of the MTZ.

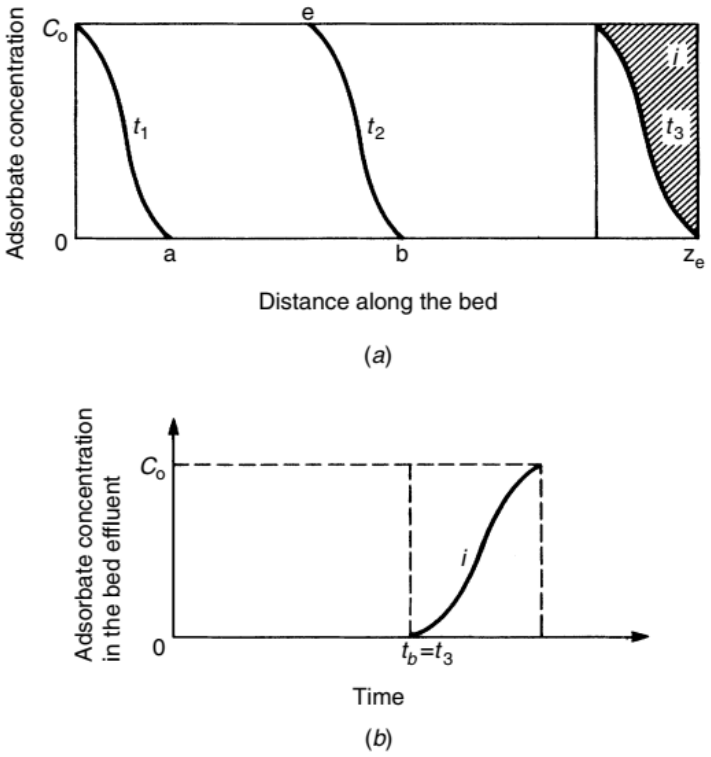

Figure 6: A mass transfer zone (a) and its breakthrough curve (b) (Reproduced from Richardson *et al.* (2002), p1009, with permission from Elsevier).

The shape of the breakthrough curve gives certain insight into the nature of the mass transfer within the adsorbent. Given knowledge of the inlet flowrate and bed diameter, the MTZ length can be calculated for a given system by measuring the time taken for the outlet concentration to recover to that of the inlet concentration of adsorbate. In general shorter mass transfer zones are desirable, because they indicate superior mass transfer properties of the adsorbent as supported which means the adsorbent is being more efficiently used and cycle times can be more rapid when used in industrial applications (Yang 2003).

The shape of the breakthrough curve is also linked to the mass transfer behaviour and isotherm data for the particular system which allows for the investigation of mass transfer coefficients and diffusivity by fitting mass transfer models to experimental breakthrough

data (Knox *et al.* 2016). Various models exist for interpreting breakthrough curve data to determine the mass transfer characteristics of an adsorbent bed. Two such models are the Yoon-Nelson model and the Thomas model. A Bohart-Adams model is also reported in the literature, but is functionally identical to the Thomas model (Chu 2010).

The Yoon-Nelson was developed focussing on the adsorption of gases and vapours onto activated carbon and has a linearized form as follows (Recepoğlu *et al.* 2018):

$$\ln\frac{C}{C_0 - C} = K_{YN}t - t_{50}K_{YN} \quad (1)$$

Where K_{YN} is the Young-Nelson rate constant and t_{50} the time taken for 50% adsorptive breakthrough.

The Thomas model on the other hand assumes highly favourable type 1 adsorption and that mass transfer is the limiting process in the adsorption breakthrough instead of the adsorption process itself. The Thomas model has a linearized form as follows (Chu 2010):

$$\ln\left[\left(\frac{C_0}{C_t}\right) - 1\right] = \left(\frac{k_{Th}q_0 m}{Q}\right) - k_{Th}C_0 t_b \quad (2)$$

Where k_{Th} is the Thomas rate constant, q_0 the equilibrium uptake of the adsorbent, m the adsorbent mass, t_b the breakthrough time and Q the volumetric flowrate. In order to estimate the Thomas rate constant data from the experimental data, the linearized form of the Thomas model can be used to replot the breakthrough curves in terms of $\ln\left[\left(\frac{C_0}{C_t}\right) - 1\right]$ against time to obtain the Thomas rate constant from the gradient of the linearized breakthrough curve divided by the initial concentration of the adsorbate.

The choice of model will be determined by the choice of adsorbent given their differences in assumptions of adsorption behaviour, but both can potentially be used to extract mass transfer rate data from breakthrough curves.

2.2.3 Choice of adsorbent

The focus of this thesis is the investigation of supporting an adsorbent in a suitable structure for low pressure drop characteristics, as opposed to optimising and investigating adsorbent behaviours themselves. However to create an effective material for respiratory protection the structure must not only have excellent pressure drop characteristics, but also contain an active component capable of giving protection against respiratory hazards which can be accessed by the gas stream in a timely manner, and the nature of this component will determine which support structures are possible and practical to synthesise. This section thus reviews types of adsorbent suitable for incorporation into the support for the purposes of the research.

The choice of adsorbent is driven primarily by the types of toxic gases that the adsorbent is expected to remove. In the respiratory protection environment, there are countless different potential toxic threats but some gases are more common and typically encountered than others. As discussed previously, standards literature gives the following list of model gases for various categories: Cyclohexane (A), chlorine, hydrogen sulphide and hydrogen cyanide (B), sulphur dioxide (E), ammonia (K), and dimethyl ether and isobutane (X) (British Standards Institution 2004), which have to be removed in the presence of humidity (National Institute for Occupational Safety and Health 2008). In order to provide effective respiratory protection an adsorbent, or group of adsorbents which can be layered or used in a mixture to protect against multiple categories(Mansdorf 2019), must be used to remove these from the airstream to very low concentrations. This requires that the adsorbent have a favourable isotherm toward these gases, one which has significant uptake at low concentrations, in order to remove them to this degree with a practical amount of adsorbent. The six major categories of adsorbents are, as previously discussed, activated carbons, zeolites, silica gel, activated alumina, metal organic frameworks and polymers of intrinsic microporosity. The chosen adsorbent must be effective at removing the test gas whilst also being resilient enough for practical use.

2.2.3.1 Activated carbon

Activated carbon is an extremely broad category of adsorbents, with different adsorption properties being possible based on the carbon source used to produce the adsorbent and their surface properties, which can vary significantly between carbons and the treatments used in their activation. It is known for being moisture tolerant and not requiring pre-drying

for effective separation (Yang 2003). Activated carbon has poor to negligible uptake towards hydrogen sulphide (Turk *et al.* 1989) and ammonia (Park *et al.* 2005; Halim *et al.* 2010) (Model gas categories B and K) without chemical treatment to change the nature of the surface chemistry of the materials and allow for uptake via chemisorption.

Activated carbons are available which show uptake for cyclohexane (Pietrowski *et al.* 2012), whilst activated carbons also have some affinity for uptake of hydrogen sulphide which can be enhanced significantly by chemical modification (Turk *et al.* 1989). Activated carbon also has reported uptakes of up to 80 mgg^{-1} of sulphur dioxide in the literature with favourable isotherms suitable for respiratory protection but with significant decline with temperature (Aik Chong *et al.* 2001). Chemical modification of activated carbon can again significantly improve this uptake by impregnating the carbon surface with potassium hydroxide. This uses the activated carbon as a support to hold potassium hydroxide on the surface and provide a basic surface chemistry to increase uptake of sulphur dioxide by chemisorption. This reduce the surface area of the material and the pore volume, but increases uptake by 13.2 times for SO_2 compared to untreated activated carbon whilst maintaining favourable isotherm characteristics (Lee *et al.* 2002). Unmodified activated carbon is reported to have poor uptake properties for ammonia in the literature due to poor surface properties for adsorbing ammonia (Halim *et al.* 2010). Chemical modification of activated carbons via oxyfluorination to improve this uptake is possible and has been reported to significantly increase breakthrough times in adsorption studies but this may have detrimental effects on the uptake of other gases (Park *et al.* 2005). Finally, as an organic compound isobutane has significant and favourable adsorption uptake reported in the literature on activated carbons without need of modification (Whittaker *et al.* 2014). As a result, activated carbon is a strong choice for consideration as an adsorbent for use in respiratory protection as long as it has been treated chemically with the correct treatments to offer protection against a wide range of threats, as without such treatment it is totally ineffective against large sections of the threat gases.

Structured activated carbon materials however are not a novel field by any means. Activated carbon fabrics (Moreno-Castilla *et al.* 2011), foams (Saeidi *et al.* 2015) and monoliths (Zabiegaj *et al.* 2015) have all been reported in the literature as well as the traditional activated carbon beads or pellets. As a result, it is unlikely there is scope for significant improvement in the field in developing a structured activated carbon adsorbent.

2.2.3.2 Zeolites

Zeolites are aluminosilicate materials which can be both found naturally and synthetically made and are known for their very defined pore structures and sizes, giving rise to their name of molecular sieves. Zeolites exist in several forms depending upon the ratio of aluminium to silicon in their structure, as well as the crystal structure which determines the size of the molecular cage which provides the adsorption sites. As aluminosilicate structures are also negatively charged, the choice of cation to balance the charge of the structure can also affect it's adsorption behaviour (McCusker *et al.* 2001). Existing in their most basic form as crystals, adsorptive molecules must diffuse through the solid crystal structure in order to reach the adsorption sites (Thomas *et al.* 1998). This mass transfer is relatively slow, so in processes which require low contact times, such as gas adsorption in respiratory protection, the crystals are used practically in a finely divided crystalline powder. Powders impose significant resistance to pressure drop, so in applications where this factor is significant, such as respiratory protection, these require integration into a supporting material structure with lower pressure drop characteristics for use. As a result incorporating them into a foam matrix offers no inherent disadvantages compared to existing products, as is the case with activated carbons.

Considering the model gases from the literature, as a large and non-polar molecule, cyclohexane is one of the more challenging toxins for zeolites to adsorb given their small adsorption sites, pore sizes of 0.3-1 nm being typical depending on the zeolite structure (Thomas *et al.* 1998), and charged natures. Adsorption uptake of up to 10wt% at relatively low partial pressures of cyclohexane has however been reported in the literature for faujasite, a natural form of a zeolite which can be synthetically made as 13X (Nikolina *et al.* 1960). Modified copper ion exchanged zeolites have also been reported in the literature capable of offering protection against chlorine gas at concentrations hazardous to health (Liu *et al.* 2016). The adsorption of hydrogen sulphide is driven by the acidity of the zeolite in question, but the uptake of hydrogen sulphide by zeolites is well reported in the literature with better uptake seen on zeolites with wider pore structures (0.51 cm^3g^{-1} compared to 0.47 cm^3g^{-1}), and more basic surface chemistries (Gaillard *et al.* 2004; Pavlova *et al.* 2013; Sigot *et al.* 2016). Copper ion exchanged zeolites have also been reported to be effective as adsorbents for the removal of hydrogen cyanide, with the uptake being superior in smaller pore volume zeolites (0.2131 mlg^{-1} treated compared to 0.2232 mlg^{-1} untreated) which had a higher density of copper ions (Ning *et al.* 2013). Significant

favourable uptake of up to 20 wt% of sulphur dioxide on zeolites has also been reported in the literature (Marcu *et al.* 2004), but this has also been reported to be significantly inhibited by moisture content in the zeolites, which is problematic given their significant affinity for water uptake (Srinivasan *et al.* 1999) and the humid environments offered by respiratory protection. This can be mitigated by prior moisture removal with more zeolite, at the cost of reduced adsorption capacity. Uptake of ammonia gas onto zeolite has been reported in the literature of up to 12 wt%, but the nature of the isotherm was not reported (Tehrani *et al.* 2005). Zeolites have also been reported to show uptake of dimethyl ether in the literature with a linear isotherm and increased uptake for larger molecular cage sizes (0.5 nm compared to 0.4 nm) with uptakes of up to 11.5 wt% (Lad *et al.* 2014). Favourable isotherms are also reported in the literature for isobutane on mordenite, with increasing accessibility following cation exchange to increase the free space inside the molecular cage, with loadings of 2.5 wt% reported at temperatures above ambient and a reported trend of increasing adsorption with reductions in temperature (Lozano-Castello *et al.* 2006).

As a result, zeolites have significant potential for inclusion as an adsorbent, with potential activity towards the entire range of respiratory hazards identified in the standards literature. Of the various zeolites, choices with larger molecular cages will be more suitable for inclusion due to their superior adsorption performance towards larger molecular toxins such as cyclohexane and isobutane.

2.2.3.3 Silica Gels and Activated Alumina

Silica gels, solid aerogel structures comprised of silicon dioxide, and activated alumina, formed of aluminium oxide produced by dehydroxylation of aluminium hydroxide to create a form of the oxide which has adsorbent activity, are both families of adsorbent most widely used as desiccants but require consideration for their potential as agents in respiratory protection. Cyclohexane is reported to be poorly adsorbed by both silica gel, which showed strongly unfavourable isotherms (Shiko *et al.* 2013), and activated alumina where affinities were reported to be poor (Hsing *et al.* 1974). Hydrogen sulphide was not adsorbed at all by silica gel (Sigot *et al.* 2016), whilst no data was available for activated alumina. Data was similarly unavailable for the uptake of hydrogen cyanide for either activated alumina or silica gel at conditions relevant to respiratory protection. Activated alumina also showed very minor uptake of chlorine gas at temperature of 27^{o}C of 175 micromoles per gram of adsorbent (Réti *et al.* 1987). However no isotherm data was

reported and this uptake is extremely low, so it is likely to be unsuitable for respiratory protection.

Favourable adsorption of ammonia of up to 4.25 wt% has been reported at ambient conditions for activated alumina (Saha *et al.* 2010), suitable for respiratory protection against this test gas. Sulphur dioxide is also reported to have a favourable adsorption isotherm on alumina, and uptakes of 3wt% have been reported on commercially available chromatography aluminas at 15^{o}C, useful for respiratory protection (Fellner *et al.* 2006). Uptake of dimethyl ether has been reported at 24^{o}C on activated alumina with loadings of 3.26 wt% via breakthrough curve data, but the shape of the isotherm was not reported so the applicability of this data towards respiratory protection is unclear, given the necessity of a favourable isotherm (Desai *et al.* 1992). The authors also only tested very low partial pressures of dimethyl ether of 0-1.5 kPa, which leaves higher concentrations, which are respiratory hazards as well, unexplored.

Silica gel can be judged to be unsuitable immediately as an adsorbent given the lack of adsorption towards many of the model gases where data is available and unfavourable isotherms for those which it does show adsorption of which is unsuitable for respiratory protection. Activated alumina has more useful properties allowing for removal of ammonia and sulphur dioxide but the lack of isotherm data for dimethyl ether and chlorine, as well as extremely low capacities or lacking data for other test gases, mean it must be considered unsuitable for use as an adsorbent for incorporation into the support structure in this work.

2.2.3.4 Metal Organic Frameworks and Polymers of Intrinsic Microporosity

Metal organic frameworks are structured molecules made up of metal atoms connected together in a cage via long organic compounds, giving rise to their name of metal organic frameworks. A relatively recently developed family of porous materials, they offer an extremely wide range of adsorption behaviours depending upon the choice of metal ions and cross linking organic molecules, which allows for their pore structures to be controlled as well as their surface chemistry, which is extremely important for the uptake of test gases such as ammonia, chlorine, hydrogen sulphide and sulphur dioxide.

Uptake of toxic gases by MOFs has been reported in the literature, with favourable uptake of H_2S being observed for various MOFs at room temperature for capacities up to 38 mmol

per gram, but with significant variance between materials (Hamon *et al.* 2009). One of the most prominent MOFs developed to date is MIL 101, comprising of chromium linked with terephthalic acid, which has been investigated for its performance in adsorbing volatile organic compounds by Zhao *et al.* (2011), who reported uptake of 9.52 $mmolg^{-1}$ of p-xylene, a typical respiratory hazard, which was reported by the author to be over 4 times the uptake of conventional zeolite and activated carbon adsorbents, with isotherms reported to be strongly favourable as well. Favourable uptake of cyclohexane by MIL 101 has also been reported in the literature by Belarbi *et al.* (2017) with capacities of 220 cm^3g^{-1} claimed. These suggest that MIL101 could be highly effective as an adsorbent for respiratory protection.

Ammonia uptake has been reported for a range of MOFs by Kajiwara *et al.* (2014) who synthesised a range of MOFs in their work and found that ZIF-8, MIL-53(Al), Al-BTB, MOF-74(Mg), MIL-101(Cr) and MOF-76(M) were stable in the presence of ammonia, which was also linked to stability in the presence of water. Of these MOFs, adsorption uptake towards ammonia was reported for MOF-74(Mg) (>300cm^3g^{-1} at standard temperature and pressure), MIL-53 (Al) and Al-BTB (Both ≈100cm^3g^{-1} at standard temperature and pressure) which were all deemed suitable for use in ammonia removal, with MIL-53(Al) showing extremely favourable isotherms.

The uptake of sulphur dioxide onto MOFs has been explored computationally by multiple authors. Song *et al.* (2014) performed simulations of the interaction between SO_2 and IRMOF-1, -8, -9, -10 and -15 as well as MOF-177 and -505, Cu-BTC, MIL-47 and ZIF-8. They found effective adsorption over a range of materials tested, with effective uptake being strongly linked to increasing heats of adsorption and pore sizes of more than 0.4 nm. As a result they predicted ZIF-8 would be ineffective as an adsorbent for SO_2 uptake but predicted significant uptake for the other materials over a range of SO_2 pressures. In their work Sun *et al.* (2014) perform simulations on IRMOF-1, Cu-BTC, MIL-47(V), MOF-177, Mg-MOF-74, Zn-MOF-74, ZIF-8 and ZIF-10. Whilst done at lower pressures (0-100 kPa compared to 1-1000 kPa) and slightly higher temperatures (40^oC compared to 25^oC) than the work in Song, they reported similar results for the shared materials including the link between heat of adsorption and adsorption uptake. Particularly favourable isotherms at low pressure were reported for Mg-MOF-74.

Zeolitic Imidazolate Framework 8, or ZIF 8, is another form of MOF which replicates the structure of zeolites to create a framework with a large internal space which can be used for adsorption and gas storage, with zinc ions linked together by methylimidazole ions. ZIF-8 was reported by Gao *et al.* (2017) to have a significantly greater surface area of 1425 m^2g^{-1} for ZIF 8 compared to 375 m^2g^{-1} for ZSM-5. Adsorption isotherm uptake for 1-butanol was also reported to be significantly higher with 0.3 gg^{-1} for 1-butanol reported for ZIF 8 compared to 0.12 gg^{-1} for the comparison zeolite ZSM-5, with both materials having strongly favourable isotherms but with significantly slower kinetic uptake with equilibrium times of 60 minutes reported for ZIF 8 compared to 10 minutes for the ZSM-5. This was attributed to pore size limitations present only in the ZIF 8 and is not likely to be relevant for smaller molecules which are more likely to be encountered in respiratory protection applications. These results suggest that ZIF 8 offers a significant improvement on zeolites as an adsorbent whilst retaining their favourable adsorption properties. Chen *et al.* (2016) report similar conclusions in their investigation of the separation of n-hexane from 2-methylpentane, finding ZIF 8 to offer adsorption capacities of 0.5 gg^{-1} compared to capacities of 0.1 gg^{-1} for the comparison zeolite 5A, with both showing favourable isotherms.

Adsorption isotherms towards the model gases for ZIF 8 have not been investigated with the exception of ammonia and sulphur dioxide as previously mentioned and isobutane which was investigated by Awadallah-F *et al.* (2019) who report isotherm capacities of 3 $molekg^{-1}$ for isobutane on ZIF 8 with a strongly favourable isotherm. However they also report a more significant version of the pore limitations encountered by Gao, where below a certain threshold pressure there is no uptake of isobutane whatsoever in the ZIF 8 and it is only when this threshold is exceeded that the structure can sufficiently rearrange to allow access to the active sites by the adsorbate. This makes ZIF 8 unsuitable for respiratory protection as it offers no protection at low partial pressures of adsorbate, but other ZIFs based on different zeolite frameworks with larger pore sizes can overcome this limitation.

However, MOFs are still in their infancy and large scale production techniques have not been developed for most of these materials (Jiang *et al.* 2011), particularly given the vast number of potential chemistries involved. As a result of this MOFs are extremely expensive and not commercially available pre-made, with typical prices in the order of £$1g^{-1}$ for ZIF 8.

This is cost prohibitive in a respiratory protection application where a protective canister is used once and then discarded, each containing up to several hundred grams of adsorbent. As a result, they are an impractical choice for incorporation into a support at this time, but this may change in the future if lower cost variants are developed.

Polymers of intrinsic microporosity (PIMs) are a recently discovered family of polymers which, due to their molecular structure being specifically tuned to pack very poorly together in three dimensional space, have microporous structures inherent in their structure (McKeown 2012). These can have surface areas of over 1400 m^2g^{-1} depending upon the particular polymer used. Adsorption activity has been reported at ambient pressure for various PIMs towards hydrogen at -196^oC at weight loadings of up to 1.6 wt%, but uptake of larger organic molecules can vary significantly between PIMs depending upon the pore structure of the particular polymer, which can lead to molecular sieving and exclusion effects (Qiu *et al.* 2016). However the adsorption properties of PIMs toward relevant toxic gases has not been investigated in the literature. As a result, it is not suitable to choose PIMs for use as an adsorbent for respiratory protection applications at this stage, but PIMs are a young family of adsorbent with significant potential for applicability against a wide spectrum of molecules given the variety in potential chemical precursors to create them, and more suitable PIMs for respiratory protection with relevant adsorbent properties may be discovered in the future.

Potential does exist however for the use of PIMs as an active support material for incorporating another adsorbent within if a suitable chemistry can be identified to support the production of a polymeric foam of intrinsic microporosity. In their review paper McKeown (2012) list several routes to the production of PIMs based on a polyimide chemistry, which is a family of polymers which is known for making high physical performance foams (Weiser *et al.* 2000). However PIM foams based on this chemistry have not been reported, and the development of a new polymer foam chemistry is beyond the scope of this thesis.

Of the families of adsorbents considered, only the zeolites offered the possibility of favourable adsorption uptake over the entire range of toxic gas threats at ambient temperature and pressure which are the conditions relevant for respiratory protection applications. Other adsorbents either lacked uptake towards some of the gases, or have

significant practicality issues which make them unsuited for respiratory protection. Given the wide variety of types of activated carbon materials which already exist, there is little opportunity for developing a novel material based on activated carbon, and it has significant difficulties adsorbing sulphur dioxide and hydrogen sulphide, requiring chemical treatment to modify their surface chemistry to do so. As a result the family of adsorbent chosen for incorporation into an adsorbent support structure are zeolites. Of the zeolites, a zeolite with a large molecular cage is most desirable due to the ability this gives to allow for adsorption of large organic molecules such as cyclohexane, which are the most challenging for this family of materials. As a result, 13X was chosen as the zeolite which was found in the literature to have adsorption uptake for cyclohexane, as this would offer a reliable baseline adsorbent to develop the support material around.

2.3 Analysis of structured adsorbents

2.3.1 Theory of structured adsorbent materials

Gas adsorption occurs at the solid surface of an adsorbent material. As a result, effective adsorbent materials have extremely high specific surface areas to pack large amounts of surface for gas to bind to into very small amounts of space and material. These materials typically take the form of fine flowing powders which are not practical for industrial or respiratory protection applications due to the extremely high pressure drops that beds of fine powdered materials impose. The solution to this problem is to bind or encase the adsorbent into a support structure which gives it a shape which has more favourable pressure drop characteristics.

A support structure must encase and support the adsorbent in a way which allows for the gas in the bulk phase to access the surface where adsorption occurs at a sufficiently fast rate to allow for practical use. This is done via a network of pores which connect the surface of the support to the active surface in a micropore via a series of increasingly large mesopores and macropores (Figure 7) which permeate the material, and can be made of either the support itself in the case of activated carbons, or some other material in the case of zeolites (Thomas *et al.* 1998). Zeolites in particular, given their molecular sieving properties which are a result of a very strictly defined microporous structure, need to be supported for practical use.

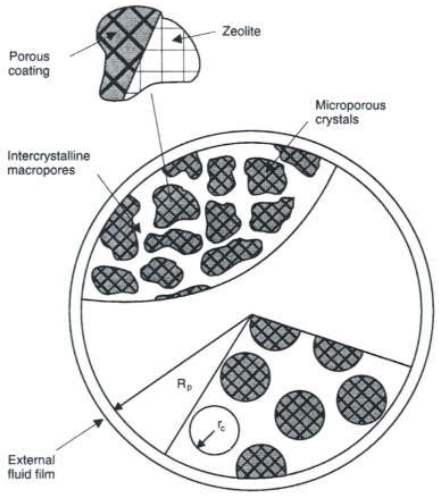

Figure 7: Schematic diagram of mass transfer into an adsorbent pellet via pore network diffusion. (Reproduced from Thomas *et al.* (1998), p80, ©1998, with permission from Elsevier)

Existing support structures for adsorbents are made via mixing the active adsorbent with another material which forms a binder between the adsorbent particles which then are extruded into the desired shape, typically spheres or pellets (Richardson *et al.* 2002). Kaolinite clay is most typically used in commercial beads, which is mixed with zeolite powder in a wet mixture to create a paste which can be moulded or extruded into the desired shape and then undergoes calcination to solidify the material and provide mechanical strength (Breck 1977).

An effective support structure thus has to balance several properties: The bulk pressure drop characteristics of the packed bed, which is a function of the morphology of the material, be it pellets, a monolith or something more exotic; the accessibility and activity of the adsorbent surface which is determined by interactions between the choice of binder and the zeolite, as well as the preparation conditions and the effects of the support on the mass transfer characteristics of the adsorbent, which is a function of the pore network within the support.

Adsorbents have been made in a variety of shapes via use of binders, with beads being most commonly used but cloths (Figure 8) (Moreno-Castilla *et al.* 2011; Nieto-Delgado *et al.* 2019), monoliths (Figure 9) (Li *et al.* 2001), and foams (Amarsanaa *et al.* 2006) also all being reported by various authors as shapes which adsorbents could be made and employed in. Other forms that adsorbents are found in include fabrics and felts, particularly in the case of activated carbons which can be created by the carbonisation of polymeric fibre precursors which can then be woven or felted into sheets as desired (Balanay *et al.* 2013). Adsorbent cloths have been particularly of interest in the field of adsorption of impurities from liquid phases and in wastewater treatment (Świątkowski 1999; Masson *et al.* 2016)

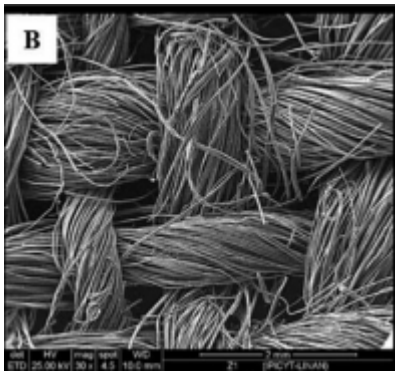

Figure 8: SEM image of activated carbon cloth, 30x magnification (Adapted from Nieto-Delgado *et al.* (2019), p653, ©2019, with permission from Elsevier).

Adsorbent monolith structures, as seen in Figure 9, have also been reported and are formed using a similar formulation technique to adsorbent beads where an adsorbent powder, such as zeolite 5A, is mixed with a binder, but instead of being moulded into bead shapes, the mixture is extruded into a single rigid shape comprising of multiple channels through an entirely solid adsorbent matrix. Clays are typically used as the binder, with bentonite being used in the examples seen in Figure 9 (Li *et al.* 2001). Monoliths are well known for their extremely low pressure drop characteristics.

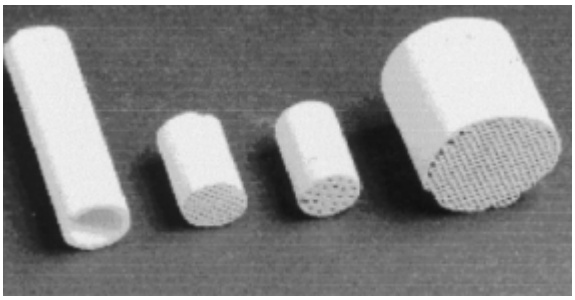

Figure 9: Extruded 5A/bentonite adsorbent monoliths (Reproduced from Li *et al.* (2001), p90 ©2001 with permission from Elsevier).

Adsorbent foams, an example of which from this research is shown in Figure 10, have been reported in the literature as well, although not to the extent of monoliths, granules or cloths. Foams produced by the addition of 7.5wt% of zeolite to polymeric foams during foam production have been reported for investigation into wastewater treatment (Amarsanaa *et al.* 2006), but the applicability of this to gaseous adsorption was not investigated, and this mass loading is impractically low for respiratory protection. Activated

carbon foams have also been made by using polymeric foams as precursors in a similar technique to the production of activated carbon fibres (Zabiegaj *et al.* 2015).

Figure 10: A polyurethane 13X adsorbent foam as produced in the research.

A pore structure within the supported zeolite which can offer good rates of mass transfer from adsorption sites to the bulk gas phase is particularly important for a practical adsorbent. Zeolites which are simply sintered or pressed into pellets retain a very highly microporous pore size distribution, even with the addition of pore forming agents such as aluminium acetate which can be removed from the structure during sintering (Figure 11). However, the use of binders can also reduce the microporosity, as well as the surface area of the material and thus reduce their total adsorption uptake. Improving the pore size distribution by the addition of meso and macropores which can be done via the addition of binders, pore forming agents and templates can lead to significantly increased mass transfer properties (Chen *et al.* 2012).

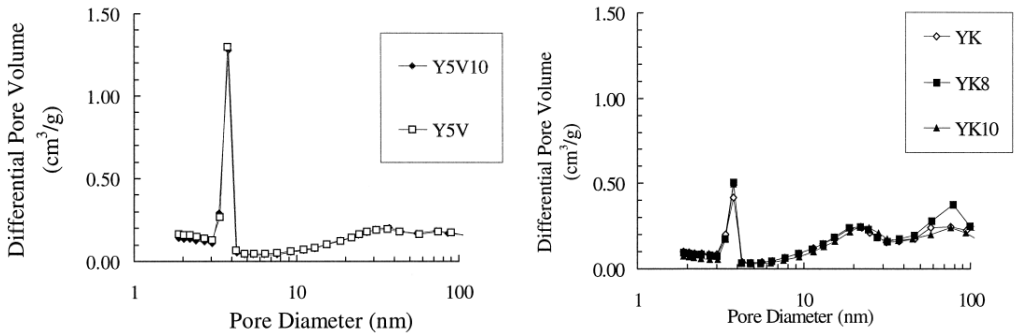

Figure 11: Pore size distributions for binderless (left) and kaolinite binder (right) zeolite Y (Reproduced from Klint *et al.* (1999), p729, 730, ©1999 with permission from Elsevier).

2.3.2 Evaluation of structured adsorbents reported in the literature

In their various works (Rezaei *et al.* 2009; 2010), Rezaei and Webley consider the optimal structure for an adsorption based gas separation problem, deliberating between packed bed, monolith, laminate fabric and foam structures. In this process they create and implement mass transfer models for a selection of geometries for each of the four structure types. These are combined with pressure drop models for the structures, again obtained from literature correlations, in order to produce an overall process model for adsorption through the various structures. This allowed for comparison between the geometries on several metrics.

In terms of mass transfer, both beaded systems and foam systems offer very good performance in terms of transfer rates due to their comparatively high specific surface area, but this comes at a cost of either high pressure drop in beaded systems or low adsorbent packing density in foams, both of which translate into poorer performance when considered in terms of a mass transfer zone length (MTZ).

Pressure drop (Figure 12) for foam structures was found to be lower than packed bed structures, but higher than both monolith and laminate structures of similar void fractions, a variation likely due to the differing nature of the flow path through the materials, with both foams and beads having a far more tortuous flow path which whilst beneficial for mass transfer is generally a hindrance for pressure drop.

Specific productivity (Figure 13) becomes a factor of several of the other variables, particularly pressure drop and mass transfer zone length due to the cyclical nature of adsorbent processes as employed in industry. A maximum thus results for each system as higher velocity allows for shorter cycle times as gas, and thus adsorbate, is put through the adsorbent faster which allows for it to be removed faster, assuming sufficient mass transfer. However this also increases the pressure drop through the bed and increases the MTZ length which leads to the bed being used less efficiently. Here too foams offer improvements over the packed bed structure, whilst falling below monoliths and laminates, but this parameter is of lesser importance in respiratory protection as adsorbents are typically only used once before being discarded.

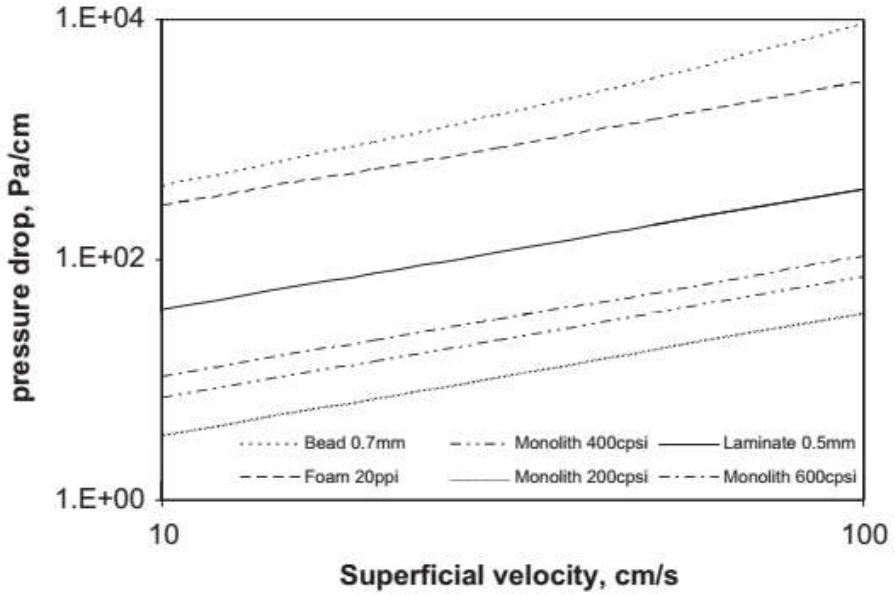

Figure 12: A comparison of modelled pressure drops for various adsorbent structures (Reproduced from (Rezaei *et al.* 2009), p5187 ©2009 with permission from Elsevier).

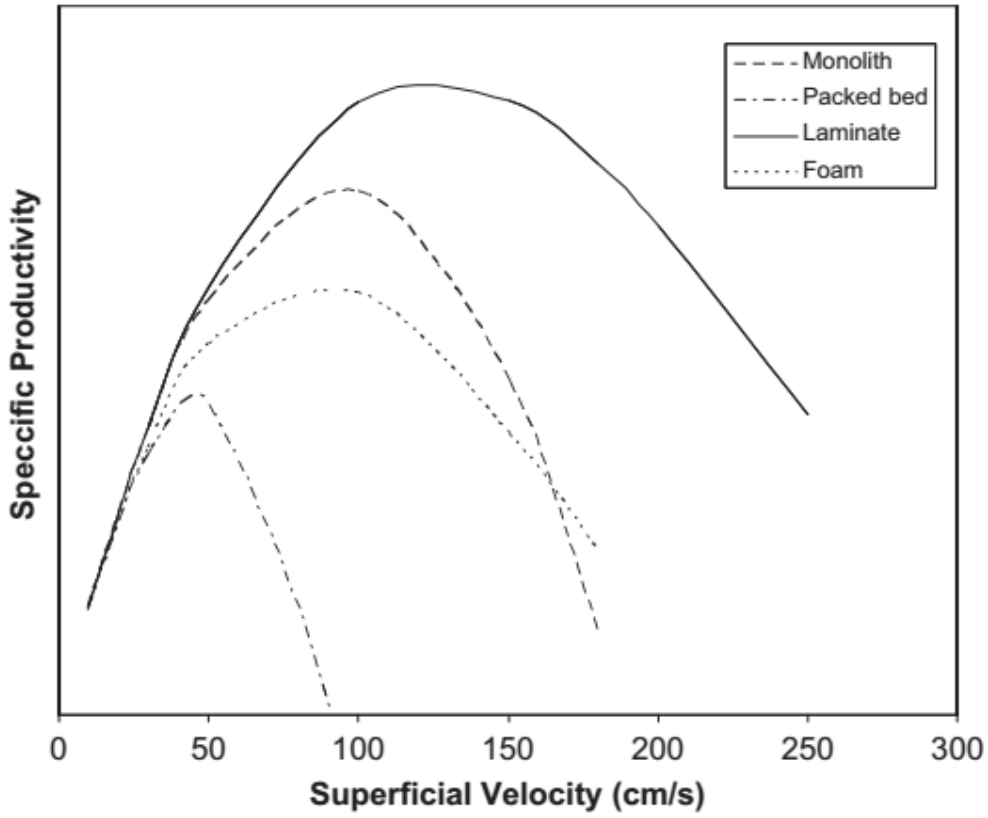

Figure 13: A comparison of modelled specific productivity for various adsorbent structures (Reproduced from (Rezaei *et al.* 2009), p5189, ©2009 with permission from Elsevier).

Following this investigation, it can be seen there is merit in the further investigation into foam based adsorbent structures as these offer benefits both in pressure drop and specific productivity in the modelled results over the packed bed structure which is currently widespread in respiratory protection applications. Other structures may also have potential benefits worthy of investigation but for the purposes of this work, it is foam based adsorbents which are chosen for investigation due to the advantages they offer in terms of freedom of design in terms of shape and size, which are highly valued for development of new and improved respiratory protection designs.

The choice of a foam structure then drives the choice of binder. Foams are difficult shapes to synthesise, given their formation from a suspension of gas bubbles in a solid matrix, but zeolite foams have been reported in the literature. In their various works (Pinto *et al.* 2004; Pinto *et al.* 2005), Pinto and Pires describe the technique of adding both organic and inorganic adsorbent powders to a polyurethane foam via adding the powders to the pre-foam mixture, which takes the form of a single-pot chemical blowing technique similar to that described and employed by Liu *et al.* (2011), only employing a polyurethane chemistry in place of a polyimide one.

As a result of their work, Pinto and Pires managed to successfully synthesise polyurethane foams containing zeolites, activated carbons and pillared clays in a variety of morphologies, forming a total of 5.3% of the total weight of the produced foam material. These were then characterised to determine the effects that the foam production process had on the resulting adsorbent performance.

In both experiments with nitrogen adsorption at -196 ^{o}C and toluene adsorption at room temperature, it was reported that there was a significant loss in adsorption uptake from the process of supporting the adsorbent in the polymer, although this varied between the adsorbent and adsorbate in question. This was attributed to the polymer coating the adsorbent material during the production process, shown in smaller reductions in toluene uptake which was known to be soluble in the polymer matrix when compared to nitrogen. Losses of uptake were particularly pronounced in the case of powdered materials for both organic and inorganic adsorbents.

Amarsanaa *et al.* (2006) also describe the synthesis of polyurethane foams containing added zeolite powder produced via a one pot chemical blowing method. Their formulation adds zeolite powder equal to 7.58 wt% of the resulting foam structures achieving loadings similar to Pires. The resulting foams showed adsorption uptake of tolulene from an aqueous environment of 0.665 wt%, but the structures had a very low specific surface area of 0.717 m^2g^{-1} reported, which suggests very little potential for adsorption given the low loading of zeolite used. No reduction in adsorption uptake due to the polymer was reported. Whilst these structures are polymer foams that contain zeolite, the applicability of these results to respiratory protection is low. The extremely low mass loading of zeolite is not suitable for respiratory protection due to the resulting low uptake of the material, whilst adsorption uptake in an aqueous environment cannot be assumed to also apply to a gaseous one due to the significantly lowered contact times in a gaseous environment, which require significantly faster kinetic uptake on the adsorbent in order to provide effective protection. Similarly the use of biofiltration as a mechanism for the removal of toluene is not applicable to respiratory protection applications, so the materials synthesised by Amarsanaa are not suitable for the needs of this research.

A different technique is reported by Barg *et al.* (2011) where they use an open cell aluminium foam to synthesis zeolite X in situ using the surface of the aluminium foam as a support for the zeolite crystallisation process. Adsorption uptake of N_2 at ambient conditions for the zeolite-metal foams was reported to be 100cm^3g^{-1}, with the reference zeolite sample reported as 180cm^3g^{-1}, whilst the aluminium foam itself had negligible adsorption uptake. The surface area of the zeolite X aluminium foam composite was also significantly increased, with a surface area of 267 m^2g^{-1} reported compared to 4 m^2g^{-1} for the base aluminium foam, but the mass fraction of zeolite in the resulting material was not reported, but can be assumed to be in the region of 50wt% given the large increase in isotherm uptake values. The resulting material provides an effective zeolite in a foam structure, which the authors reported could have its morphology controlled by altering the conditions of the aluminium foam synthesis, and is potentially practical for respiratory protection. Concerns exist however as to what the upper limit of adsorbent loading is, as 50wt% is insufficient for an effective low pressure drop adsorbent structure, but the author's technique uses the aluminium foam itself as an aluminium source for the zeolite synthesis, leading to a limit where the foam support will collapse if excess zeolite formation is pursued, so it is unclear how much further this mass fraction can be increased. Saini *et*

al. (2011) describe in their work the use of polyurethane foam as a template for the synthesis of a zeolite foam in which the zeolite is deposited on the surface of the foam which is destroyed in the process of the zeolite crystallisation. The resulting physical or adsorption properties of the zeolite foam were not reported, but it was reported that the zeolite synthesis process was significantly restricted by the conditions required to preserve the polyurethane foam for long enough to act as a template and not be destroyed too quickly, which potentially limits the zeolite formulations possible.

In terms of potential for further investigation, the addition of zeolite powders to foams during the foam formation stage appears to have the greatest potential. Although literature published on the matter shows only very low proportions of zeolite in the produced materials, it does not directly impose any limit on the adsorbent used other than that it can be acquired in a powdered form, unlike the templating technique. Literature on the production of polymeric foams suggests that additional content of adsorbent should be possible compared to that already reported, as foams with filler powder contents of 20wt% have been reported by Yetgin *et al.* (2014), whilst adsorption activity may be retained from the supporting process as well. A polymer foam should also be used rather than an aluminium foam due to the advantages this offers in terms of weight saving and potential loading not being limited by the need for a solid aluminium support.

2.4 Foam theory

Following the selection of foams as the structure for the supported adsorbent in the previous section, it is necessary to consider how foams are produced and the relevant physical properties governing their formation in order to select and control a process for the creation of a foam containing an active and accessible adsorbent fraction.

A foam can be characterised as a dispersion of gas bubbles inside another solid or liquid phase (Hansen *et al.* 2004). The accumulation of these bubbles against each other, forcing the liquid or solid phase into the space in between the bubbles, is what forms the foam structure, which is similar for all types of foams. Solid foam can be produced from a variety of substances including polymers (Figure 10), metals, typically light metals such as aluminium (García-Moreno 2016) (Figure 14) and ceramics (Figure 15).

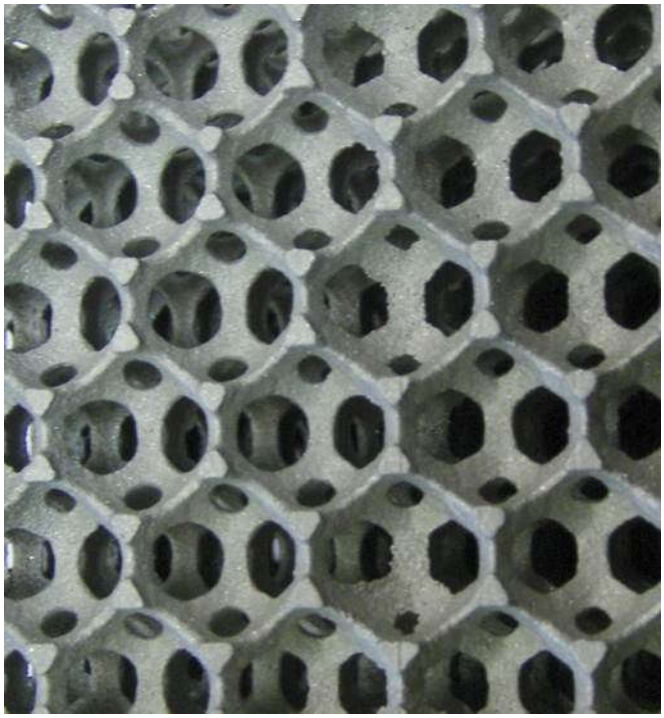

Figure 14: A metal foam (Reproduced from Alvéotec (2012) under the Creative Commons Attribution-Share Alike 3.0 Unported license).

As a result of the structure of foams, they have several key characteristics based on their formation. These are bubble size, window size, strut diameter and void fraction (Figure 16). These are investigated and used to interpret the pressure drop properties of the foams by various authors in the literature in section 2.6.2.

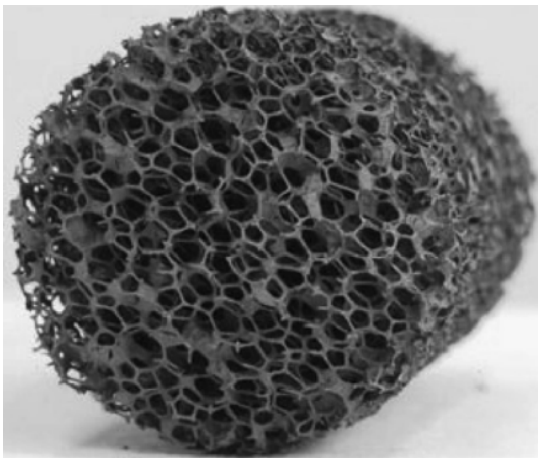

Figure 15: A ceramic silicon carbide foam showing struts formed by bubble agglomeration (Reproduced from (Lacroix *et al.* 2007), p3260 ©2007 with permission from Elsevier).

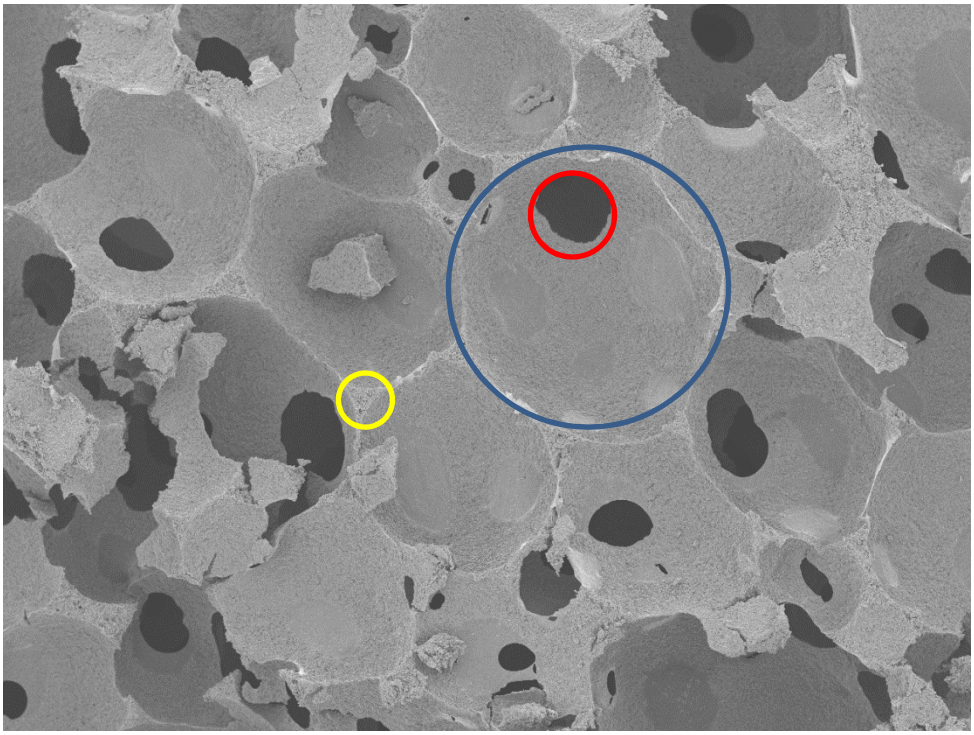

Figure 16: SEM image of a polymer foam with example characteristic dimensions marked. (Bubble diameter in blue, window diameter in red, strut in yellow).

In order to make an adsorbent foam it is necessary to build an understanding of the production of foam structures without adsorbent content in order to develop and adapt the techniques to the production of a foam material with a significant adsorbent content. Foams of various materials are known to exist, but for the purposes of a low material weight and acceptable levels of physical resilience polymeric foams were chosen for further investigation over other options such as ceramic or metallic foams.

In polymeric foams, the solid or liquid phase of the foam is the polymer itself. However to create a polymer foam gas must be added to the polymer as a liquid as the creation of bubbles within a solid is impossible in the scope of producing a material useful for further applications. Various methods are known for achieving this for polymeric foams.

In all cases the production of a foam takes the following form. Gas is introduced into a liquid phase via dissolution or chemical reaction in situ. Once the concentration of gas reaches a critical concentration, bubbles then begin to form at nucleation sites within the liquid. These bubbles then expand against the resistive force of the liquid until they reach an equilibrium size which in turn is also a factor of liquid properties.

Bubble growth rate is given by the following equation (Hansen *et al.* 2004):

$$R_{bub} = \frac{k\left(P_{bub} - \frac{2\gamma}{r}\right)}{\mu} \quad (3)$$

Whilst the equilibrium size is given by the following (Hansen *et al.* 2004):

$$P_{bub} = \frac{2\gamma}{r} \quad (4)$$

where r is the bubble radius (m), P_{bub} the internal bubble pressure (Pa), R_{bub} the rate of bubble growth (ms^{-1}), μ the viscosity of the fluid (m^2s^{-1}), γ its surface tension (Nm^{-1}) and k a proportionality constant (m^4kg^{-1}).

The growth of bubbles leads to the beginning of foam formation as seen in the left of Figure 17. Bubble growth will continue as long as gas continues to be produced within the liquid, leading to the bubbles which initially form growing larger and larger as more gas enters them, leading to expansion of the mixture as the bubbles lift up the liquid leading to the expansion phase of the foam.

Once the production of gas from the liquid slows, the foam begins the aging process. As bubbles expand against each other, the liquid is forced out into the spaces between the bubbles, leading to increasingly thin liquid films in between the individual bubbles. As this process continues, these films rupture and lots of smaller bubbles agglomerate into fewer larger bubbles which can in turn support less liquid. As this process continues, the foam then shrinks and eventually collapses.

If not halted in some way, the foam then begins to age and collapse via the agglomeration of bubbles as seen in Figure 17 until the mixture is fully liquid once again. In the case of solid foams, this halting is done via the solidification of the liquid phase by physical or chemical means.

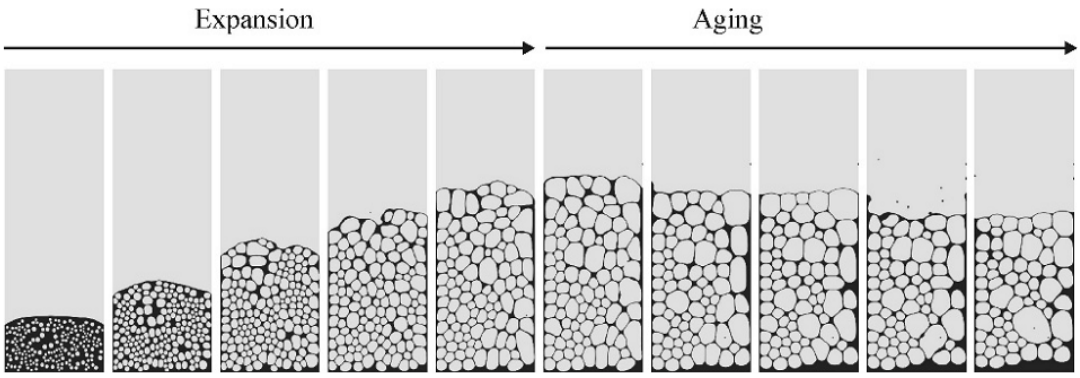

Figure 17: Lifecycle of a foam without any stabilisation process (Reprinted by permission from Springer Nature: [Springer [Integral Foam Molding of Light Metals Technology, Foam Physics and Foam Simulation] by (Koerner 2008) ©2008).

Equation (3) and equation (4) display two important facts for the control of foam formation which are of particular note. Firstly the presence of surface tension in both equations confirms the well-known property of surface tension altering additives, or surfactants, to alter and supress foam formation. Surfactants are chemicals which due to their combination of hydrophobic and hydrophilic properties will adsorb onto the liquid interface, forming a monolayer. As a result, they have a significant impact on surface tension even at low concentration as the surface, and thus the surface tension, is based mostly on the surfactant and not the bulk liquid (Birdi 2009). Secondly the presence of viscosity in equation (3) reveals that foam growth will be particularly sensitive to changes in the viscosity of the fluid, which is highly dependent on the temperature. As a result, both control and alteration of the temperature and viscosity in which the foam is produced offer possibilities to control the end properties of the foam.

2.5 Polymer foam chemistry and manufacture

Following the selection of polymers as the material to form the foam support in section 2.3.2., it becomes necessary to consider both the types of polymer suitable for the production of a foam for use as a support, and the techniques with which the polymers can be formed into a foam structure in order to choose both a technique and polymer most suitable for the production of a successful adsorbent structure.

A polymer is a large complex molecule formed by the reaction of several repeating smaller molecules known as monomers together to form one single molecule. A vast variety of polymers exist depending upon what monomer is used to produce the polymer and the details of the chemical reaction involved (Schaschke 2014).

Polymeric foam production can be categorised based upon the technique used to introduce gas into the structure. This can be achieved by either directly injecting gas into the polymer in some liquid state, known as physical blowing, or having the gas created in situ by some chemical reaction, known as chemical blowing (Kishan 1997). The choice of technique is typically dependent upon the polymer being synthesised. Physical injection requires the use of molten polymers which restricts its use to thermosoftening materials. Chemical blowing however can be integrated into the polymerisation process as either an additive or integral part of the reaction itself which means it can be applied to all polymer varieties.

Physical blowing is widely seen in foam extrusion processes, where a gas can be injected into molten polymer and prevented from forming bubbles until it passes through the extruder die. The choice of gas for use in physical blowing is dependent upon its solubility in the polymer chosen and its melt temperature, but due to the wide reliance on extrusion techniques it is restricted to geometries which can be achieved via this process. The choice of polymer naturally follows from the choice of foam blowing technique. Given the ability to produce materials in arbitrary shapes due to their mouldable properties and the low equipment requirements, chemically blown foams are preferable for investigation in this work.

For the purposes of this work, the choice of polymer is driven by the need to make polymeric open celled foam to provide the support for the adsorbent. This narrows the available options to families of polymer which are suitable for foam production. The most

straightforward way of producing foams is the use of the one pot chemical blowing technique where liquid monomers are mixed together and in the process of reacting a gas is liberated which foams the liquid mixture as it polymerises and solidifies. Several families of foams are compatible with this technique, listed below in Table 2.

Table 2: Families of thermosetting foams suitable for single stage foam formation (Reproduced from (Ashida *et al.* 1995), p12, ©1995, with permission from Elsevier).

Type of foam	**Reaction type**	**Physical properties**
Polyurethane	Polyaddition	Flexible and rigid
Polyisocyanurate	Cyclotrimerization	Rigid
Polyamide	Polycondensation	Flexible and rigid
Polyimide	Polycondensation	Semi-rigid
Pyranyl	Radical polymerization	Rigid
Polyurea	Polyaddition	Flexible and rigid
Epoxy	Ring-opening polymerisation	Rigid
Phenolic	Polycondensation	Rigid
Urea-formaldehyde	Polycondensation	Rigid
Polycarodiimide	Polycondensation	Rigid
Polyoxazolidone	Ring-opening polyaddition	Semi-rigid
Unsaturated polyester	Radical polymerisation	Rigid
Rubber	Vulcanisation	Flexible
Viscose	Regeneration of cellulose	Flexible
Polyvinyl alcohol	Formal formation	Flexible

Of these families of polymers, ones which produce foams which are either flexible or rigid with good physical strength properties are good choices for resisting the mechanical stress of a respiratory protection environment. Polyurethane has also been reported in the literature as a choice of polymer in which zeolites have been successfully supported. Polyimides have been reported as a polymer suitable for the production of foams which has excellent physical properties as well (Pan *et al.* 2010). As a result, both families of polymers are suitable for further consideration, particularly as they can share a monomer in the form of polyisocyanates (Ashida *et al.* 1995). The use of isocyanate as a base monomer is of particular note, as isocyanates are well known for their applicability in a wide variety of polymeric chemistries, which when combined with the isocyanate-water

reaction for creating a blowing gas in-situ provides a wide variety of options for polymers to produce the supporting foam from (Ashida *et al.* 1995).

An example of a widely used polyurethane chemistry is shown below in Scheme 1, which shows an example of a polyurethane being produced by a reaction between the polyol and isocyanate functional groups on each monomer to form a polyurethane bond.

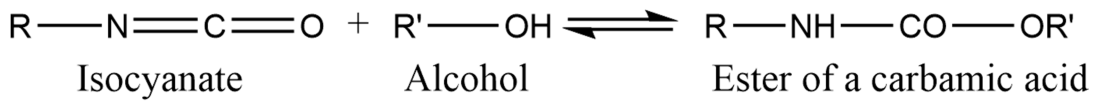

Scheme 1: Generic polyurethane chemistry (Adapted from Drobny (2007), p216, ©2007 with permission from Elsevier).

Depending upon the chosen nature of the monomers, which can be any molecule with the required functional groups in accessible positions, the resulting produced polymer can have a wide range of properties. An example of polyimide chemistry is also shown below in Scheme 2 in which an anhydride monomer is reacted with an isocyanate to create a polyimide.

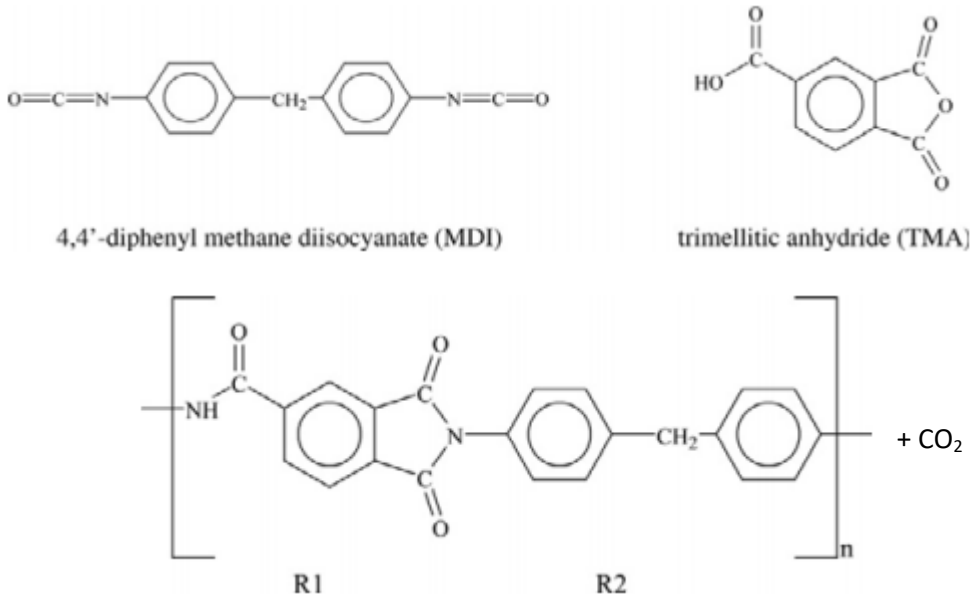

Scheme 2: A typical polyimide chemistry from anhydride and isocyanate monomers (Adapted from McKeen (2012), p107-108, ©2012 with permission from Elsevier).

Liu *et al.* (2011) describe in their work the production of a polyimide foam, a polyimide being a polymer formed by the condensation of an organic dianhydride (PMDA in Scheme 3) with a diamine group (The nitrogen in the isocyanate in Scheme 3) (Gooch 2007). This was done via the chemical blowing technique, which demonstrates the significant advantages this technique offers. In this technique they use a single pot process to mix the chemical precursors of polyimide together along with additional water to allow the polymerisation and blowing reactions to occur simultaneously, as seen in Scheme 3 and Scheme 4.

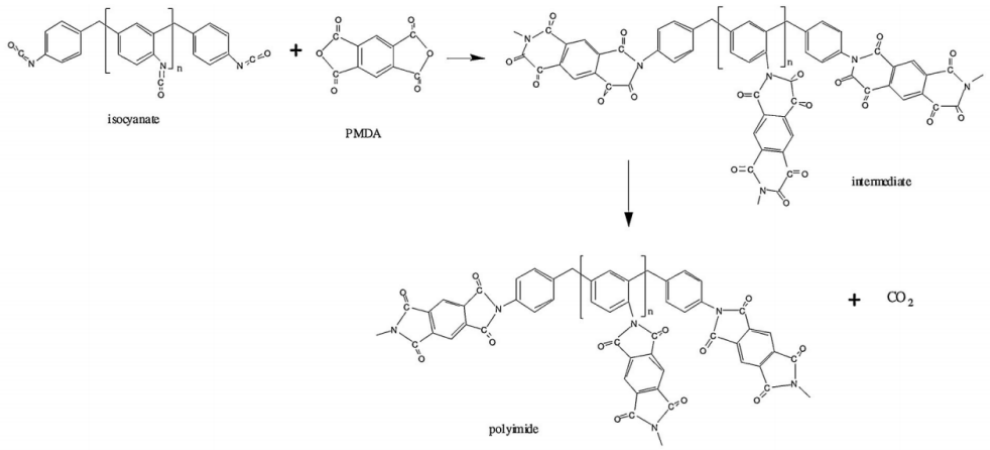

Scheme 3: Chemistry for producing a polyimide foam (Liu *et al.* 2011) (Reproduced from (Liu *et al.* 2011) with permission from John Wiley and Sons, ©2011).

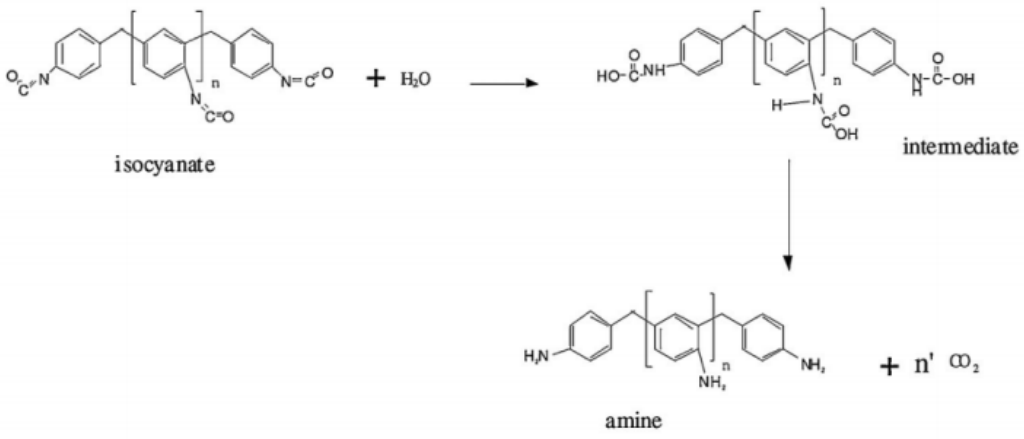

Scheme 4: Isocyanate-water blowing reaction (Liu *et al.* 2011) (Reproduced from (Liu *et al.* 2011) with permission from John Wiley and Sons, ©2011).

The resulting foams were reported to have a high degree of resulting expansion, taking on the form of the container in which the components were mixed, and reacted in an order of seconds, making this a particularly favourable production route given the control over the reaction's occurrence and produced shapes it can offer.

As a result of the scoping efforts, both polyimide foams and polyurethane foams are selected for investigation as a support polymer for the zeolite, due to the literature suggesting polyurethane foams can support zeolite as well as the potential for improved physical and thermal properties from polyimide as well as the similar chemistries allowing for the sharing of a monomer. Both also were compatible with the chemical blowing foaming technique which was preferable due to the lack of need for extensive gas injection equipment for physically blown foams and the ability to produce foams in arbitrary geometries via use of moulds.

2.6 Pressure drop in foam structures and comparison to packed bed structures

In order to evaluate any produced foam material supporting an adsorbent for favourable pressure drop characteristics, it is important to consider the existing work performed on modelling and understanding pressure drop through foam materials. As a foam is geometrically the inverse structure of a packed bed, such efforts are typically adaptations of the original efforts to understand pressure drop through packed beds by Ergun (1952).

2.6.1 Packed bed structures

A packed bed can be described as a mass of solid particles, typically spherical, which provide a path for fluid flow in the void space between the particles, held in place either by gravity or by some physical containment (Figure 18).

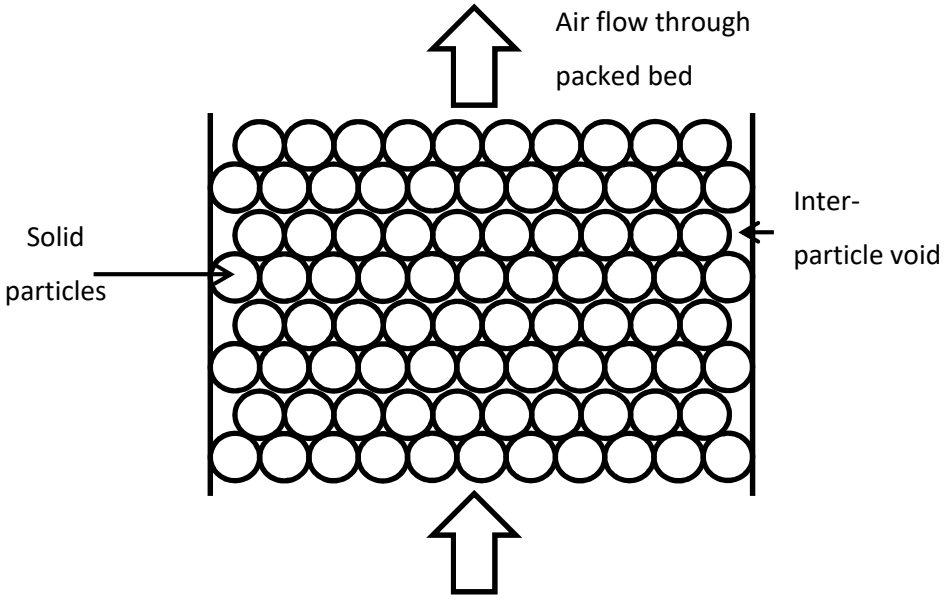

Figure 18: Schematic diagram of a packed bed structure.

The pressure drop through this bed of particles can be described by the Ergun equation, shown below (Ergun 1952):

$$\frac{\Delta P}{L} = E_1 \frac{\mu(1-\varepsilon)^2 u_g}{\varepsilon^3 d_p^2} + E_2 \frac{\rho(1-\varepsilon)u_g^2}{\varepsilon^3 d_p} \quad (5)$$

Where ε is the void fraction of the bed (dimensionless), d_p the particle diameter (m), u_g the superficial gas velocity (ms^{-1}), ρ the fluid density (kgm^{-3}) and μ the fluid viscosity (Pas). This

equation is true for incompressible gas flow. E_1 (dimensionless) and E_2 (dimensionless) are known as the Ergun constants and in practice are empirical fitting parameters for the equation to fit a given set of systems depending on how the packing compares to spherical packing. In the case of the packed beds of spheres described by Ergun, E_1=150 and E_2= 1.75 are used.

2.6.2 Foam structures

Given that a foam is by its nature a structure comprised of a series of interconnected bubble shaped voids encased by a solid framework, it is logical that the Ergun equation has formed the basis for understanding and modelling pressure drop through such structures as it originally modelled their inverse structure, namely the packed bed of particles. Indeed, literature work exists both in modelling and practical investigation which supports this route of analysis.

One of the requirements in order to create a working adaptation of the Ergun equation is to find a characteristic dimension which is the equivalent of the particle diameter. In order to do this, published works including Richardson *et al.* (2000) create a geometric model to describe the foam structure. This is based on the regular packing of tetrakaidecahedral cells, as seen in Figure 19.

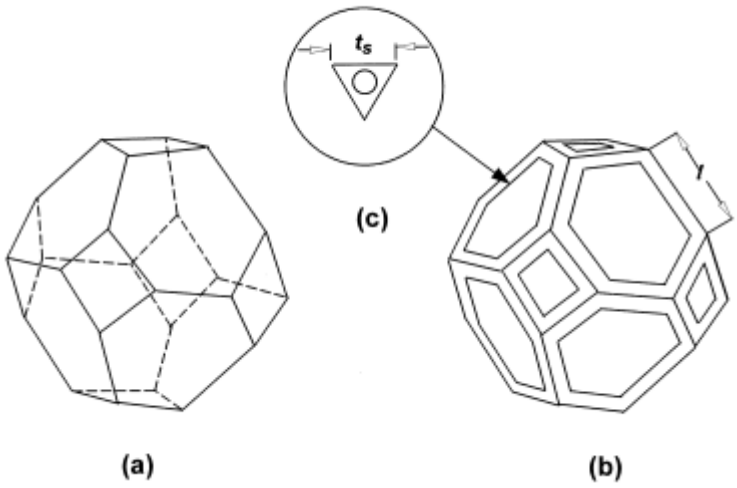

Figure 19: The tetrakaidecahedral geometry model for foams (Reproduced from (Richardson *et al.* 2000), p26 ©2000 with permission from Elsevier).

In this model, the struts are the solid material left by the expanding of bubbles inside the foam and the windows between bubbles are represented by the open hexagonal and square faces. This model is built upon in further published work in order to create adaptations of the Ergun equation to apply it to foam materials, which are discussed below.

In their work Lacroix *et al.* (2007) describe their efforts to modify the Ergun equation for modelling pressure drop through silicon carbide foams. In this work, they use a substitution to link an effective spherical particle diameter d_p (m) to the foam properties as follows:

$$d_p = \frac{6}{4} d_s \tag{6}$$

$$d_s = \frac{a[(4/3\,\pi)(1-\varepsilon)]^{1/2}}{1-[(4/3\,\pi)(1-\varepsilon)]^{1/2}} \tag{7}$$

$$a = \frac{\phi}{2.3} \tag{8}$$

Where ϕ (m) is the bubble or cell diameter of the foam being investigated.

The value for the bubble diameter was found in the work via optical microscopy of the foams tested and used to validate the model, with a mean diameter of a selection of 20 cells used to provide a value for ϕ.

Using this set of substitutions, the authors report good agreement between pressure drop modelled using their technique and measured pressure drops through foam porosities of 0.5-0.92 and fluid velocities of up to 6ms^{-1} without any requirement to alter the Ergun constants.

Other methods of adapting the Ergun equation for foams have also been published. Dietrich (2012) uses a technique based on the work of Ergun and the application of a friction factor approach to obtain the following correlation for pressure drop through foams:

$$\frac{\Delta P}{\Delta L} = 110\frac{\mu}{\varepsilon d_h^2}u + 1.45\frac{\rho}{\varepsilon^2 d_h}u^2 \tag{9}$$

Where d_h (m) is the hydraulic diameter for fluid flow. As in other published work, the difficulty comes in the determination of the characteristic diameter for gas flow. Dietrich *et al.* (2009) defined the hydraulic diameter in terms of the specific surface area as follows:

$$d_h = 4\frac{\varepsilon}{S_v} \tag{10}$$

Where S_v, the specific surface area (m^2kg^{-1}), is found by the following correlation:

$$S_v = 2.87\frac{1}{d_{strut}+d_w}(1-\varepsilon)^{0.25} \tag{11}$$

It was reported that this showed good agreement with published data for pressure drops through foam materials for a range of Reynolds numbers from 10^{-1} to 10^5 with errors of up to ±40%.

Inayat *et al.* (2011) develop correlations for the Ergun constants as well as equations relating the hydraulic diameter to foam properties (Inayat *et al.* 2011).

Starting from the following basic form of the Ergun Equation:

$$\frac{\Delta P}{L} = \frac{E_1 S_v^2(1-\varepsilon)^2\mu}{\varepsilon^3}u + \frac{E_2 S_v(1-\varepsilon)\rho}{\varepsilon^3}u^2 \tag{12}$$

They propose the following correlations for the Ergun constants:

$$E_1 = \left[\left(\frac{1-0.971(1-\varepsilon)^{0.5}}{0.6164(1-\varepsilon)^{0.5}}\right)\varepsilon\right]^{-1} \tag{13}$$

$$E_2 = \left[\left(\frac{1-0.971(1-\varepsilon)^{0.5}}{0.6164(1-\varepsilon)^{0.5}}\right)(1-\varepsilon)\right] \tag{14}$$

These coefficients are based on a standard tetrakaidecahedral packing foam model with triangular struts, in particular the ratio between window diameter to strut thickness.

However, the authors also consider more realistic structures in their work and how this might affect the resulting correlations. Inayat *et al.* (2011) consider the base case of

triangular struts as well as cylindrical struts and concave triangular struts. The case of concave triangular struts is of particular interest as these structures bear most resemblance to a foam likely to be produced via a bubble based blowing technique.

For concave triangular struts, the authors found the following equations building on the tetrakaidecahedral geometric model:

$$d_{s(\text{triangular concave,effective})} = \frac{0.6164 d_w (1-\varepsilon)^{0.5}}{1 - 0.971(1-\varepsilon)^{0.5}} \quad (15)$$

Where d_w is the window diameter of the foam (m).

$$S_{v\ \text{triangular,concave}} = 6.49 \frac{[1 - 0.971(1-\varepsilon)^{0.5}]}{d_w (1-\varepsilon)^{0.5}} (1-\varepsilon) \quad (16)$$

This allows for further adaptation of the author's correlations for the Ergun equation to the foam geometry actually being encountered.

As can be seen, a wide variety of techniques exist for the adaptation of the Ergun equation to a foam structure, with seemingly little consensus within the literature for a preferred technique. Correlations for fitting Ergun constants to datasets are fairly common and date back as far as the original Ergun paper itself. The difference when considering the foam system is the disagreement over what comprises the characteristic diameter for fluid flow. In the case of packed beds it is given by the particle diameter, but in the case of foams window diameter, strut diameter and bubble diameter are all potential candidates and have been applied in the literature. Whilst the discussed papers provide a useful guide, it will be necessary to perform experimental analysis against the real foam structures produced in order to find an effective model for interpreting pressure drop results in the research described in this thesis.

2.7 Conclusions for the development of materials relevant to the research

Investigation into the standards literature governing respirators has highlighted cyclohexane, chlorine, hydrogen sulphide, hydrogen cyanide, sulphur dioxide, ammonia, dimethyl ether and isobutane as examples of the major chemical respiratory hazards which a respirator must protect against. Of the major families of adsorbents activated carbons and zeolites were found to offer potential removal of the entire range of these hazards, of which zeolites were selected due to the potential novelty of supported zeolite materials. Of the zeolites, 13X was selected due to it having the largest cavity in its microcrystalline structure offering superior uptake towards larger organics such as cyclohexane.

The theoretical reviews performed by Rezaei *et al.* (2010) support the assertion from the introduction that investigation into a foam structured support has merit for further development and benefit over existing solutions for respiratory protection. This in combination with the review of the standards literature confirms the case for a lower pressure drop support.

The work of Pinto *et al.* (2005), when taken into consideration with more basic work on the production of foams, such as that of Liu *et al.* (2011), provides a guide for further development of a workable concept. Whilst Pinto synthesised a foam containing an adsorbent material, the loading by weight of adsorbent achieved was far too low to be a useful material in the application relevant to this thesis. Investigations into increasing this loading will be of significant interest, particularly if it can be done to a degree such that the polymeric covering of the adsorbent surface can be prevented, which was an issue highlighted in the work. Published data from the polymeric foam industry supports the assertion that the fraction of a powder component within a foam can be increased from the published values in the work, and attempts will have to be made to increase the mass fraction by over an order of magnitude compared to published examples.

Investigation into techniques for the production of polymeric foams has identified chemical blowing techniques as the most suitable for the production of a practical adsorbent support material, and of the various families of polymers compatible with this process highlighted polyurethanes and polyimides as suitable choices for investigation, as well as found a suitable chemistry to develop based upon the isocyanate monomer chemistry

highlighted by Liu *et al.* (2011) with adaptations and developments as may prove necessary to create a functional material. As a result, adsorbent supported in polymeric foam matrix has been chosen as the material for development.

The literature surrounding pressure drop through foam materials has also been discussed to provide a background for analysis of the pressure drop behaviour of foams and allow them to be compared to pressure drop of traditional packed bed materials. No consensus was found in the literature on the characteristic dimension of a foam to compare to the particle diameter seen in Ergun style relationships so various models which adapted Ergun to fit the foam geometry were selected for further use and analysis, with Ergun being used as a basis due to the physical similarities between a packed bed structure and an open celled foam.

3 Development of adsorbent foam materials

This Chapter describes the experiments performed to develop a technique to produce a foam material which contains an active adsorbent fraction, based on the areas identified in the literature review. It also highlights the produced experimental materials relevant to this development.

The Chapter has an experiment by experiment description of the early formulation development, highlighting experiments where important observations and breakthroughs were made. This starts with foam chemistries which are described in more detail, explaining the process of adaptation of the published formulations into those used in this work, and how working formulations were developed for both polyimide and polyurethane foams.

Following the success in creating working formulations to make adsorbent foams, the development of the physical processing techniques is discussed. This covers the efforts required in order to make foams in suitable shapes and sizes for testing and further analysis, the development of drying techniques to remove solvents used during production, and the methods used to ensure production is consistent and reliable. The development of post-production processing techniques is also described, justifying the need for post processing and describing the methods investigated and chosen to improve the accessibility of adsorbents within the foams. The methods used focus on removing polymer from the foam material in a controlled and limited fashion.

The foams produced in this Chapter are then used to provide samples for the physical and adsorption characterisation efforts which form Chapters 4 and 5 of this thesis and allow for judgements on their suitability and effectiveness as adsorbent support structures to be made.

3.1 Production process development

The development of the foam production technique involved three areas of work: adaptation of the published foam chemistries to the needs of the research and desired products, the choice of an appropriate adsorbent for incorporation into the foams and devising a physical process for ensuring the resulting product had a suitable form for further investigation work with minimal wastage.

In order to achieve this, various experiments were performed to find a formulation that was successful in supporting an adsorbent. This section highlights those experiments which were critical in guiding the development of the formulations, whilst omitting experiments which did not provide useful information for this development for clarity.

3.1.1 Choice of adsorbent

The focus of this thesis is the investigation of supporting an adsorbent in a suitable structure for low pressure drop characteristics, as opposed to optimising and investigating adsorbent behaviours themselves. However it is necessary to choose an adsorbent for incorporation into the foam for investigation of their properties as an adsorbent support. Section 2.2.3 highlighted 13X as the best choice for an adsorbent for further investigation into use as a supported adsorbent, which is used in this work in the form of commercially available 13X powder, supplied by Brownell Ltd. This then must be incorporated into a polymeric foam, the development of which is discussed below.

3.1.2 Foam chemistries

Two foam chemistries were explored in this work to form the polymeric support, a polyimide (PI) based foam, and a polyurethane (PU) based foam. These were both developed by adaptation of and improvement upon work published in the open literature, with the PU foams being an offshoot of work in developing the PI foams. As such, the work on PI foams is discussed first before going into detail on PU foams.

3.1.2.1 Polyimides

As discussed in Chapter 2, Liu *et al.* (2011) identified a formulation for the production of a polyimide foam (Scheme 3). From the literature, the preparation technique was described thusly: Pyromelletic dianhydride (PMDA) was weighed and mixed in N, N dimethyl formamide (DMF) at 80^{o}C until all the PMDA was dissolved. To this solution was added 5wt% methanol, 3wt% water, 20wt% polyether modified polysiloxane surfactant, 0.05 wt% triethanolamine and 0.05wt% dibutyltin dilaurate. The resulting solution was mixed and allowed to cool to 30^{o}C to form the first solution. This solution then had added to it polyaryl polymethylene isocyanate, which formed the second solution. The two solutions were then vigorously mixed with a mechanical mixer and then poured into a mould and allowed to rise. The amount of polyaryl polymethylene isocyanate in the second solution was varied in the published work as part of the author's investigation based on a weight ratio to the first solution with weight ratios of 0.5, 0.65, 0.80, 0.95 and 1.10 of polyaryl polymethylene isocyanate:first solution being reported.

The initial developments in the chemistry came from attempting to replicate the published technique in the laboratory. Polymethylene polyphenyl isocyanate (PMDI) was sourced from Aldrich (average molecular weight 400), along with PMDA (Aldrich, 97% purity), DMF (Aldrich, 99% purity), triethanolamine (Aldrich, 98% purity), dibutyltin dilaurate (Aldrich, 95% purity) and methanol (Aldrich, 99.8% purity). Due to the inability to source the modified polysiloxane surfactant described in the literature, it was omitted. For the initial foam making experiment the following formulation was used (Table 3) which was derived from the proportions reported in Liu *et al.* (2011):

Table 3: Formulation used for sample 0

Component	**Amount**
PMDA	21.8g
Water	0.7g
Methanol	1.2g
Triethanolamine	0.01g
Dibutyltin dilaurate	0.01g
DMF	As sufficient to dissolve PMDA
PMDI	26.2g

The PMDA was added to a beaker, followed by sufficient DMF to dissolve the PMDA crystals entirely into the liquid. To this solution was then added the triethanolamine, dibutyltin dilaurate and water, and the solution thoroughly mixed. This formed one part of the two part reaction. The second part of the reaction, the PMDI, was then weighed into the beaker, stirred briefly and vigorously using a metal spatula and the resulting mixture allowed to rise and set before being removed from the beaker.

This formulation allowed for the production of a polyimide foam which showed good expansion characteristics; had interconnected bubbles which would allow for the passage of air through the material; and the characteristic yellow colour of a polyimide (Figure 20). As a result it was deemed suitable for the attempted inclusion of an active adsorbent component.

Figure 20: A fragment of the produced pure polyimide foam (sample 0).

Immediate refinements were made to the formulation based on this experience, before adding adsorbent was attempted. The PMDA needed an excessive amount of DMF in order to be dissolved properly. Additionally it was found exceedingly difficult to measure and dispense the two catalysts on a mass basis. As a result of this, for the first experiment involving adsorbent, the PMDA was dissolved under an elevated temperature of 80^{o}C and the catalysts were dispensed via pipette, but otherwise the technique was unchanged. The following formulation was used (Table 4). 13X powder was acquired from Brownell Ltd and used as received:

Table 4: Formulation used for sample 1

Component	**Amount**
PMDA	21.9g
Water	1g
Methanol	1g
Triethanolamine	0.01g
Dibutyltin dilaurate	0.01g
DMF	47 ml
PMDI	28.5g
13X zeolite powder	10g

This formulation was chosen so that the added fraction of 13X zeolite would not be an excessive proportion of the whole in order to test for the viability of adding 13X powder and was approximately a 20 wt% fraction of the resulting polymer based on a mass balance of the components and assuming total removal of the solvent.

Figure 21: A fragment of sample 1 showing a coarser foam structure compared to sample 0.

The resulting produced foam, sample 1 (Figure 21), foamed very successfully, but the reaction proceeded at an unexpectedly fast and difficult to control rate following the addition of the PMDI, and overflowed the reaction vessel. This resulted in visibly lower density foam with large voids compared to sample 0. The elevated reaction temperature was suspected to be responsible, but could not be confirmed due to the potential of interference from the addition of the zeolite powder. This lead to further developments in the technique for sample 2.

Sample 2 used the elevated heating of sample 1 to properly dissolve the PMDA in the DMF as in sample 1, but instead of mixing in the PMDI immediately and letting the reaction occur at that elevated temperature, the mixture was allowed to cool to 30^{o}C before mixing in the PMDI to react. 13X was also eliminated from the formula to prevent any possible interference in the foaming reaction, resulting in the formulation in Table 5.

Table 5: Formulation used for sample 2

Component	**Amount**
PMDA	21.9g
Water	1g
Methanol	1g
Triethanolamine	0.01g
Dibutyltin dilaurate	0.01g
DMF	47 ml
PMDI	28.5g

This sample behaved differently from the previous efforts. Whilst it did react and expand as previous efforts had done, the foam then proceeded to collapse again and then more slowly rise and react following the addition of extra heating to attempt to encourage the reaction to resume.

As sample 2 showed fast foaming and reaction, followed by a collapse, which was not seen in the ambient temperature conditions used for sample 0, it confirms that elevated temperature are accelerating the foaming process, which can lead to the expansion seen in sample 1. As sample 2 was a failure however, and sample 1 successful, the zeolite can also be confirmed to have an effect. As foam collapse is caused by a lack of bubble and gas formation, the high expansion of the foam in sample 1 suggests that the zeolite is promoting gas formation. This is expected from foam theory due to it providing nucleation sites.

Further adaptations thus chose to use both elevated temperature and 13X addition to improve the performance of the polyimide foams and build on the successful sample 1. In further samples, whilst the reaction mixture was cooled, the reaction did not occur at room temperature, instead being performed at 50^{o}C which was chosen as a compromise

between the temperature required for effective dissolution of the PMDA and temperatures too low for effective foaming to occur. Triethanolamine and dibutyltin dilaurate were also dispensed via a 100μl pipette on a volume basis to remove difficulties in measurement on a mass basis. Sample 13 was the first experiment with 13X and polyimide which used this new technique, including a 30wt% fraction of adsorbent with the formulation listed in Table 6. This foam expanded and set successfully, producing a solid material without unexpected complications.

Following the successful adaptations of technique shown in sample 13, further experiments focussed upon increasing the fraction of adsorbent which could be successfully added without complications using the same formulation for other components.

Table 6: Formulation used for sample 13

Component	**Amount**
PMDA	11g
Water	1 ml
Methanol	0.5 ml
Triethanolamine	6 drops
Dibutyltin dilaurate	0.05 ml
DMF	24 ml
PMDI	14.3g
13X	10g

Foams with 38 wt% adsorbent (sample 14) were successful, but attempts to make foams with 44 wt% adsorbent (sample 16, Table 7) resulted in the foam expanding in volume very quickly before collapsing before the polymerisation process could occur (Figure 22). Additional difficulties were encountered in handling the extra solid fraction of 13X powder, the method of overcoming which is discussed in section 3.1.2.3.

Table 7: Formulation used for sample 16

Component	**Amount**
PMDA	11g
Water	1 ml
Methanol	0.5 ml
Triethanolamine	6 drops
Dibutyltin dilaurate	0.05 ml
DMF	24 ml
PMDI	14.3g
13X	17.3g

Figure 22: Example of a foam formed after collapse of the bubble structure.

Foam theory, as discussed in section 2.4 and Figure 17, suggests that foam collapse is due to the foam aging process occurring faster than the chemical reaction causing it to solidify. As a result of this, the addition of a surfactant was trialled to see if this could overcome the limit encountered. The surfactant chosen was a silicone oil of 350 cSt viscosity, purchased from Aldrich and was added in during sample 17 (Table 8). Liu *et al.* (2011) report using 20 wt% of surfactant in their work, and this value was used as a guide for choosing to use 5ml of silicone oil in sample 17. The fraction of DMF has also been increased in order to ensure proper liquidity of the solution given the greatly increasing fraction of solid 13X powder, which is discussed in further detail below in section 3.1.2.3.

Table 8: Formulation used for sample 17

Component	**Amount**
PMDA	5g
Water	0.5 ml
Methanol	0.25 ml
Triethanolamine	3 drops
Dibutyltin dilaurate	0.025 ml
DMF	25 ml
PMDI	5g
Silicone oil	5 ml
13X	10g

This formulation resulted in a slower foaming process due to the addition of surface tension increasing silicone oil, as predicted by the general foam theory discussed in section 2.4 and equation (3), and solidified without any sign of collapse, but did have a somewhat rubbery feel when removed from the mould which suggested that silicone oil was distributed throughout the structure. Further samples would thus reduce the fraction of silicone oil used to attempt to mitigate this excess.

Following the success of sample 17 at supporting higher mass fractions of adsorbent, further increases in adsorbent were attempted in sample 19, using compositions as shown in Table 9. Increasing amounts of DMF have been added as a result of the increasing solid fraction of adsorbent, and the silicone oil additions have been reduced. The result was a slow rising foam which solidified following good expansion and showed no signs of collapse.

Table 9: Formulation used for sample 19

Component	**Amount**
PMDA	5g
Water	0.5 ml
Methanol	0.25 ml
Triethanolamine	3 drops
Dibutyltin dilaurate	0.025 ml
DMF	30 ml
PMDI	5g
Silicone oil	2 ml
13X	20g

Following the success of sample 19, few changes were thus needed to create a set formulation for the production of a foam over a wide range of adsorbent fractions. Given issues with supply in DMF and the desire to apply existing knowledge from solvent extraction in polymer membrane systems, 1-methyl-2-pyrrolidinone (NMP) (Acquired from Aldrich, 99% purity) was substituted in as a solvent for DMF in sample 27 (Table 10) which was otherwise identical to sample 19.

Table 10: Formulation used for sample 27

Component	**Amount**
PMDA	5g
Water	0.5 ml
Methanol	0.25 ml
Triethanolamine	3 drops
Dibutyltin dilaurate	0.025 ml
NMP	30 ml
PMDI	5g
Silicone oil	2 ml
13X	20g

This foam again foamed successfully, showing slightly increased reaction speed, foam expansion and bubble size compared to sample 19. As a result, NMP was chosen for use as

a process solvent in all future foam work to avoid further supply issues. The other significant formulation change was the elimination of methanol as a component. The original literature did not state a reason for its inclusion, and foam theory as discussed in section 2.4 did not offer an explanation for its purpose. As a result it was removed, which had no impact on the resulting performance in foam production.

The resulting generic formulation could thus be created for polyimide foams, which allowed for the scaling of the mixture to any desired size for a variety of shapes for further testing. It calculates component amounts as a function of the desired adsorbent fraction (m%) and an arbitrary scaling factor (n) (Table 11).

Table 11: Generic formulation for PI-13X adsorbent foams

Component	**Amount**
Arbitrary scaling factor	n
Desired adsorbent fraction of foam (in decimal form)	m
PMDA	10n g
Water	n ml
Triethanolamine	6n drops
Dibutyltin dilaurate	0.05n ml
NMP	1.4*(20n*(m/(1-m)) ml
PMDI	10n g
Silicone oil	4n ml
13X	20n*(m/(1-m)) g

This formulation uses the ratios between components as published in the literature, with the amount of process solvent set as a 1.4 ratio of the 13X powder present. This value was found via investigation as discussed later in section 3.1.2.3. Implementations of this formula are used for all further experiments with PI-13X foams.

Given the development of a generic formulation for PI-13X foam production, the remaining area to investigate in formulation development was the upper limit on adsorbent content. Given the nature of the materials as active adsorbent supported in a polymer structure, it is logical that at some point the structure should be unable to support the addition of more

structurally inert powder. For the generic formula described in Table 11 this was found to be 67wt%. Formulations made with 13X fractions in excess of this failed to foam. As a result PI-13X foams became of less interest to investigate compared to a different formulation using polyurethanes which showed the capability to overcome this limit, described in the following section.

3.1.2.2 Polyurethanes

As discussed in Chapter 2, polyurethanes are characterised by the urethane links between the chosen monomers, and are typically produced by the reaction between an isocyanate group and a hydroxyl group. Due to this chemistry, it is reasonably simple to modify the polyimide chemistry to a polyurethane one by substituting the dianhydride monomer used previously with a monomer containing hydroxyl groups.

The monomer chosen to replace the dianhydride was polyethylene glycol (PEG), which was chosen to investigate because PEG was chemically similar to the pyromelletic dianhydride component it was replacing in that it has two functional groups per molecule (Figure 23).

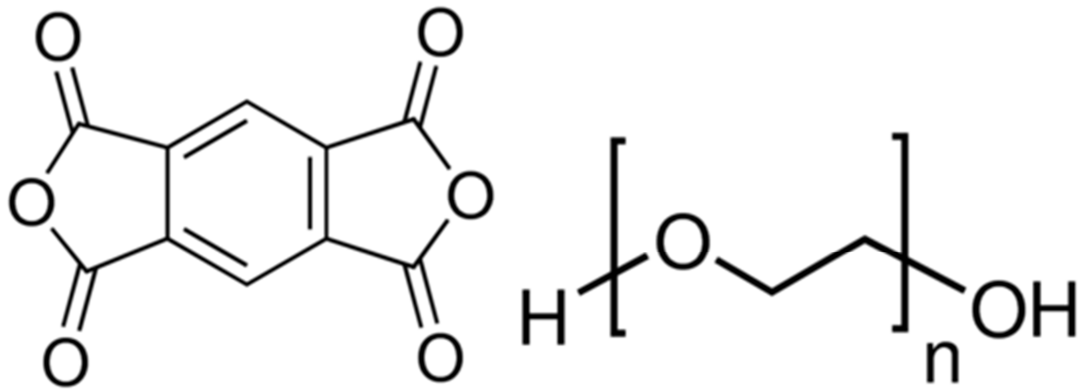

Figure 23: Pyromelletic dianhydride (Left) and polyetheylene glycol (Right) showing two functional groups each.

PEG was substituted into the existing polyimide chemistry as refined in the previous section and tested for its effectiveness in producing a polyurethane foam using the formulation in Table 12. PEG was acquired from Aldrich, with an average molecular weight of 400gmol^{-1}.

Table 12: Formulation for sample 33, a 67wt% PU-13X foam.

Component	**Amount**
Polyethylene glycol	5g
Water	0.5 ml
Triethanolamine	3 drops
Dibutyltin dilaurate	0.025ml
NMP	28 ml
PMDI	5g
13X	20g
Silicone oil	2g

Sample 33 used a direct substitution of the PMDA monomer for PEG in an existing formulation known to produce a successful high adsorbent loading foam with PI (Sample 27). The resulting foam rose in a very sluggish fashion, eventually forming a very dense but flexible material in contrast to the PI foams of similar loading. This flexibility was lost upon thorough solvent removal.

The slow foaming process and high density according to foam formation theory, as discussed in section 2.4 and equation (3) and (4), is a sign of an excessive amount of surfactant added. PEG is known to have surfactant properties, which means that the formulation contains two substances providing surfactant properties: silicone oil and PEG. Due to this duplication of properties and poor foaming, the formulation can be simplified by eliminating the silicone oil, giving the formulation shown in Table 13, providing an additional benefit to the choice of PEG as a monomer.

Table 13: Experimental formulation for sample 36, a 67wt% PU-13X foam without additional surfactant

Component	**Amount**
Polyethylene glycol	5g
Water	0.5 ml
Triethanolamine	3 drops
Dibutyltin dilaurate	0.025ml
NMP	28 ml
PMDI	5g
13X	20g

As expected by foam formation theory (section 2.4), this formulation showed increased expansion compared to sample 33 and retained the flexibility of the previous material. As a result, the elimination of silicone oil as an additional surfactant was successful, encouraging the use of polyurethane as a supporting polymer and a generic formula for PU-13X foams could be produced as follows (Table 14). This formula was thus used for all PU-13X based samples.

Table 14: Generic formulation for PU-13X foams

Component	**Amount**
Arbitrary scaling factor	n
Desired adsorbent fraction of foam (in decimal form)	m
PEG	10n g
Water	n ml
Triethanolamine	6n drops
Dibutyltin dilaurate	0.05n ml
NMP	1.4*(20n*(m/(1-m)) ml
PMDI	10n g
13X	20n*(m/(1-m)) g

As done previously, the upper limit for adsorbent content in the PU-13X foams was investigated. This limit was encountered in sample 54, given below in Table 15.

Table 15: Formulation for sample 54, an attempted 80wt% PU-13X foam

Component	**Amount**
PMDA	20g
Water	2 ml
Triethanolamine	12 drops
Dibutyltin dilaurate	0.1 ml
NMP	240 ml
PMDI	20g
13X	160g

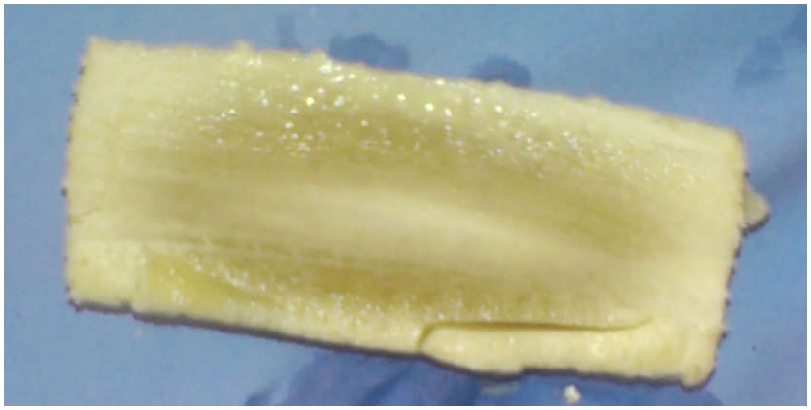

Figure 24: Cross-section of sample 54 showing a total failure to rise.

As can be seen in Figure 24, an attempted foam containing this fraction of adsorbent shows a total failure to undergo the foaming process. During the experiment it was necessary to add excessive solvent to maintain liquidity and the polymerisation reaction was very slow. Insufficient bubbles were also produced to foam the structure.

This result is an expected consequence of the increasing amount of 13X in the reaction mixture. As both the 13X and the required solvent in order to ensure the mixture remains liquid with the powder increase, the concentrations of active components in the form of the monomer and blowing agents are reduced. Due to this, there exists an upper limit past which an insufficient rate or amount of blowing gas will be produced to foam the mixture whilst polymerisation occurs, which has thus been determined to be between 75 wt%, the highest loading formulation successfully made with the formulation in Table 14, and 80 wt% which failed to foam.

3.1.2.3 Liquidity ratios

During the development of the polyimide chemistry it was discovered that as the fraction of adsorbent increased relative to all other ingredients, the resulting precursor mixture became increasingly thick and paste like if all other components were kept in the same proportions. This was due to the increasing amount of 13X which must be added for a small relative increase in adsorbent fraction (Figure 25). This results in an increasingly slurry or paste like consistency in the precursor. As a result, additional liquid must be added in order to ensure that the mixture has suitable properties to support the formation of bubbles, and thus produce foams.

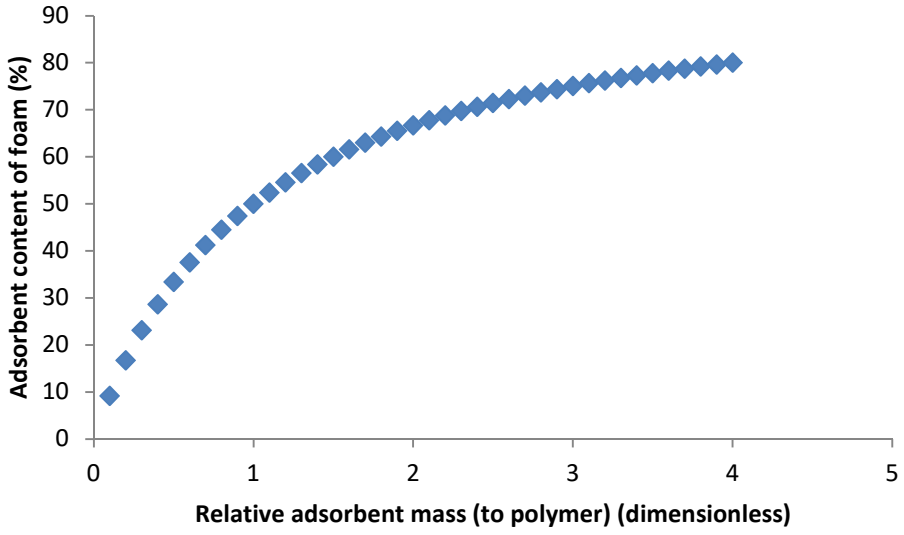

Figure 25: The diminishing effects of additional adsorbent on the adsorbent fraction of a resulting polymer-adsorbent foam composite.

However increasing the proportion of liquid components which are retained in the final polymer structure undoes the effort to increase the fraction of active adsorbent in the material. The chosen solution was to increase the fraction of solvent used to dissolve the monomer to ensure the solution remained liquid as the solvent was removed after foam formation. The chosen liquidity ratio was set as a function of the 13X powder present, as in the foams of practical use the 13X powder was either the only, or the most abundant solid ingredient used in the procedure.

The chosen liquidity ratio should add as little solvent as necessary to maintain the desired liquid properties to minimise the resulting effort required to remove it once the polymer structure has solidified, and use successful foam formulations as a guideline for acceptable values to begin from.

As discussed in section 2.4, the fluid properties with the most impact upon the formation of bubbles within a liquid, and as a result the formation of foams, are the surface tension and viscosity of the liquid. As a result, how both of these were affected by changes in the formulation was investigated to allow for the choice of a suitable liquidity ratio for the generic formulations previously mentioned.

3.1.2.3.1 Surface tension

The surface tension of the precursor solutions was investigated via use of the pendant drop technique, which was chosen for its ability to handle sample materials containing a significant fraction of particulate matter and use relatively small sample sizes. This technique works by solving a force balance over the drop being suspended, with surface tension suspending the drop against gravitational forces.

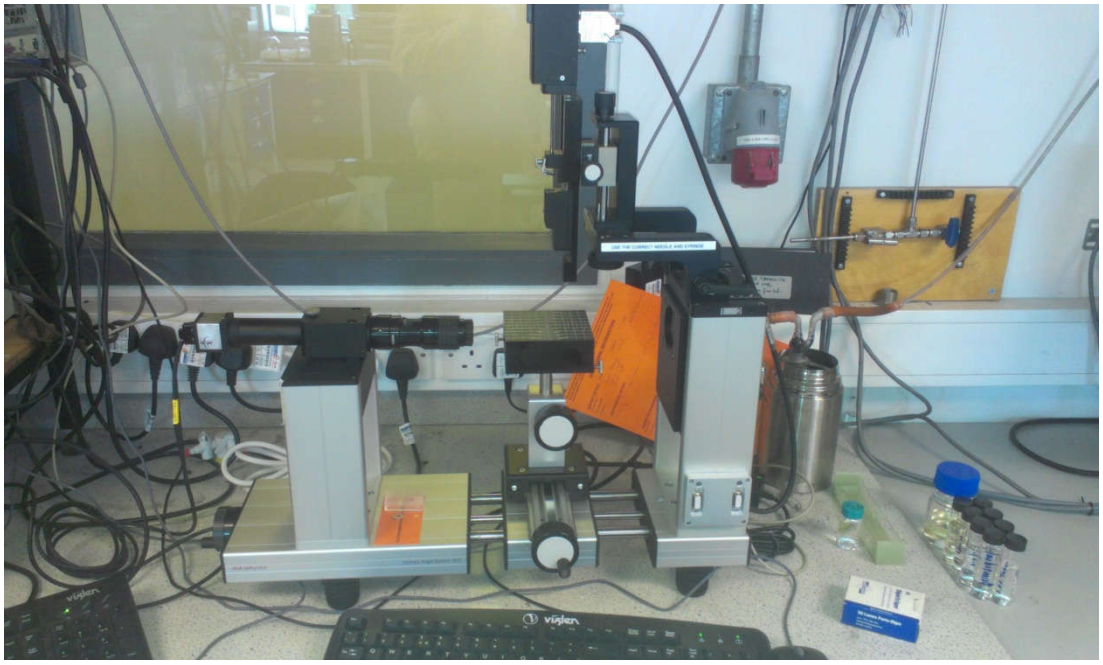

Figure 26: Pendant drop apparatus as used in the research.

In the apparatus used (An OCA 25 DataPhysics optical contact angle measurement system, DataPhysics Instruments GmbH) (Figure 26), a known amount of the solution is dispensed via use of a computer controlled syringe through a needle of known diameter to form a drop hanging from the end of the needle, preferably as large as possible. An image of the drop is then recorded on camera against a blank background to allow for an accurate outline of the drop to be recorded (Figure 27).

Figure 27: Example image of a fluid pendant drop as used to measure surface tension (1.4 liquidity ratio, 75 wt% 13X).

For a cylindrical needle, the force due to surface tension acts upon the interface between the fluid and the surrounding air and is in equilibrium with the weight of the drop. It can be described as follows (Hansen *et al.* 1991):

$$\gamma = \Delta\rho g r^2/\beta \qquad (17)$$

where γ is the surface tension of the fluid (Nm^{-1}), g the acceleration due to gravity (ms^{-2}), $\Delta\rho$ the difference in density between the air and the fluid being tested, r the radius of the drop at the apex and β a shape factor determined by the shape of the drop.

The shape factor, β, is calculated by fitting drop profiles to the shape of the drop, which is dependant on the contact angle between the drop and the air and the ratio of the neck of the drop to the widest point. Various methods exist to approximate this but in practice this

calculation is performed automatically via the software supplied with the equipment. The volume of the drop is known due to the controlled method in which the syringe dispenses fluid to fill the drop, whilst the contact angle between fluid and air is found optically (Figure 28). Given this and knowledge of the density of the solution, found via measurement of the test solutions before use, the surface tension of the solution being measured can be calculated.

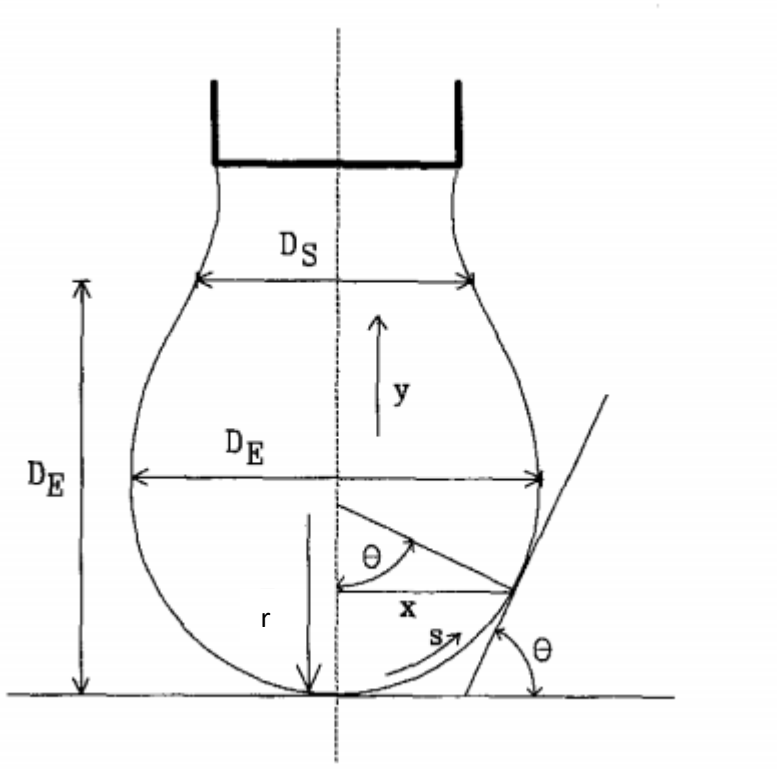

Figure 28: Schematic diagram of the pendant drop technique (Adapted from (Hansen *et al.* 1991), p4 ©1991 with permission from Elsevier).

A variety of partial precursor solutions were synthesised for testing using the generic formulation in Table 14, comprising of PEG, NMP and 13X in varying proportions as would correspond with formulations used in certain 13X weight loadings of foam. The catalyst components were eliminated due to safety concerns in handling, whilst PDMI was eliminated as this would cause a foaming reaction to occur. A Design of Experiments technique was used to reduce the amount of required experimental work resulting in the following samples being chosen for investigation (Table 16).

Table 16: A Design of Experiments matrix showing the chosen solutions for surface tension measurement.

13X Loading/Liquidity Ratio	1.2	1.4	1.6	1.8	2.0
1.2	X		X		X
1.4		X		X	
1.6	X		X		X
1.8		X		X	
2.0	X		X		X

Liquidity ratios below 1.2 failed to produce a consistent liquid phase, whilst ratios above 2.0 used impractically large amounts of solvent compared to the active components. These samples had their surface tension data measured using the technique described above and the resulting surface tension data was used to plot a 3D graph (Figure 29) of various formulations being tested, with gaps in between known data points being filled via linear interpolation. This was then used to identify which formulation variables affected surface tension, so that areas which had a significant effect on the surface tension could be avoided.

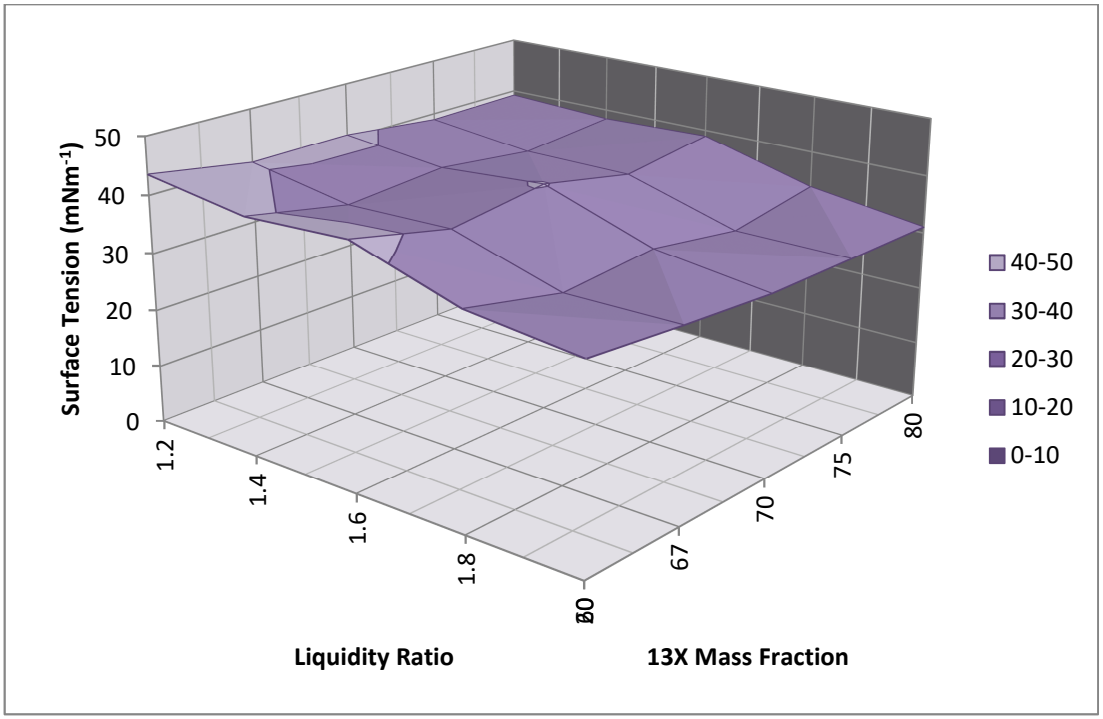

Figure 29: A 3D plot showing the change in surface tension of precursor foam solutions when liquidity ratio and 13X fraction were varied.

As can be seen in Figure 29, the surface tension of the precursor solutions is not strongly affected by changes in the liquidity ratio, particularly as the 13X fraction of the solution increases. As a result the effects of surface tension on the foam formation behaviour can be concluded to be reasonably constant.

3.1.2.3.2 Viscosity

Using the same choice of solutions to investigate as was used in the surface tension investigation (Table 16), the viscosity of these solutions was also measured experimentally in order to determine which choice of liquidity ratio would be most suitable. The technique chosen for this was the use of a Bohlin CS Rheometer rotary viscometer as seen in Figure 30.

Figure 30: A Bohlin CS Rheometer, as used to test the viscosity of the solutions.

A rotary viscometer involves the rotation of a specially shaped cone which is in contact with the solution to be tested across its entire surface and kept at a constant temperature (Figure 31). This cone can be rotated at a variety of speeds in order to impose any desired choice of shear stress on the solution. By measuring the power required to impose such a movement speed a force balance can be performed in order to determine the viscosity of the solution.

Viscosity is defined as the ratio of shear stress to shear rate as follows:

$$\mu = \frac{\text{Shear stress}}{\text{Shear rate}} = \frac{\sigma}{\dot{\gamma}} \tag{18}$$

In the cone and plate system, the shear stress is given by the torque applied to the rotational disk by the motor multiplied by a form factor for the cone to find the force upon the fluid itself:

$$\sigma = \tau c_1 \tag{19}$$

where the shear stress form factor for the cone (c_1) is a function of the radius r:

$$c_1 = \frac{3}{2} r^3 \tag{20}$$

The shear rate $\dot{\gamma}$ is given by the rotational speed of the cone through the fluid (ω) (assuming the bottom plate is stationary), multiplied by a form factor constant for the cone in use (c_2):

$$\dot{\gamma} = \omega c_2 \tag{21}$$

where the form factor for shear rate in a cone system (c_2) is given by the contact angle of the cone with the plate (α):

$$c_2 = \frac{1}{\alpha} \tag{22}$$

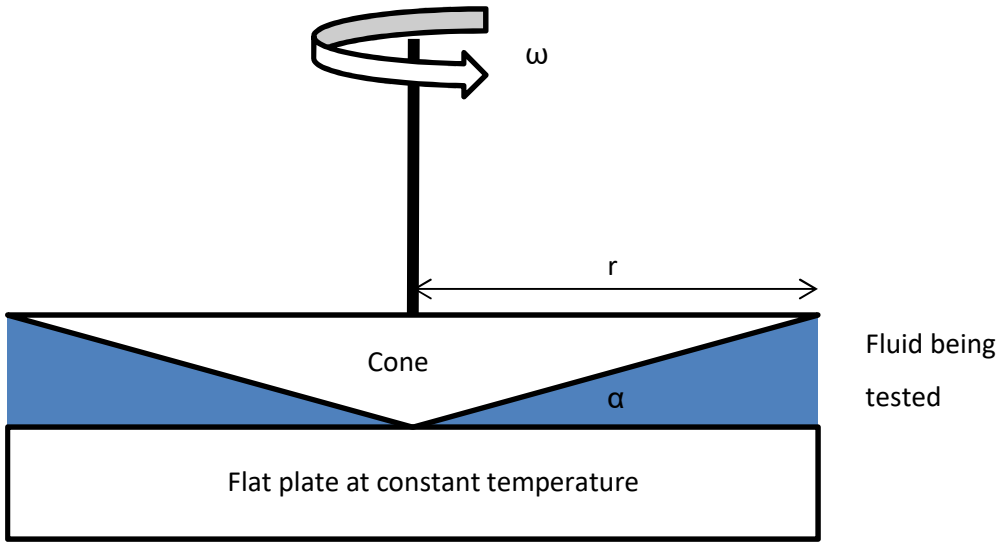

Figure 31: Schematic diagram of a cone and plate rotary viscometer.

The equipment measures the torque imposed upon the fluid and directly controls the rotational speed of the cone in real time, and as a result can directly measure and plot the viscosity of the fluid given knowledge of the cone being used in the measurement.

Preliminary scoping work was performed to determine which range of shear stresses would best differentiate between the solutions being tested. Higher stresses showed higher differences in viscosity between solutions, and as a result a shear stress range of 0-5 Pa was chosen to measure viscosity across. Higher stresses were also viewed as more representative of the initial bubble expansion in foam formation which was particularly affected by liquid properties.

Viscometry data was taken as the average of three different measurements. As in the investigation of surface tension, a Design of Experiments matrix was used to reduce the amount of measurements required (Table 16). Missing data was estimated using linear interpolation. The acquired viscosity data for the top end of the measured shear stress range was plotted in a 3D plot (Figure 32) to examine which properties of the precursor solutions had the most effect on the viscosity of the solution.

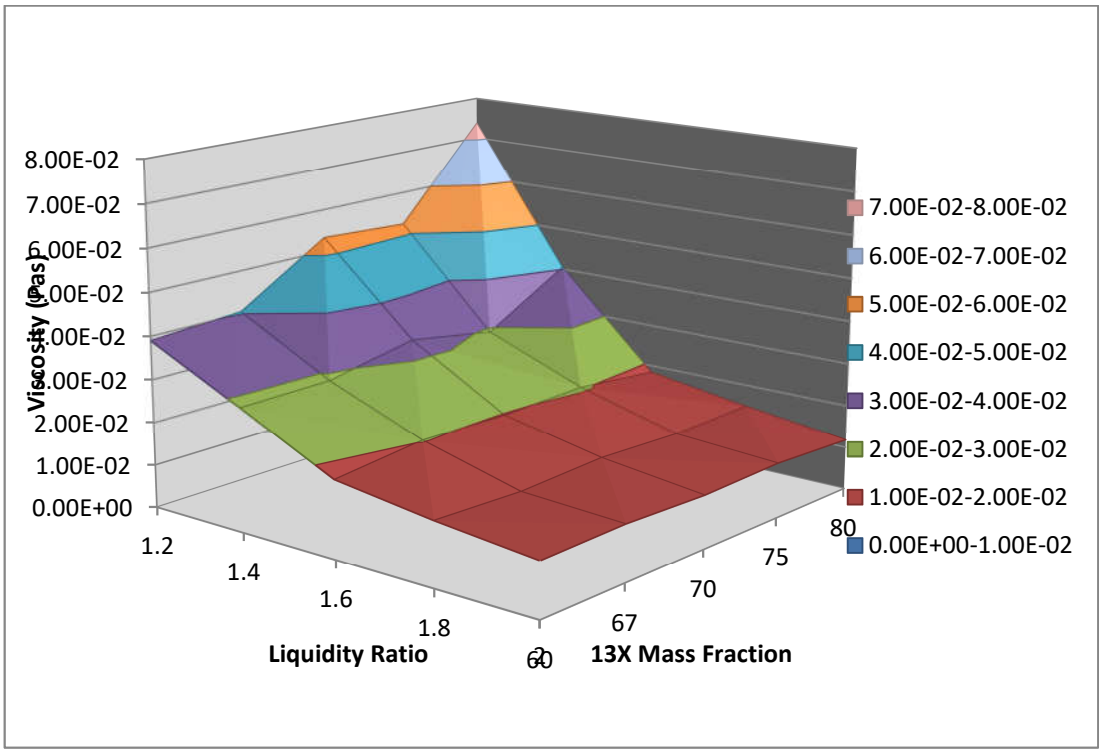

Figure 32: A 3D plot showing the variance in viscosity of precursor foam solutions when liquidity ratio and 13X fraction were varied.

As can be seen here, as the liquidity ratio decreases viscosity of the precursor solutions increases, particularly for higher 13X loadings, which makes it increasing difficult for foam formation to occur. Solutions with higher liquidity ratios have a less pronounced increase in viscosity with 13X loading, if any at all.

Given the lack of sensitivity of surface tension to the formulation of the precursor solution, and the obvious downsides of increasing liquidity ratio too much in adding difficulties in the solvent removal process and diluting the active polymerisation components, a compromise value of 1.4 was chosen for the liquidity ratio to be used in the generic formulations, as this greatly reduced the viscosity increase as a factor of 13X loading.

3.1.2.4 Formulation development conclusions

The formulation development efforts have resulted in a general formula (Table 17) which can be used for foam production of either polyurethane or polyimide based adsorbent foams. This formulation scales to a wide variety of foam loadings as well as desired sample sizes depending on the size of mould and amount desired for testing. Greater 13X loading was found to be possible using PU chemistries in place of PI ones.

Table 17: Generic formulation used for foam sample production.

Component	**Amount**
Arbitrary scaling factor	n
Desired adsorbent fraction of foam (in decimal form)	m
Monomer (PEG or PMDA)	10n g
Silicone oil (PI only)	4n g
Water	n ml
Triethanolamine	6n drops
Dibutyltin dilaurate	0.05n ml
NMP	1.4*(20n*(m/(1-m)) ml
PMDI	10n g
13X	20n*(m/(1-m)) g

This formulation proved reliable in allowing for the successful production of samples to support the rest of the research when used with proper physical processing techniques, discussed in the following section. This formulation was used to manufacture all the foams which were used in physical characterisation and testing as discussed in Chapter 4, as well as the adsorption investigation in Chapter 5.

3.1.3 Physical processing development

The initial technique for foam production was simply mixing the components together in a two part procedure, keeping the active monomers separate until the last moment so the time foam production began could be controlled (Figure 33). This was done on the bench in standard laboratory glassware.

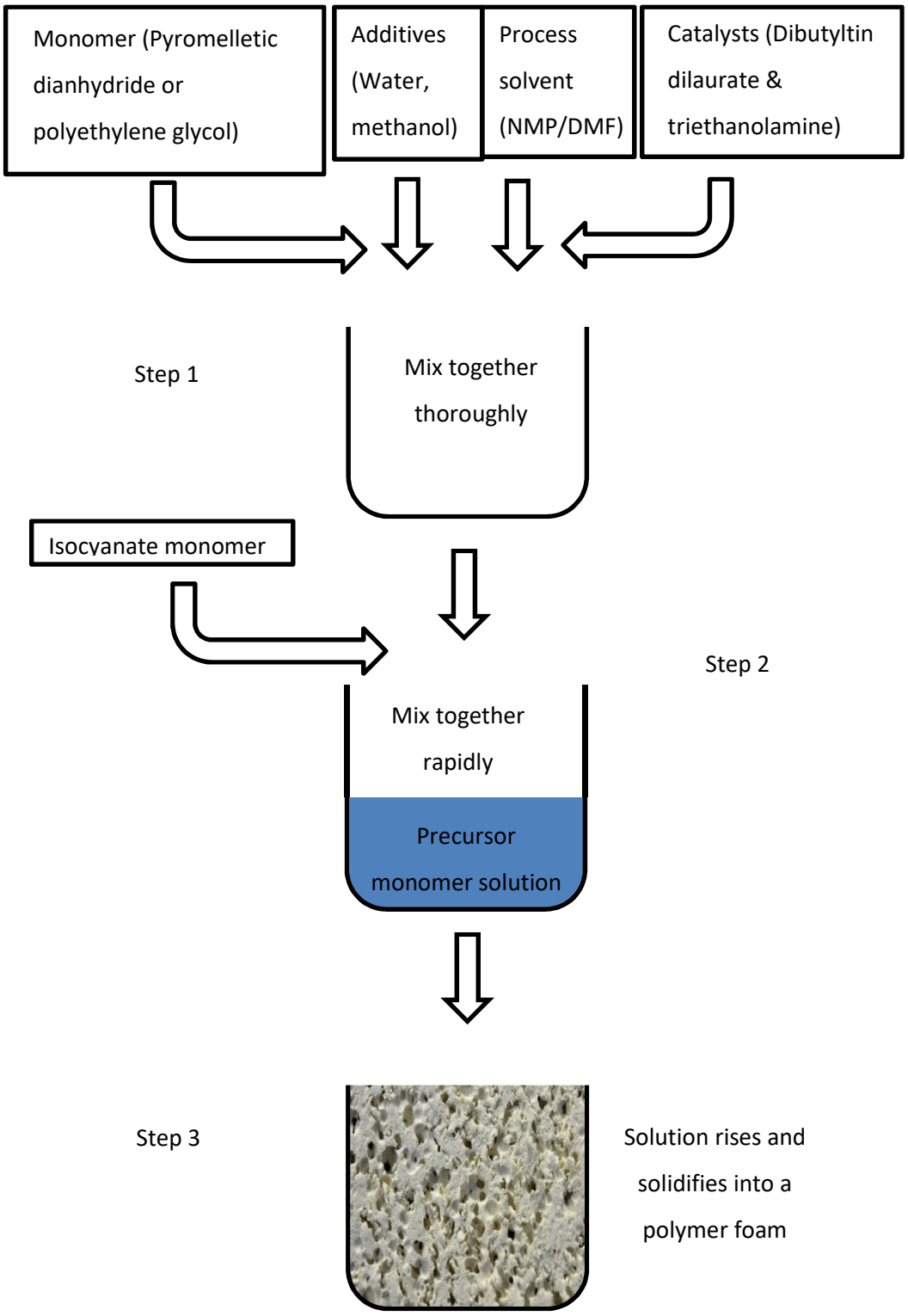

Figure 33: Diagram of the initial foam production process.

Various problems immediately became apparent which required refinement of the technique. The first of these was the difficulty in removing the resulting polymeric foam from the beaker once it had formed, as the resulting foam had a tendency to be bound to the sides and bottom of the beaker quite firmly. Furthermore, the shape of a beaker was not the most suited to producing foams for further testing. As a result, investigations were made into the use of moulds for the production of foams inside.

Figure 34: PU-13X foam being produced in a removable tin mould.

Removable tin moulds proved very effective at allowing the produced foam to be removed in a single piece, as seen in Figure 34. These were used for several experiments during the formulation development process. However they suffered from the same difficulties as found in glass beakers in that the shape of foam they produced was not particularly suitable for characterisation testing, which became clear as the testing regime was developed.

As a result of this, the process was adapted to use a cylindrical mould (Figure 35), as long cylindrical morphologies were particularly suited to further testing and this allowed for economical use of chemicals and produced foam materials.

Figure 35: PU-13X foam being produced in a tube mould.

This then introduced difficulties in removing the sample from the mould, but these were overcome by use of a plant oil based mould release agent which the mould was coated with as necessary before use. PU foams were found to be easier to remove without assistance compared to PI foams.

Following the development of techniques to characterise the produced foam materials, a need for larger samples to support destructive processing and testing became clear. As a result, the formulation was simply scaled up linearly for larger samples, resulting in formulations as seen in Table 18.

Table 18: Formulation for sample 45, an enlarged 67 wt% PU-13X foam.

Component	**Amount**
Polyethylene glycol	10g
Water	1 ml
Triethanolamine	6 drops
Dibutyltin dilaurate	0.05ml
NMP	56 ml
PMDI	10g
13X	40g

During the mixing process of adding the solvent to the mixture of 13X, monomer and additives, a significant degree of heat was generated, as well as a tendency to create lumps of paste-like powder within the solution. These combined effects led to the resulting foam having an undesirably high density and poor distribution of 13X within the structure due to these two unwanted properties.

Following this, the production process was altered to move away from hand mixing, and towards the use of a mechanical homogeniser (Ultra Turrax T25 homogeniser (IKA Werke)) (Figure 36) to ensure that the 13X powder was evenly distributed within the precursor solutions and resulting foams. The mixer also allowed for very good mixing of the isocyanate component within the brief window allowed before the foaming reaction begins. Cooling steps after mixing were also added to allow for the reaction to occur at a constant room temperature. This mixer was particularly effective when used with the cylindrical mould, providing very good mixing and consistent resulting foam properties without any large voids or pouring patterns.

The other main area of process development that arose was in the safe and effective drying of the samples and removal of any remaining solvent. As increasingly large amounts of solvent had to be added in order to keep the precursors liquid, as previously discussed, the removal of this solvent became a new and pressing issue.

Figure 36: Ultra Turrax T25 homogeniser (IKA Werke) as used in foam production.

Given the samples contained adsorbent which was desired to be tested, vacuum oven drying was required as part of the process. However, simply directly transferring the sample from the beaker to the oven and applying heat and negative pressure until dry proved ineffective. This was because the excessive solvent load lead to long drying times, poor removal efficiency and a tendency for the solvent to cause thermal damage to the equipment or cause the sample to thermally degrade at lower than expected temperatures.

As a result of these initial efforts, the samples initially underwent liquid-liquid solvent extraction before being subjected to drying via a thermal technique. The sample was first immersed into a bath of either water or a solvent-water mixture overnight. This was followed by two more baths in pure water, to remove as much solvent as possible by extraction into the surrounding liquid. The use of a solvent-water mix for the initial removal was investigated as part of surface modification, discussed later (section 3.2.1). Following this, samples were patted dry with tissue paper and then underwent vacuum oven drying until they reached constant weight. This technique, whilst slower, resulted in samples more reliably surviving the drying process as well as avoided damage to the equipment by only having to remove water, rather than solvent. If samples were particularly wet after extraction, an intermediate stage of drying using only vacuum was employed to minimise demand for the vacuum oven.

Given the issues with exposure to high temperatures, samples were dried using moderate temperatures and used vacuum to ensure effective drying, with temperatures of 80^{o}C found acceptable for simple drying of the samples.

3.1.3.1 Finalised production procedure

Following the development into the production process in this section, the final production procedure was as shown in Table 19, using the two part process as previously described in Figure 33:

Table 19: Step by step production procedure for making 13X-polymer foams.

Procedure step	**Action**
1	Pre-fill a beaker with the chosen extraction bath composition (water or a water/solvent mix)
2	Weigh the polyethylene glycol directly into the mould
3	Using a pipette, add water, dibutyltin dilaurate and triethanolamine to the mixture in the mould
4	Weigh the 13X powder into the mould
5	Add NMP as measured by measuring cylinder to the 13X powder
6	Homogenise the mixture using the homogeniser at 6,500 RPM for 60 seconds
7	Allow the mixture to cool to ambient temperature
8	Homogenise the mixture again at 6,500 RPM for 30 seconds
9	Weigh the polyisocyanate into the mixture inside the mould
10	Homogenise the mixture at 6,500 RPM for 5 seconds
11	Allow the solution to rise and set for 3 minutes or until the surface has set firm to the touch
12	Gently remove the sample from the mould using a spatula
13	Immerse the sample in the extraction bath and leave overnight
14	Remove the sample from the extraction bath and immerse in a water bath for 1 hour
15	Pat the sample dry gently with paper towel
16	Dry the sample in a vacuum oven at 80^{o}C until it reaches constant weight

3.2 Post-processing development and techniques

During examination of the produced foam materials via scanning electron microscopy (SEM) (The technique employed being discussed in detail later in section 4.2.1.1), it became apparent that the bubble surface between the void space of the foam and the polymer-adsorbent matrix has a solid polymeric skin obstructing gas flow between the void space and the adsorbent surface, as can be seen in Figure 37.

However due to the nature of foams being a material formed by the agglomeration of bubbles, it is impossible to remove this skin by controlling bubble formation during the foam production process. As a result, techniques have been investigated and developed in this work to mitigate or remove entirely the polymeric skin in post-production processing, which are discussed in this section.

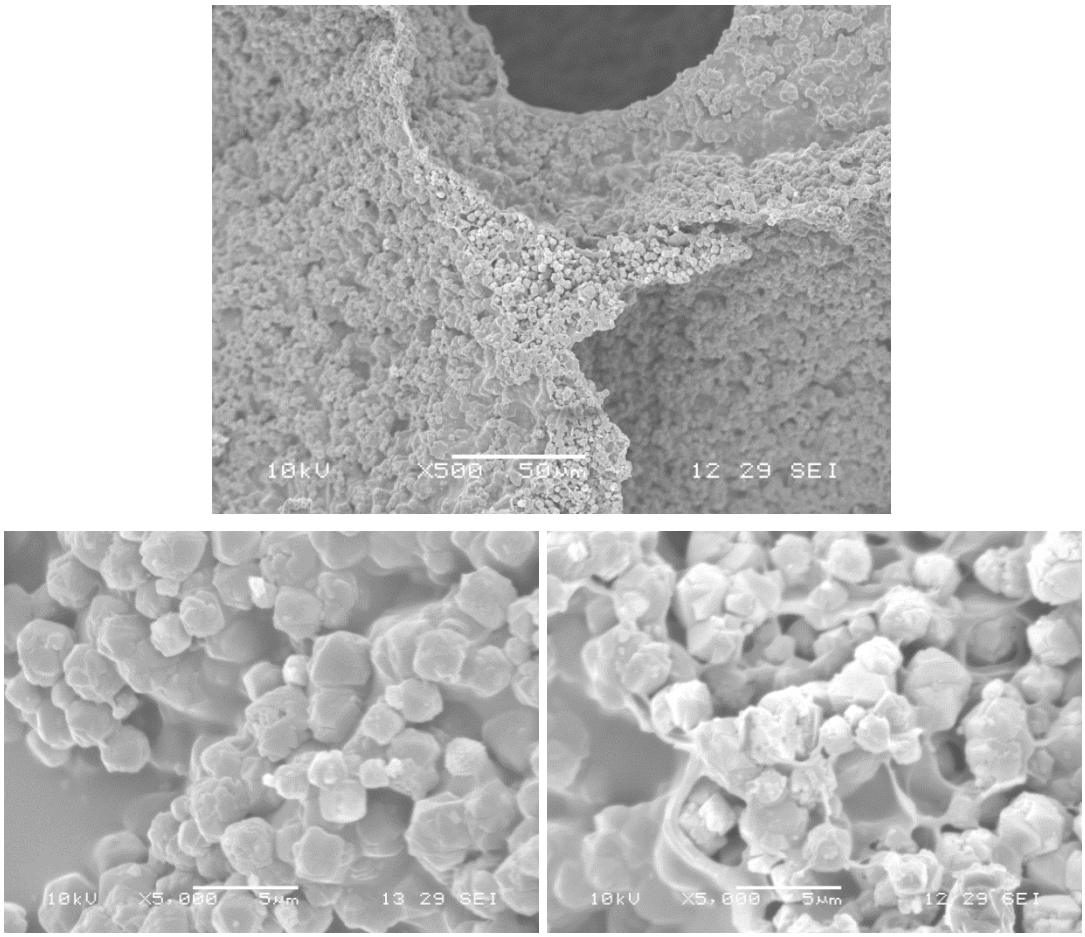

Figure 37: SEM Images of sample 82 before surface modification treatment. Top shows the overall foam structure. Bottom left shows the bubble skin obscuring the zeolite crystals in the structure, whilst bottom right shows the contrast between this and the internal structure.

3.2.1 Solvent removal

The process of producing polymeric foams containing adsorbent powder includes the addition of a significant fraction of solvent in order to ensure the monomer solution remains sufficiently liquid for bubbles to form and to foam properly, as discussed in section 3.1.2.3. This solvent is retained within the resulting polymer matrix and must be removed before the material can be activated to have adsorbent properties.

The speed at which the solvent is removed from a solid-solvent mixture, as well as the technique used, can have significant effects upon the resulting solid produced. This is well known in the field of membrane production where polymeric membranes are produced via a phase inversion process. In phase inversion processes the polymer is suspended in a solvent, which is removed into a non-solvent via absorption thus causing the polymer phase to solidify. This is similar to the solvent removal technique used in this work as discussed previously.

In the case of separation via contact with a non-solvent liquid, this formation process is known as non-solvent induced phase separation. Guillen *et al.* (2011) in their review of the topic discussed the effects of the speed of solvent removal on the resulting morphology of polymeric membranes as shown in Figure 38.

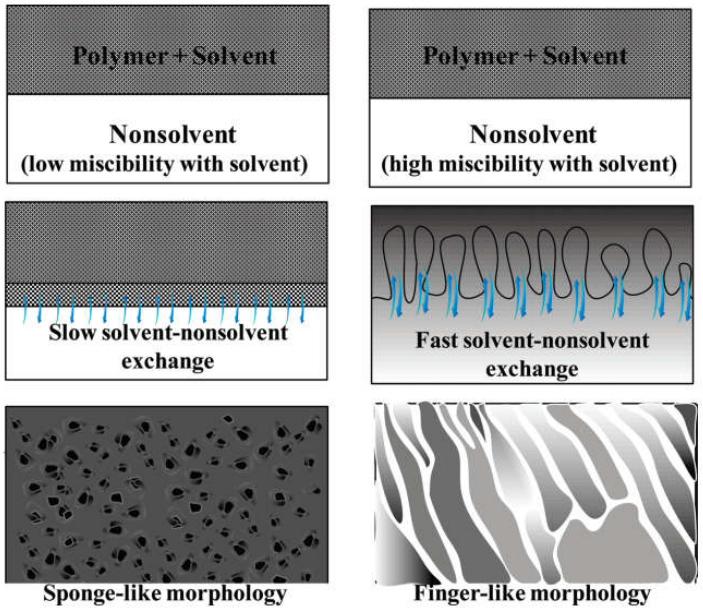

Figure 38: The effects of varying solvent removal speed on resulting membrane morphology (Reprinted with permission from (Guillen *et al.* 2011), ©2011 American Chemical Society).

Initial production techniques of adsorbent containing foams used a pure water bath in order to extract the retained solvent so that they could be safely activated. This was considered likely to promote quick solidification in the surface, followed by inhibition of extraction from areas deeper inside the foam matrix. As a result extraction with a 50:50 mixture of solvent:water was attempted to slow the solvent exchange by reducing the further solubility of the solvent within the surrounding water, as well as a second 40:60 mixture of solvent:water (Figure 39). These were then compared with a sample of similar loading of 13X with solvent extraction into pure water (Figure 40).

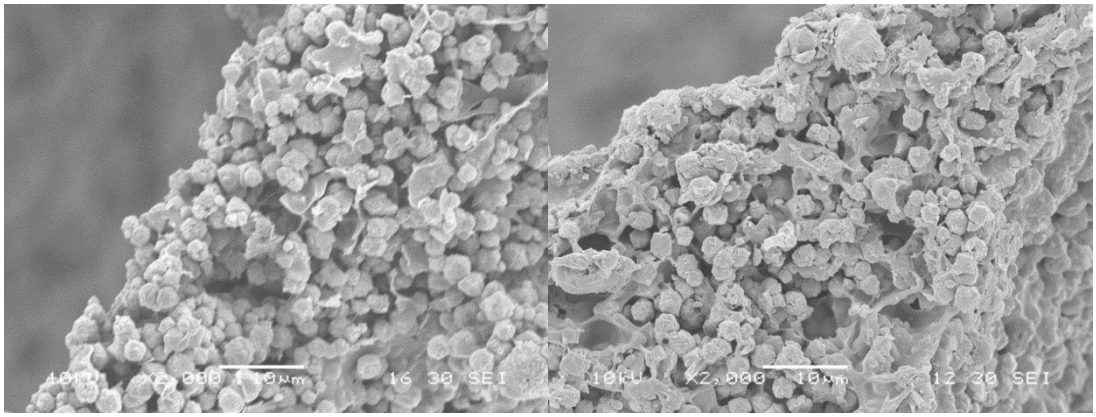

Figure 39: SEM images of sample 77 (Left) and 65 (Right) showing the bubble skin after extraction in 50:50 and 40:60 water:NMP mixtures.

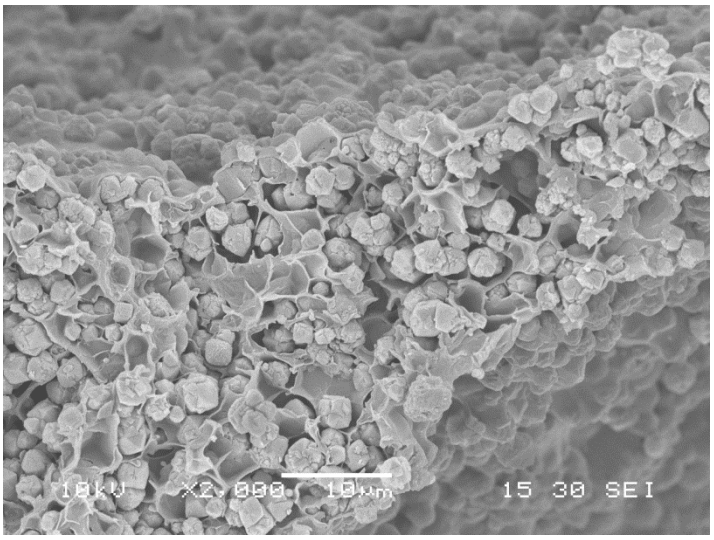

Figure 40: SEM image of sample 72 showing the bubble skin after water extraction.

Physically there is little noticeable difference between the foams produced in any of the three extraction mixtures, although all of them successfully removed the solvent within the polymer and allowed for the production of useful samples. Any difference in their properties, and thus merit as a support, will thus be shown in their relative adsorbent activity which is discussed later in Chapter 5.

Further investigation into using this technique to alter the bubble surface properties may have merit for further work, particularly in tuning the composition of the solutions used for initial solvent extraction to promote desired surface properties. However, due to time constraints, this was not pursued during the research beyond the three extraction mixtures investigated.

3.2.2 Surface dissolution

Removing the bubble surface by dissolving and washing away the polymer in a solvent was also investigated to see if it was suitable for use as a technique for improving access to the adsorbent within the structure. Sodium hydroxide was chosen as a solvent in order to dissolve the bubble surface due to its reporting in the literature as a suitable compound for the roughening and etching of both polyimide and polyurethane surfaces prior to the use of adhesives (Ebnesajjad 2011).

A sample (sample 32) of polyimide-13X foam underwent etching in a solution of sodium hydroxide to allow for dissolution of the surface in a controlled manner. Samples were immersed into the solution for two hours and four hours respectively and then examined using scanning electron microscopy in order to investigate the effect that the treatment had on the bubble surface.

Whilst some surface cracking from the treatment can be seen (Figure 41), particularly after longer duration exposure as seen in Figure 42, the material removed from some portions of the material has simply been redeposited elsewhere on the structure. This can be seen by comparing the internal strut appearance of Figure 43 after treatment to a similar structure without treatment in Figure 44. Compared to the rough surface that should be present from a fractured strut, the material is smooth and similar to the polymer skin of the bubbles. Therefore it could be concluded that the etching technique was not removing material as desired, but merely moving it to other parts of the foam. As a result, the solvent etching technique could be concluded to be ineffective.

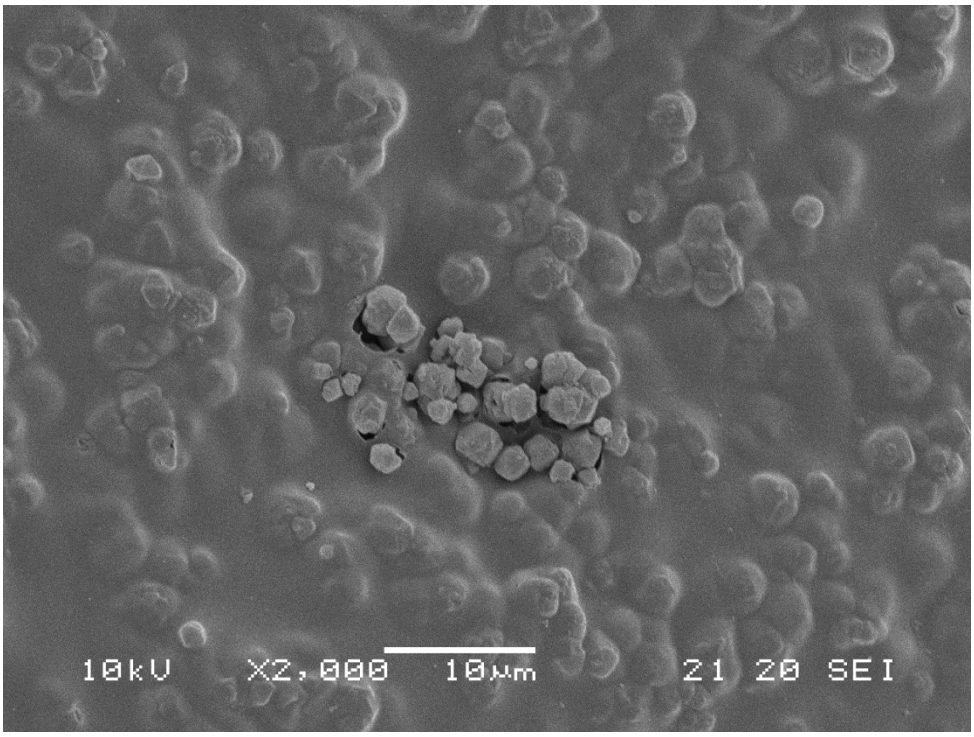

Figure 41: PU-13X foam surface after 2 hours in sodium hydroxide etching solution.

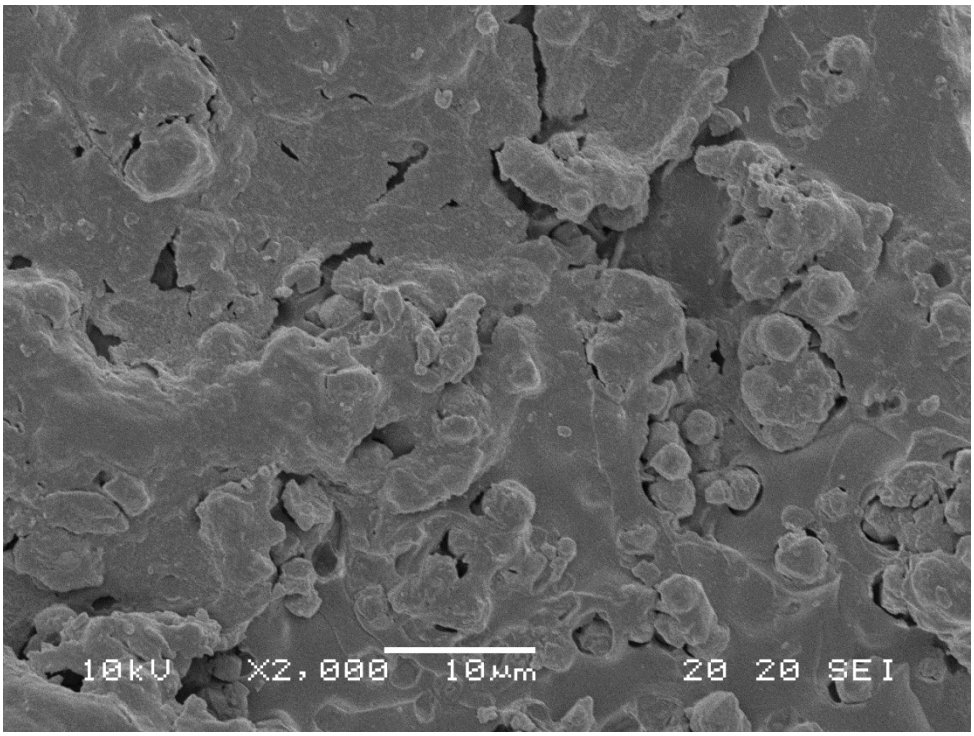

Figure 42: PU-13X foam surface after 4 hours in sodium hydroxide etching solution.

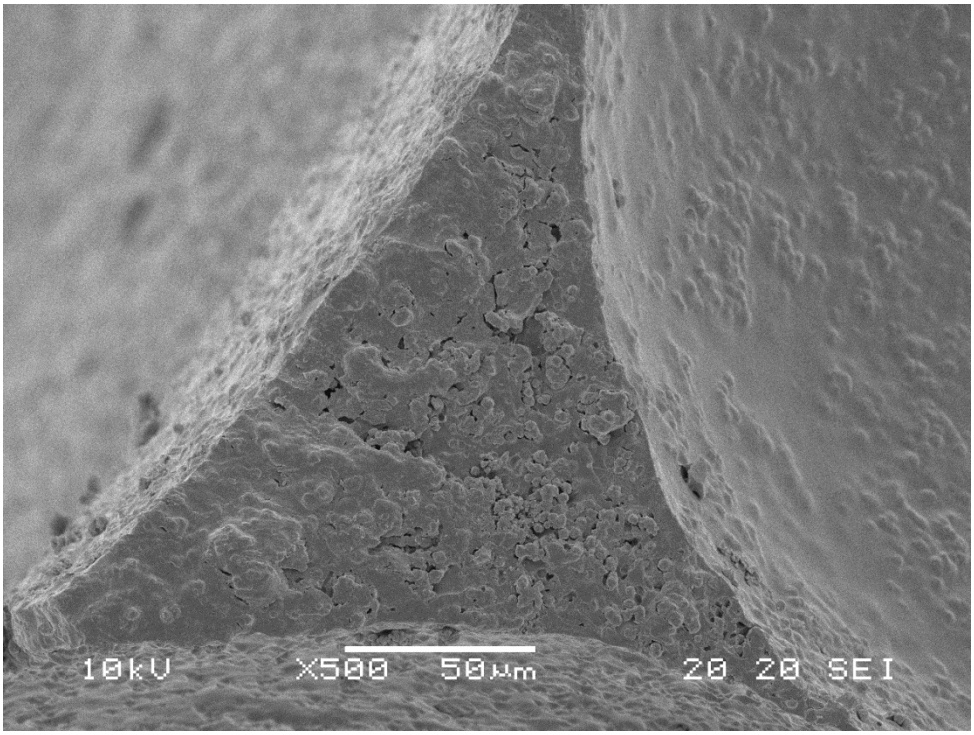

Figure 43: PU-13X foam strut after 4 hours in sodium hydroxide etching solution.

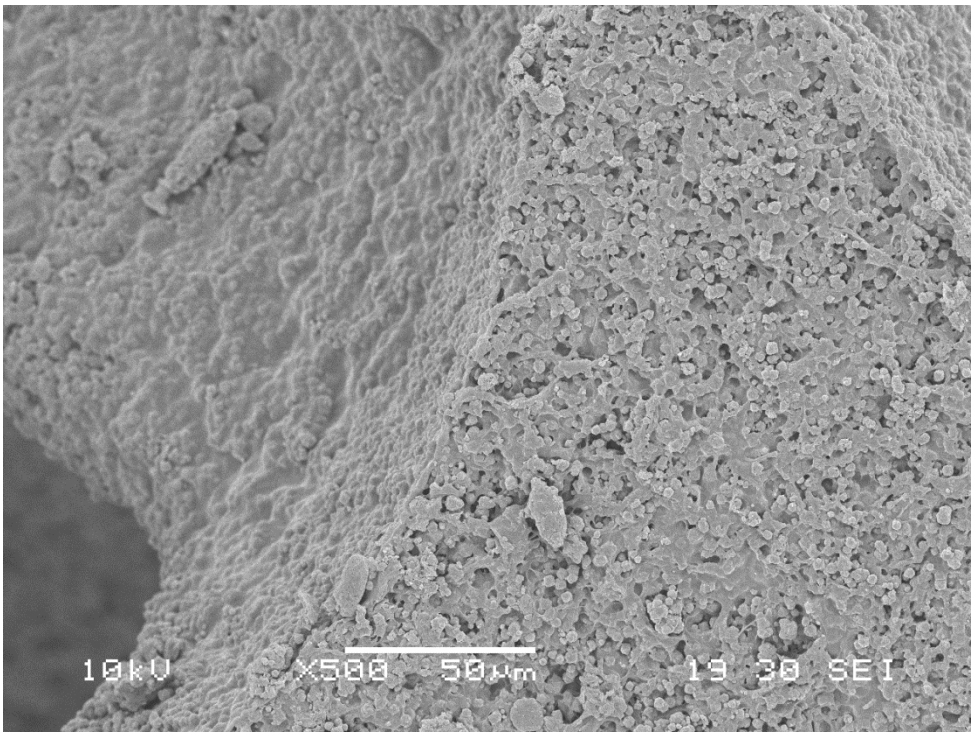

Figure 44: A PU-13X strut that has not undergone sodium hydroxide etching.

3.2.3 Heat treatment

The removal of the bubble surface by oxidation was investigated as a method of exposing the internal adsorbent in foam samples to airflow. This technique was of particular interest as the first parts of the material to undergo combustion would necessarily be those parts impeding gas flow to the inside of the material. This is due to the need for oxygen from the ambient environment in the combustion process of the polymer.

Initial experiments used a closed Memmert SM100 oven exposing a dry PU-13X sample to temperatures of 200^{o}C, chosen for being close to but below the typical combustion temperature of polyurethane to promote degradation. This temperature was found via thermal gravimetric analysis (TGA) of the samples as discussed later in section 5.2.1. These experiments showed limited degradation, with samples tending towards a dark caramel colour (Figure 45).

Figure 45: A section of sample 67 having undergone preliminary heat treatment.

This heat treatment technique was further attempted on a whole cylindrical sample, sample 86, for further testing and showed similar results as can be seen in Figure 46.

Figure 46: Sample 86 having undergone stagnant air heat treatment.

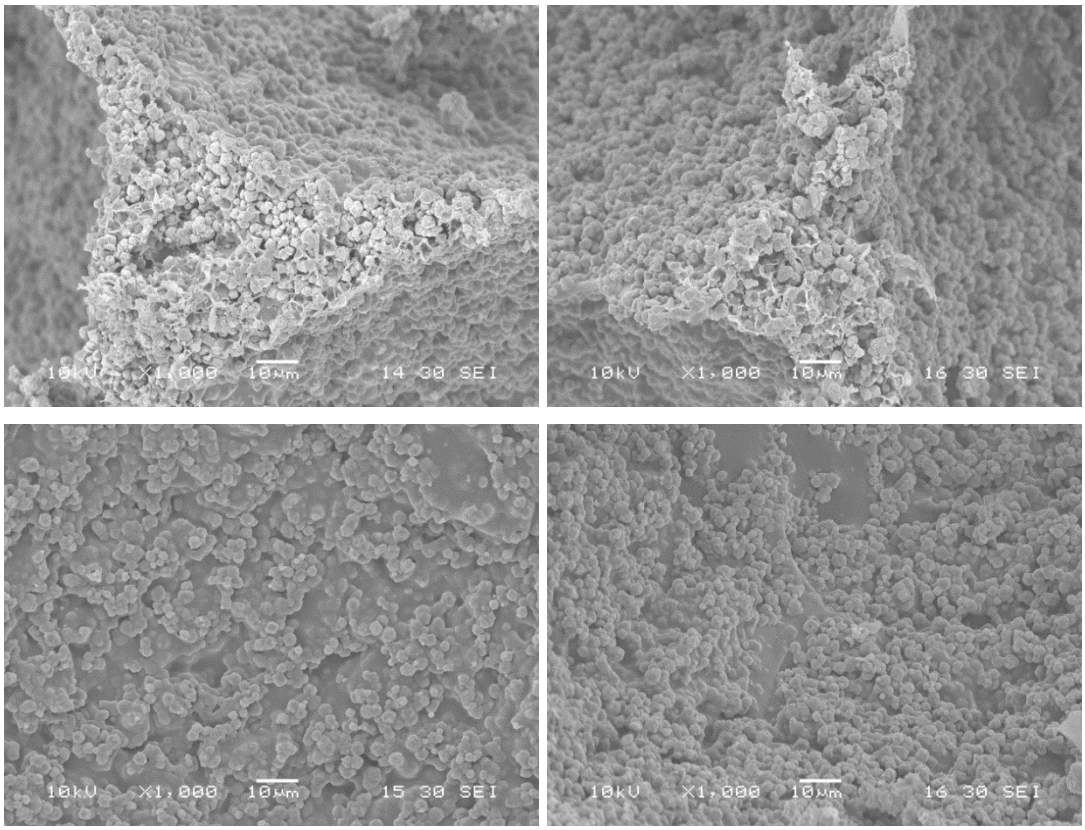

Figure 47: SEM images of sample 86 before (top and bottom left) and after (top and bottom right) stagnant air heat treatment.

The resulting samples were investigated using SEM and as can be seen in Figure 47, there are some signs of the surface being slightly removed. This was supported by further testing into the properties of the resulting material, discussed much later in section 6.2 following studies on dynamic adsorption breakthrough which are discussed in Chapter 5. However this improvement was minor.

Further development of the technique focussed upon ways of increasing the extent of the degradation to expose more of the adsorbent within the material to airflow. As a result, the technique changed to holding the sample at a raised temperature within flowing air. This was done in order to allow for an ample supply of oxygen to contact the polyurethane and allow for further oxidation of the polymer. This was successful, resulting in much darker samples as seen in Figure 48 compared to previous efforts and the starting material.

Figure 48: Samples of sample 74 before (right) and after (left, centre) heat treatment.

Following this success, the flowing air technique was used on three testing size cylindrical samples, samples 82, 83 and 84, which all showed signs of significant degradation (Figure 49 and Figure 50).

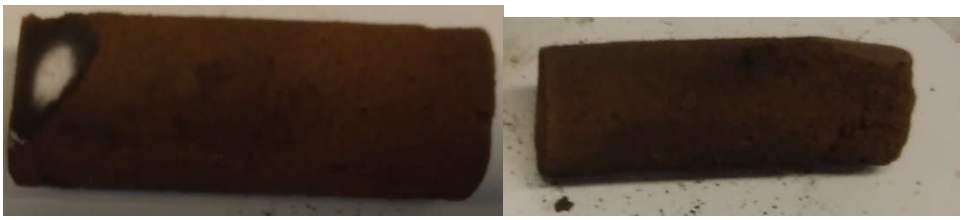

Figure 49: Sample 82 (Left) and sample 83 (Right) after heat treatment.

Figure 50: Sample 84 after heat treatment.

One difficulty encountered in the improved heat treatment process was the fact that if exposed to heat for too long, the samples would degrade to a sufficient degree that the entire structure would disintegrate. This is particularly clear in Figure 50 where the white colour observed is almost identical to the precursor 13X powder, which suggests almost the entire polymer matrix has been removed. Whilst this has the potential for very high adsorption performance, the resulting foam was extremely fragile and eventually disintegrated during handling and testing.

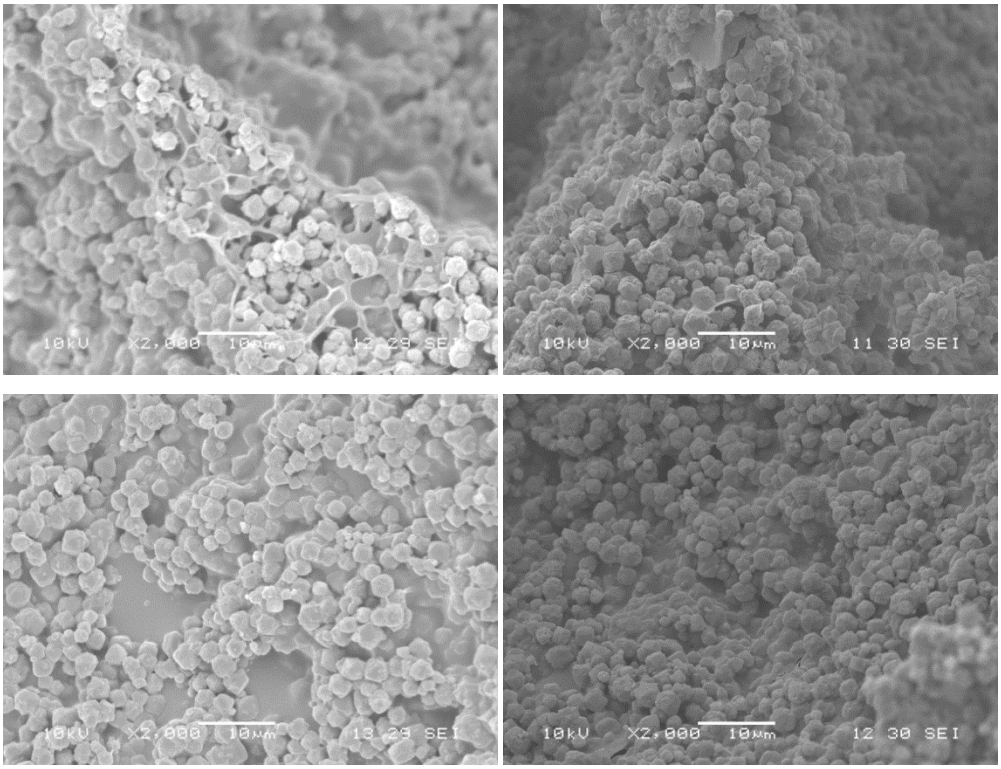

Figure 51: SEM Images of the bubble surface of sample 82 before (top and bottom left) and after (top and bottom right) heat treatment.

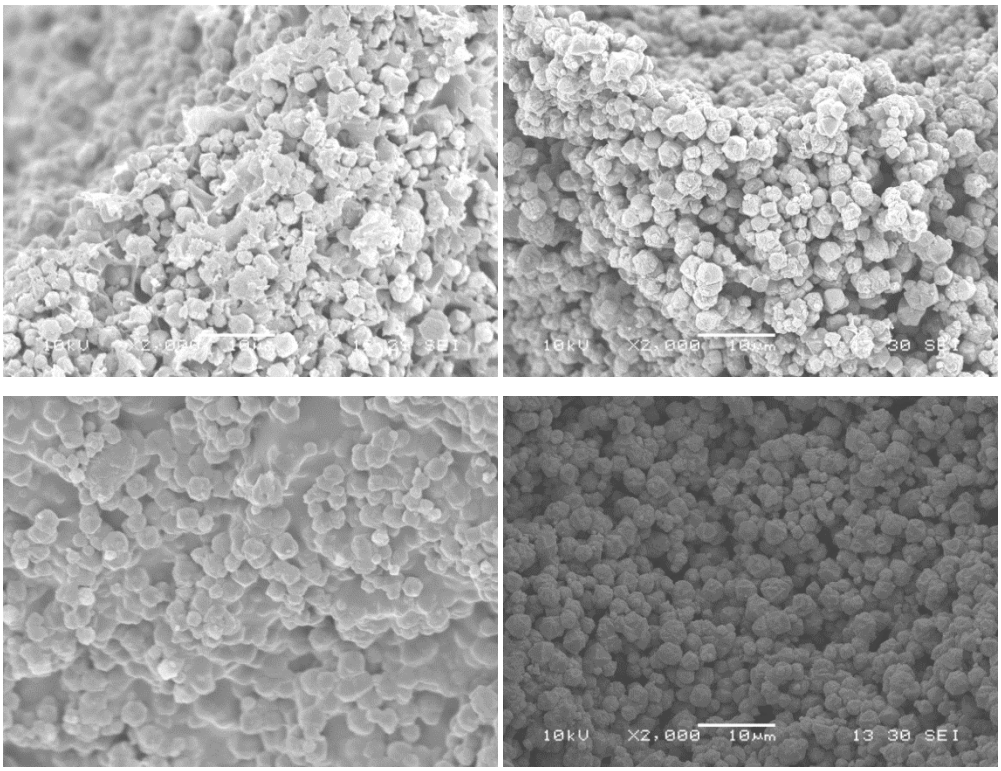

Figure 52: SEM images of the bubble surface of sample 83 before (top and bottom left) and after (top and bottom right) heat treatment.

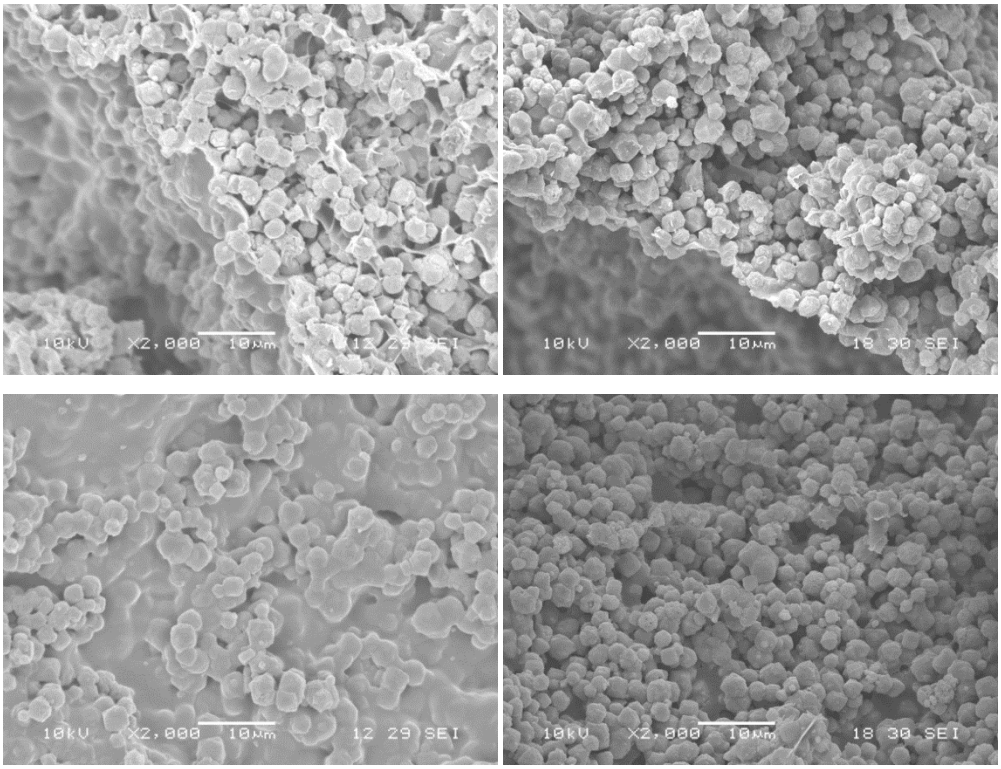

Figure 53: SEM images of the bubble surface of sample 84 before (top and bottom left) and after (top and bottom right) heat treatment.

As can be seen in Figure 51, Figure 52 and Figure 53, the thermal treatment has a clear and noticeable effect of thinning the polymer skin present and making the shape and presence of the 13X crystals more noticeable. This suggests the potential for beneficial effects on adsorption performance. This is investigated later in the work, and the effects of this removal process on adsorbent activity are discussed in section 5.2.3.4.

As a result of the difficulty in maintaining a resilient material, the need for a controllable heat treatment process where the removal of the polymer could be halted at a desired phase became obvious. Samples where the removal was halted earlier were significantly more resilient, as was observed in sample 82 (Figure 49), where the external polymer was a lighter brown compared to dark black and provided a protective outer coating to handle the sample with. However significant investigation into this process for either PU or PI foams did not occur due to time constraints and as such has significant interest for further work. Given the lack of TGA data to drive the development of heat treatment for PI-13X foams, heat treatment of these foams was not pursued in this work.

3.3 Conclusions

Following significant development work, an initial chemistry for a pure PI polymeric foam found in literature has been modified and adapted to support the inclusion of significant fractions of adsorbent powder within the structure. 13X was chosen as the adsorbent most suitable for inclusion for materials worthy of investigation and a generic formulation (Table 17) was devised for the production of either PI or PU-13X foam composites of any size and desired adsorbent loading. A wide variety of foams were made using these techniques for further investigation in this thesis, which are described below in Table 20

A practical upper limit of adsorbent content within a foam was discovered, lying somewhere between 75% and 80% by weight based upon mass balance over the generic formulation for PU-13X foams, which allowed for the selection of a series of formulations for further investigation in Chapter 4.

Moulding and processing techniques were similarly developed to allow for the production of usefully sized and shaped materials for further testing and examination. This allowed for the consistent production of cylindrical shaped foams for pressure drop testing and adsorption breakthrough investigation.

Finally post-production processing techniques were developed and investigated to allow for both the removal of undesirable components from the materials and improve their adsorbent properties, of which the thermal removal of excessive polymer blocking gas flow into the foam-adsorbent matrix was found to be most effective.

Following these efforts, foam samples could then be produced and processed reliably, to allow for more detailed investigation into the suitability of the structure as an adsorbent support. Polyurethane foams were selected for further testing due to the ability to synthesise PU-13X foams with high adsorbent mass fractions and their ease of heat treatment to improve their adsorbent properties, whilst PI-13X foams were not tested further. It is the development of the investigative techniques to do so and the results acquired which are the topics of the following chapters.

3.3.1 Samples and compositions relevant to this thesis

Table 20: Sample numbers, 13X mass fractions and formulation notes for foam samples relevant to this thesis

Sample number	13X Mass fraction by formulation	Polymer	Additional information
0	0 wt%	PI	Pure polyimide
1	20 wt%	PI	-
2	0 wt%	PI	Pure polyimide
13	30 wt%	PI	-
14	38 wt%	PI	-
16	44 wt%	PI	Collapsed
17	50 wt%	PI	Silicone oil added
19	67 wt%	PI	-
27	67 wt%	PI	NMP solvent introduced
32	67 wt%	PI	-
33	67 wt%	PU	Silicone oil included
36	67 wt%	PU	Silicone oil removed from formulation
45	67 wt%	PU	-
48	67 wt%	PU	-
49	75 wt%	PU	-
54	80 wt%	PU	Failed to foam
59	75 wt%	PU	50:50 NMP:Water solvent extraction stage introduced
62	60 wt%	PU	-
63	70 wt%	PU	-
65	75 wt%	PU	-
67	50 wt%	PU	-
68	60 wt%	PU	-
70	70 wt%	PU	Pre-drying of 13X powder introduced to improve weighing
72	75 wt%	PU	Silicone oil added
73	67 wt%	PU	Reaction performed in ice bath

74/A	72 wt%	PU	-
77/A	75 wt%	PU	Tin catalyst omitted
78/A	75 wt%	PU	-
80	0 wt%	PU	Pure polyurethane
82/A	75 w%	PU	Repeatability study
83/A	75 wt%	PU	Repeatability study
84/A	75 wt%	PU	Repeatability study
85	60 wt%	PU	-
86/A	67 wt%	PU	-
87/A	70 wt%	PU	-
88/A	75 wt%	PU	Silicone oil added

Notes: The letter A after a sample denotes a sample which has undergone subsequent heat treatment.

4 Physical characterisation of adsorbent foam materials

4.1 Introduction

In Chapter 2, literature models by Ergun (1952); Lacroix *et al.* (2007); Dietrich *et al.* (2009); Inayat *et al.* (2011) for pressure drop through foam materials were introduced with significant disagreement as to what model was most effective for foams, as well as what the characteristic dimension of a foam was and what other physical characteristics govern pressure drop through a foam structure.

In this Chapter, these models are applied to the foams produced during the research in order to investigate the performance of the materials and guide a deeper understanding of the foams produced. In order to achieve this goal, experimental effort is required to acquire data for modelling purposes. A pressure drop experiment apparatus was designed and used to acquire pressure drop data over a range of flowrates for various produced foams, both with and without heat treatment, as well as comparison data for commercial adsorbent beads.

Photographic techniques using SEM imaging are developed and implemented in the Chapter to allow for the determination of both bubble and window diameters for the foam materials, and helium pycnometry is used to determine their voidage, all of which are required physical characteristics of the foams in order to apply the literature models described in Chapter 2.

Using the acquired physical data the models published by Ergun, Inayat, Lacroix and Dietrich are applied to foams produced during this research in order to evaluate their suitability in describing pressure drop. Adaptations to improve their accuracy when applied to PU-13X foam composites are also considered in order to find a model which identifies the critical physical properties governing pressure drop through the foams, and allow for improvement of the materials in further work.

4.2 Measuring foam structure characteristics

As discussed in section 2.6, the pressure drop behaviour of foams is a function of their morphology (Figure 54), particularly the bubble size of the foams and the true void fraction, with the Dietrich model also referring to window size. Bubble size in the context of foams describes the size of the gas bubbles which form the empty space in the foam structure, and given the nature of foams as an agglomeration of bubbles is typically described as an average diameter. Window size describes the size of the gaps between bubbles where two bubbles have connected to form an open cell foam structure and again is typically described as an average.

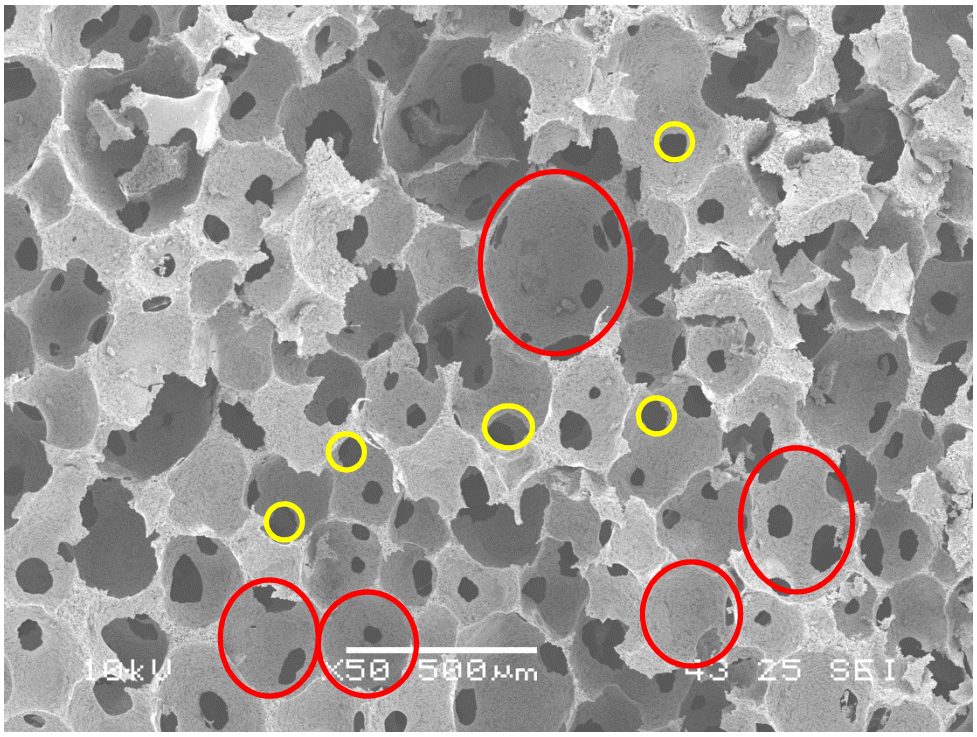

Figure 54: 50x magnification SEM image of a sample from sample 74A highlighting selected bubble diameters (red) and window diameters (yellow).

As a result of the need for data on the physical foam characteristics, techniques for measuring these properties in the foams produced had to be developed. These techniques are discussed in this section.

4.2.1 Development of bubble size measurement technique

The measurement of bubble size in solid foams is an area of some difficulty. Relatively few techniques allow for the direct 3 dimensional measurement of the bubbles. These techniques typically involve magnetic resonance imaging (MRI) of samples, and are expensive, slow (taking in the order of hours to measure a single sample), and require access to significant computing power in order to interpret the results (Große *et al.* 2008).

It is far more common in the literature to estimate bubble size via a 2 dimensional photographic technique with images acquired via scanning electron microscopy (SEM) (Lee *et al.* 2001; Abdel Hakim *et al.* 2011; Liu *et al.* 2011). This technique was chosen for this work as it provided images with a known scale which could be used to calibrate the analysis, and also provided high resolution images at a magnification significant enough such that the bubble edges could be seen in detail. A typical image as acquired for analysis can be seen in Figure 55 with example bubbles which make up the structure marked in red, whilst 13X crystals are too small to be found at the magnification used for this technique. SEM also allows for the acquisition of raw data for several produced samples in one session as image acquisition is relatively speedy at 80s per image, and several samples can be put into the equipment at once.

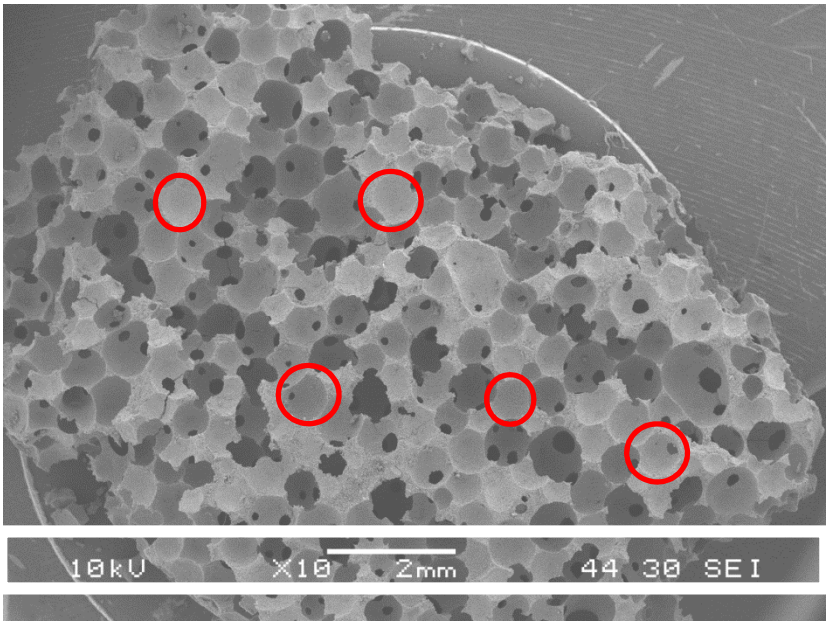

Figure 55: A high resolution image of a cross section of a sample from sample 72, showing several bubble cross sections and image scale (highlighted in white).

4.2.1.1 SEM Imaging technique

First it is necessary to acquire an image of a cross section of the foam material to analyse. This image must be as high a resolution as reasonably practical, and within it contain as many bubble cross sections as possible in order to allow for investigation into the size distribution of the bubbles, as not all bubbles will be the same size.

Samples were cut from dried foams, as produced by the experimental technique previously discussed in Chapter 3, into cubes with edges approximately 1cm long. Samples were taken from the inside of the cylindrical foam morphology to avoid any edge effects in the sample being analysed. Samples were mounted onto stainless steel stubs using double sided carbon tape and degassed under vacuum for a minimum of 24 hours in a Bio-Rad film desiccator, before undergoing sputter coating with gold under argon for 5 minutes in an Edwards S150B sputter coater to provide sample conductivity. SEM images were captured using a Jeol 6480 LV scanning electron microscope with an accelerating voltage of 10kV and a beam spot size of 30 at a working distance as close to the sample as reasonably practical, typically 14mm.

Images were acquired in versions both with and without the white scaling bar imposed upon the bottom of the image by the SEM software (Highlighted in white on Figure 55). Once acquired, the scaled image would be opened in ImageJ, the chosen image analysis software, and the scaling used to calibrate the size of one pixel for analysis. Once done, the non-scaled image was opened using ImageJ to perform the analysis.

4.2.2 Bubble size measurement technique

The first step to measuring the bubble size is to crop the image to only the bubbles being investigated, to prevent interference in image processing or transformations from the image background. Once performed, this results in an image as seen in Figure 56. The image is then put through ImageJ's built in normalisation filter. The normalisation filter alters the value of each pixel so that as an overall image they are distributed over the entire black to white scale. This makes further processing to distinguish between bubble edges and bubble interiors easier, and results in an image as seen in Figure 57.

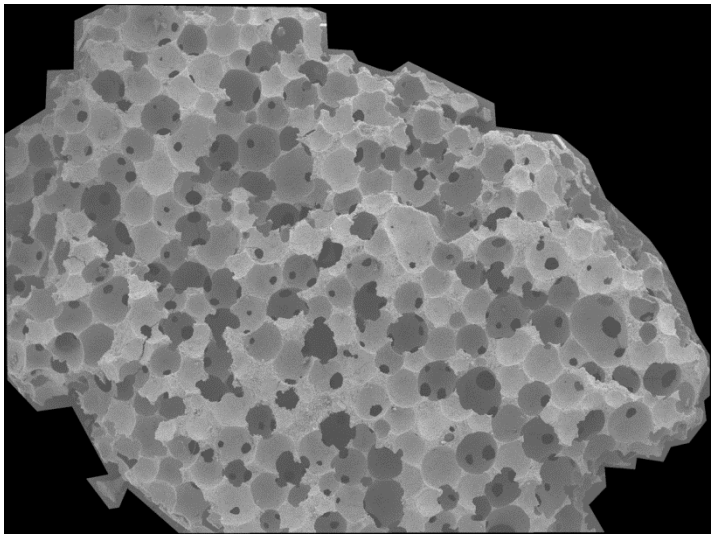

Figure 56: A high resolution image of a cross section of a sample from sample 72, cropped to the area of interest for analysis.

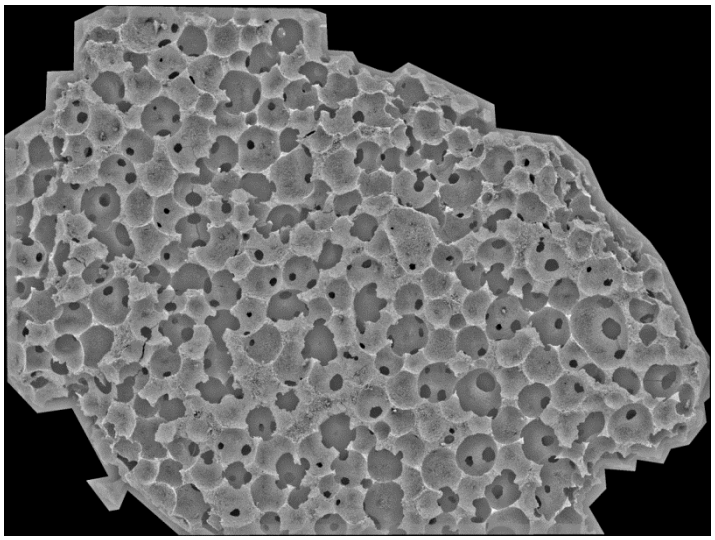

Figure 57: A high resolution image of a cross section of a sample from sample 72, after image normalisation.

The next step is to enhance the contrast of the image. This serves to increase the distinction between the borders of the bubbles, which are closer to the camera, and the insides of the bubbles which are further away. This is done by applying a threshold value to the image where pixels below the chosen value are set to black and those above it are set to white and is picked on an image by image basis such that the bubble outlines are clearly shown as in Figure 58. The threshold value typically used is in the region of 216 on a 0-255 scale. ImageJ's despeckling filter is also run to remove random dots produced by this

process due to the rough nature of the foam surface caused by 13X crystals. This filter replaces each pixel with the median value of the 3x3 pixel grid surrounding the pixel.

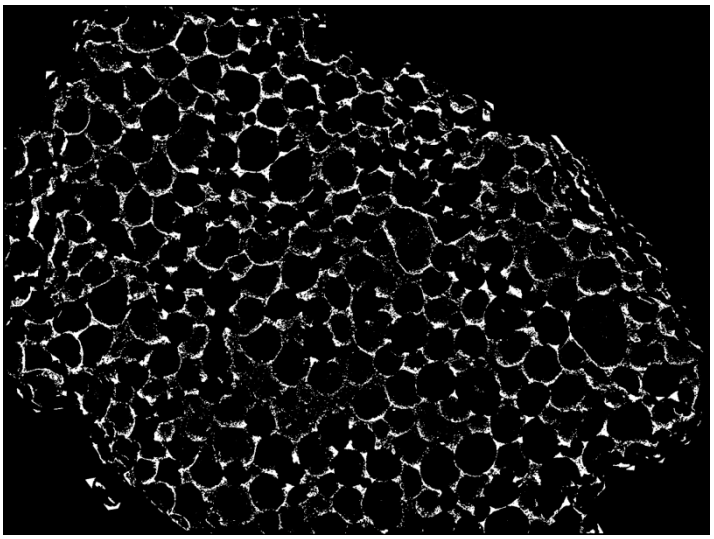

Figure 58: A cross section of a sample from sample 72, after contrast adjustment showing the distinctive bubble edges only.

After this, an algorithm is used to detect the presence of circles and measure their average diameter which is known as the circle Hough Transform as implemented into an ImageJ plugin. This uses the Hough Transform on the image data in order to detect the edges of the circles within the image, and consequently attempt to fit circles of arbitrary size to the shape of the edges depending upon if a certain circularity threshold is met. Size thresholds for the circles are set on this process in order to prevent the acquisition of false positive data. The number and diameter of the resulting bubbles are then collated by the plugin.

In this work, the circularity threshold was set at 0.75, with allowable radii between 0.1 and 1 mm as a range which covered the circle features found in the images and avoided excessive computational time requirements. The resulting bubble diameters were averaged in order to give an average bubble size diameter for the foam sample in question.

4.2.3 Window size measurement technique

Window sizes for the foams were determined via a similar technique to bubble sizes, but instead of focussing on processing the image to highlight the bubble edges, the processing was focussed on highlighting the windows which allow for airflow between the bubbles.

A higher resolution image is used than for bubble processing, as can be seen below in Figure 59, shown without scaling bars to prevent them from interfering with the analysis. After applying a scale to the image using a scaled version beforehand, the image has a threshold applied to it, a value above which each pixel is set to black and below which each pixel is set to white, in order to reduce the image down to just the windows between bubbles. These are picked up in the thresholding due to their higher darkness than the surrounding foam due to being further away from the camera.

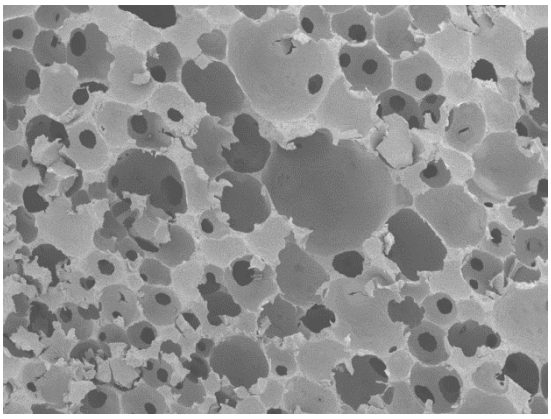

Figure 59: A 20x magnification SEM image of a sample from sample 83.

Thresholding results in the image seen in Figure 60, leaving the windows as partly circular black shapes on a white background. These can be thus analysed as particles using ImageJ's inbuilt Analyse Particles function. Higher resolution images are used to allow for a minimum particle size to be set to allow for the elimination of dots and background noise for the analysis, resulting in a list of particle areas acquired as a result within the chosen range of circularity and particle areas. For the purposes of results, a circularity threshold of 0.5 is used and no upper limit of particle size. Window diameters are then calculated by assuming a perfect circle and applying the equation for the area of a circle, $A = \pi r^2$.

Figure 60: A 20x magnification SEM image of a sample from sample 83 after applying thresholding.

4.2.3.1 Measured bubble and window sizes

Table 21: Bubble diameters and window diameters for various samples as measured via the Hough's detect circles method and analyse particle functions.

Sample number	Average bubble diameter (mm)	Standard deviation for bubble diameter (mm)	Average window diameter (mm)	Standard deviation for window diameter (mm)
65	0.748	± 0.164	0.312	± 0.0983
66	0.449	± 0.118	0.119	± 0.0466
67	0.384	± 0.0328	0.114	± 0.0358
68	0.300	± 0.0707	0.0585	± 0.0242
71	0.622	± 0.142	0.207	± 0.0268
72	0.433	± 0.107	0.121	± 0.0749
77	0.518	± 0.150	0.145	± 0.0405
78	0.685	± 0.181	0.124	± 0.0326
82	0.303	± 0.0596	0.101	± 0.0281
82A	0.274	± 0.102	0.0734	± 0.0193
83	0.405	± 0.127	0.143	± 0.0391
83A	0.188	± 0.0593	0.114	± 0.0433
84	0.349	± 0.0966	0.112	± 0.0298
84A	0.261	± 0.0802	0.0942	± 0.0364
85	0.257	± 0.0729	0.133	± 0.0426
86	0.403	± 0.154	0.125	± 0.0406
86A	0.257	± 0.0764	0.101	± 0.0216
87	0.274	± 0.0927	0.106	± 0.0264
88	0.416	± 0.161	0.175	± 0.0760

Table 21 shows average bubble and window diameters for various samples which are calculated by averaging the detected values for each experiment over an entire image which contains several bubbles or windows to detect. Image analysis was run a single time for a given image to produce the results. Values are averaged for the purposes of modelling using these results as the literature models are written assuming a constant value for the

foam properties, instead of a range of values which are found in a more realistic polymer foam structure.

The error in the bubble and window size measurements can come from three sources. The first source is the uncertainty introduced due to the pixel size of the images from which the measurements are being taken. This is a function of the pixel size and the magnification used. For a 20x magnification image, the resolution of 0.005 mm per pixel gives a total error of $\pm$0.000451mm in the calculated values for bubble or window size for an error of 0.5%. This has been kept to a minimum by using as high an image resolution as possible. The second source of error is the image processing techniques used to extract the data from the images. These are a result of the filters used to enhance the contrast of the image and remove random noise from the image and may cause inaccuracy in where the bubble edges are compared to reality. This cannot be quantified but will be more significant for the bubble size measurements as more image processing steps are necessary to extract this data. Finally the use of a 2 dimensional technique to extract data on a 3 dimensional property introduces another inaccuracy for the bubble size diameters as the photographs are of 2 dimensional slices of bubbles, which vary in diameter depending on what height the bubble is sliced as seen in Figure 61. This also cannot be quantified but will result in bubble diameter data underestimating the true bubble diameters and having a larger range of values than may be true. This error is not present for the window diameter data, as this is a 2 dimensional value.

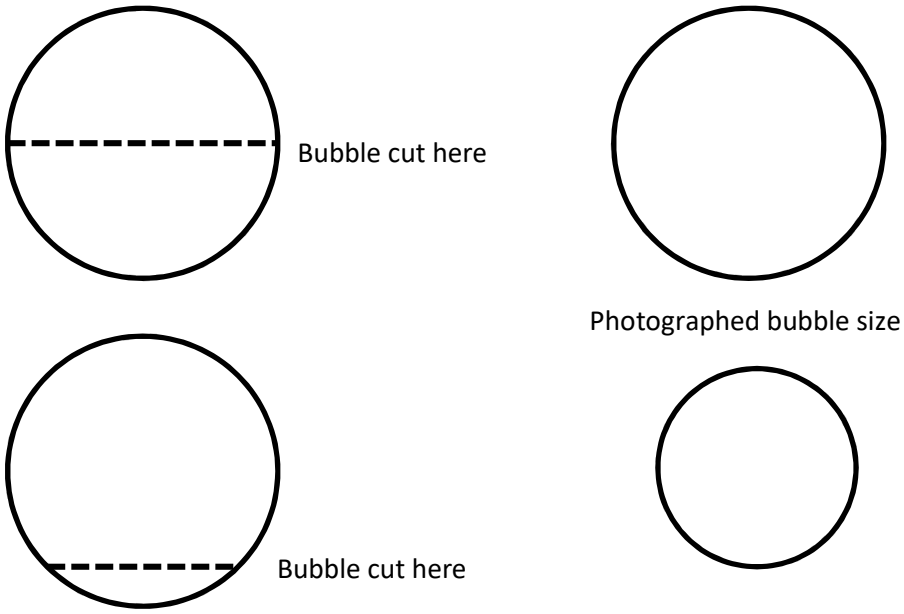

Figure 61: Diagram showing the error introduced in bubble size diameter via 2 dimensional sampling technique.

4.2.4 Determining void fraction

The voidage of the foams is a critical parameter in analysing and modelling their pressure drop via modified versions of the Ergun equation, as discussed in section 2.6. Fractional voidage is defined as the fraction of the volume of the foam bed which is not occupied by solid material and can thus be linked to the volume of bed occupied as follows (Chhabra *et al.* 2019).

$$\text{Fractional solid volume} = (1 - \varepsilon) \tag{23}$$

The total volume is determined easily by measuring a chosen sample via a micrometer and elementary geometry, and describes the combined volume of the sample's solid and void fractions. As a result, in order to find the void fraction it is necessary to measure the solid fraction, which is the solid volume of a given sample without any contribution from the external voids.

The technique chosen for measuring the solid volume was pycnometry. This technique describes the method of determining an unknown volume by the introduction of a known fluid to fill that volume which can be metered as it is introduced into the volume to allow for its measurement. For this work helium pycnometry was chosen over mercury

pycnometry for reasons of safety and ease of work. Helium pycnometry allowed for the faster testing of materials, and samples could be retained after testing rather than disposed of as hazardous waste.

Helium pycnometry uses the expansion of a gas into a chamber containing the sample, followed by expansion of the gas into a reference chamber of known volume in order to calculate the volume of the sample (Figure 62, Figure 63). The system is first purged with helium gas in order to fill the entire working volume with helium. The sample chamber is then pressurised up to a set pressure with helium and allowed to equilibrate. This chamber is then opened and exposed to the reference chamber, which causes a drop in pressure due to the additional volume which the helium gas can now occupy. The extent of this pressure drop can thus be used to calculate the volume of the sample relative to the volumes of the empty sample chamber and the reference chamber, as given in the working equation (24)

$$V_{sam} = V_C + \frac{V_r}{1 - \frac{P_1}{P_2}} \tag{24}$$

where V_c is the sample chamber volume (m^3) whilst empty, V_{sam} the sample volume (m^3), V_r the reference volume (m^3), P_1 the pre-expansion pressure (Pa) and P_2 the post expansion pressure (Pa).

Figure 62: Helium pycnometry apparatus as used in the research.

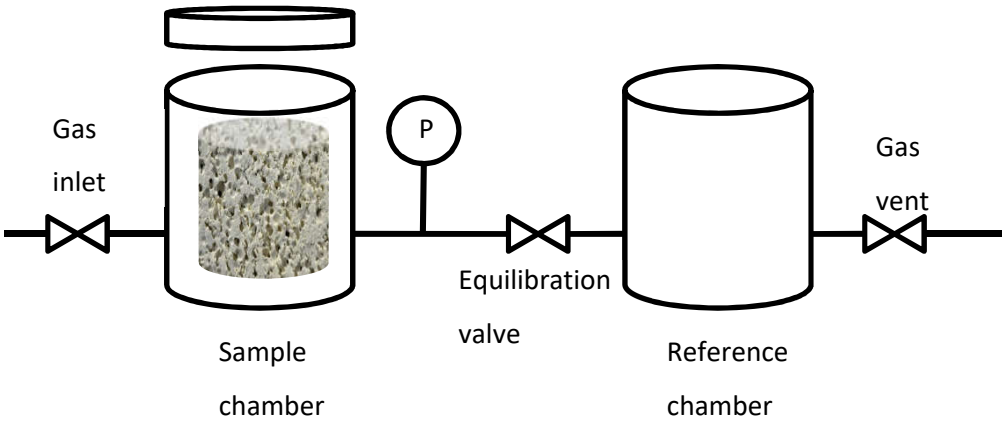

Figure 63: Schematic diagram of helium pycnometer.

Figure 64: A sample holder (left) and foam sample (right) as used for helium pycnometry (Sample from sample 87A).

4.2.4.1 Experimental technique for helium pycnometry

Samples were cut using a cylindrical punch from the foam desired to be tested, with samples made as long as possible, and the ends cut flat to create a regular cylinder. The height and diameter of the cylinder were measured via a micrometer and used to calculate its superficial volume. The skeletal volume was then measured using an AccuPyc 1330 helium pycnometer which had been calibrated beforehand using spheres of a known standard volume, with the volume of the samples being measured 10 times and the average volume of the tests used to calculate the resulting foam voidage.

As an example of how voidage is calculated consider a sample of sample 87A as seen in Figure 64. This cylindrical sample was measured using a micrometer to find its height of 27.92mm and its diameter of 17.2mm. The superficial volume of the sample can then be calculated as follows:

$$V_{cylinder} = \pi r^2 h = \pi \times \left(\frac{17.2}{2}\right)^2 \times 27.92 = 6487 mm^3 \quad (25)$$

The pycnometer measured a series of skeletal volumes for the sample in Figure 64 of which the average of 468mm^3 was taken, and used to calculate the voidage by comparing the fraction of the superficial volume of the cylinder which was empty space to the total volume as follows:

$$\varepsilon = \frac{V_{superficial} - V_{skeletal}}{V_{superficial}} = \frac{6487 - 468}{6487} = 0.928\ (-) \quad (26)$$

4.2.4.2 Helium pycnometry results and discussion

The pycnometry technique previously described was used on all the samples tested and results are shown in Table 22. The error in this experimental data comes from two sources. The first is the measurement error in determining the superficial volume of the foam samples. This is a function of the micrometer accuracy of ±0.001mm which results in an error in the superficial volume of ±10^{-6}mm^3, which is extremely low compared to the calculated superficial volumes. A more significant cause of error is measurement error in the pycnometer itself in determining the skeletal volume of the samples. This error was reported by the manufacturer of the equipment to be equal to ±0.03% of the measured value ±30 mm^3. For the measured skeletal volumes, this is a significantly larger error at approximately 10% of the measured values and forms the largest source of error. However as this is a constant inaccuracy which is a function of the equipment size this cannot be mitigated except by using larger samples. The error this introduces into the calculated voidage is variable due to the variance in sample sizes, but is no more than ±0.01.

It is interesting to note that the standard deviation for heat treated foams was larger than for their non-heat treated equivalents, which suggests that access into the internal structure of the foam was interfering with the test gas, resulting in less accurate data. This conclusion is further supported by the extremely high voidage shown in Table 22 for the adsorbent beads. The voidage of 0.746 is significantly higher than would be expected for a packed bed structure with typical values of 0.45 for packed spheres being reported in the literature (Mota *et al.* 2001). As helium is not significantly adsorbed at room temperature

(Brandani *et al.* 2016; Abouelnasr *et al.* 2017), this is unlikely to be due to helium adsorption. However as it is most pronounced in the adsorbent beads it is possible that the pycnometry is detecting the internal pores of the structure which are not present in the untreated foams and are not relevant for dynamic gas flow. Similarly, the heat treated foams have thinner bubble skins and more access to the internal part of the structure that the helium may be detecting. The beads may also have mesoporosity which is being detected.

The voidage of the foams measured varied from 0.85 to 0.94 which was significantly more than the 0.75 shown in the bead materials, with heat treated foams showing greater voidage than their non-heat treated counterparts. These voidage values are typical for foam materials (Richardson *et al.* 2000; Li *et al.* 2014) and polymeric foams in particular (Ma *et al.* 2013). This suggests that the results obtained for the foam materials are accurate, particularly for the non-heat treated foams.

Table 22: Measured void fractions for various PU-13X samples and 13X adsorbent beads.

Sample number	Measured geometric volume (mm^3) $\pm 10^{-6} mm^3$	Average skeletal volume (mm^3) $\pm 30 mm^3$	Standard deviation of skeletal volume (mm^3)	Voidage (dimensionless)
Adsorbent beads	1.01×10^4	2.57×10^3	$\pm 7.61 \times 10^1$	0.746
67	6.92×10^3	5.87×10^2	$\pm 1.78 \times 10^0$	0.915
68	2.84×10^3	4.16×10^2	$\pm 1.42 \times 10^0$	0.854
70	2.56×10^3	2.90×10^2	$\pm 2.26 \times 10^0$	0.887
80	2.56×10^3	1.21×10^2	$\pm 2.40 \times 10^0$	0.953
82	5.54×10^3	5.34×10^2	$\pm 1.86 \times 10^0$	0.904
82A	5.15×10^3	4.39×10^2	$\pm 5.37 \times 10^0$	0.915
83	2.75×10^3	3.48×10^2	$\pm 1.87 \times 10^0$	0.873
83A	3.42×10^3	2.87×10^2	$\pm 3.64 \times 10^0$	0.916
84	2.95×10^3	3.19×10^2	$\pm 8.29 \times 10^{-1}$	0.892
84A	2.82×10^3	2.58×10^2	$\pm 4.46 \times 10^0$	0.908
85	7.80×10^3	5.10×10^2	$\pm 1.73 \times 10^0$	0.935
85A	7.28×10^3	4.17×10^2	$\pm 4.90 \times 10^0$	0.943
86	5.62×10^3	4.20×10^2	$\pm 1.65 \times 10^0$	0.925
86A	5.01×10^3	3.43×10^2	$\pm 2.68 \times 10^0$	0.931
87	5.48×10^3	5.46×10^2	$\pm 1.21 \times 10^0$	0.900
87A	6.49×10^3	4.68×10^2	$\pm 2.10 \times 10^0$	0.928
88	3.30×10^3	3.51×10^2	$\pm 1.10 \times 10^0$	0.894
88A	3.10×10^3	3.05×10^2	$\pm 2.74 \times 10^0$	0.902

4.2.5 Experimental measurements of pressure drop

In order to fully investigate the suitability of the produced materials as low pressure drop adsorbent supports, measuring their pressure drop behaviour was necessary. This was performed in the laboratory using a benchtop apparatus as shown in Figure 65.

In the setup used (Figure 65, Figure 66), compressed air from a centralised supply was passed through a holder containing a cylindrical section of the foam sample being tested. Air was used as is without any drying or further treatment. Given the low moisture content of the compressed air supply compared to the ambient lab conditions the samples were stored in, as well as exposure to the air supply during setup, this effect this moisture would have on the pressure drop tests was not viewed as significant. The sample was chosen to be as long as possible from the produced material with a minimum height of 3.3 cm. It was dried and free of dust and closed top or bottom sections were removed. Samples had their size measured using a micrometer before being tested, and were fit into the holder using impermeable gas tape wrapped around the top and bottom to ensure a snug fit to avoid bypass.

Airflow through the sample was controlled via a needle valve in combination with a rotameter to measure the flowrate of air through the sample holder and sample if present. Pressure drop over the holder was measured via use of a water filled U-tube manometer, giving a resulting pressure drop in terms of water height. Gas flowrates were then steadily increased up to the largest flowrate for which a pressure drop on the manometer scale could be measured, or as high as the rotameter scale would allow, whichever was lower.

In order to calculate the true pressure drop of a given sample, the equipment was first used to measure the pressure drop of the sample holder whilst empty. These results are shown in Figure 67. This data is then subtracted from the measured pressure drops of experiments run with foam samples present in the holder in order to find the pressure drop imposed by the sample itself.

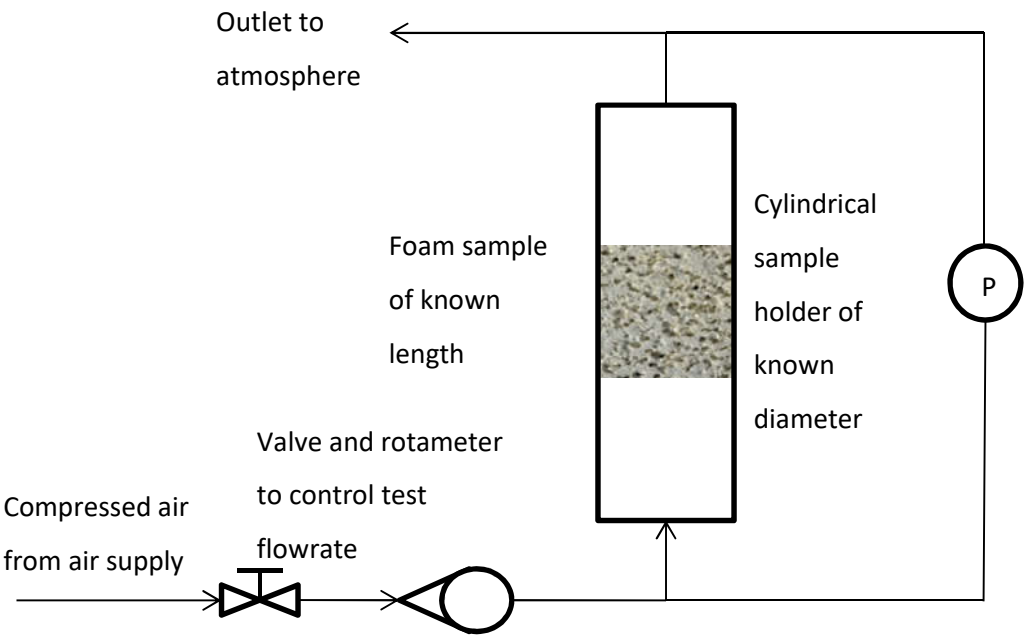

Figure 65: Schematic diagram of pressure drop testing apparatus.

Figure 66: Pressure drop apparatus as used in the research. Foam sample tested highlighted in yellow.

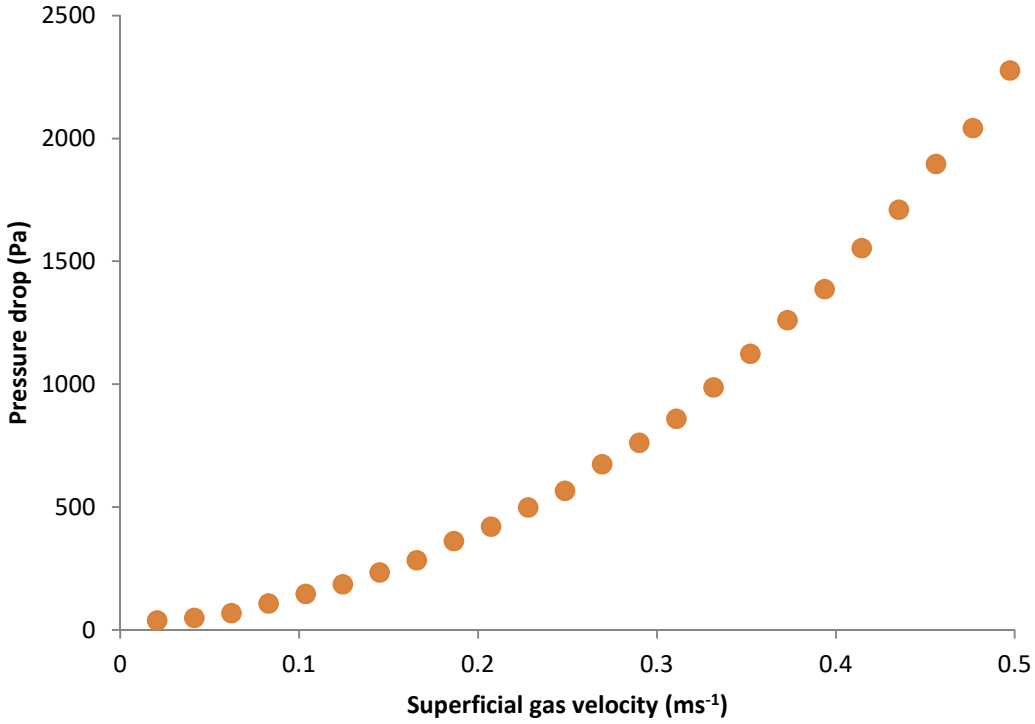

Figure 67: Baseline pressure drop of the apparatus as measured using the apparatus, used for data correction.

In order to convert the raw pressure drop data into a form useful for analysis, it is necessary to perform subsequent processing. Firstly, the raw data in terms of water height is corrected to remove the effects of the apparatus by simple subtraction of the data seen in Figure 67. Using the knowledge of the diameter of the sample holder, the gas flowrate is converted from volumetric terms into a superficial gas velocity. The pressure drop is similarly converted into a pressure drop per unit length to compensate for differing sample lengths using the measured length of the sample via the micrometer. This results in data expressed as pressure drop per length as a function of gas velocity, suitable for further analysis, as displayed in Figure 68. The samples tested covered a range of 13X mass fractions, formulations and synthesis techniques in order to investigate the effects of various changes in the foam synthesis process on pressure drop behaviour, and these are described in Table 23.

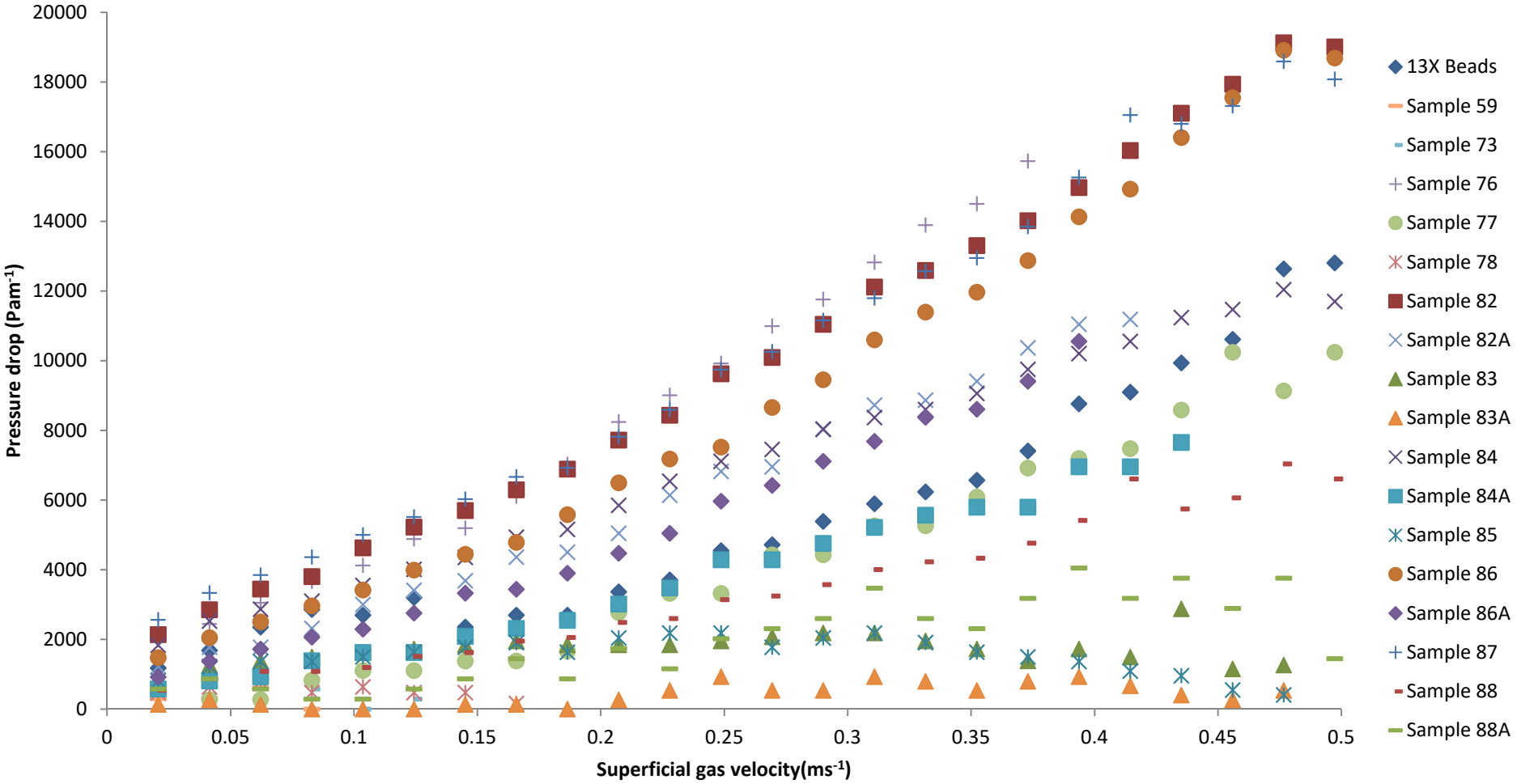

Figure 68: Measured pressure drops for various PU-13X samples, as well as 13X adsorbent beads.

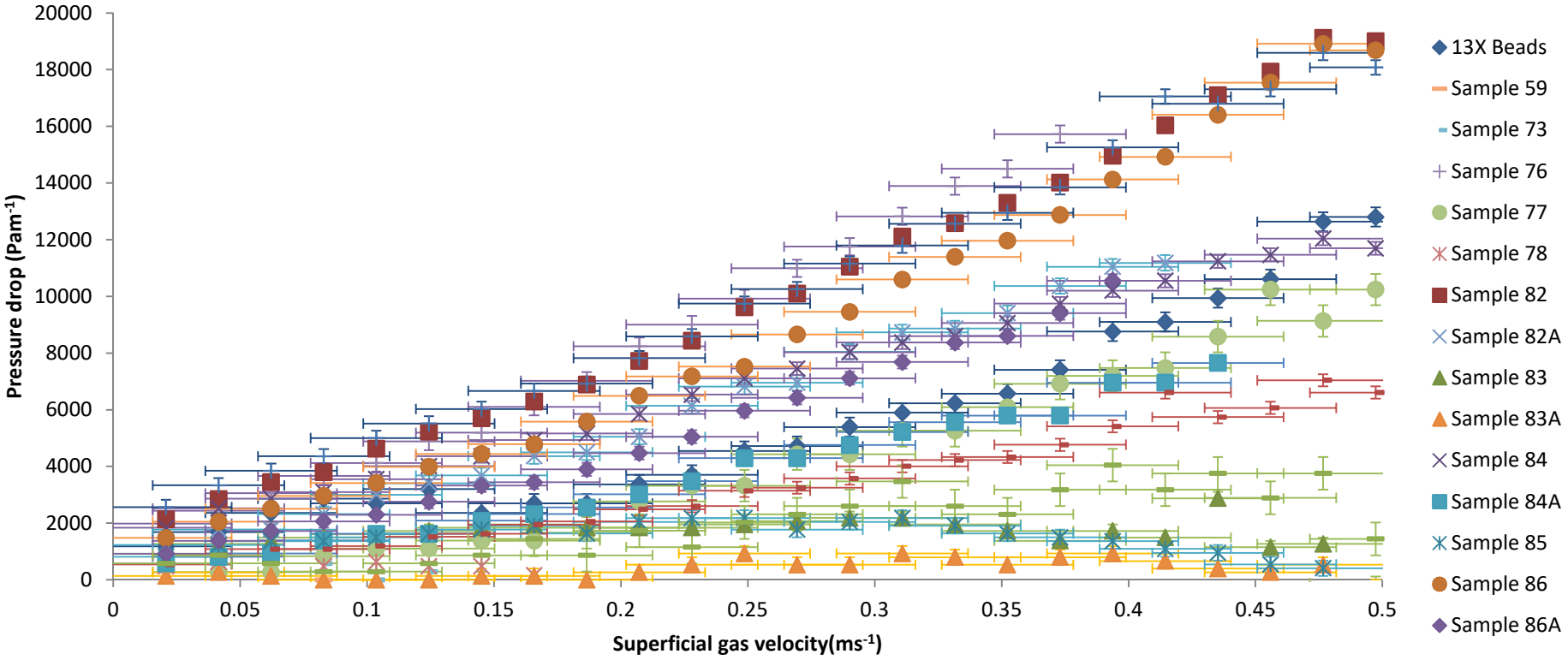

Figure 69: Measured pressure drops for various PU-13X samples, as well as 13X adsorbent beads showing experimental errors.

Table 23: Experiment samples undergoing pressure drop testing with 13X content and formulation notes.

Sample number	13X content (Weight % by formulation)	Other formulation notes
87	70	
82	75	Single batch with 83, 84
86	67	
82A	75	Heat treated, single batch with 83, 84
86A	67	Heat treated
84	75	Single batch with 82, 83
Beads	-	-
84A	75	Heat treated, single batch with 82, 83
88	75	Silicone oil added
88A	75	Heat treated, silicone oil added
83	75	Single batch with 82, 84
85	60	-
83A	75	Heat treated, single batch with 82, 84
73	67	Reaction performed in ice bath
77	75	Tin polymerisation catalyst omitted
59	75	-

The error in the pressure drop data, displayed in Figure 69, comes primarily from the measurement of the raw pressure drop values via the U-tube manometer. The accuracy of the measurements of the length and width of the sample is sufficiently high ($\pm$0.02 mm) that contributions to the overall error of the data from this source are insignificant. In calculating the pressure drop data seen in Figure 68 however, the water height must be measured 4 times, twice to calculate the baseline pressure drop of the equipment seen in Figure 67, and twice to determine the pressure drop with the sample being measured,

comparing the difference in water heights each time. This results in a total error of 4 times the measurement error of the ruler (±0.5 mm), which can have a variable effect on the total error depending on the sample length. This is worst for shorter samples with a maximum error observed of ±610 Pam^{-1} for sample 59. This could be reduced by increasing the sample length, which was done in later experiments, but would ideally be improved by using a more precise pressure sensor in future tests.

An additional source of error exists in the superficial gas velocity values. As before, the contribution from calculating the cross sectional area of the sample can be taken to be negligible due to being measured via the micrometer. The rotameter however has a significant error of 5% of the full scale of 25 lpm, which corresponds to an error of ±0.0259 ms^{-1}. Another source of error is also present at higher air flowrates, where oscillation of the airflow can occur following changes in the flowrate. This cannot be quantified but is controlled for by introducing wait periods between measurements to allow for the flow regime in the apparatus to stabilise before taking measurements.

4.2.6 Pressure drop analysis

As can be seen in Figure 68, the beads have similar pressure drop characteristics compared to the various foams tested. Several foams showed significantly lower pressure drop per length than the beads, heat treated foams in particular.

The reason for this improvement however is not immediately clear, as there is a significant variance in the pressure drop of the foams. Part of this is likely due to the inherently random nature of the foam production process. Samples 82, 83 and 84 were all made in a consistent manner in identical conditions and have a wide range of pressure drop behaviour and voidage and bubble diameters, as seen in Table 24. The table, when sorted in terms of pressure drop, also shows no clear correlation between either voidage or the characteristic dimension, and improved pressure drop performance.

Heat treated foams were however consistently found to have lower pressure drop than their precursor foams. These foam pairs can thus be considered to determine the cause of the lower pressure drop behaviour as these pairs will be the most similar foams to each other. The heat treatment process causes both an increase in the voidage of the foams and a decrease in their bubble and window diameters. This suggests that the voidage of the foams has a significant effect on their pressure drop behaviour. The effect of the

characteristic dimension of the foams is significant enough that it cannot be neglected however, as whilst the adsorbent beads have the lowest voidage of any sample tested, their pressure drop is competitive with the foams which have far higher voidages, which can be attributed to the bead diameters being an order of magnitude larger than the bubble or window diameters of the foams.

The density of the foams may also have a significant effect. Samples 73, 77 and 88 all took steps to increase the density of the foams by supressing foaming behaviour. These resulted in larger characteristic dimensions compared to other foams and can explain the improved pressure drop behaviour compared to other foams of similar voidage.

The nature of the flow regime through the foams is unclear. The nature of a flow and if it is laminar or turbulent is given by the Reynolds number for a system. A definition for particle Reynolds number has been reported in the literature for foams to be as seen in equation (27) (Richardson *et al.* 2000), where the particle diameter d_p is the mean cell diameter for the foam. The velocity of gas flowing through the foam must also take the foam voidage into account as the solid fraction will block gas flow, resulting in equation (28) (Beer *et al.* 2019). The literature work is based on open celled metal foams and uses bubble diameter as their characteristic dimension, an assumption which may not hold true in this work where bubbles are less interconnected and windows are smaller, so window diameters are also used in this case. This results in Reynolds numbers for the foam system tested of between 0.282 to 24.3 for bubble size and 0.110 to 6.48 for window size.

$$\mathrm{Re_p} = \frac{\rho V d_p}{\mu} \tag{27}$$

$$V = \frac{Q}{\varepsilon A_{cs}} \tag{28}$$

Given the importance of two different physical properties to the pressure drop behaviour of the foams, it becomes useful to consider models for pressure drop through foam materials in order to gain a more detailed understanding of the relative importance of these properties. It is also desirable to find which of bubble or window diameter is the characteristic dimension of a foam in the same way that bead diameter is for the adsorbent beads, which occurs in the following section.

Table 24: Voidage, window diameter and bubble diameter data where available for samples used in pressure drop experiments, from highest to lowest pressure drop.

Sample number	Voidage (dimensionless)	Bubble/Bead diameter (mm)	Window diameter (mm)	Formulation notes
87	0.900	0.274	0.106	
82	0.904	0.303	0.101	Single batch with 83, 84
86	0.925	0.403	0.125	
82A	0.915	0.274	0.0734	Single batch with 83, 84
86A	0.931	0.257	0.101	
84	0.892	0.349	0.112	Single batch with 82, 83
Beads	0.746	1.6-2.5	N/A	-
84A	0.908	0.261	0.0942	Single batch with 82, 83
88	0.894	0.416	0.175	Silicone oil added
88A	0.903	-	-	Silicone oil added
83	0.873	0.405	0.143	Single batch with 82, 84
85	0.934	0.257	0.133	-
83A	0.916	0.188	0.114	Single batch with 82, 84
73	0.879	-	-	Reaction performed in ice bath
77	0.850	0.518	0.145	No tin polymerisation catalyst
59	0.676	-	-	-

4.3 Modelling and analysis of gas flow through foams

4.3.1 Introduction

In order to guide the design and development of adsorbent foam materials in practical applications a model which can effectively predict their pressure drop given knowledge of their physical characteristics is useful. Such a model can be used for process design and for developing the foams to have lower pressure drops by control of the production procedure and altering their physical properties. This section aims to achieve this goal, building upon the experimental work done earlier in this Chapter and the literature review in Chapter 2 on the subject. This is not a simple task however, as there is no consensus on what the characteristic dimensions of a foam are. Additionally the inherently random nature of bubble formation in chemically blown polymeric foams means that there is natural variance in their voidages and bubble and window sizes before the difficulties and uncertainties of measuring these are taken into account. As a result modelling these types of foams has novelty and value.

The initial analysis of the pressure drop data in section 4.2.6 found that the pressure drop of the foams was dependant both upon their voidage and their characteristic dimension. However there was no clear conclusion as to if the window size or the bubble size of the foams was their characteristic dimension, and the relative importance of voidage to their characteristic dimension was also unclear. As a result, an accurate model must be developed to determine the sensitivity of pressure drop to these physical characteristics.

Section 2.6.2 reviewed the literature on pressure drop through foam materials and identified four models for investigation. These are the Ergun equation and three models which modify the Ergun equation in some way to fit a foam structure instead of a packed bed: the Lacroix model (Lacroix *et al.* 2007), the Dietrich model (Dietrich 2012) and the Inayat model (Inayat *et al.* 2011). These models use different characteristic dimensions, Lacroix uses bubble diameter whilst Inayat and Dietrich use window diameter and also modify the Ergun constants in different ways. In this section, all four models are applied to the pressure drop data for the foams found in the previous section and analysed in detail in order to deepen understanding of the foam's pressure drop characteristics and develop an effective model for the PU-13X foam system used in this research.

4.3.2 The Ergun equation

Before any models based on the Ergun equation can be considered, it is useful to apply the unmodified Ergun equation to the foams in order to understand how effectively it models pressure drop before any changes. The basic form of the Ergun equation is shown below as introduced in Chapter 2, and is used for this purpose.

$$\frac{\Delta P}{L} = E_1 \frac{\mu(1-\varepsilon)^2 u_g}{\varepsilon^3 d_p^2} + E_2 \frac{\rho(1-\varepsilon) u_g^2}{\varepsilon^3 d_p} \quad (29)$$

The Ergun equation was developed for the flow of air through packed beds of smooth and spherical particles which exist for voidages in the region of 0.4 and has since been applied and modified to a wide variety of systems in the literature with varying results. Even systems which are close to the assumptions the Ergun equation was based on can show significant disagreement between the model and the experimental data (Macdonald *et al.* 1979), and the model makes no account for variance in the particle size, roughness of the surface and the E_1 and E_2 constants have to be empirically found for each particular application for it to be effective. It is also extremely sensitive to changes in voidage. Nonetheless it is widely used.

Equation (29) is applied to a subset of the pressure drop data for which reliable voidage and bubble/window diameter data is available and samples which are likely to be relevant to practical respiratory protection applications. As a result, the chosen dataset was the pressure drop profiles for samples 82, 82A, 83, 84, 84A and 88.This includes two heat treated non-heat treated pairs, the repeatability study of samples 82, 83 and 84 and also covered the entire range of pressure drops measured. The adsorbent bead data was also modelled with the Ergun equation to test its reliability in situations it was designed for.

Window and bubble diameters as determined by experiment were used to implement the Ergun equation to model the foam dataset by using both the bubble and window diameter in the place of the particle diameter, whilst the adsorbent beads used the average bead diameter supplied by the manufacturer. All of the foams used voidage data as determined via experiment. The adsorbent beads, due to the inaccuracies in the voidage data, used a correlated voidage value of 0.396 calculated for packed spheres using the correlation

below as published in Benyahia *et al.* (2005) which compares particle diameter (d_p) to the tube diameter (d_{tub}). The values of E_1=150 and E_2=1.75 as calculated by Ergun were used.

$$\varepsilon = 0.390 + \frac{1.740}{\left(d_{tub}/d_p + 1.140\right)^2} \tag{30}$$

This resulted in the modelled data seen in Figure 70 for the 13X adsorbent beads, Figure 71 for the Ergun equation using bubble diameters and Figure 72 for the Ergun equation using window diameters, compared against the experimental pressure drop data for these samples seen in Figure 73.

As can be seen in the graphs, the Ergun equation models the foams poorly compared to the beads, underestimating the pressure drop of the foams by an order of magnitude. The beads themselves are also modelled poorly, but significantly closer to the experimental data than was seen with the foams, and with significantly less reliable data used to inform the model. As expected, the Ergun equation on its own cannot be used to model the foams via a direct substitution of bubble or window diameter for particle diameter. The window diameter values offered closer agreement with the data, which is likely because these were smaller values than the bubble diameters but this was still insufficient for agreement with the experimental data. More elaborate modifications of the Ergun equation are thus necessary to model the foams successfully, which are described in the following sections.

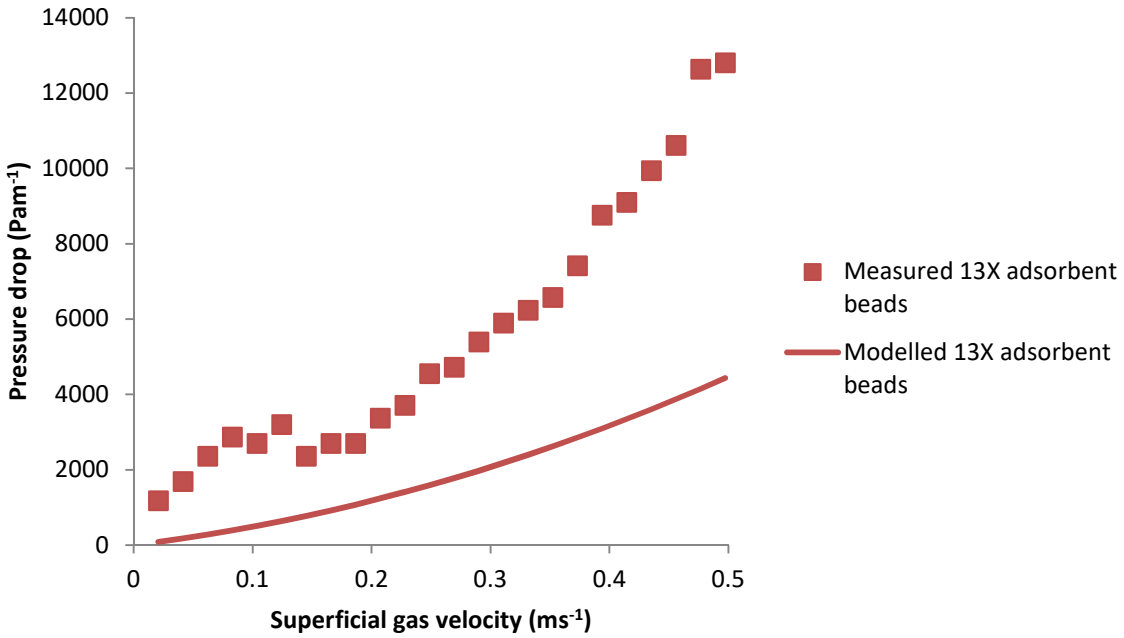

Figure 70: The Ergun model implemented for 13X adsorbent beads plotted against experimental pressure drop data for the beads.

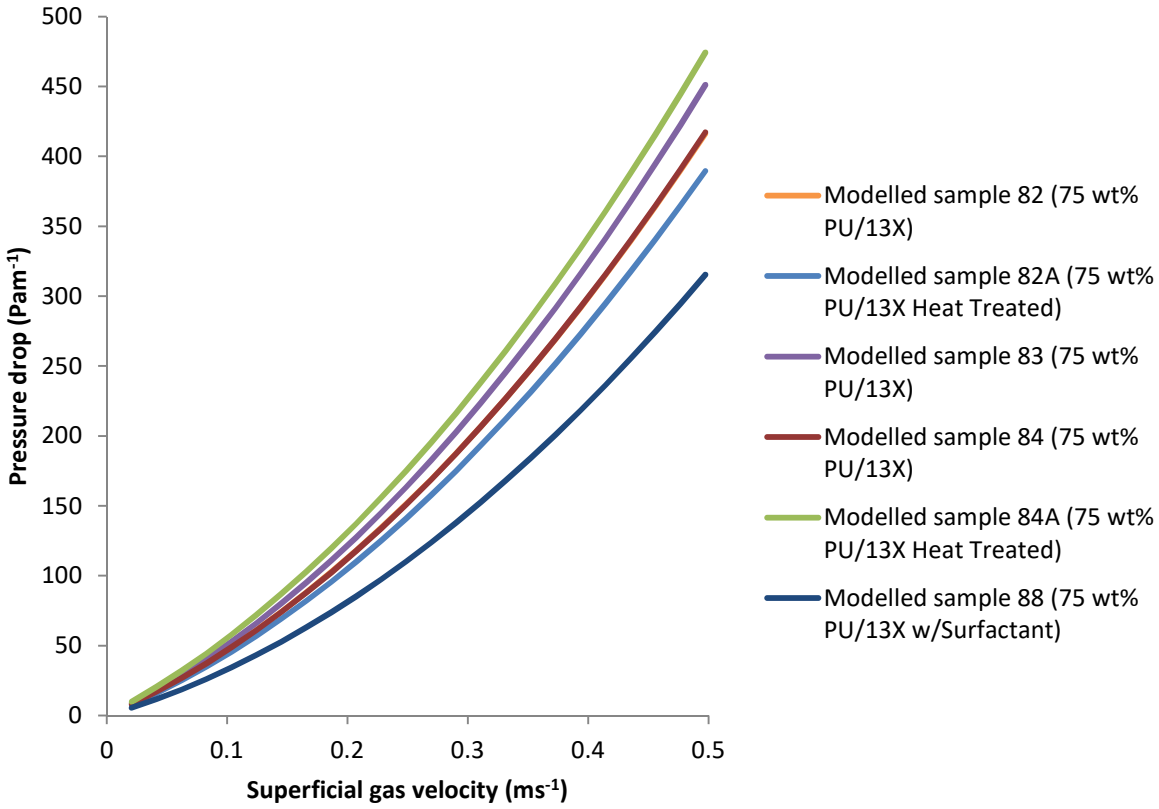

Figure 71: Ergun models for foams of samples 82, 82A, 83, 84, 84A, and 88 using bubble diameter as particle diameter.

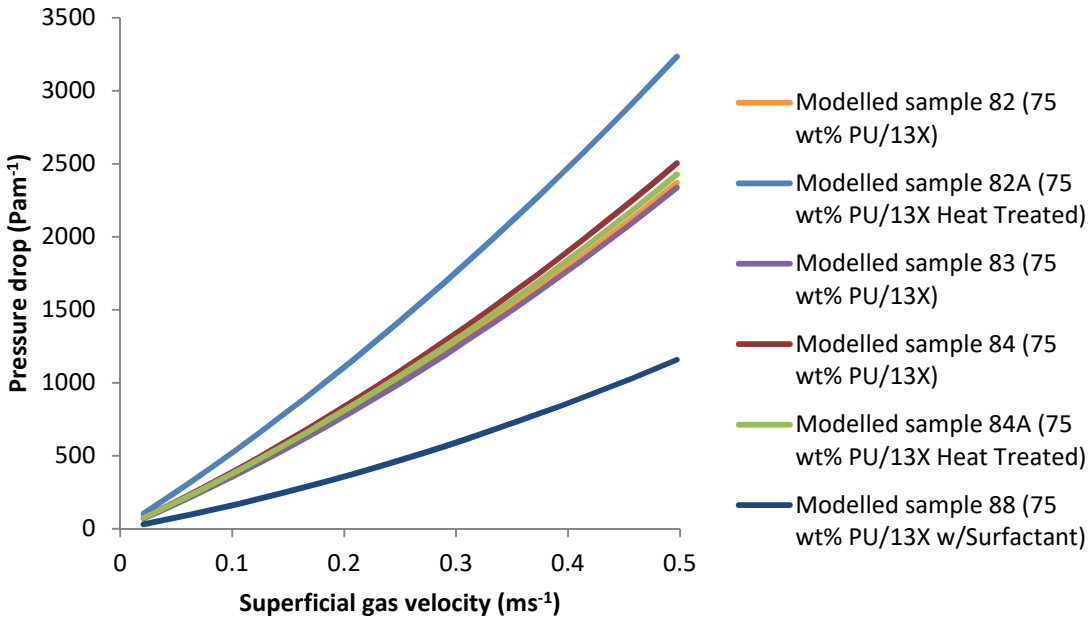

Figure 72: Ergun models for foams of samples 82, 82A, 83, 84, 84A and 88 using window diameter as particle diameter.

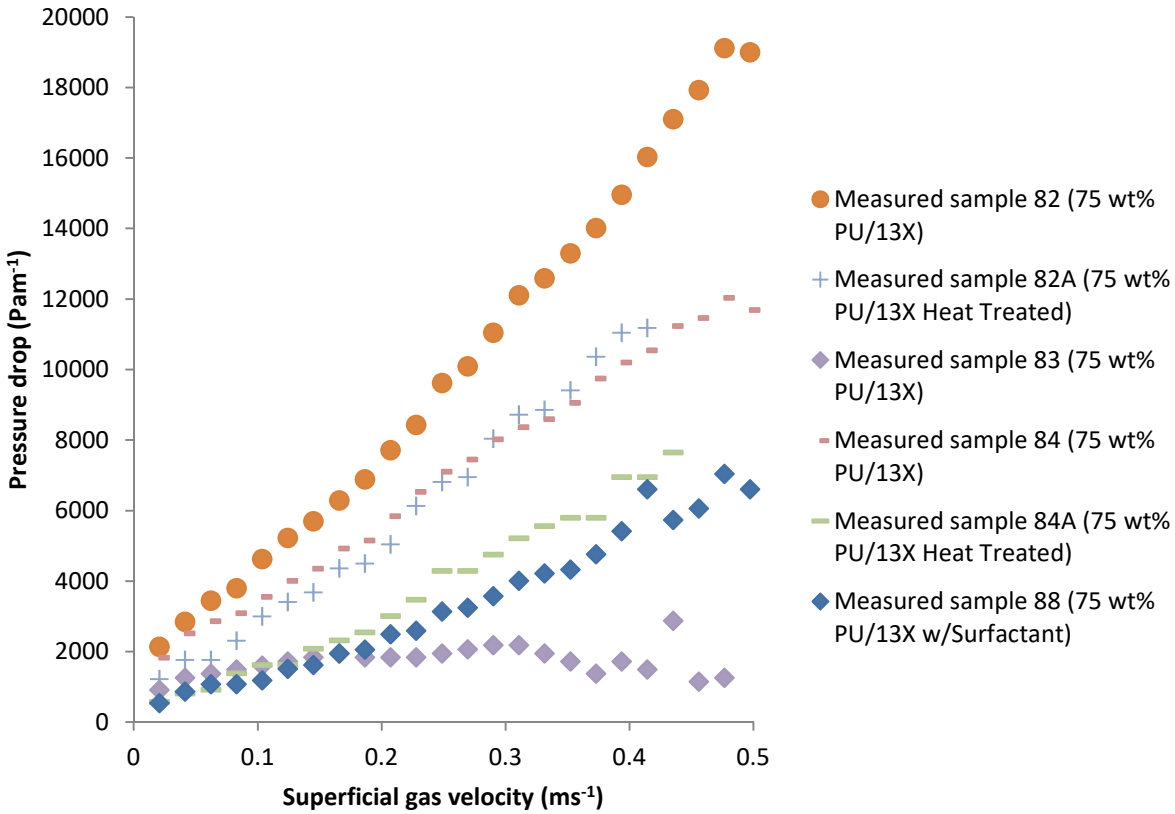

Figure 73: Experimental pressure drop data for foams of samples 82, 82A, 83, 84, 84A and 88.

4.3.3 The Lacroix model

As discussed in section 2.6, one model which is used to adapt the Ergun equation to foams is the work by Lacroix *et al.* (2007). In this work, they use a cubic cell model where foams are treated as a three dimensional lattice of cubes where the solid fraction forms the interface between the cubes in the form of solid cylinders. This is used to find an effective particle diameter for the foams in terms of the strut diameter of the cubic lattice by way of equating the external specific surface area for structures of identical voidage. This then allows for the effective particle diameter to be estimated from the foam properties, where the bubble diameter was used for the cell size of the cubic cell model as seen below in equations (31) (32) and (33), where ϕ was the bubble diameter of the foams being measured. They do not modify the Ergun constants, but use the values of E_1=150 and E_2=1.75 as are typical for packed beds.

$$d_p = \frac{6}{4} d_s \tag{31}$$

$$d_s = \frac{a[(4/3\,\pi)(1-\varepsilon)]^{1/2}}{1-[(4/3\,\pi)(1-\varepsilon)]^{1/2}} \tag{32}$$

$$a = \frac{\phi}{2.3} \tag{33}$$

This model was applied to samples 82, 82A, 83, 84, 84A and 88 and compared with pressure drop profiles measured via experiment using voidages and bubble sizes as determined via experiment previously in this section. This resulted in the comparisons shown in Figure 74 with experimentally measured pressure drop data in Figure 73. These models show no improvement over the Ergun equation and are entirely ineffective at modelling the pressure drop behaviour of the foams, underestimating their pressure drops by an order of magnitude. This is most likely due to the fact that the Lacroix model performs very few modifications to the Ergun equation, using the same Ergun constants and only changing the particle diameter. The calculated particle diameters are shown below in Table 25 compared to the bubble sizes of the foams.

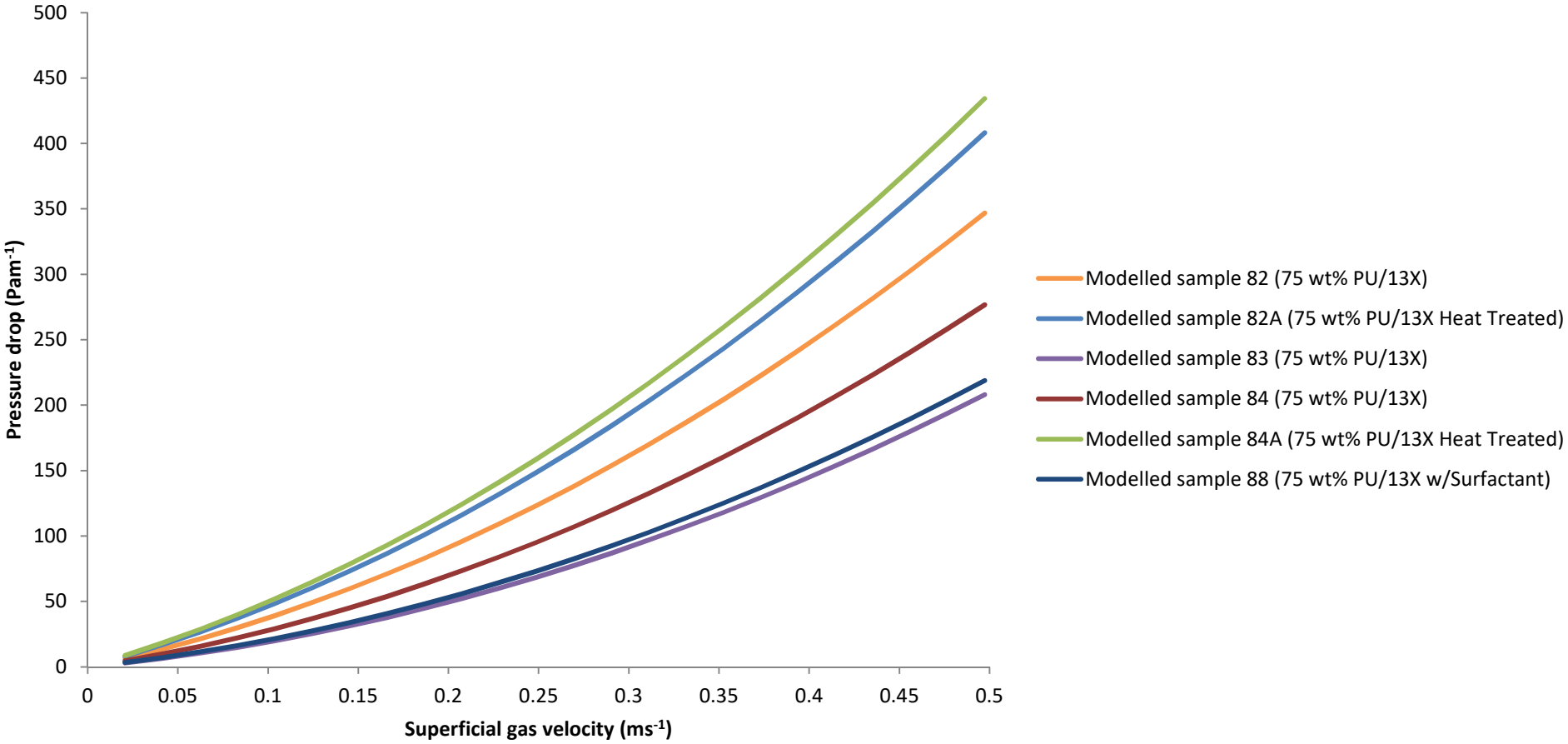

Figure 74: Lacroix models for foams of samples 82, 82A, 83, 84, 84A, and 88 using the particle diameter as calculated by Lacroix with Ergun constants as in Ergun and voidage measured via experiment.

Table 25: Effective particle diameters calculated by the Lacroix model compared to bubble diameters measured via experiment and foam voidage.

Sample number	Effective particle diameter calculated using Lacroix's method (m)	Bubble diameter measured via experiment (m)	Voidage (dimensionless)
82	3.44×10^{-4}	3.03×10^{-4}	0.904
82A	2.65×10^{-4}	2.74×10^{-4}	0.912
83	7.10×10^{-4}	4.05×10^{-4}	0.873
84	4.66×10^{-4}	3.49×10^{-4}	0.892
84A	2.77×10^{-4}	2.61×10^{-4}	0.908
88	5.43×10^{-4}	4.16×10^{-4}	0.894

As can be seen from these calculated particle diameters, there is relatively little change in the particle diameter calculated by the Lacroix method compared to the measured bubble diameters, which leads to the resulting lack of improvement in the modelled pressure drop. This is likely due to the fact the Lacroix model is validated by Lacroix for superficial gas velocities of up to $6ms^{-1}$ and voidages of 0.75 to 0.92. The pressure drop experiments are well within this gas velocity range but the foam voidages are at the upper end of the range validated, and are poorly modelled by Lacroix as a result. This is supported by the fact that the experiment with the greatest change in particle diameter was sample 83, which in turn had the lowest measured voidage.

The morphology of the foams Lacroix used to develop their model is also significantly different from the foams used in this work. Lacroix used silicon carbide foams which had a very large window size and open structure compared to the foams in this work (Figure 75). This lead to a similarity between the SiC foams and the cubic cell model which Lacroix used which may not hold true for the PU-13X foams in this work. Similarly the cubic cell model has very similar bubble to window size ratios, due to this highly open structure. Smaller windows as seen in the polymeric foams will increase the tortuosity of the path for gas flow, increasing the resulting pressure drop without a significant decrease in the voidage. As a result of these issues, the Lacroix model can be discounted as an effective model for the PU-13X foams.

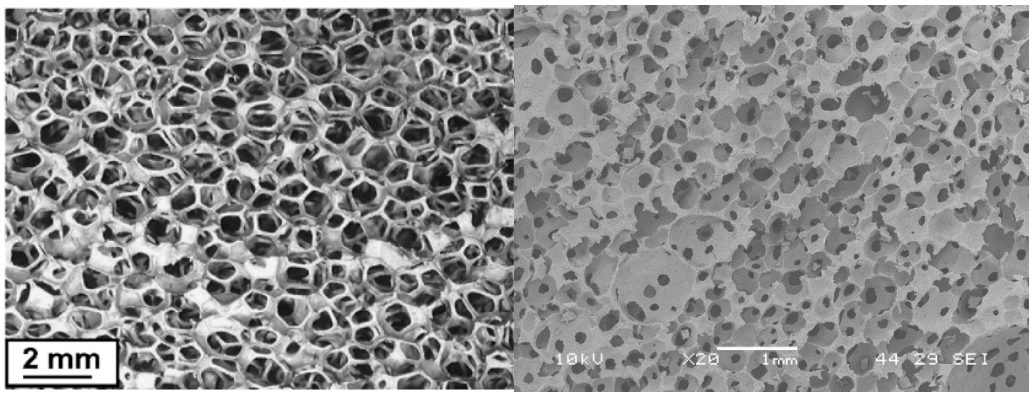

Figure 75: Microscopy images for SiC foams as used in Lacroix *et al.* (2007) (left) (Reproduced from (Lacroix *et al.* 2007), p3262, ©2007 with permission from Elsevier) and PU-13X foams as produced in this work (Sample 82, right).

4.3.4 The Inayat model

The model suggested by Inayat *et al.* (2011) uses a different geometric model for foams which employs a regular tetrakaidecahedral cell model instead of the cubic cell model used by Lacroix. This model assumes that the solid fraction of the foam takes the form of solid struts which form the vertices of the tetrakaidecahedrons. This model uses the basic form of the Ergun equation as shown below (34), but uses correlations for the Ergun constants based on the foam voidage. This model was developed using superficial gas velocities of up to 6 ms^{-1} and voidages of 0.799 to 0.871, a similar flow regime to the pressure drop experiments in this work.

$$\frac{\Delta P}{L} = \frac{E_1 S_v^2 (1-\varepsilon)^2 \mu}{\varepsilon^3} u + \frac{E_2 S_v (1-\varepsilon) \rho}{\varepsilon^3} u^2 \tag{34}$$

The following correlations for the Ergun constants are given by Inayat:

$$E_1 = \left[\left(\frac{1 - 0.971(1-\varepsilon)^{0.5}}{0.6164(1-\varepsilon)^{0.5}}\right)\varepsilon\right]^{-1} \tag{35}$$

$$E_2 = \left[\left(\frac{1-0.971(1-\varepsilon)^{0.5}}{0.6164(1-\varepsilon)^{0.5}}\right)(1-\varepsilon)\right] \tag{36}$$

Inayat *et al.* (2011) also give a correlation for the specific surface area of foam materials in terms of window diameter for foam structures which have concave triangular struts as

seen in the produced materials. This is based on their regular tetrakaidecahedral cell model and is found geometrically by allowing the specific surface area to be linked to the foam voidage and window sizes.

$$S_{v\ triangular,concave} = 6.49\frac{[1-0.971(1-\varepsilon)^{0.5}]}{d_w(1-\varepsilon)^{0.5}}(1-\varepsilon) \quad (37)$$

This model was applied to samples 82, 82A, 83, 84, 84A and 88 and compared with pressure drop profiles measured via experiment using voidages and bubble sizes as determined via experiment previously in this section. This resulted in the models shown in Figure 76 and the pressure drop data in Figure 73. This shows very poor modelling of the foams compared to the experimental data, with significantly worse performance than both the Ergun equation using window size and the Lacroix equation using bubble size.

Given the use of the Ergun equation as a basis, it is worth investigating further as to why the Inayat model offers no improvement on this baseline. Firstly, the Ergun constants can be considered as seen in Table 26.

Table 26: Calculated Ergun constants and particle diameters for the Inayat model compared with measured values and original Ergun constants.

Sample number	Calculated E_1 value from Inayat correlation	Calculated E_2 value from Inayat correlation	Effective particle diameter calculated via Inayat (m)	Bubble diameter via measurement (m)
Ergun	4.17	0.292	-	-
82	0.303	0.352	4.32×10^{-4}	3.03×10^{-4}
82A	0.275	0.339	3.24×10^{-4}	2.74×10^{-4}
83	0.384	0.378	5.67×10^{-4}	4.05×10^{-4}
84	0.333	0.363	4.65×10^{-4}	3.49×10^{-4}
84A	0.291	0.347	4.07×10^{-4}	2.61×10^{-4}
88	0.329	0.361	7.28×10^{-4}	4.16×10^{-4}

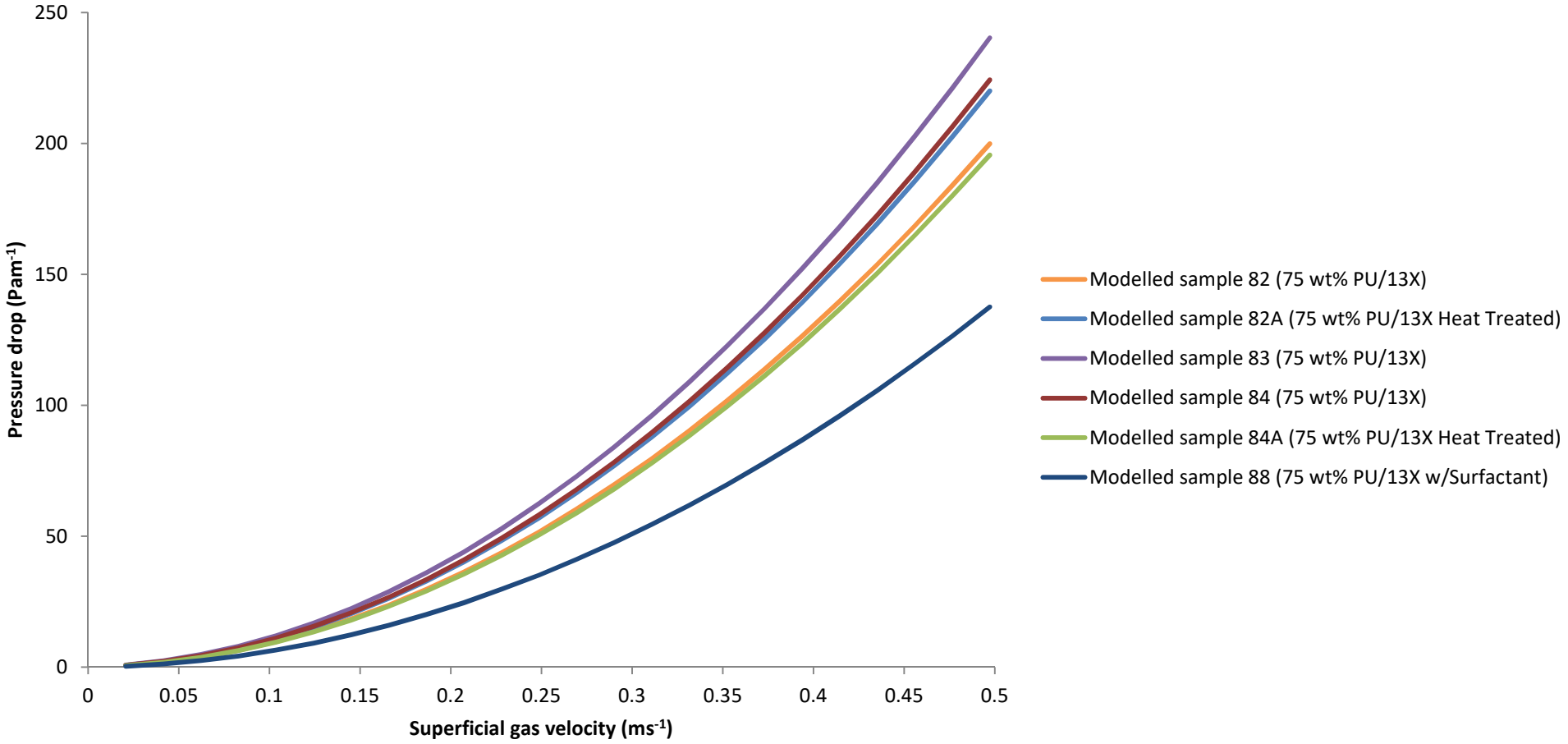

Figure 76: Inayat models for foams of samples 82, 82A, 83, 84, 84A, and 88 using the specific surface area and Ergun constants as calculated by Inayat with voidage measured via experiment.

The effective particle diameters for comparison were found via the equation below as given in Inayat.

$$d_p = \frac{6}{S_v} \tag{38}$$

As can be seen in the table, the Inayat model increases the effective particle diameter used to model the pressure drop, and greatly decreases the Ergun constants, which as seen in equations (35) and (36) are highly dependent on the foam voidage, which was significantly less for the foams considered by Inayat than the foams produced in this work. In order to attempt to improve on this, the Inayat model was revised to use the original values for E_1=4.17 and E_2=0.292 as proposed by Ergun for the equation in terms of specific surface area as seen in equation (34). This model was applied to samples 82, 82A, 83, 84, 84A and 88 and compared with pressure drop profiles measured via experiment using voidages and bubble sizes as determined via experiment previously in this section. This resulted in the models shown in Figure 77 with pressure drop data in Figure 73.

As can be seen in the figure, the use of the original Ergun constants increases the modelled pressure drops but is still insufficient to model the pressure drop for the foams as used. As a result it must be concluded that the geometric model which Inayat use is not applicable to the foams in this work. The tetrakaidecahedral cell model used by Inayat is shown below in Figure 78. As can be seen here, the model has a large degree of open interconnectivity between the bubble cells, which was also reported by Inayat in their work developing the model based upon SiC foams (Figure 79). However, this is not present in the PU-13X foams in this work, which have significantly less interconnectivity as seen in Figure 80. As a result of the greater tortuosity seen in the polymeric foams made in this work, the model significantly underestimates the pressure drop of the PU-13X foams.

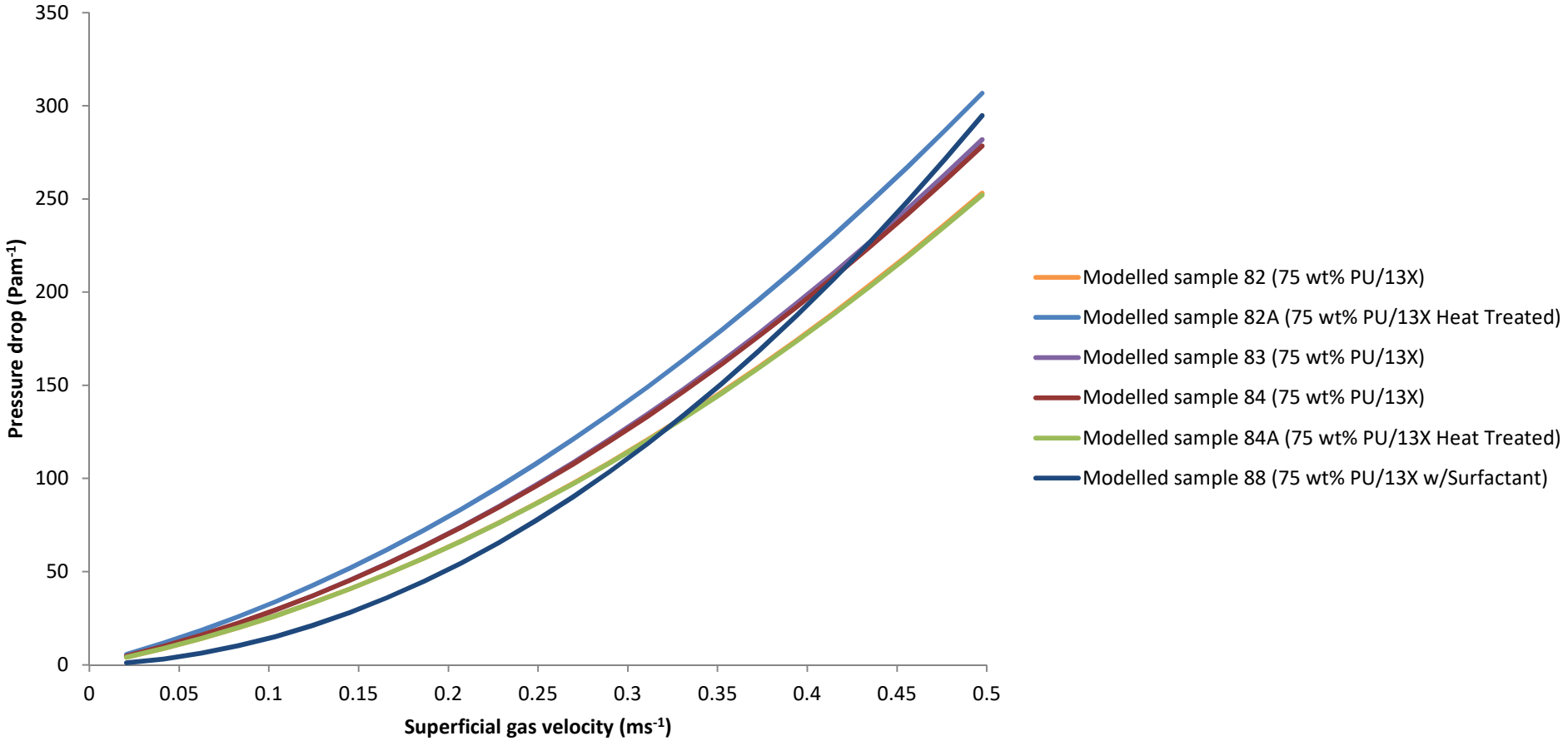

Figure 77: Inayat models for foams of samples 82, 82A, 83, 84, 84A, and 88 using the specific surface area as calculated by Inayat and Ergun constants as used by Ergun with voidage measured via experiment.

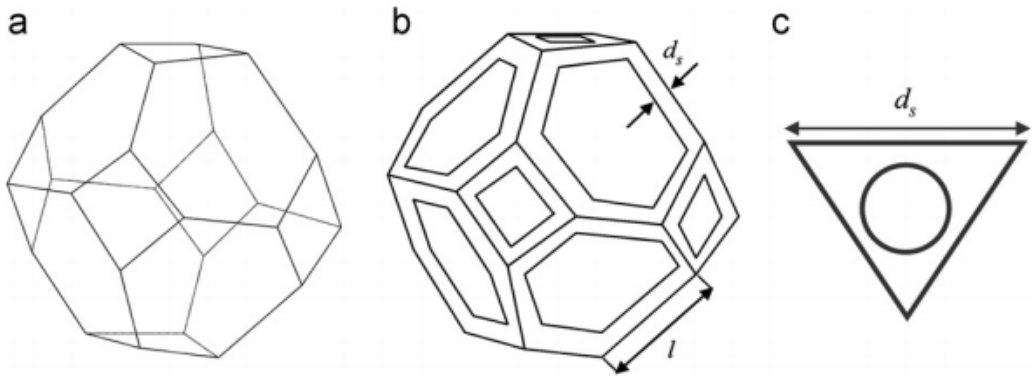

Figure 78: The tetrakaidecahedral unit cell geometric model used by Inayat *et al.* (2011) (Reproduced from (Richardson *et al.* 2000), p26 ©2000 with permission from Elsevier).

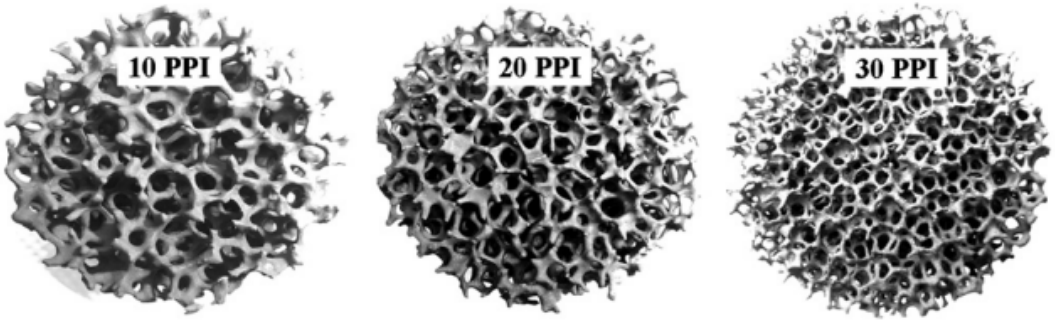

Figure 79: Samples of SiC foam as used by Inayat *et al.* (2011) to develop their foam pressure drop model. (Reproduced from (Inayat *et al.* 2011), p1181 ©2011 with permission from Elsevier).

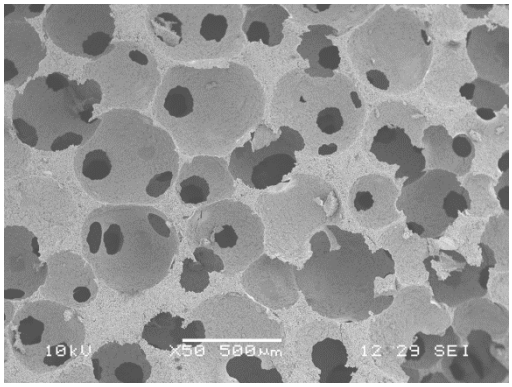

Figure 80: SEM image of sample 84 showing the PU-13X foam structure.

4.3.5 The Dietrich model

The last correlation mentioned in section 2.6.2 is the model developed by Dietrich (2012). The Dietrich model is based on an adaptation of the Ergun equation to foam materials which uses new Ergun constants of E_1=110 and E_2=1.45 which are found by fitting the Ergun equation to a series of experimental data for pressure drop through various ceramic and metal foams. The specific surface area of the foams is also used to calculate an effective hydraulic diameter which governs the flow of air through the materials. The approach Dietrich uses for this is to equate this to the porosity of the foam materials by using the tetrakaidecahedral cell model modified to use coefficients found by fitting to experimental foam data for specific surface area, resulting in the equations below (39), (40) and (41).

$$\frac{\Delta P}{\Delta L} = 110\frac{\mu}{\varepsilon d_h^2}u + 1.45\frac{\rho}{\varepsilon^2 d_h}u^2 \tag{39}$$

$$d_h = 4\frac{\varepsilon}{S_v} \tag{40}$$

$$S_v = 2.87\frac{1}{d_{strut} + d_w}(1-\varepsilon)^{0.25} \tag{41}$$

In their work, Dietrich mentions that in the case of cell diameter data being available but combined strut and window diameter data being absent, cell diameter was used in place of strut diameter and window diameter added together. This model was applied to foams 82, 82A, 83, 84, 84A and 88 using bubble diameters and voidages determined experimentally, resulting in the comparisons seen in Figure 81. This shows that the Dietrich model is ineffective at modelling the foams tested, although better than the other models used and the Ergun equation, and underestimates the pressure drop of the foams. This could be due to their choice of Ergun constants of 110 and 1.45 which are based on curve fitting to ceramic and metal foams, which have significantly different morphologies and pressure drop behaviour to polymeric foams as previously discussed. However their technique to calculate the Ergun constants can be applied to polymeric foams.

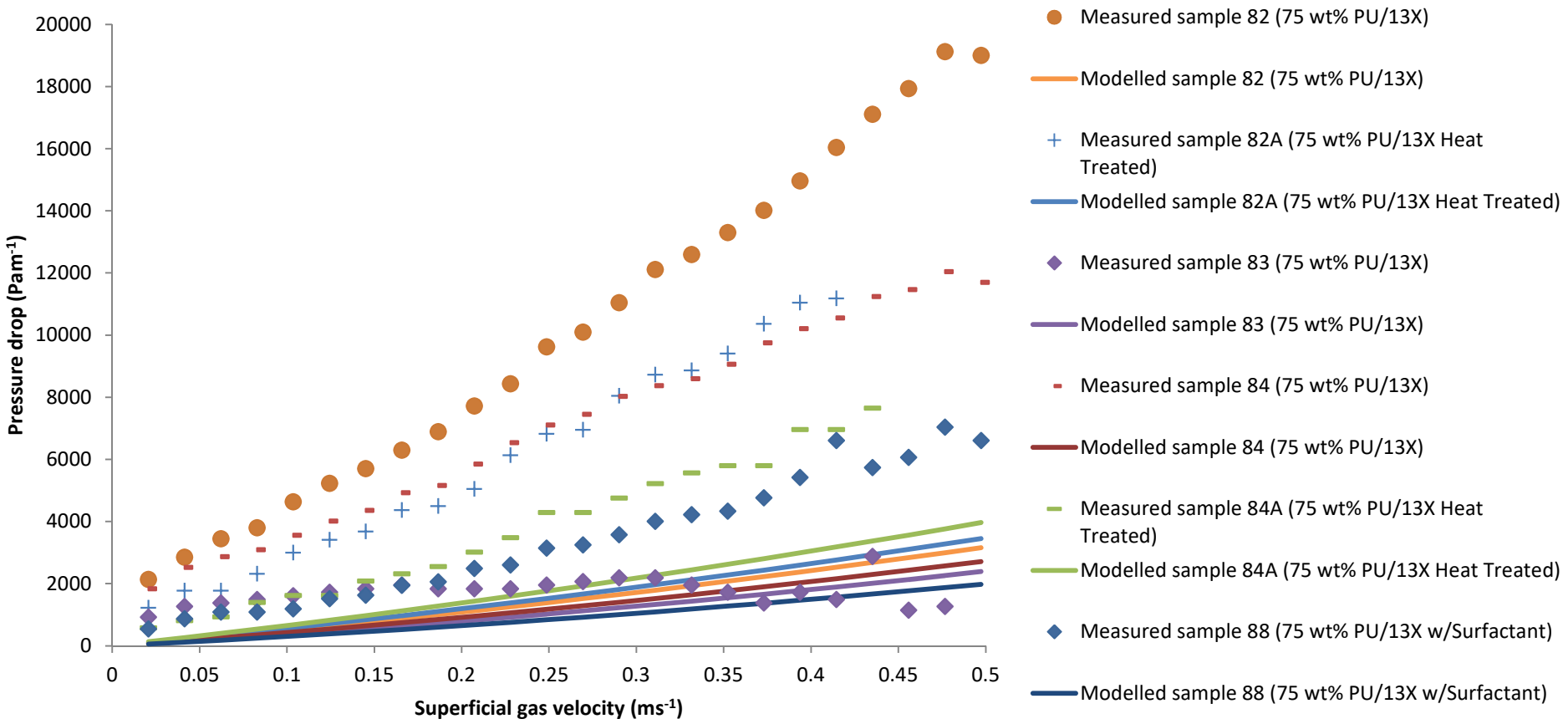

Figure 81: Dietrich models for foams of samples 82, 82A, 83, 84, 84A, and 88 using the specific surface area and Ergun constants as calculated by Dietrich with voidage measured via experiment plotted against experimental pressure drop data for these materials.

In their previous work (Dietrich *et al.* 2009), Dietrich describes the technique by which they calculate these values of 110 and 1.45 as follows. Using the Ergun equation in the form shown in equation (42) and by comparison with the more general Darcy-Forcheimer equation in (43) Dietrich could determine values of A and B in terms of K_1 and K_2 as shown in equations (44) and (45), where the hydraulic diameter was defined as used in the Dietrich model and mentioned previously in equations (40) and (41).

$$\frac{\Delta P}{\Delta L} = A\frac{\mu}{\varepsilon d_h^2}u + B\frac{\rho}{\varepsilon^2 d_h}u^2 \tag{42}$$

$$\frac{\Delta P}{\Delta L} = \frac{\mu}{K_1}u + \frac{\rho}{K_2}u^2 \tag{43}$$

$$A = \frac{\varepsilon d_h^2}{K_1} \tag{44}$$

$$B = \frac{\varepsilon^2 d_h}{K_2} \tag{45}$$

By obtaining values of K_1 and K_2 by fitting a second order polynomial to experimental data of pressure drop through an alumina sponge, Dietrich thus calculated the values of A=110 and B=1.45 which they use for their pressure drop model. However, the maximum voidage that was used to calculate these values was 0.85, significantly lower than the typical voidage for the PU-13X foams considered in this work, and the alumina foams had quite large bubble sizes compared to the PU-13X foams.

This technique can however also be employed to calculate new values of A and B for use in this work based on pressure drop data through PU-13X foams. By fitting a second order polynomial to experimental data for sample 77, shown in Figure 82, values for the coefficients of the u and u^2 terms of equation (43) were found, which resulted in the following equations:

$$\frac{\mu}{K_1} = 6.64 \times 10^3 \therefore K_1 = \frac{6.64 \times 10^3}{\mu} = 2.78 \times 10^{-9} \tag{46}$$

$$A = \frac{\varepsilon d_h^2}{K_1} = 298 \tag{47}$$

$$\frac{\rho}{K_2} = 2.95 \times 10^4 \therefore K_2 = \frac{2.95 \times 10^4}{\rho} = 4.15 \times 10^{-5} \tag{48}$$

$$B = \frac{\varepsilon^2 d_h}{K_2} = 17.2 \tag{49}$$

This then allows for the Dietrich model to be revised to equations (50), (51) and (52), using the new values for the Ergun constants.

$$\frac{\Delta P}{\Delta L} = 298\frac{\mu}{\varepsilon d_h^2}u + 17.2\frac{\rho}{\varepsilon^2 d_h}u^2 \quad (50)$$

$$d_h = 4\frac{\varepsilon}{S_v} \quad (51)$$

$$S_v = 2.87\frac{1}{d_{bub}}(1-\varepsilon)^{0.25} \quad (52)$$

This model was applied to samples 82, 82A, 83, 84, 84A and 88 using bubble diameters and voidages determined experimentally, resulting in the comparisons seen in Figure 83. As can be seen, these modelled values are significantly more accurate than any previously attempted model, with results in the same order of magnitude as the pressure drop data. Particularly accurate results were seen for sample 88, sample 84 and sample 82A. There exists some discrepancy for the other samples however. To determine if this is significant, the models are plotted again against the pressure drop results with the experimental error in gas velocity as seen in Figure 84, whilst models which take into account the ±0.01 error in voidage are plotted in Figure 85. As can be seen, the significant error in the superficial gas velocities means that the models are in better agreement with the experimental data than might have been previously thought. The error in voidage also results in significant variance in model results, particularly for the foams with higher voidages such as sample 82.

Sample 84A, shown in green in Figure 83, is significantly overestimated by the model compared to the non heat treated foams. The reason for this is not immediately clear but the foam properties shown in Table 27 for sample 84A compared to other samples show it to have a very small bubble diameter for its comparative voidage, compared to sample 82. As a result, given the fact that the model is very sensitive to changes for high voidage samples it is possible that uncertainties in the bubble diameter have lead to inaccurate modelling. It is unlikely to be due to changes in the foam geometry due to the heat treatment process as sample 82A is very well modelled by the modified Dietrich model.

Table 27: Bubble diameter, window diameter and voidage for the modelled foam samples.

Sample number	Bubble diameter (m)	Window diameter (m)	Voidage (dimensionless)
82	3.03×10^{-4}	1.01×10^{-4}	0.904
82A	2.74×10^{-4}	7.34×10^{-5}	0.915
83	4.05×10^{-4}	1.43×10^{-4}	0.873
84	3.49×10^{-4}	1.12×10^{-4}	0.892
84A	2.61×10^{-4}	9.42×10^{-5}	0.908
88	4.16×10^{-4}	1.75×10^{-4}	0.894

The model is effective in modelling both heat treated samples and non-heat treated samples well, with agreements and discrepancies being seen in both types of samples. This is an encouraging result and expected as the foams remain geometrically similar both before and after treatment and as a result should behave in a consistent manner with changes being due to the differences in their physical properties instead of a significant difference in morphology.

The model itself also has flaws which can introduce errors. The constants of 2.87 and 0.25 in equation (52) were found by Dietrich by an empirical curve fitting technique to fit an alumina foam to specific surface area data found via means of magnetic resonance imaging. As previously discussed, the alumina foams have a significantly different morphology to the PU-13X foams used in this work, but the MRI based technique could not be practically replicated in this work. As a result the values of Dietrich were used without modification which is likely to have introduced inaccuracies in the model. One particular discrepancy between the models and the measured results is in how the models tend to the origin, whilst some of the measured data, such as sample 82, does not. Due to the significant errors in the superficial velocity (Figure 69), and the lack of a rational basis for pressure drop existing without flow, this offset was viewed at being due to experimental error and was not considered for inclusion into the model.

The model developed is sufficiently accurate to use in sensitivity modelling to provide input on the relevant design parameters for effective low pressure drop foams which occurs in the following section.

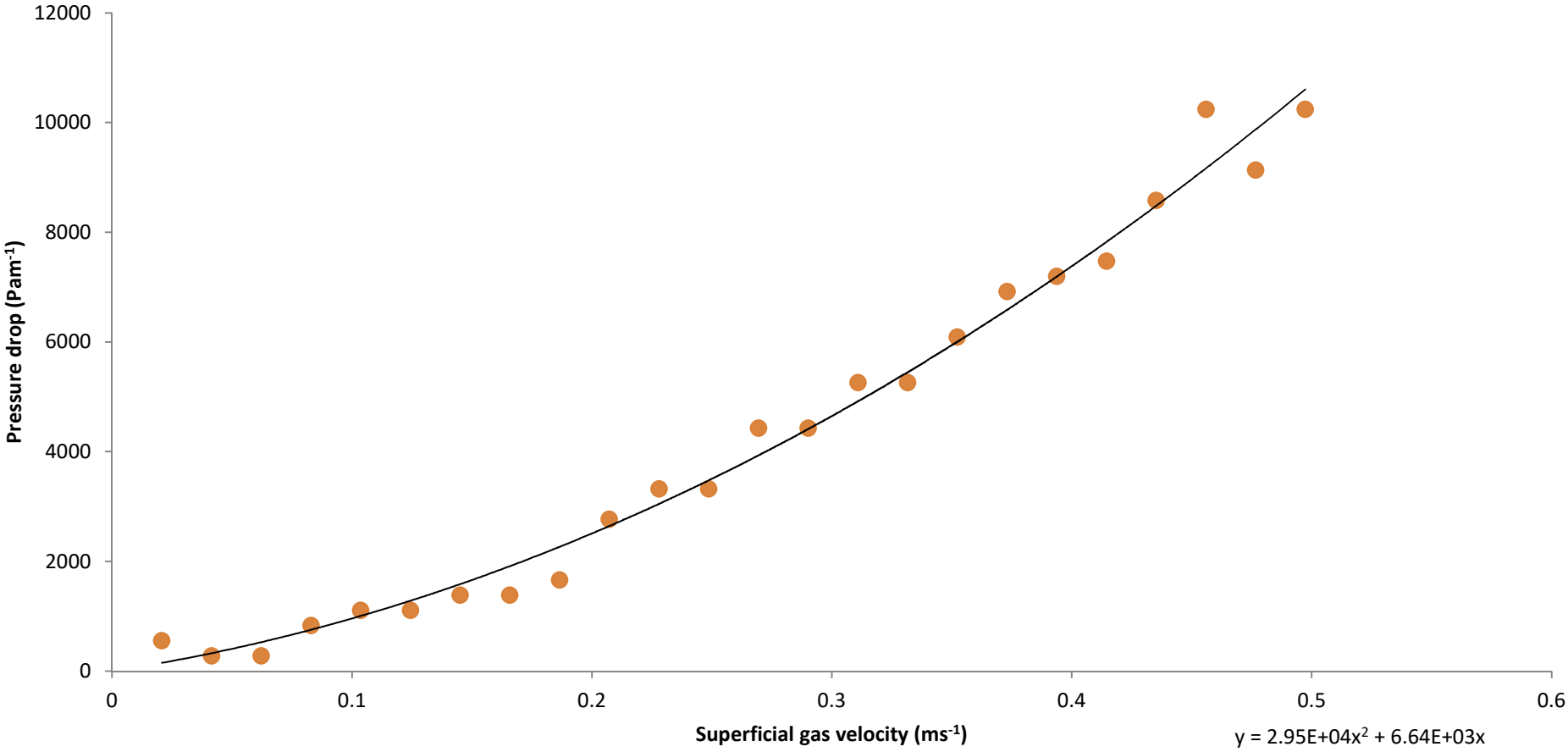

Figure 82: Pressure drop profile for sample 77 (75 wt%, no catalyst, ε=0.85, d_b=5.18x10^{-4}m) with fitted second order polynomial shown as used to calculate Ergun constants for the modified Dietrich model.

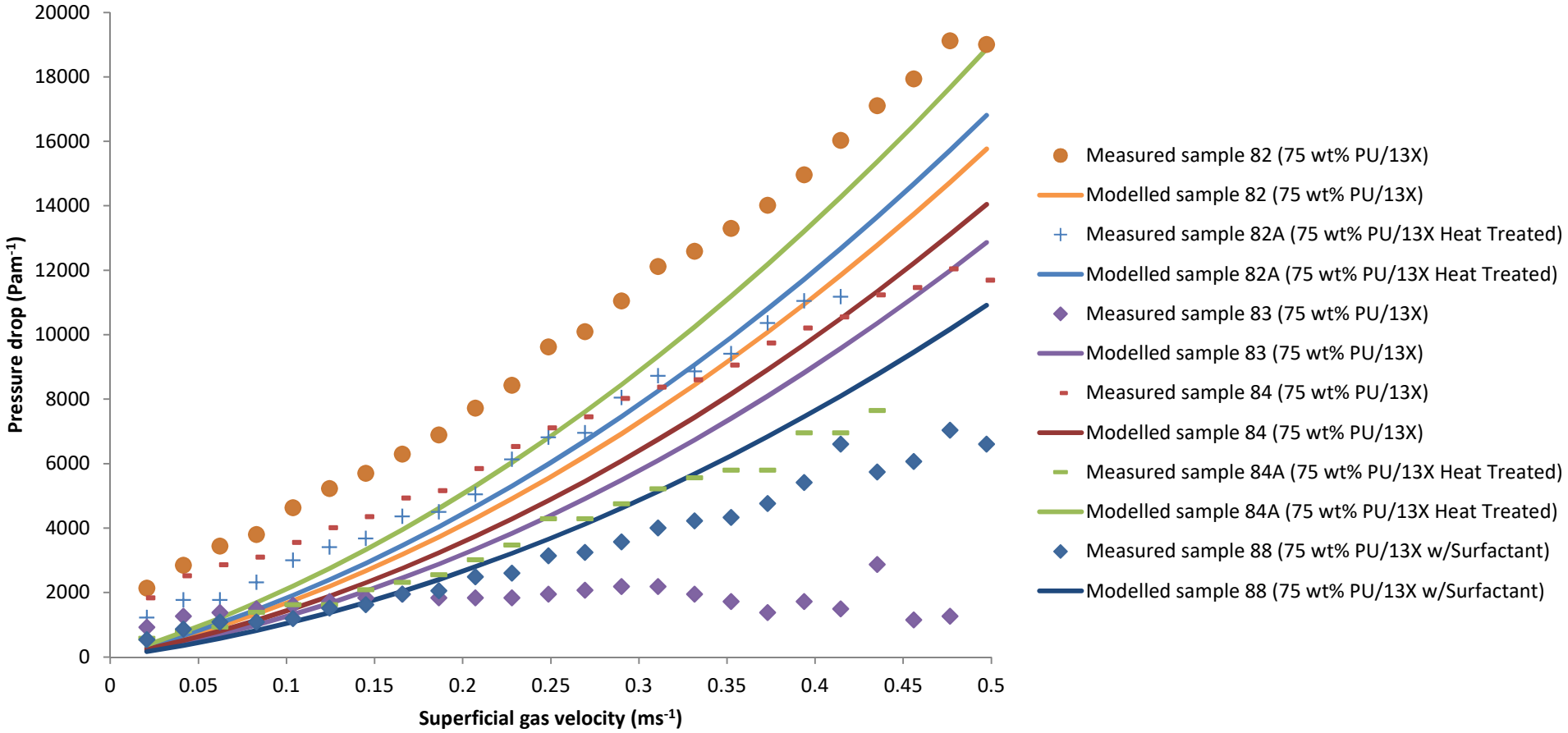

Figure 83: Dietrich models for foams of samples 82, 82A, 83, 84, 84A, and 88 using the specific surface area as calculated by Dietrich with revised Ergun constants as calculated in this work with voidage measured via experiment plotted against experimental pressure drop data for these materials.

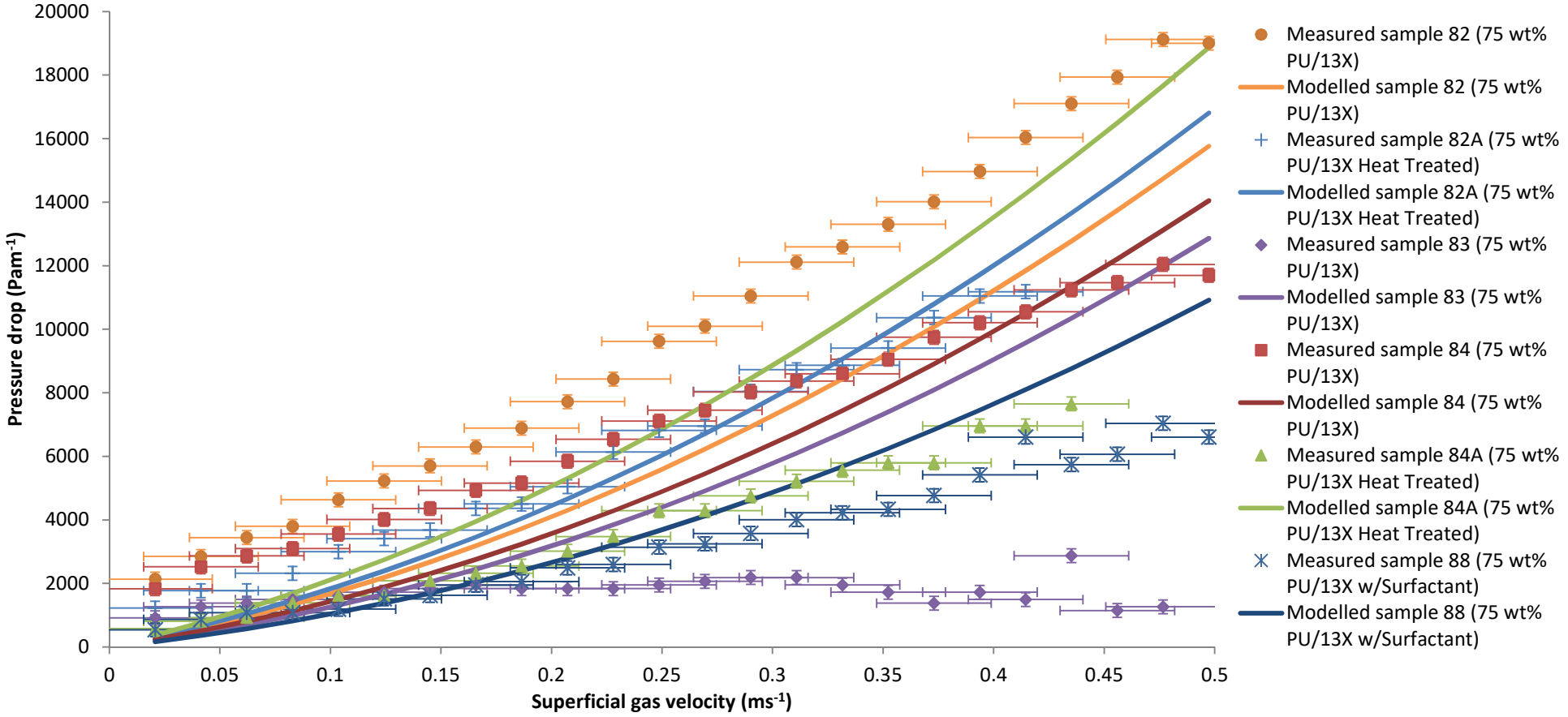

Figure 84: Dietrich models for foams of samples 82, 82A, 83, 84, 84A and 88 using the specific surface area as calculated by Dietrich with revised Ergun constants as calculated in this work with voidage measured via experiment plotted against experimental pressure drop data for these materials with pressure drop experimental data bars.

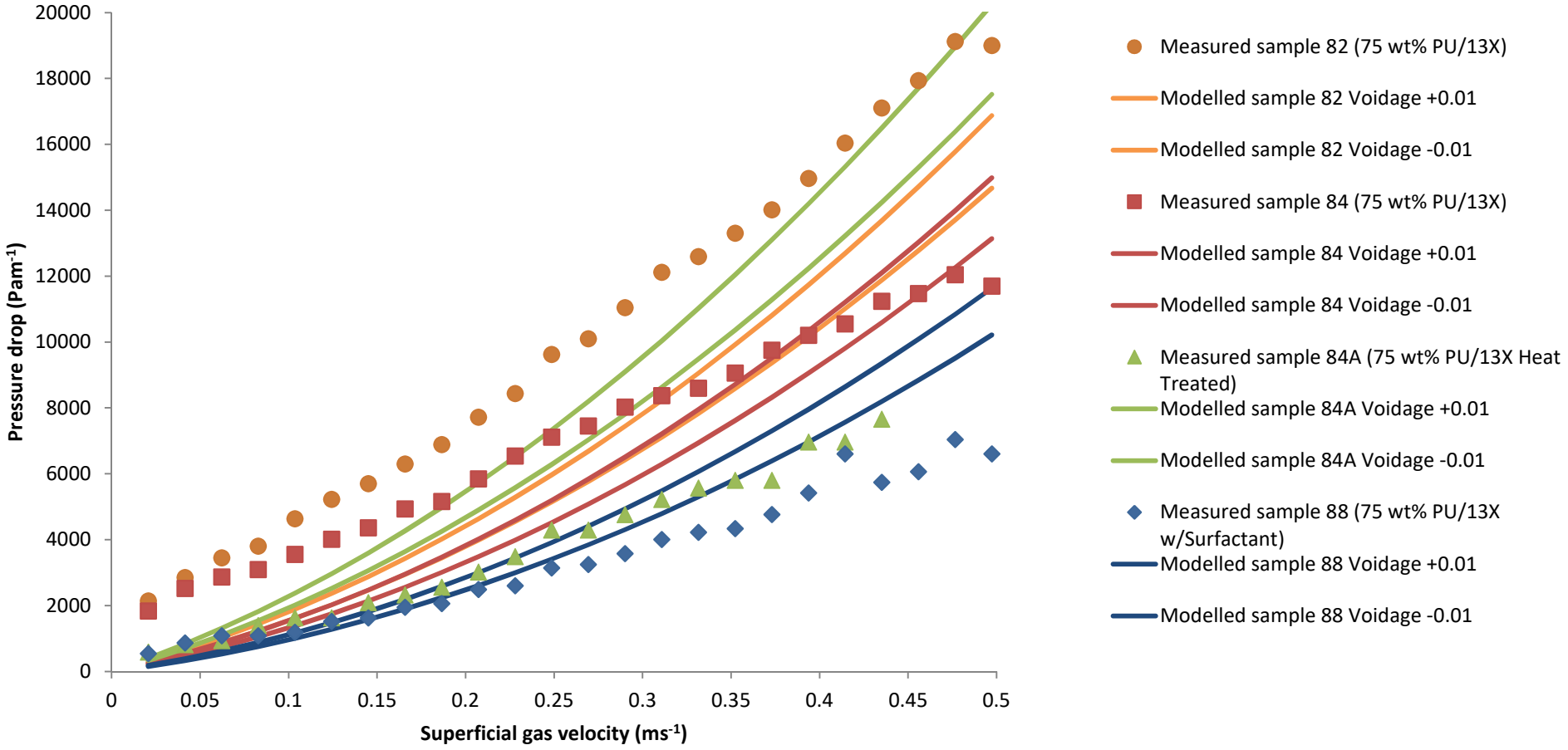

Figure 85: Dietrich models for foams of samples 82, 84, 84A, 88 using the specific surface area as calculated by Dietrich with revised Ergun constants and voidage measured via experiment plotted against experimental pressure drop data for these materials showing model variance due to voidage errors.

4.3.6 Sensitivity analysis of the modified Dietrich model

The previous section developed an effective model for pressure drop through PU-13X foams in the form of the modified Dietrich equation shown below in equations (53), (54) and (55).

$$\frac{\Delta P}{\Delta L} = 298\frac{\mu}{\varepsilon d_h^2}u + 17.2\frac{\rho}{\varepsilon^2 d_h}u^2 \quad (53)$$

$$d_h = 4\frac{\varepsilon}{S_v} \quad (54)$$

$$S_v = 2.87\frac{1}{d_{bub}}(1-\varepsilon)^{0.25} \quad (55)$$

As can be seen in these equations the pressure drop is highly dependent on the voidage and bubble size of the modelled foams due to the ε^2 and d_h^2 terms, a fact supported by the pressure drop analysis. A sensitivity analysis is therefore performed in order to determine what magnitude of effect these physical characteristics of the foam have on its overall pressure drop behaviour. This was performed using voidage and bubble size data from samples 82, 84, 84A, and 88 and varying the voidage by $\pm$0.05 and the measured bubble size by $\pm$10% of the experimental values. The resulting modelled data was plotted and compared to experimental pressure drops for these samples, resulting in Figure 86 and Figure 87.

The figures clearly show that voidage is the most significant variable in the pressure drop model as relatively small changes in voidage of $\pm$0.05 lead to changes in the modelled pressure drops of up to +28.5%/-37.4% of the unmodified model. This non linear dependence of the pressure drop on voidage is particularly important when the pressure drops of the thermally treated foams are considered as it explains their improvement in pressure drop despite the reduction in their bubble and window sizes. There is also a significant change in pressure drop when the bubble size is varied (Figure 87) which is also slightly non linear with pressure drop varying by +14.2%/-12.7%. The change in modelled pressure drops were more consistent when varying the bubble size compared to when voidage was varied. Foams with voidage values of 0.9 or higher showed extremely large changes in pressure drop compared to foams with lower initial voidage.

Table 28: Bubble diameter, window diameter and voidage for the modelled foam samples.

Sample number	Bubble diameter (m)	Window diameter (m)	Voidage (dimensionless)
82	3.03×10^{-4}	1.01×10^{-4}	0.904
82A	2.74×10^{-4}	7.34×10^{-5}	0.915
83	4.05×10^{-4}	1.43×10^{-4}	0.873
84	3.49×10^{-4}	1.12×10^{-4}	0.892
84A	2.61×10^{-4}	9.42×10^{-5}	0.908
88	4.16×10^{-4}	1.75×10^{-4}	0.894

Table 28 shows the bubble diameters, window diameters and voidage for the foams used to model the pressure drop behaviour. In all of the cases the heat treated foams showed lower pressure drop than their non-treated counterparts, despite having smaller bubble and window diameters. The improved pressure drop is therefore due to their higher voidage, and the mechanism behind this is the high sensitivity to voidage shown in Figure 86.

This sensitivity to voidage provides a method of improving the design of the foams, as both voidage and the bubble diameter can have significant effects on pressure drop. As these can be varied independently of each other to a limited extent during the foam production process, the pressure drop of the foams can be controlled in their design. An example of this is in sample 88. This formulation used a 75wt% foam with the addition of silicone oil to supress the foam formation and lower the voidage, but its large bubble size means this has not caused higher pressure drop behaviour but instead allowed for a coarser foam to be made.

This is desirable as lower voidage foams allow for more adsorbent to be packed into the same volume of foam, which increases their overall effectiveness at providing respiratory protection, provided that it can be done without disproportionately increasing the pressure drop. Larger bubble sizes can be used to compensate for this reduction in voidage and porosity, and correspond with foams which have been allowed to foam longer before solidifying.

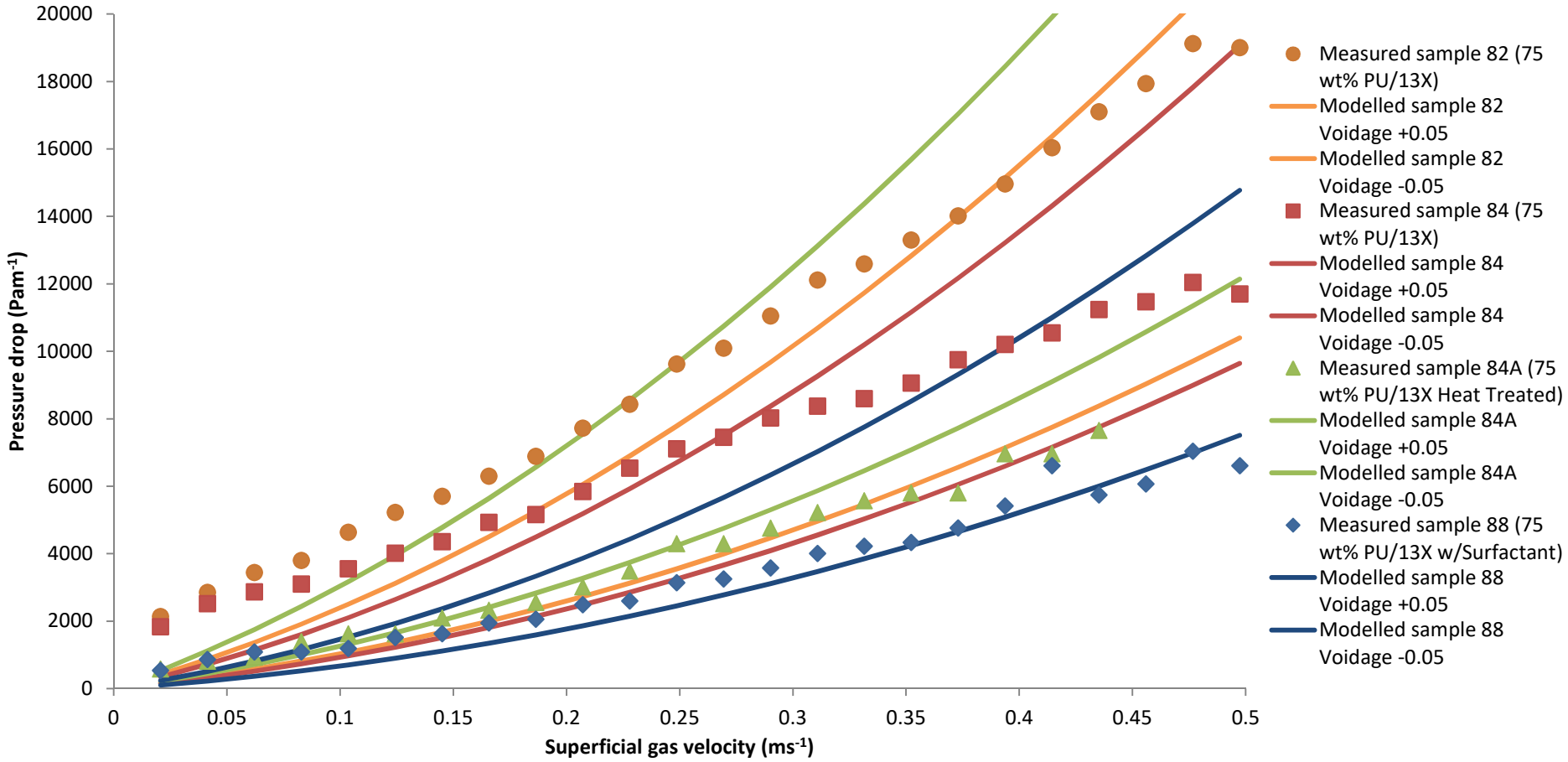

Figure 86: Modified Dietrich models for foams of samples 82, 84, 84A, 88 showing effects of varying input voidage plotted against experimental pressure drop data for these materials showing model sensitivity.

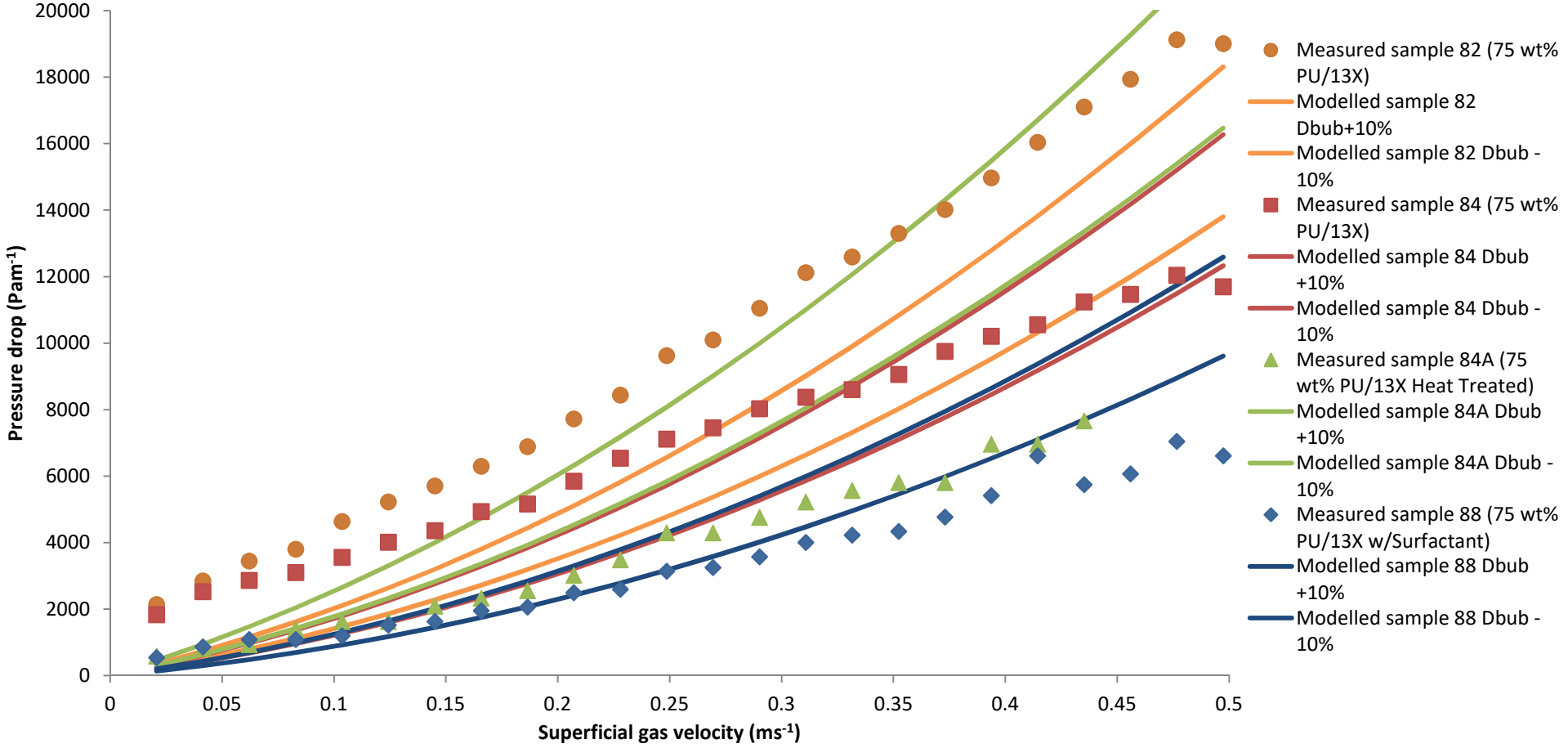

Figure 87: Modified Dietrich models for foams of samples 82, 84, 84A, 88 showing effects of varying input bubble diameter plotted against experimental pressure drop data for these materials showing model sensitivity.

4.4 Conclusions

In this Chapter, techniques were developed and implemented for the physical characterisation of foam materials against the existing materials of 13X beads. Helium pycnometry was implemented successfully to find voidage for the produced PU-13X foams. SEM based photographic techniques were developed and applied to estimate the bubble size without the need for slow and costly 3D measurement techniques and directly measure the window sizes of the PU-13X foams. This could be performed over a large number of bubble cross sections to compensate for the natural range of bubble sizes in chemically blown polymer foams.

Pressure drop measurements were taken for a variety of heat treated and non heat treated foams as well as 13X adsorbent beads and carbon granules. Heat treated PU-13X foam materials showed marginal improvements over the 13X adsorbent beads. Heat treated foams showed improved pressure drop behaviour than their non-treated precursors in all cases, behaviour which was linked to the improvement in foam voidage caused by the thermal treatment process.

Using the physical characteristic data as well as the pressure drop data, the models published in the literature by various authors were applied to the foams in this work to determine how the pressure drop of the foam materials could be predicted and controlled. The published literature models were found to fit the experimental data poorly due to differences in the geometric models used in the literature based on highly open celled metal foams, which did not reflect the more tortuous geometry of the PU-13X foams produced in this work. Modelling difficulties were also compounded by significant experimental errors in the superficial gas velocity and a high sensitivity of the models to voidage in the 0.85-0.95 range of voidage the experimental materials occupied, which amplified any errors in the measured voidage.

Models which were based very rigorously on a geometric model of foams were found to model the PU-13X foams very poorly, but models which used a more empirical curve fitting approach had an improved fit which could be used for further development of their performance by repeating the curve fitting procedure for foams produced in this work. As a result a successful model for the PU-13X foams was found in a modification of the Dietrich model, which recalculated the Ergun constants for the Dietrich equation using the same

technique as described by the authors of fitting to a pressure drop curve for the PU-13X system. This was then applied successfully to the experimental dataset used for the modelling work with good agreement with the experimental data.

Sensitivity modelling on the modified Dietrich model as well as comparisons between various foam results concluded that the superior pressure drop characteristics of the foams, particularly the heat treated foams, were a result of the superior voidages of the foams compared to adsorbent beads. This conclusion was supported by the superior pressure drop shown in activated samples which had a noted increase in void fraction and decrease in bubble diameters from the heat treatment process. Bubble diameter was also found to have a significant influence on the pressure drop of the foams, though less than that of voidage. This allows for the design of the foams to be improved by balancing one variable against the other, with denser but coarser foams able to offer comparable pressure drop to foams with higher voidages and smaller bubble sizes, which can be achieved by control over the foam formulation and production process. This allows for foams to be allowed to foam more before polymerising, resulting in a foam with improved overall adsorption uptake.

5 Measurement and analysis of adsorbent mass fraction, equilibrium uptake and kinetic uptake behaviour

5.1 Introduction

In this Chapter the techniques used to analyse adsorbent behaviour of the foams are introduced, developed and used to provide data for further analysis of the adsorbent foams produced, and allow them to be compared to commercial 13X adsorbent beads.

Thermogravimetric analysis (TGA) techniques are developed and employed for PU-13X foams to allow for the true mass fraction of 13X inside the produced foams to be measured, in order to evaluate how much adsorbent was within the material to allow for analysis of how accessible to adsorptive it was in conjunction with isotherm data.

The technique used for determining adsorption isotherms is introduced and described, providing various isotherms for produced adsorbent foam samples, as well as for precursor 13X powder. This was used to provide data for determining how accessible the adsorbent within the PU-13X foams is to adsorptive gases in the bulk phase.

The technique for acquiring dynamic adsorption breakthrough curves for the foams is also developed and described, and is used to give an insight into the kinetic behaviour of the produced adsorbent foams in comparison to 13X adsorbent beads. As part of this analysis, SEM techniques for measuring the skin thickness of non-heat treated and heat treated foams are also developed and implemented to investigate the effects of the heat treatment process on the kinetic adsorption behaviour of the foams.

The data gathered from the techniques is then used to analyse the adsorbent behaviour of the samples to determine which formulations offer the best adsorptive accessibility within the structure, and how well their adsorption uptake compares with existing materials, as well as providing some insight into techniques which can be used to improve this.

5.2 Measurement and analysis of adsorbent content, uptake and uptake behaviour in foam materials and beads

5.2.1 Measuring adsorbent content of the foams

In Chapter 3, various foam formulations were discussed in terms of their adsorbent loading. This loading was determined via a mass balance of the ingredients, and assuming that all the solvent was removed from the resulting polymer matrix. However, the validity of this assumption requires testing if these values are to be used to assess the adsorbent accessibility of the resulting material.

As a result of this uncertainty, it was necessary to develop a technique to accurately measure what proportion of any particular sample was 13X adsorbent in a form as would be used in further testing, i.e. after any post-processing stages. The technique chosen to do this was thermogravimetric analysis (TGA). Thermogravimetric analysis is the measurement of the effects of the exposure of a material to a chosen temperature profile on the mass of the sample, and can be conducted in either flowing air or an inert atmosphere as desired.

TGA was chosen as the technique because of the nature of the samples in the form of PU-13X composites, chosen for analysis due to their ease of heat treatment. Due to this choice of materials, it was theoretically possible to remove the polymer fraction via oxidation, whilst leaving the 13X fraction untouched by the process, save for being degassed of any adsorbed compounds. By measuring the mass after the TGA process, the true adsorbent mass fraction of the foams could then be calculated.

5.2.1.1 Thermogravimetric analysis methodology

In the apparatus used in the research, a Setaram TG-92 thermogravimetric analyser (Figure 88), a section of the sample (approximately 15 mg) which is desired to be tested is placed into an alumina crucible which has been previously calibrated against an empty crucible on the other side of a balance. This sample is then weighed on the balance which is itself suspended and lowered into the furnace. Once inside, the furnace then heats up to a temperature as chosen by the user for the desired length of time. Gas can also be introduced into the furnace during heating, and in this case compressed air is used to allow for a supply of oxygen for oxidation. The weight of the sample and the temperature of the furnace are measured and recorded in real time, as well as the heat given off or taken up by the sample.

Figure 88: TGA apparatus as used in the research.

5.2.1.2 Development of TGA profiles

In order for TGA to be used to calculate adsorbent mass fractions of the foams it was necessary to develop a temperature profile which would allow for the polymer to be fully removed. This development was done with pure polyurethane foam synthesised using the same chemistry as used to make the PU-13X composites.

The first step to developing a thermal profile was simply to expose samples of pure polyurethane foam and 13X powder separately to a rising temperature profile as seen in Figure 89 and examine the resulting TGA profiles for each material, particularly the rate of heat flow into or out of the sample. This would allow for the determination of temperatures at which mass loss occurred, and guide further development.

Figure 90 shows the TGA data acquired from imposing the profile in Figure 89 to a 13X powder sample. In the figures it can be seen that the sample mass of 13X steadily declines with the increasing temperature until reaching a constant mass at a temperature of 400^{o}C.There is an initial peak of heat inflow into the sample at 100^{o}C associated with sample drying, followed by a significant inflow of heat into the 13X sample at 200^{o}C, higher than the heat inflow seen at other temperatures, which corresponds with mass loss in the sample. This means that the sample is absorbing more heat than is required to raise its temperature if it were an inert mass and is thus undergoing a physical or chemical process

which requires heat input to occur. Due to the endothermic nature of this mass loss, it can be concluded to be a result of desorption of compounds from the 13X powder. These compounds are most likely to be atmospheric moisture held in the 13X which is released by the absorption of heat into the 13X powder. It can be concluded that once the sample has reached 400°C however that none of these compounds remain and that it is fully regenerated and all the mass that remains is 13X. The rate of mass loss was greatest in the temperature range of 200°C to 300°C, which indicates most desorption is occurring in this region, which is supported by the high values for heat flow into the sample associated with this.

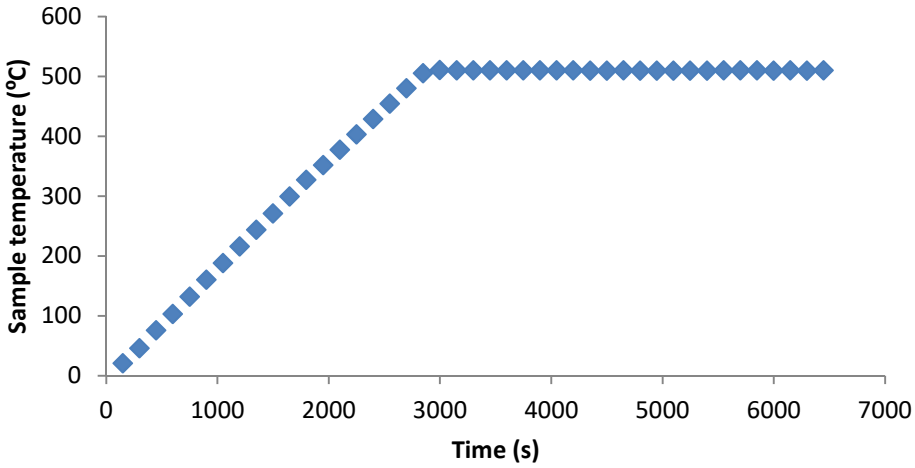

Figure 89: Thermal profile used for initial TGA experiments.

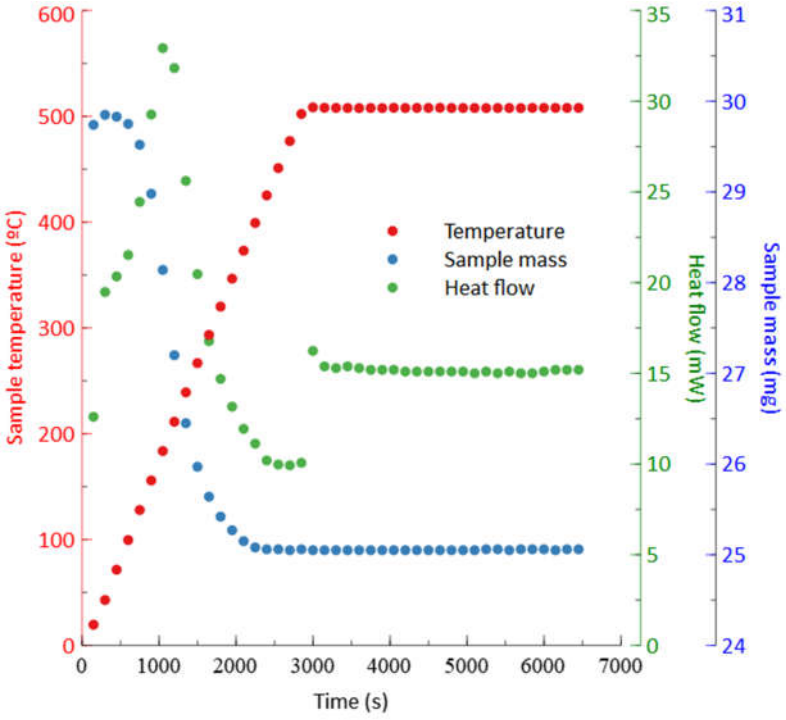

Figure 90: A TGA profile of pure 13X powder, relating sample mass to temperature and heat flow into the sample.

A TGA investigation was also performed using the thermal profile in Figure 89 for a sample of pure polyurethane foam, manufactured using the same formulation as for the composite foams, resulting in the TGA profile seen below in Figure 91.

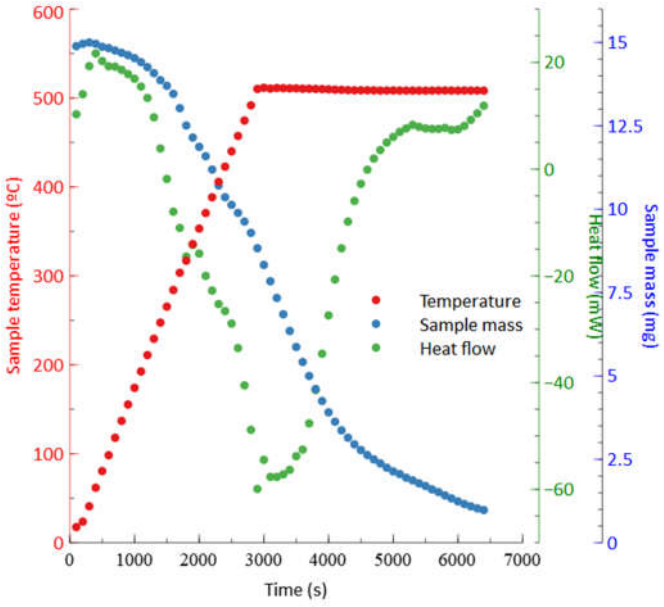

Figure 91: A TGA profile of pure PU foam, relating sample mass to temperature and heat flow into the sample.

As can be seen in Figure 91, the mass of PU declines with increasing temperature, increasingly so once the sample temperature reaches 300°C. However the most significant decline can be seen to happen at 500°C as this is where the heat flow given off by the sample is highest. This indicates that combustion of the PU is happening mostly around this point, as this heat output is also associated with mass loss. The heat flow into the sample has an initial peak at 100°C associated with drying of moisture before remaining stable until the sample begins losing mass at 200°C which is a temperature where polyurethane begins to thermally degrade. The sample then begins giving out heat strongly as it loses mass until the sample reaches constant mass, and the heat flow declines with the decline in mass loss until reaching a constant rate at 500°C.

Due to the temperatures needed to cause desorption of adsorbed compounds on 13X and combustion of PU discovered in the preliminary experiments, the chosen TGA profile used to investigate actual PU-13X samples used two different temperatures to support both processes; first raising the sample to 200°C to degas the 13X within the sample, followed by raising the temperature to 500°C to burn off the PU fraction of the material. The chosen temperature profile is shown in Figure 92.

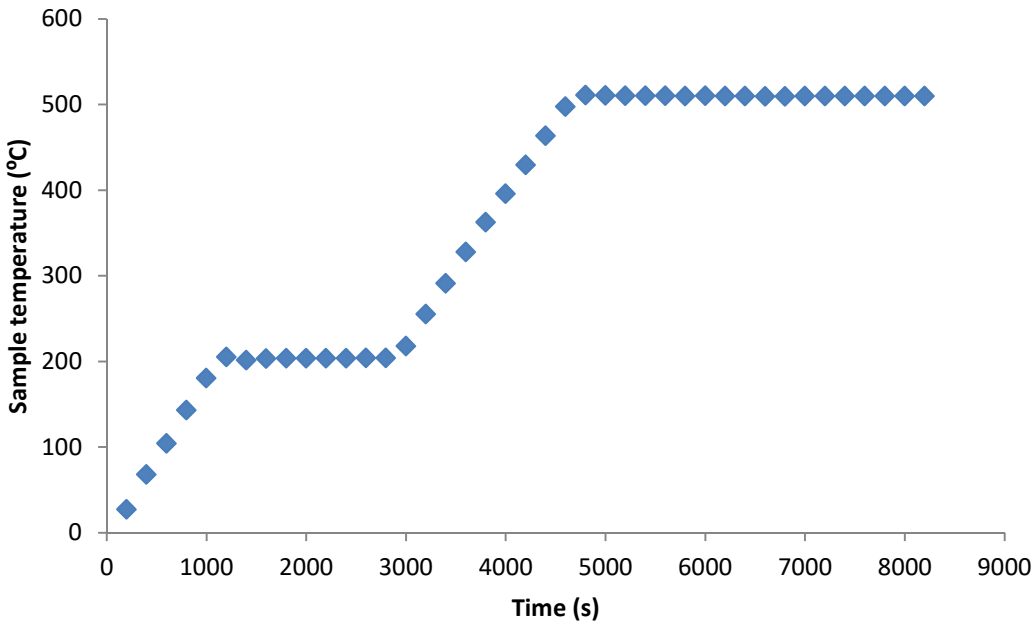

Figure 92: Thermal profile used for TGA experiments with degassing step for 13X.

By using this profile, the mass of active adsorbent within the material can be calculated as a fraction of the total material, whilst also accounting for the weight of adsorbed gases onto the 13X.

5.2.2 Measured adsorbent mass loading of the produced materials

Applying the test profile developed in the previous section to a sample of PU-13X foam, in this case from sample 82, results in a typical TGA profile as seen below in Figure 93, where the behaviours of both the 13X degassing and PU combustion can be seen happening in turn. As can be seen in the figure, there is an initial peak in heatflow into the sample at 100°C associated with moisture drying, followed by a steady increase of heat into the sample at 200°C as the zeolite in the sample is degassed. As the temperature is increased from 200°C to 500°C the sample then gives off a large amount of heat as the polyurethane fraction combusts, which slowly decreases as the sample stops losing mass until reaching a steady state at 500°C where only fully activated 13X remains.

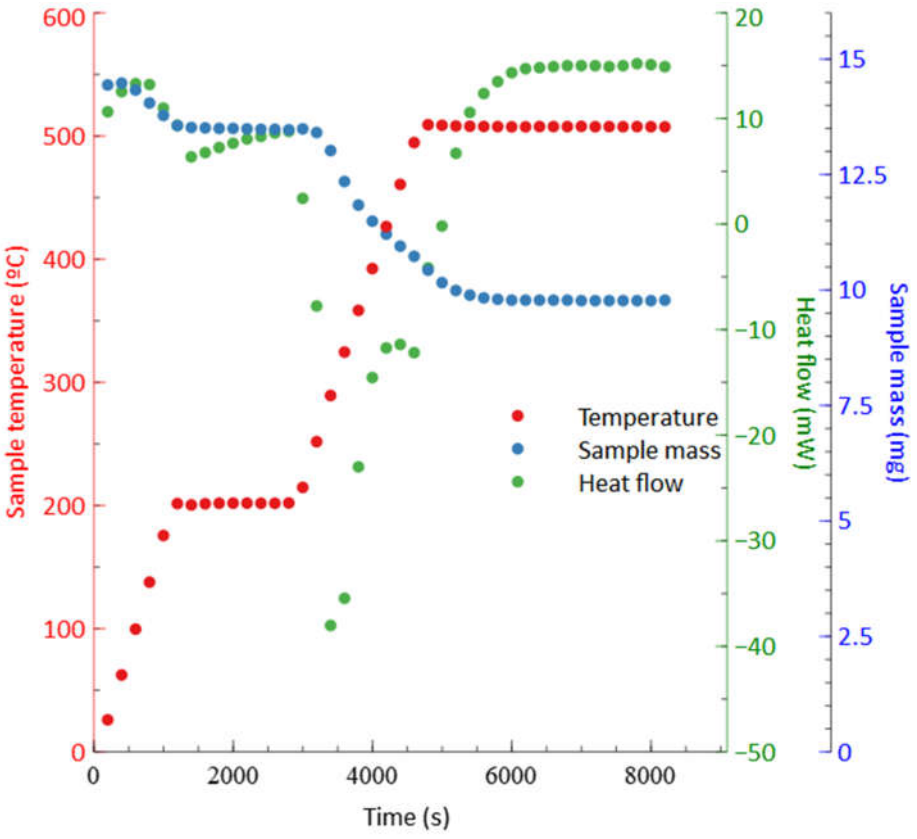

Figure 93: A TGA profile for sample 82 showing sample mass as a function of temperature and heat flow into the sample.

In order to calculate the mass fraction of 13X from this TGA data, the mass of the sample is recorded at the end of the degassing step, as the temperature is held at 200°C, and then also recorded at the end of the experiment after being held at 500°C. In the case of Figure 93 this results in the following:

$$\frac{\text{End Mass}}{\text{Dry Mass}} = \frac{9.77}{13.47} \times 100 = 72.5\% \tag{56}$$

This is a slightly lower mass fraction than would be predicted by mass balancing of the formulation (Table 29). Assuming all the liquid components (water, NMP, triethanolamine, dibutyltin dilaurate) are removed by the drying process, the resulting material comprises only of polyethylene glycol, PMDI and 13X powder. The mass fraction can be estimated by mass balancing then as follows:

$$\frac{\text{13X Mass}}{\text{Total Mass}} = \frac{30\text{g}}{5\text{g}+30\text{g}+5\text{g}} = \frac{30\text{g}}{40\text{g}} = 75\% \tag{57}$$

As can be seen, equation (56) predicts a slightly lower 13X mass fraction than equation (57). This could be due to adding more PMDI than the formulation required, which was possible due to the sticky and difficult to measure consistency of the PMDI, or moisture uptake on the 13X powder during manufacture causing it to seem as though more 13X was present than was actually added to the mixture. Both of these can cause the mass balance in equation (57) to overestimate the amount of 13X present compared to the TGA technique in equation (56), which only considers 13X after the desorption of compounds from the 13X and combustion of the polyurethane fraction of the foam.

Table 29: Experimental formulation for sample 82.

Component	**Amount**
Polyethylene glycol	5g
Water	0.5 ml
Triethanolamine	3 drops
Dibutyltin dilaurate	0.025ml
NMP	42 ml
PMDI	5g
13X	30g

Various samples of PU-13X foams were analysed using the TGA technique developed and described in section 5.2.1. This resulted in the following true adsorbent mass fractions as shown in Table 30, with heat treated samples labelled with an A to distinguish them from their precursor samples. Predicted adsorbent mass fractions for heat treated samples were unavailable as it was not known how much polymer had been removed by the heat treatment process. The predictions for the mass loading via formulation for the non-heat treated foams were compared to their measured mass loadings via TGA in Figure 94. As can be seen here, there is good agreement between the predicted and measured mass fractions of 13X for the foam materials, with the mass balancing slightly overestimating the amount of 13X present, which makes the TGA technique reliable for measuring the mass fractions of the heat treated materials for which formulation predictions cannot be made. As a result it can also be concluded that the heat treatment of the foams is significantly increasing the mass fraction of 13X in the materials, which is likely due to the partial removal of the inert polymer fraction.

It can also be seen that the foam production process does have some degree of variance to it. In Table 30 it can be seen that there is a 3 wt% variance between samples 82, 83 and 84 which were made in the same conditions as part of the repeatability study. This shows the level of consistency and control that is possible in the foam production process, which is subject to some variance due to the previously mentioned difficulties in accurately metering the PMDI.

Table 30: TGA adsorbent mass fractions for various experiments compared to mass balance estimates.

Sample number	Predicted adsorbent mass fraction (via mass balance on formulation) (wt%)	Measured adsorbent mass fraction (via TGA technique) (wt%)
67	50	50.1
69	67	64.1
70	70	62.2
71	75	68.1
72	75	69.2
73	67	65.6
74	72	68.3
77A	-	82.5
78A	-	78.2
82	75	72.5
82A	-	92.3
83	75	69.4
84	75	69.7
84A	-	81.1

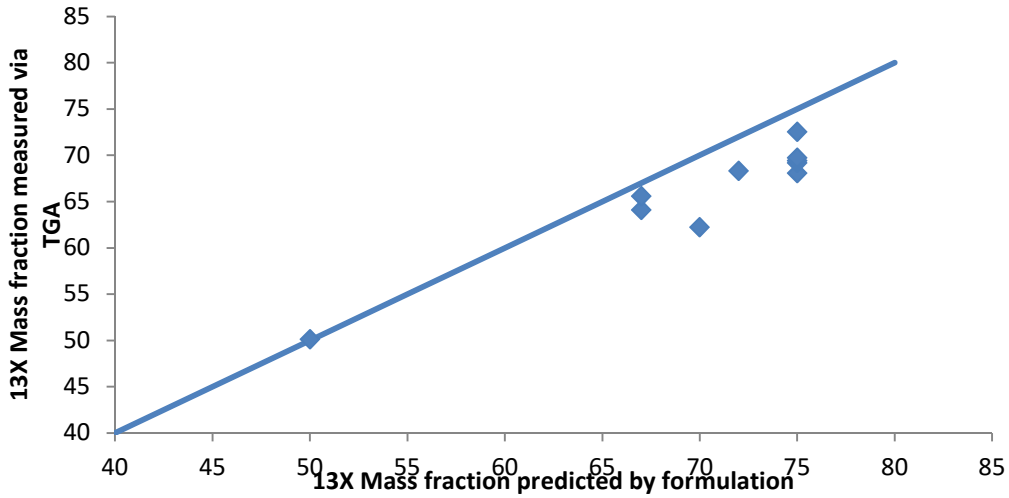

Figure 94: Predicted 13X mass fractions compared with TGA measured 13X mass fractions for non-heat treated samples listed in Table 30 plotted against a modelled line for equal measured and predicted mass fractions.

5.2.3 Measuring adsorbent activity of the foams

In order to judge the effectiveness of an adsorbent support, it is necessary to be able to measure the adsorption uptake behaviour of the materials as manufactured. In this work this is done by measuring the adsorption isotherms of the foams using a known reference gas and comparing this isotherm against an isotherm for unsupported precursor 13X adsorbent powder, and using the knowledge of the adsorbent content of the foams gained in the previous section.

Adsorption isotherm testing was chosen to evaluate the overall adsorption uptake of the materials because it offers excellent accuracy in measuring adsorption uptake, and requires extremely small sample sizes. As a result it can offer insight into adsorption uptake which may be missed in breakthrough testing where the dynamic nature of the testing can lead to adsorption uptake not being detected due to poor accessibility of the adsorption sites, or the slow sampling rate of breakthrough testing as performed giving large uncertainties in the total adsorption uptake for low breakthrough times. Isotherm testing was however very slow, taking up to several days for slowly equilibrating samples, and could only be performed on limited numbers of samples due to competition for equipment time. Isotherm testing also provides no insight into the dynamic behaviour of the adsorption process.

5.2.3.1 Isotherm methodology

Adsorption isotherms were measured at Dstl by Martin Smith via the use of a Dynamic Vapour Sorption (DVS) Advantage 2 apparatus, time on which was kindly provided by Dstl as part sponsors of the research. This method used a gravimetric technique to determine the maximum uptake of the chosen test gas onto a sample over a range of partial pressures in order to plot a full isotherm graph for the chosen test material.

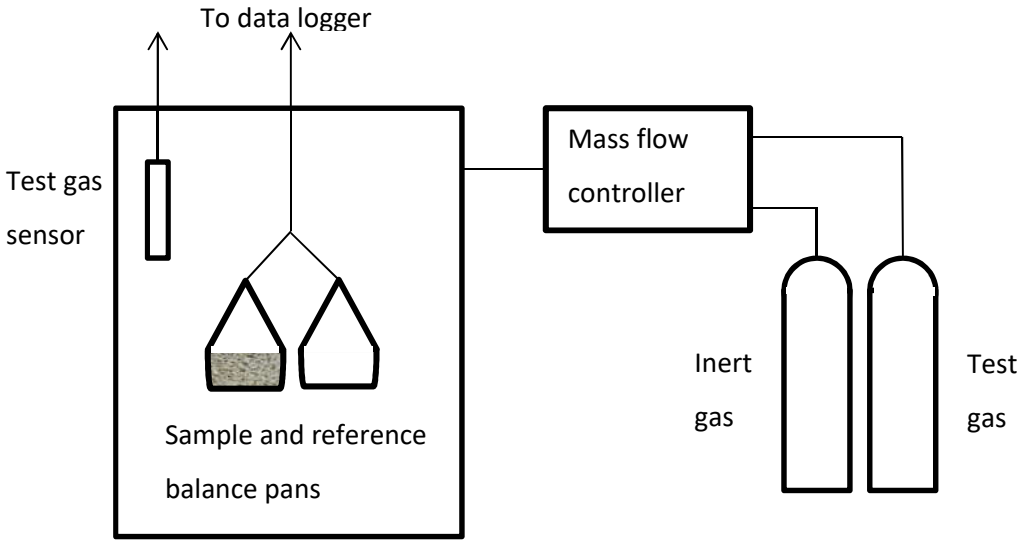

Figure 95: Schematic diagram of apparatus used for isotherm measurement.

In the experimental technique, samples were degassed prior to measurement by heating them to 200^{o}C under vacuum. The sample is first exposed to nitrogen used as an inert gas at a constant temperature inside the equipment (Figure 95) until the sample reaches a constant mass when it will have outgassed any other components that may have been adsorbed in transit. Once this has been achieved, the sample is exposed to an increasing partial pressure of the test gas, up to the critical pressure, which is achieved by mixing the test gas with the inert gas via the mass flow controller. At each point the sample is exposed to the test mixture until it reaches a constant mass which is then recorded. This also calculates the uptake of adsorbent onto the sample as a weight% based on the total sample weight including any inert fraction. This proceeds until the sample is exposed to the entire chosen range of test gas pressures. Optionally, it can also be exposed to lower partial pressures of test gas after reaching the critical pressure to examine desorption behaviour and to test for hysteresis.

The choice of test gas for the experiments was cyclohexane, a known respiratory hazard which was preferred by Dstl for its ability to be compared with a library of in house data on other materials. Foam samples were taken as a single piece from the centre of the produced foams without any skin, with a typical sample mass of 50mg. Isotherms were measured at 25^{o}C.

5.2.3.2 Adsorption isotherm results

The technique described in the previous section gives an isotherm in the typically seen graphical form, allowing for investigation and comparison of adsorption uptake under a variety of static conditions. A typical experimental data set is shown below in Figure 96, which displays an adsorption isotherm as measured for the 13X powder used in the manufacture of the foams being tested, as supplied by Brownell Ltd. This is compared to literature data for cyclohexane adsorption on faujasite (Nikolina *et al.* 1960), a natural form of a zeolite which can be synthetically made as 13X, showing excellent agreement between the published and experimentally acquired data.

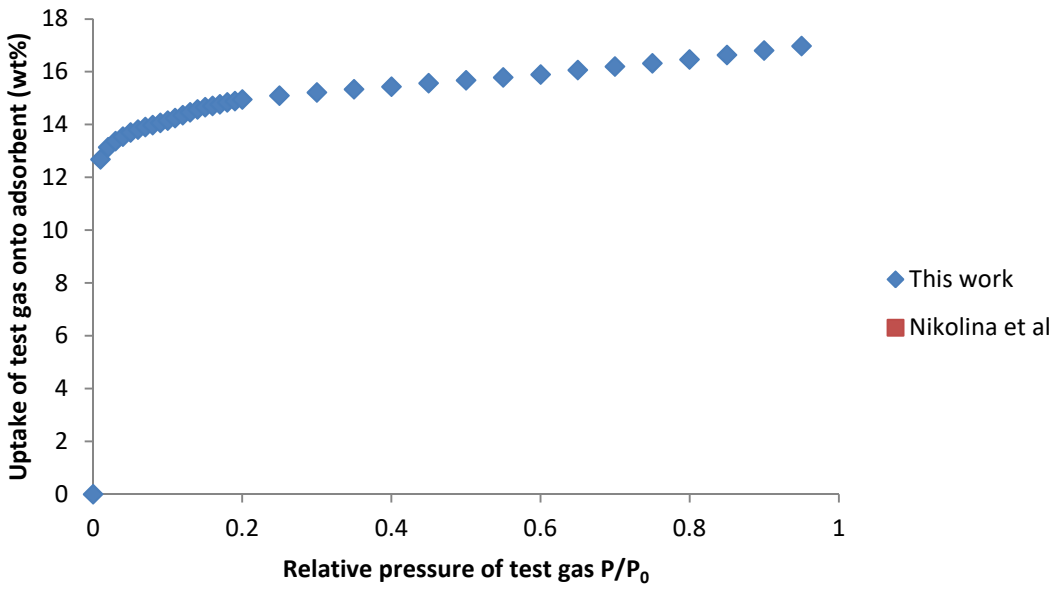

Figure 96: A set of measured adsorption isotherms for cyclohexane on 13X powder as used to make PU-13X foams compared to literature data for cyclohexane adsorption on faujasite (Nikolina *et al.* 1960).

This technique allows for the very accurate measurement of adsorption isotherms, with sample mass being measured to ±0.1μg and requires very small amounts of sample to perform, with as little as 1mg being sufficient (Surface Measurement Systems 2014), which results in a very reliable technique for finding adsorption data from the materials. Various PU-13X foams were measured for uptake of cyclohexane on a sample weight basis using this technique, as well as pure PU foam resulting in the isotherms seen in Figure 97.

As can be seen from the isotherms, the polyurethane support on its own has negligible adsorption uptake for cyclohexane and thus provides no benefit for the adsorbent materials beyond being a support. All the foams measured have a significantly reduced adsorption uptake compared to the 13X powder as well, which indicates that the polymer support is reducing the adsorptive accessibility of the 13X. Sample 72 showed extremely good uptake compared to other foams with 75 wt% of 13X, but as this result could not be repeated or replicated with other foams of the same formulation this result must be concluded to be anomalous.

Heat treated foams show better uptake than the non treated foams, suggesting that the heat treatment process is improving the uptake of the samples, as can be seen in the increase in isotherms between sample 86 and 86A and how sample 77A has a greater uptake than non heat treated samples of similar 13X content. This is further analysed quantitatively in the following section, using the adsorbent loading data from TGA.

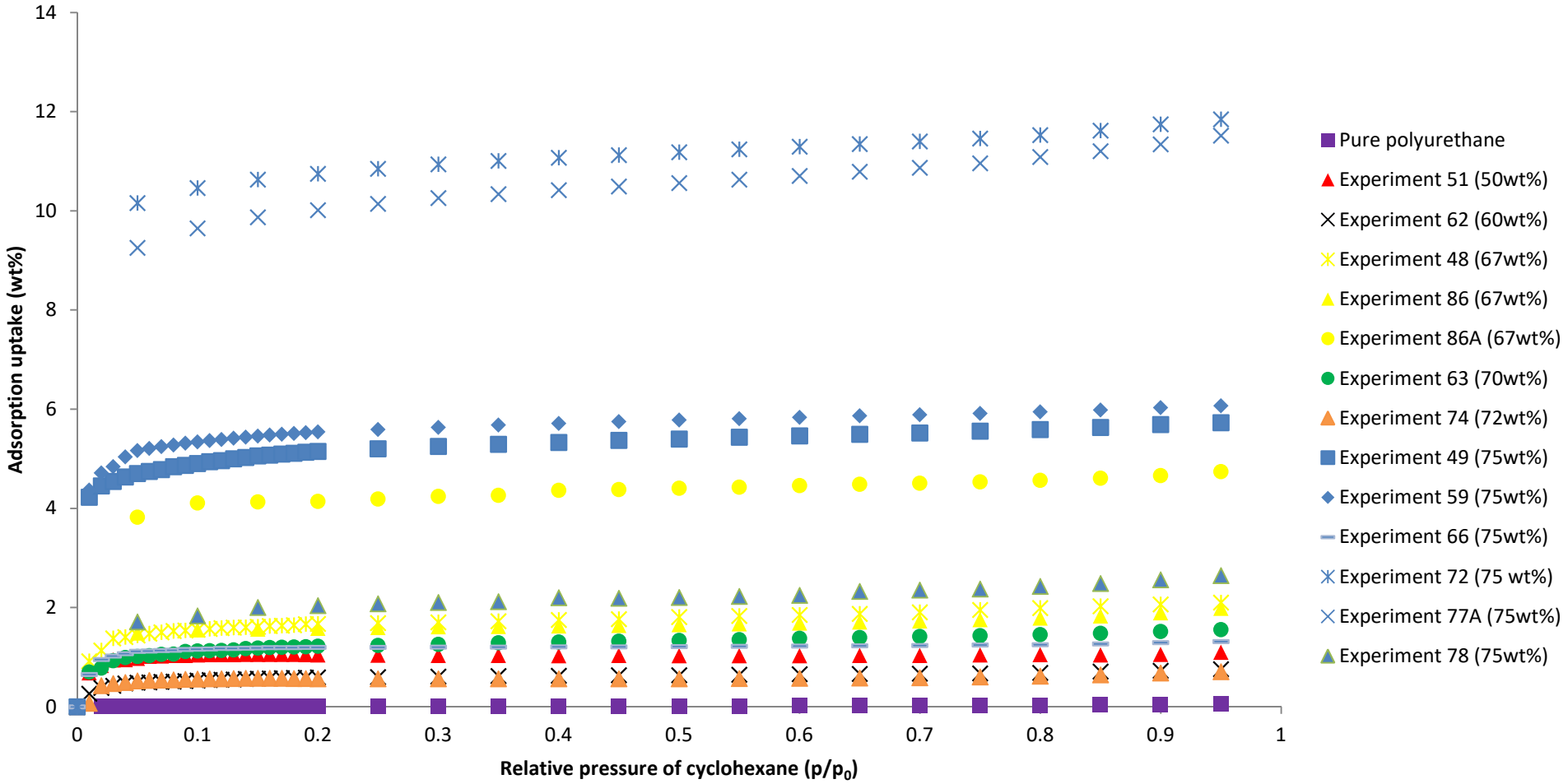

Figure 97: Isotherms measured for various PU-13X samples and pure PU foam.

5.2.3.3 Calculating adsorbent accessibility within unmodified produced foams

In order to analyse the effectiveness of polymers as a support for the adsorbent, the adsorptive accessibility of the adsorbent whilst contained within the support material must be known. The isotherms in the previous section confirmed that the polyurethane fraction of the foams has negligible adsorption uptake. As a result, the accessibility of the 13X could be analysed by comparing the measured isotherms of PU-13X foams to modelled isotherms of 13X which are calculated assuming only a certain percentage of the 13X uptake is present. This comparison allows for how much of the 13X in the foam has adsorptive accessibility to be calculated.

Using the 13X mass fraction values as calculated via mass balance of the formulations for the relevant experiment, due to an incomplete data set of true mass fractions from TGA, isotherms for 13X powder were plotted for 50%, 60%, 67%, 70%, 72% and 75% of the measured adsorbent isotherm for 13X powder with cyclohexane. These modelled isotherm values were then compared against measured isotherms for real samples with equal 13X mass fractions to find the adsorptive accessibility of the 13X adsorbent. This resulted in the comparisons in Figure 98.

Figure 98 shows modelled isotherms for 50%, 60%, 67%, 70%, 72% and 75% of the measured isotherm of pure 13X powder as well as measured isotherms for foams of these mass fractions calculated via formulation which provides the data for the calculation of accessibility. An isotherm is also shown for pure polyurethane synthesised using the same chemistry as for the PU-13X foams in order to determine if any adsorption uptake was due to the polymer and not the 13X. The adsorption uptake of the polyurethane support was found to be negligible (Figure 98), and thus using this data, the total fraction of 13X which was accessible in a sample could then be calculated as follows (shown for sample 86):

$$\text{Accessibility (\%)} = \frac{\text{Uptake of sample (wt\%)}}{\text{Uptake of 13X powder} \times \text{Weight loading (\%)}} = \frac{1.79}{16.5 \times 0.67} = 16.3\% \quad (58)$$

The accessibility varied over the range of the isotherm depending upon the pressure chosen for comparison, so for comparison purposes between samples accessibility was calculated at relative pressures of 0.25, 0.5 and 0.75 and an average value was also taken, resulting in the data seen in Table 31.

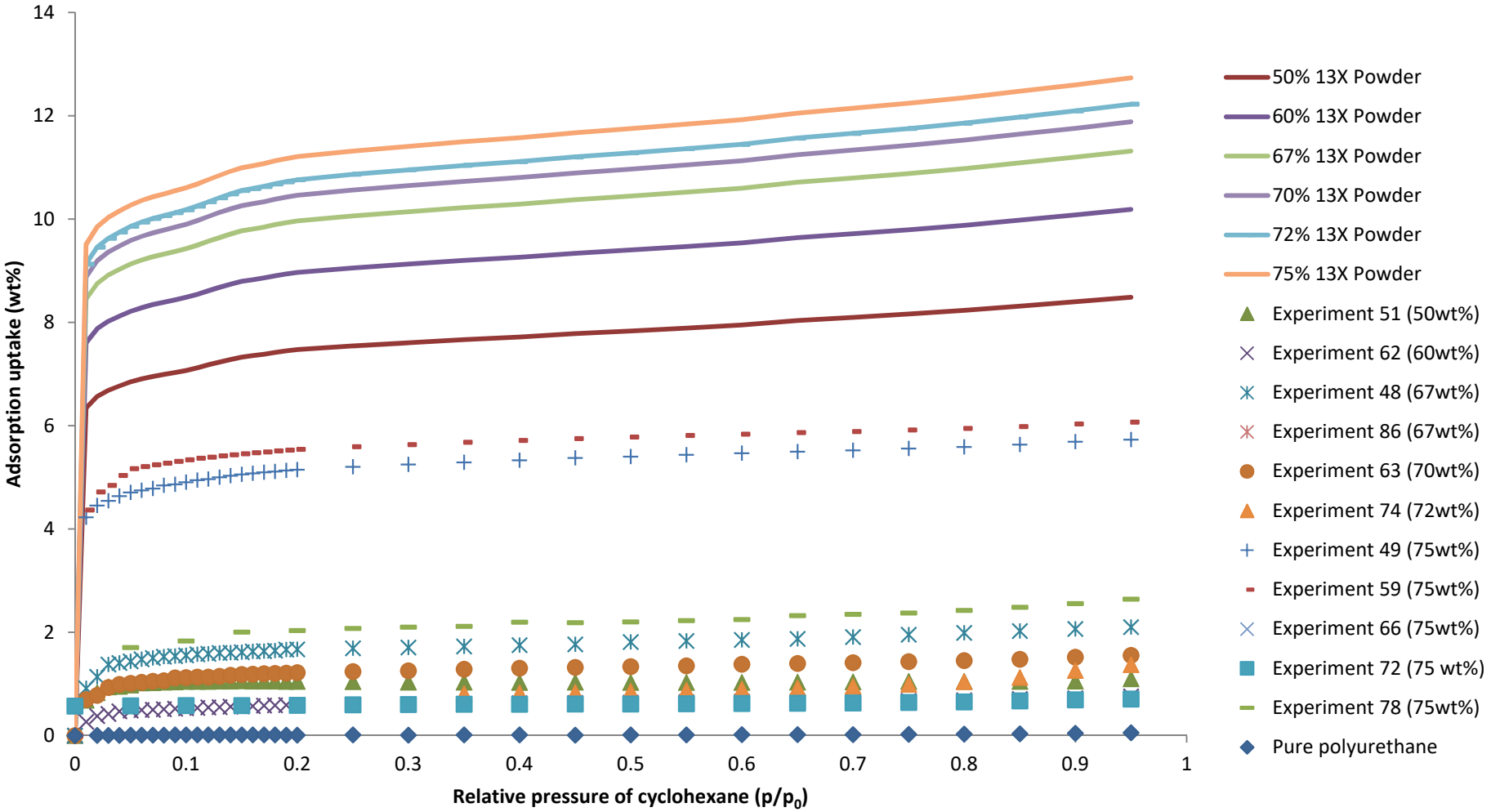

Figure 98: Cyclohexane isotherms for downrated 13X powders compared to PU-13X isotherms of experiments with equal loading and pure PU.

Table 31: Proportion of accessible adsorbent of PU-13X foams as calculated from isotherm data.

Sample number	Calculated loading (From formulation) (wt%)	Accessibility of adsorbent (p/p_0=0.25) (%)	Accessibility of adsorbent (p/p_0=0.5) (%)	Accessibility of adsorbent (p/p_0=0.75) (%)	Accessibility of adsorbent (average) (%)
51	50	13.8	13.1	12.8	13.7
62	60	6.60	6.78	6.88	6.39
48	67	16.8	17.3	18.0	16.6
86	67	15.9	15.8	16.1	16.2
63	70	11.7	12.2	12.5	11.5
74	72	5.17	4.99	5.07	5.10
49	75	46.0	46.0	45.4	45.8
59	75	49.4	49.2	48.3	49.2
66	75	10.6	10.3	10.2	10.4
72	75	95.8	95.1	93.6	95.1
78	75	18.3	18.7	19.4	18.8

As can be seen from the accessibility data in Table 31 there is no relationship between the 13X mass fraction and the accessibility of the adsorbent for non-heat treated samples. High mass fraction samples remain superior due to containing a greater concentration of adsorbent per unit volume, but the adsorbent is not more accessible on a mass basis.

There exists significant variance in accessibility for samples with similar predicted mass fractions of 13X, as can be seen in Table 31 and Figure 98. This variance is far larger than any variance in mass loading for these samples (as shown in Table 30) which could explain such a discrepancy. Sample 72 is so vastly removed from all other results to be clearly anomalous, particularly as it could not be reproduced as previously discussed.

Part of this repeatability issue can be explained by the use of 13X mass fraction from the formulation calculation. As found via TGA, the formulation values overestimate the amount of 13X in the foams and there exists variance in 13X mass fraction between samples of

identical formulation. This small variance in loading can explain small variances in accessibility as the measured isotherms are not being compared with correct modelled isotherms (such as Sample 48 and 86) but is insufficient to explain larger differences such as are seen between samples 49, 59, 66, 72 and 78 which all have a 13X mass fraction of 75% by formulation.

The other major discrepancies in samples are samples 49 and 59. These samples were the largest samples made during the research, significantly larger than the cylindrical samples made later and made in wide flat moulds which lead them to be very prone to poor mixing, even with the use of a homogeniser. As a result test samples taken from lower in the foam may have higher 13X content than would be predicted, leading to higher isotherm values.

In order to improve the data for future work, foam samples should be prepared for the testing as a dedicated batch in order to reduce variance introduced by the manufacturing process, using the same mould shape for all samples and attempting to keep sample masses as similar as possible in order to ensure mixing behaviour is as similar between samples as possible. In particular they should use an identical process for solvent removal, ideally going through such a process simultaneously.

For example, samples 59 and 66 both used a 50:50 NMP:H_2O bath to remove solvent from the produced foams, but sample 59 was exposed to the bath for 1 hour, whilst sample 66 was exposed for 12 hours. Sample 49 on the other hand used pure H_2O to remove solvent. This variance can alter the sample structure to affect accessibility independently of adsorbent mass fraction. Samples should be dried simultaneously and have isotherm testing performed as soon as possible after the drying process.

Overall, the non-heat treated samples showed extremely poor 13X accessibility, with foams managing to have only half the 13X inside the structure accessible at best, which confirms the necessity of post-processing methods to improve the accessibility of the adsorbent, as such low accessibility values are unsuitable for a useful material. This accessibility cannot simply be achieved by increasing 13X mass fraction. As a result, surface modification techniques were investigated and analysed via these techniques in the following section.

5.2.3.4 Increasing adsorbent accessibility by surface modification

As discussed in section 3.2.3, samples underwent heat treatment in order to attempt to improve the accessibility of the 13X. The effectiveness of this heat treatment method was investigated by use of acquired isotherm data. Using the technique described in section 5.2.3, isotherm data for heat treated samples was acquired for sample 77A, a 75wt% sample by formulation, and 86A, a 67wt% sample. These samples were compared against both non-heat treated samples of similar mass fractions by formulation and modelled 13X powder isotherm data for these 13X mass fractions in order to see if they offered improvements in accessibility compared with non heat treated samples.

In both cases improved adsorbate uptake was measured, with sample 86A showing an increase in accessibility from 16.2% in the untreated state to 42.0% in the post-treatment state when comparing both isotherms for 86 and 86A against the same modelled 13X isotherm for 67 wt%. This calculation assumes that there has been no effective increase in the 13X mass fraction of the material as a result of the heat treatment process. Figure 99 shows the resulting comparisons between the three modelled 13X isotherms and the measured isotherm data for sample 77A, 86A and various other non-heat treated samples of comparable 13X mass fraction. The assumption that the heat treatment process does not affect the mass fraction of 13X in the materials is not correct however, as TGA data shows that heat treatment increases the mass fraction of 13X in the samples. The increase in adsorbent uptake in the isotherm for the heat treated materials is sufficiently large however to suggest actual improved accessibility from the process, particularly given the analysis of the non-heat treated samples in section 5.2.3.3 suggesting no link between 13X mass fractions and accessibility of adsorbent.

For sample 77A, no isotherm data was available for its non-heat treated state, but TGA data was available for its true mass loading of 13X, which was calculated to be 82.5wt%. This allowed for an accurate comparison of its accessibility to other non-heat treated samples without using the incorrect assumptions used to calculate accessibility of sample 86A. This resulted in a calculated accessibility of 81.7% for sample 77A. This is significantly higher than the accessibility of the 75 wt% non-heat treated samples with the exception of the sample 72 outlier (samples 59, 66 and 78 in Figure 99), which confirms that the heat treatment process improves adsorbent accessibility as well as simply removing inert polyurethane from the structure.

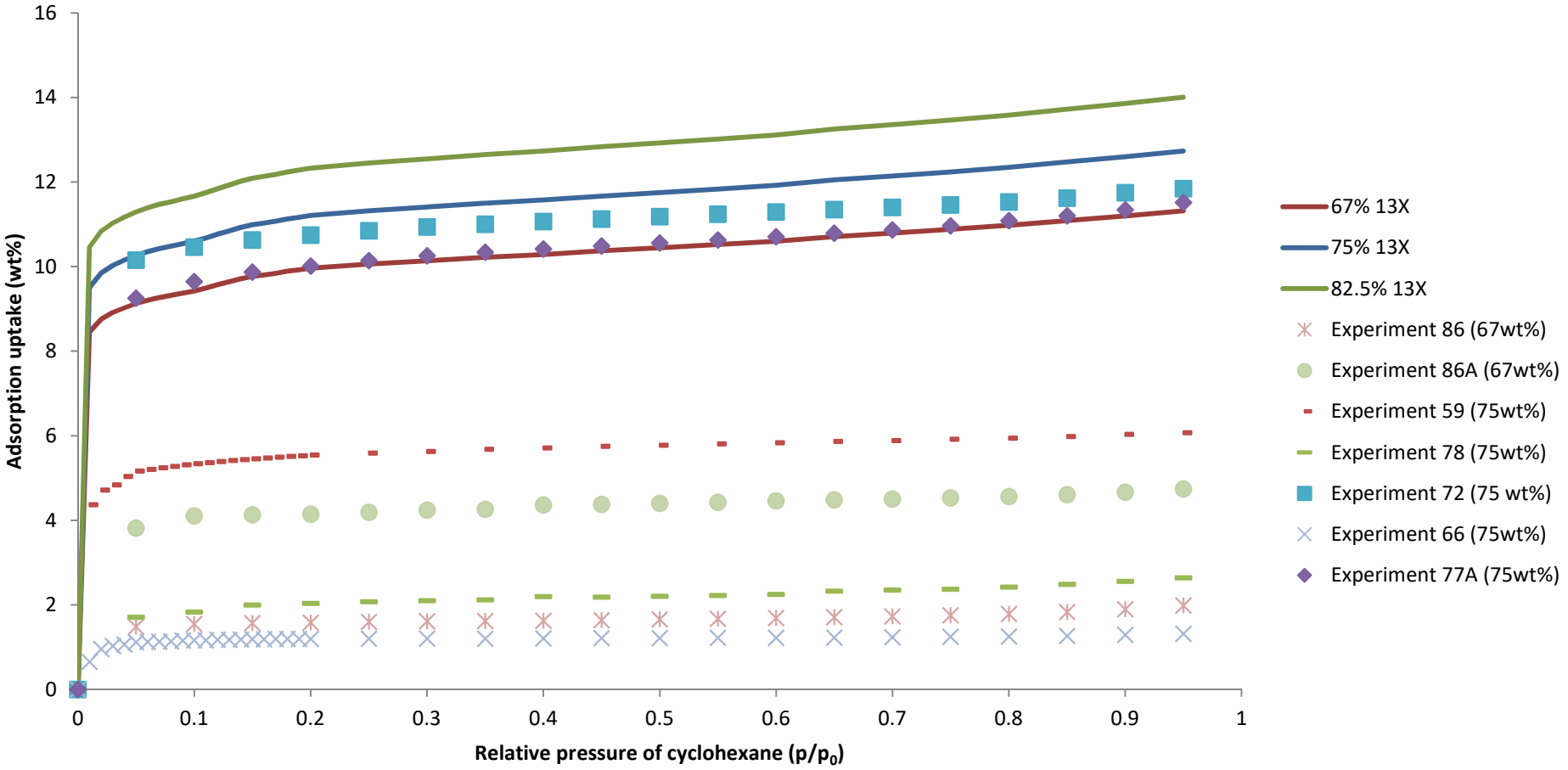

Figure 99: Adsorption isotherms for non-heat treated and heat treated PU-13X samples compared against pro-rated 13X isotherms for equal 13X mass fraction.

5.2.3.5 Adsorption isotherms compared to commercial 13X beads

Isotherms were measured for 13X adsorbent powder as used to produce the foams (Brownell Ltd.) and 13X beads (ZeoSorb 63 13X beads, diameter 1.6-2.5 mm) to compare with the foam materials, resulting in the comparison in Figure 100. As can be seen, the beads offer superior uptake than the foam materials, both before and after heat treatment for even the highest 13X mass fraction foams, but typically lower than the 13X powder except for at very high pressures.

It is not certain however what the cause of this adsorption uptake advantage in the 13X beads over the foams is. The beads support 13X powder into the bead shape via the use of a binding agent which forms part of the mass of the beads, similar to how the polymer in the foams forms part of the mass. However in the case of the beads, this binder is not inert from an adsorption perspective.

This can be seen in the shape of the adsorbent bead isotherm, which shows a sudden increase in adsorption uptake towards the highest end of the pressure axis (p/p_0 of 0.9 upwards). As no significant hysteresis was observed in the desorption curve for the 13X beads, this is unlikely to be due to mesoporosity but may be due to condensation on macropores as this only occurs at high adsorptive partial pressures. As a result of this maximum uptake being higher than the powder, it is not possible to determine how accessible the 13X is within the beads compared to the foams. This is because the weight loading of 13X in the beads is unknown and the adsorption uptake of the binder cannot be disregarded.

Regardless of the actual accessibility of the adsorbent within the beads, it is clear that on a uptake basis by weight the 13X powder is the superior material. However 13X powder is impractical for use in respiratory protection and so the choice is between the foams and the beads. In adsorption uptake terms the beads are the superior material, but this must be considered in combination with pressure drop behaviour to determine which material is more effective overall as an adsorbent structure for respiratory protection.

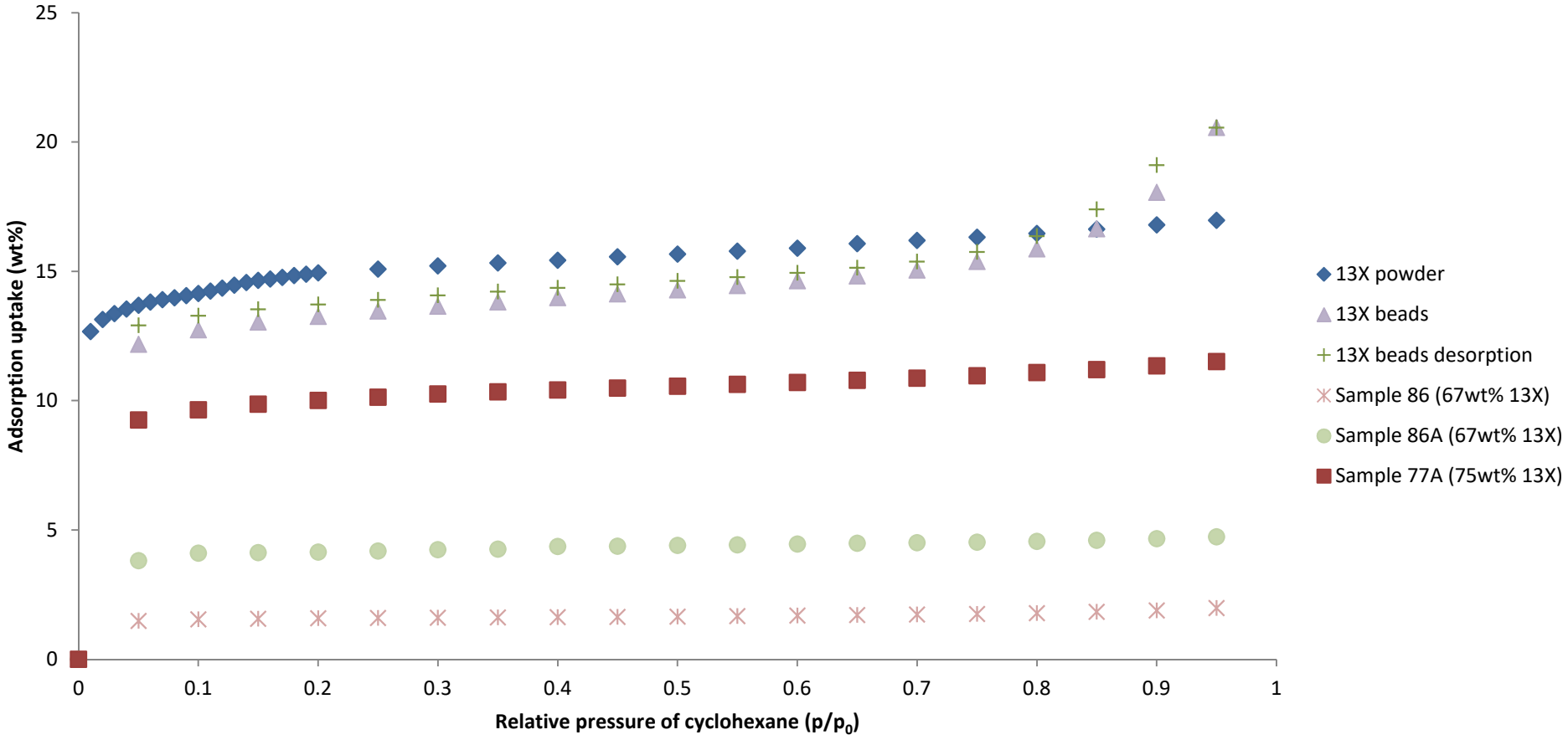

Figure 100: Isotherms comparing the performance of PU-13X foams in non-heat treated and heat treated states against the precursor 13X powder and commercially available 13X beads.

5.3 Investigation and analysis of kinetic behaviour in adsorbent foam materials

In order to investigate the kinetic behaviour of the adsorbent foams it is necessary to perform breakthrough testing to produce breakthrough curves for analysis, the technique for which is discussed in this section. Breakthrough testing was chosen to investigate the adsorption kinetics as it allowed for testing with molecules similar to those which might be seen in actual use in respiratory protection, as well as testing the foams in a form as might be practically used, allowing for data to be gathered which can easily be applied to real world applications.

This experimental technique produces a breakthrough curve from the concentration measured at the outlet over time, an example of which can be seen in Figure 101. From this figure a variety of data can be calculated. The working uptake of the adsorbent can be found by calculating the amount of test gas which has flowed into the test bed in the time from the experiment start (t=0) until the breakthrough time where a certain fraction of adsorbate can be detected in the outlet ($t=t_b$), in this case 10% of the inlet value ($C_b=0.1\ C_0$). This value is shown on the graph by the red shaded rectangle and can be converted into working uptake by multiplying the area of the rectangle by the adsorbent flowrate.

This is however not the equilibrium loading which is only reached when the entire bed is saturated with the adsorbate, a state which occurs when the concentration measured in the outlet is equal to that of the inlet ($C=C_0$). The equilibrium loading can be found by taking the area over the breakthrough curve between t=0 and the saturation time $t=t_s$, where the saturation time is defined as when the outlet has a sufficient fraction of the inlet concentration, in this case 90% of the inlet ($C_s=0.9\ C_0$), shown by the combined red and green shaded areas and multiplying this by the adsorbent flowrate.

The breakthrough curve between the breakthrough time and the saturation time is the mass transfer zone which reflects the mass transfer behaviour which occurs in the adsorbent as adsorbate containing gas passes through the sample. The shape of the mass transfer zone allows for the nature of the mass transfer in the adsorbent to be investigated. If the mass transfer zone of the adsorbent takes a constant shape, which is the case for the favourable isotherms seen in the adsorbate-adsorbent pair being investigated, the shape of

the breakthrough curve can be linked to the mass transfer characteristics of the adsorbent structure.

In this work, the Thomas model was chosen to analyse the shape of the breakthrough curves by fitting Thomas predicted curves to the experimentally determined data. This model was chosen due to its assumptions that the adsorption behaviour of the isotherm showed extremely favourable type 1 style behaviour, which was known to be the case in this work. The Thomas model has a linearized form as follows (Chu 2010):

$$\ln\left[\left(\frac{C_0}{C_t}\right)-1\right]=\left(\frac{k_{Th}q_0m}{Q}\right)-k_{Th}C_0t_b \tag{59}$$

where k_{Th} is the Thomas rate constant, q_0 the equilibrium uptake of the adsorbent, m the adsorbent mass, t_b the breakthrough time and Q the flowrate. In order to estimate the Thomas rate constant data from the experimental data, the linearized form of the Thomas model can be used to replot the breakthrough curves in terms of $\ln\left[\left(\frac{C_0}{C_t}\right)-1\right]$ against time to obtain the Thomas rate constant from the gradient of the linearized breakthrough curve divided by the initial concentration of the adsorbate.

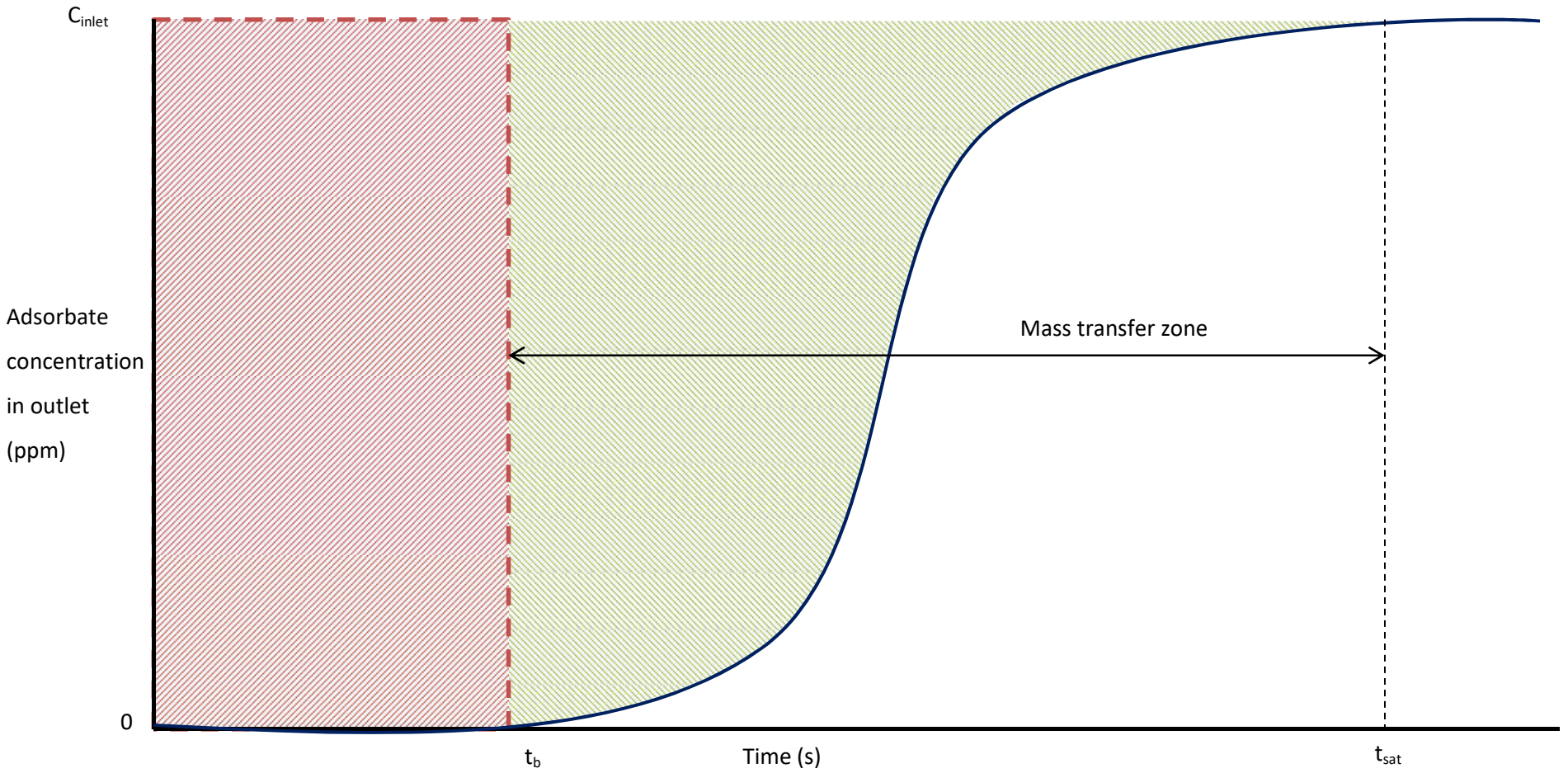

Figure 101: Schematic diagram of an adsorption breakthrough curve, showing data which can be obtained from the technique.

5.3.1 Adsorption breakthrough methodology

Adsorption breakthrough testing was performed in the laboratory using a flame ionisation detector (FID) set up for the detection of n-butane with foam samples fixed in a cylindrical holder (Figure 102, Figure 103). N-butane was chosen as a test gas due to its easy availability in a gas form compared to cyclohexane which required gas bubbling and mixing equipment, as well as being a small organic compound for which 13X is suitable as an adsorbent and a known respiratory hazard.

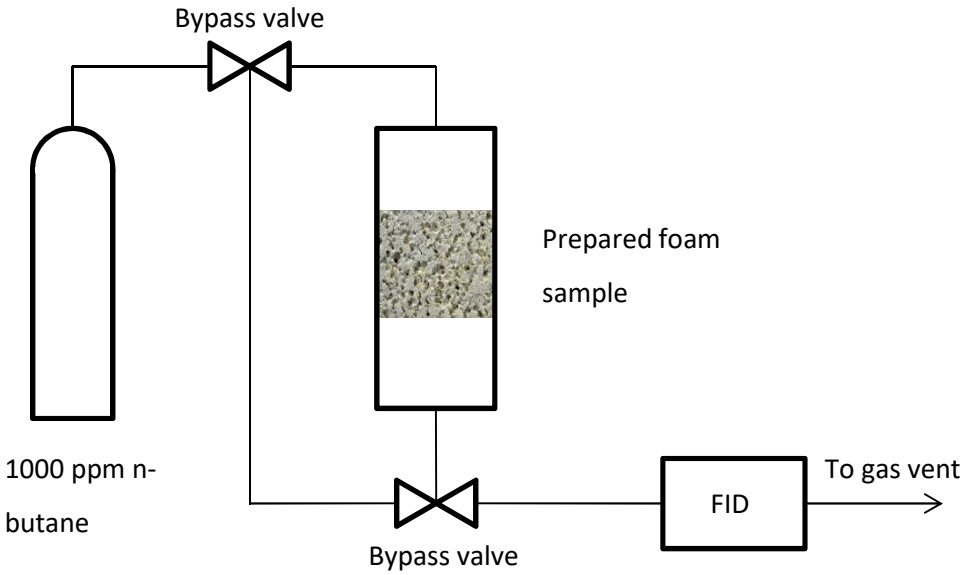

Figure 102: Schematic diagram of the adsorption breakthrough apparatus used.

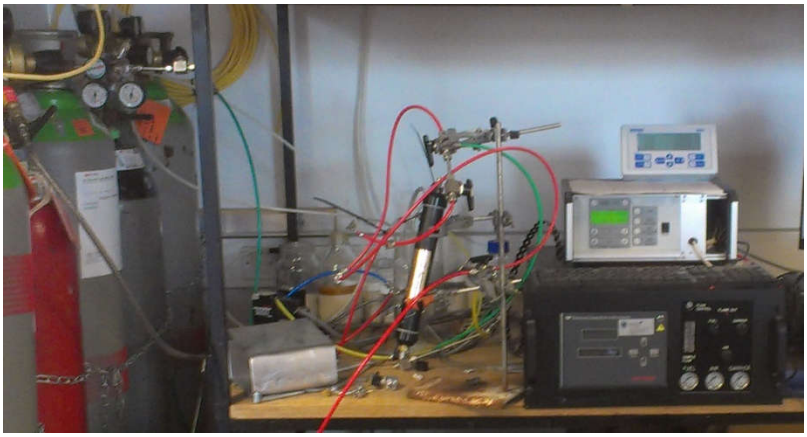

Figure 103: Adsorption breakthrough apparatus as used in the research.

Samples were prepared prior to testing for adsorption kinetics via use of a vacuum oven to remove any pre-existing adsorbed gases on the samples, being exposed to vacuum (-950 mBar) at 200^{o}C overnight prior to testing, before being fitted into the sample holders and tested immediately afterwards. Cylindrical samples of PU-13X foam were used for testing, being fitted securely within the sample holder by use of PTFE gas tape (Supplied by RS Components) wrapped around the end of the samples to prevent any bypass of the test gas containing n-butane.

The breakthrough apparatus was calibrated to the baseline of n-butane present by flowing test gas through a bypass, with butane levels being measured over time automatically by the FID. A flowrate of 1lpm (at 25^{o}C and 1bar) of test gas was chosen as the lowest flowrate the FID would accept in order to achieve the most accurate results possible, whilst 1000 ppm of n-Butane was chosen for being a representative concentration that might be seen in a respiratory protection application.

When the FID had registered three separate consecutive readings in close agreement with each other within the margin of error of the equipment ($\pm$20 ppm), and the sample was fitted into the holder and ready for use, the test was begun by switching the bypass valves so butane would flow through the sample holder. The test then continued until the outlet concentration of butane had recovered to the baseline level or until no testing time remained, whichever came sooner.

5.3.2 Adsorption kinetics analysis

Breakthrough data for sample pairs of tested foams which underwent breakthrough testing before and after heat treatment was plotted in Figure 104 to allow for investigation into the effects of the heat treatment process on the dynamic adsorption behaviour of the samples. The breakthrough data shows that PU-13X samples which had not undergone the heat treatment process showed instantaneous breakthrough of the adsorbate in breakthrough testing.

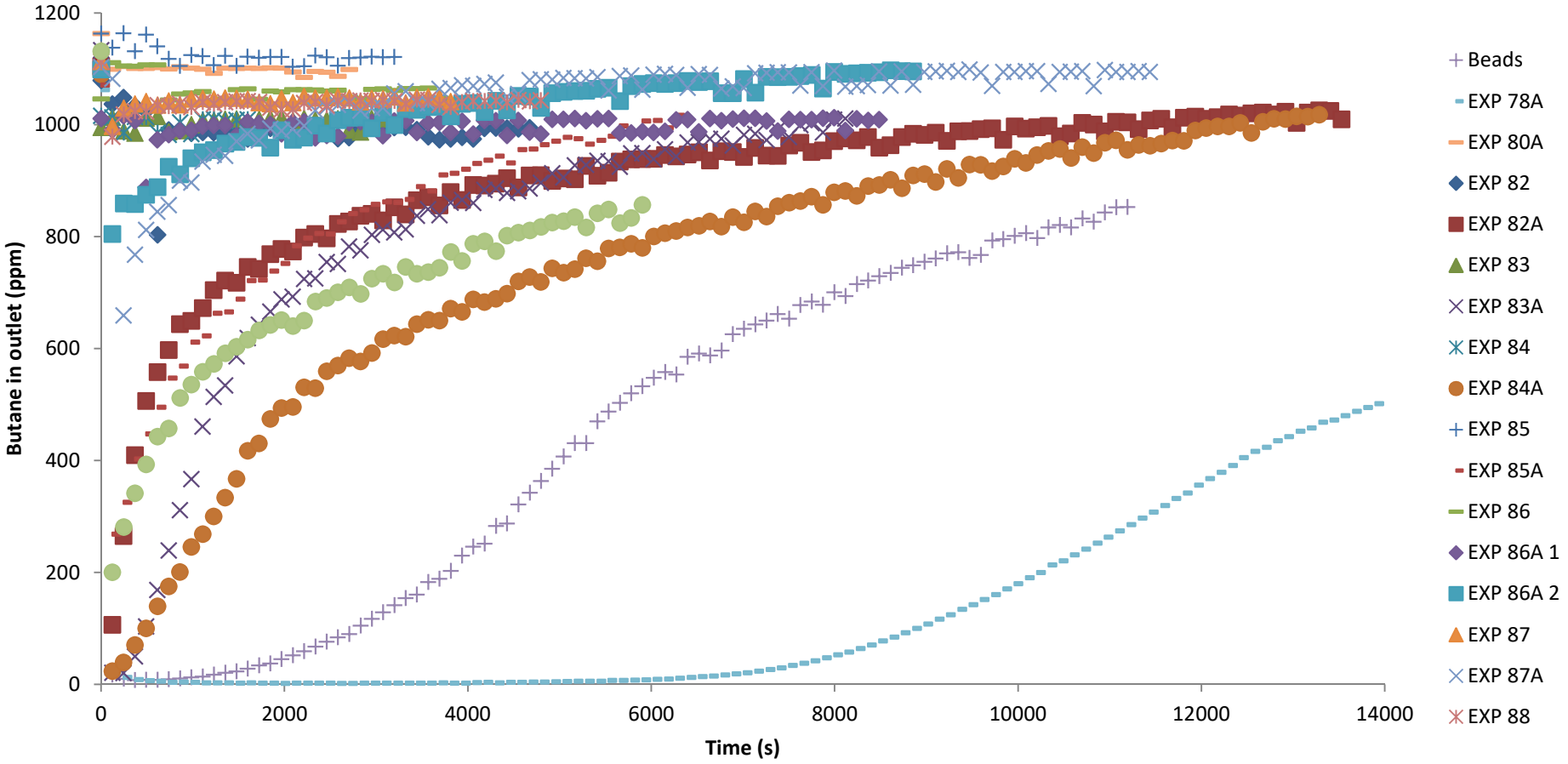

Figure 104: Adsorption breakthrough curves for PU-13X foam samples before and after heat treatment, showing improved uptake gradients, and 13X beads for comparison.

This confirms the previous assumption that the polymer on the surface of the bubbles in the foams (as seen in Figure 105) which forms part of the material was imposing a barrier between the adsorbent and the adsorptive in the gas phase. This was shown in the experiments as non-heat treated samples do have adsorbent uptake as shown in isotherm measurements, but this cannot be detected in the dynamic test environment implemented in the research. This is due to adsorptive mass transfer limitations in the non-heat treated foams. The polymer skin is restricting the rate at which adsorbate can be adsorbed from the test stream even when adsorbent uptake is available, which results in more adsorbate flowing through the sample than can be removed. This causes seemingly instant breakthrough even when uptake is available in the material. A lower choice of adsorbate flowrate would potentially avoid this problem but was not possible with the FID used in this work.

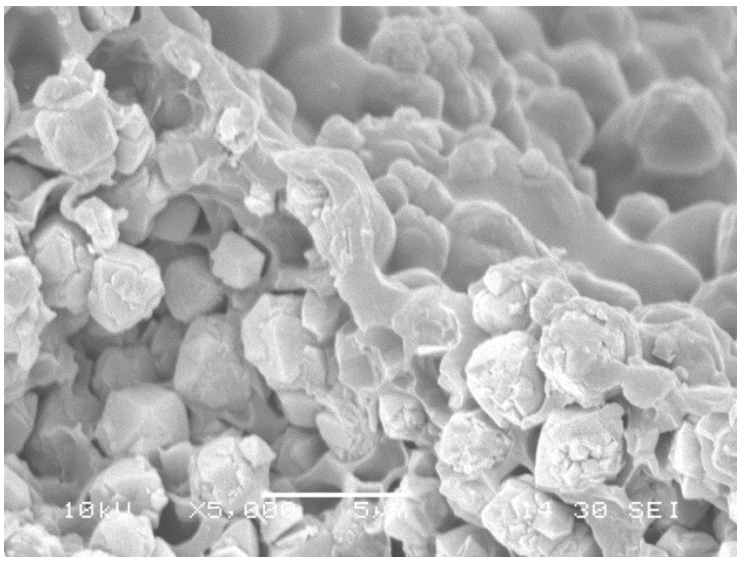

Figure 105: SEM image of a sample from sample 86 showing polymer coating the bubble surface (top right) and blocking access to 13X crystals inside the foam material (bottom left).

Further analysis of the breakthrough data allowed for investigation of the mass transfer limitations imposed by the polymer skin for each sample to determine if it was affected in any way by the heat treatment process or the thickness of the polymer skin. Qualitative comparison of breakthrough curve shapes and gradients was already possible in Figure 104. Quantitative data for the mass transfer behaviour through the materials was found by fitting the Thomas model to linearized breakthrough curves where possible using the technique discussed previously in this Chapter. Breakthrough curves which did not show

typical S shaped responses due to instantaneous adsorbate breakthrough were not suitable for analysis using this technique, and as a result Thomas constants could not be measured for most of the untreated foams.

The Thomas model resulted in the calculation of various Thomas constants as seen in Table 32. As can be seen, the beads offered superior mass transfer performance compared to the heat treated foams, which in turn were an order of magnitude superior to the non-heat treated foams as was expected. However the difference between the beads and some heat treated foams is relatively minor. The heat treatment process can therefore be concluded to be effective in increasing the accessibility of the adsorbent within the foam structures. There exists significant variance between the Thomas rate constants of the various heat treated foams however, which merits further investigation into their properties and the heat treatment process to determine the cause of this.

Table 32: Calculated Thomas constants for various foams and beads from breakthrough data.

Sample number	**Thomas constant ($ppm^{-1}s^{-1}$)**
Beads	-5.11×10^{-7}
78A	-3.12×10^{-7}
82A	-1.63×10^{-7}
83A	-4.23×10^{-7}
84A	-2.78×10^{-7}
85A	-4.91×10^{-7}
86A	-4.04×10^{-7}
87	-5.77×10^{-8}
87A	-2.76×10^{-7}
88	-5.19×10^{-8}
88A	-2.83×10^{-7}

The kinetic behaviour of heat treated samples is related to the details of the process used to treat them and reduce the polymer fraction of the materials. As a result, the skin thickness of the foams was investigated to determine if the heat treatment process had led to a reduction in the polymer coating previously mentioned, and as a result caused the improved mass transfer behaviour.

5.3.3 Measuring skin thickness

In order to measure the bubble skin thickness, SEM images were acquired for heat treated foams for which adsorption breakthrough data was available, as well as non-heat treated foams for comparison where available using the SEM technique described previously in section 4.2.1.1 (Figure 106 to Figure 109). These images focussed on capturing the cross section of the foam struts to clearly show the bubble skin between the adsorbent and the void space of the foam and were performed at as high a magnification as possible to reduce errors as a result of pixel size. Using ImageJ and the scale of the SEM image, the width of the bubble skin was then measured directly for all the samples.

5.3.4 Skin thickness results and discussion

The skin thicknesses measured via the SEM images are shown below in Table 33. These thicknesses vary significantly between foams with sample 85 being particularly thick as measured. As was predicted, the heat treatment process significantly reduces the skin thicknesses of the foams compared to their untreated counterparts, and the thickness of the heat treated skins are far more consistent with each other. These thicknesses can then be considered in combination with the rate data found previously to determine the effectiveness of the heat treatment process in improving the accessibility of the adsorbent in the structure, which occurs in the following section.

The error in the skin thickness measurements comes from two sources. First is the error from the pixel size of the SEM images used to measure the thickness, which is a factor of the resolution of the image and the magnification used, and is ± 0.01 μm. This is minimised by using high resolution images and as high a magnification as is practical for acquiring images. The second source of error is in making a judgement as to where the polymer skin begins and ends. This issue can be seen clearly in Figure 108. In the non heat treated foam on the left the polymer skin is very clearly defined against the 13X crystals, but in the heat treated version on the right there is considerably more ambiguity on what is the polymer skin cross section compared to a polymer surface. This error cannot be quantified and will vary significantly depending on the quality of the cross section being imaged.

Table 33: Bubble skin thicknesses for various heat treated and non-heat treated foams.

Sample	Skin thickness (μm) ±0.01
77A	0.175
78A	0.115
82	0.371
82A	0.107
84	0.255
84A	0.091
85	1.11
86	0.437
86A	0.125
87	0.621
87A	0.079

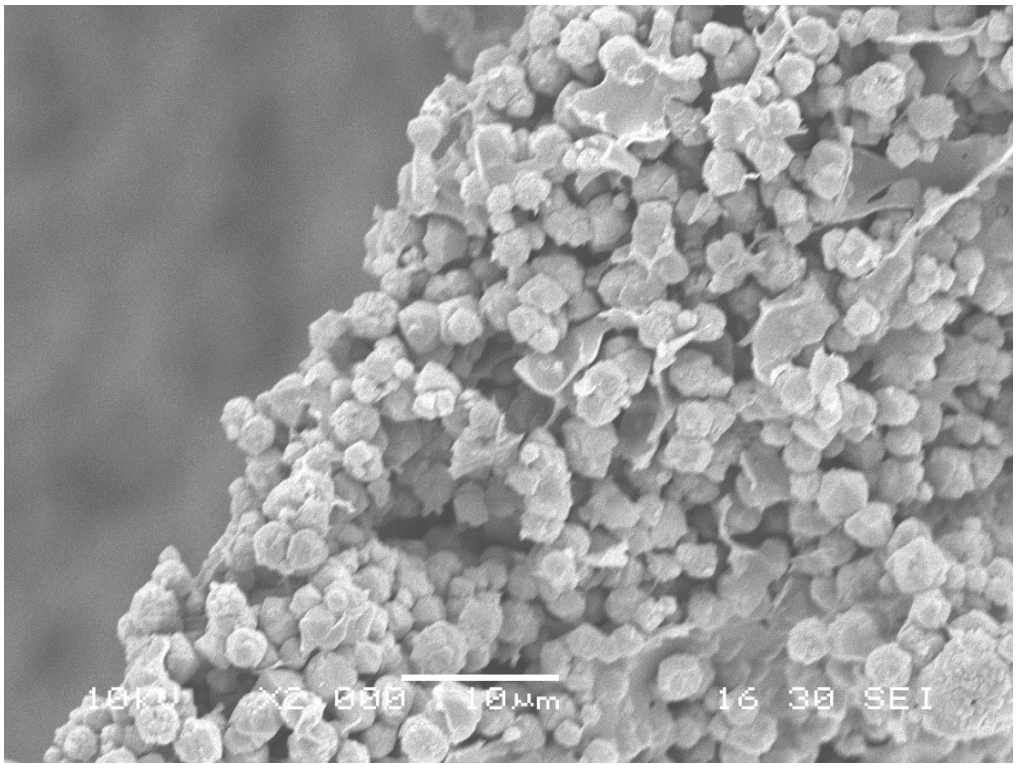

Figure 106: SEM image of a sample from sample 77A strut cross section showing polymer skin thickness.

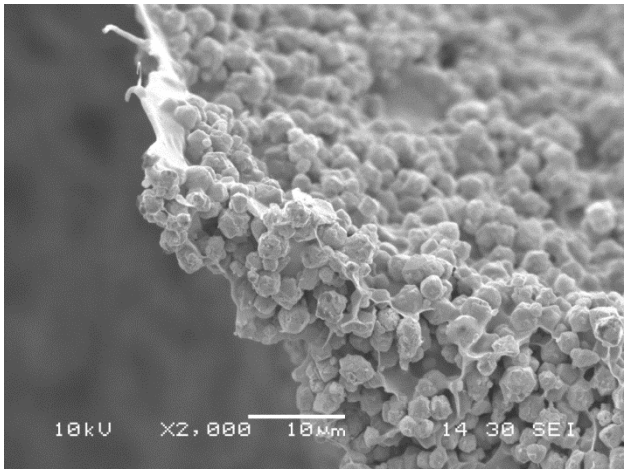

Figure 107: SEM image of a sample from sample 78A strut cross section showing polymer skin thickness.

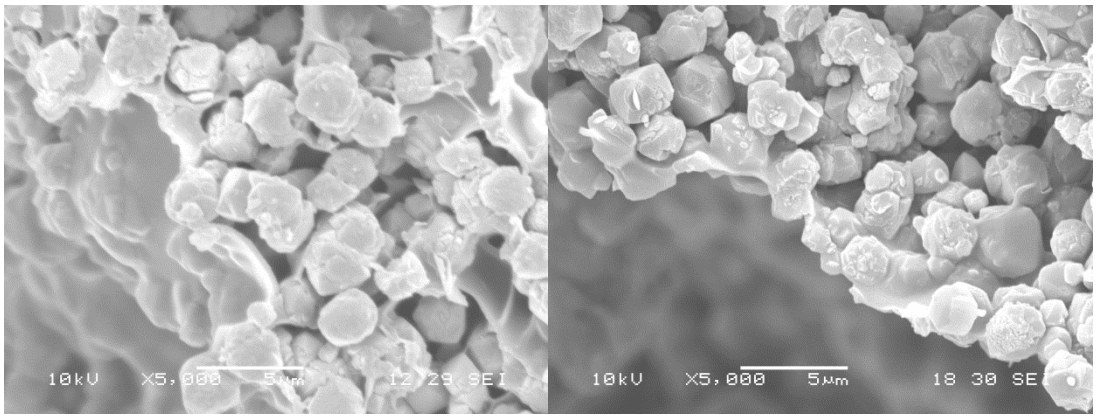

Figure 108: SEM images of a sample from sample 84 (Left) and 84A (Right) strut cross sections showing polymer skin thickness before and after heat treatment.

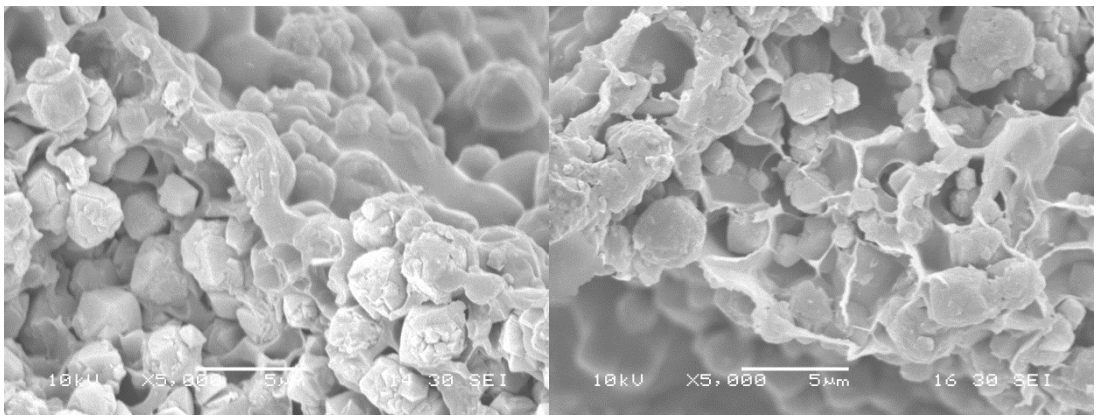

Figure 109: SEM images of a sample from sample 86 (Left) and 86A (Right) strut cross sections showing polymer skin thickness before and after heat treatment.

5.3.5 Adsorption kinetics analysis and the effects of skin thickness

The skin thicknesses measured in the previous section are compared against the Thomas rate constants for these samples where available, resulting in Table 34. As was found in the previous section, heat treatment of the samples lead to a significant reduction in the skin thickness of the polymer covering the adsorbent crystals. This reduction in skin thickness was strongly correlated with increased mass transfer rates, as shown in the Thomas constant change between sample 87 and 87A, and plotted graphically in Figure 110.

Table 34: Bubble skin thicknesses compared to Thomas rate constants for various heat treated and non-heat treated samples.

Sample	Thomas constant ($ppm^{-1}s^{-1}$)	Skin thickness (μm)
78A	-3.12×10^{-7}	0.115
82A	-1.63×10^{-7}	0.107
84A	-2.78×10^{-7}	0.091
86A	-4.04×10^{-7}	0.125
87	-5.77×10^{-8}	0.621
87A	-2.76×10^{-7}	0.079

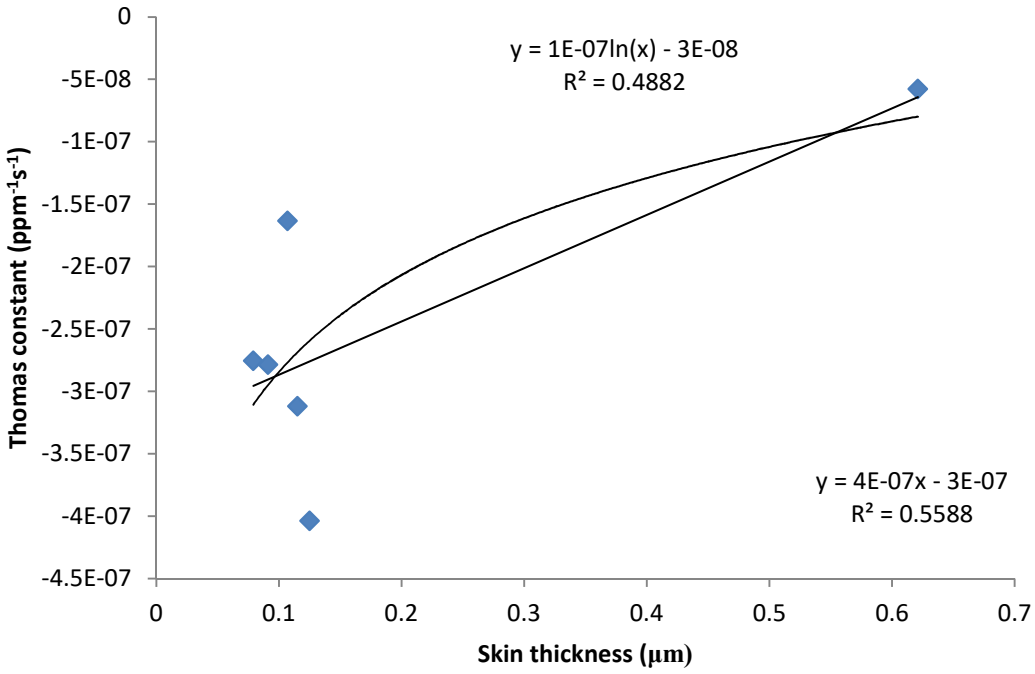

Figure 110: Thomas constants for samples in Table 34 plotted against sample skin thicknesses.

There was a strong relationship between thinner bubble skins and larger Thomas constants for the non-heat treated, heat treated sample pair 87 and 87A. However there was more variance in Thomas constants for different heat treated samples of similar skin thickness, with the samples of 82A, 78A and 86A having similar skin thickness but significant differences in Thomas constant. Similarly, the thinnest sample, 84A, did not show the greatest Thomas constant but instead the thickest, 86A, of the heat treated samples did.

This variance in Thomas constant could be explained by the preparation methods used in producing each of the precursor foams which were then heat treated. 82A and 84A were both produced using an identical synthesis process as part of the repeatability study and therefore have similar Thomas constants with the difference between the samples being due to the difference in their skin thickness.

The Thomas constant is however an overall rate constant which takes into account all forms of mass transfer limitations. Variance in the rate constant for samples of similar skin thicknesses may be due to other transfer processes such as diffusion within the foam itself which have become significant once the limitations imposed by the polymer skin are reduced. It is possible that as the 13X mass fraction of the foams increases, the close packing of the 13X crystals makes diffusion inside the foam structure more difficult. Sample 78A has a true 13X mass fraction of 78 wt%, sample 82A a mass fraction of 92 wt% and sample 84A a mass fraction of 81 wt%, showing a negative correlation between Thomas constant and 13X mass fraction.

Figure 110 can also be used to attempt to model the effects of skin thickness on the Thomas constant, an area of novelty given the general novelty of polymer supported adsorbent materials. The nature of the relationship between skin thickness and Thomas constant is unclear given the lack of data for high skin thicknesses and the potential for other variables than skin thickness to influence the Thomas constant but two models were considered. First was a linear model, shown in equation (60) and the second is a logarithmic model shown in equation (61). Neither of these model the data well, with R^2 values of 0.559 for the linear model and 0.488 for the logarithmic model.

$$k_{TH} = 4 \times 10^{-7} L_{sk} - 3 \times 10^{-7} \quad (60)$$

$$k_{TH} = 10^{-7} \ln L_{sk} - 3 \times 10^{-8} \quad (61)$$

These models were used to attempt to predict the Thomas constant of sample 78A by using the measured skin thickness of 0.115μm for this sample to predict Thomas constants for this sample, resulting in Thomas constants of -2.54×10^{-7} $ppm^{-1}s^{-1}$ for the linear model and -2.46×10^{-7} $ppm^{-1}s^{-1}$ for the logarithmic model, compared to the measured constant of -3.12×10^{-7} $ppm^{-1}s^{-1}$.

It is clear from the data that the polymer skin imposes a significant barrier to mass transfer which is mitigated by the heat treatment process. However given the lack of Thomas constant data for non-heat treated foams due to instantaneous breakthrough and the overall nature of the Thomas constant, it is not possible to draw further conclusions as to the nature of the mass transfer limitations in the foams. As a result of this finding, further work to investigate this behaviour is merited.

In order to improve the investigation into mass transfer behaviour of the foams, it would be necessary to improve both the adsorption breakthrough testing and the SEM process for obtaining images for skin thickness measurements. Breakthrough testing should be performed using larger samples and lower test gas flowrates for non-heat treated samples in order to acquire breakthrough curves which are suitable for analysis using the Thomas model and avoid instantaneous breakthrough.

SEM techniques should focus on improving the cutting and preparation process of the samples, potentially by either cryogenically fracturing the foams or mounting them in an epoxy, in order to maximise the number of triangular cross sections available for skin thickness measurements and increasing the number of images available for each sample to improve the accuracy of the skin thickness data.

The heat treatment process is also clearly significant to producing foams with acceptable mass transfer characteristics to be used in practical applications, and as such deserves further investigation, which occurs in section 6.2.

5.4 Conclusions

Adsorbent loading of the foam materials was found to be high via TGA testing and in reasonably close agreement with values calculated from the formulation for non-heat treated foams, with 13X mass fractions of up to 72.5% found. For heat treated samples the 13X mass fraction was increased to up to 92.3% 13X, showing that foams with high adsorbent content could be produced.

No PU-13X foam was found to have superior adsorption uptake compared to commercial 13X beads on a mass basis, although it was noted that some activity of the 13X beads was due to the non 13X fraction of the beads whilst the PU within the PU-13X foams was found to be inert in terms of adsorption uptake. In the one non-heat treated heat treated foam pair tested, the heat treatment showed significant uptake improvement in the isotherms.

The breakthrough testing showed that non-heat treated foams had extremely poor kinetic behaviour, with instantaneous breakthrough being seen during testing. However heat treated foams showed significantly improved Thomas rate constants, similar in magnitude to the 13X beads tested. The improvement in Thomas rate constants was found to be a result of polymer skin thinning from the heat treatment process.

It was found that both in terms of overall adsorption uptake and adsorption kinetics that heat treatment of the foam samples was necessary in order to achieve acceptable adsorption uptake and speed in the foam materials. Non-heat treated samples showed very poor adsorption behaviour both on a kinetic and equilibrium basis. As a result of this, heat treated samples were highlighted for further analysis and comparison to the adsorbent beads in the following Chapter, as well as further investigation into the effects of the heat treatment process on the physical properties and adsorption uptake of the foams.

6 Material comparisons and discussion

6.1 Introduction

This Chapter deals with a discussion of the new materials in two areas. Firstly it compares the effectiveness of the various heat treatment techniques introduced in section 3.2.3 at improving the adsorption behaviour of the foams. This is done by building upon the analysis of the adsorption data and skin thicknesses in Chapter 5 which identified skin thinning by heat treatment of the foams as an effective process. The analysis aims to identify the important parameters in the heat treatment process which make effective foam materials to allow for further optimisation.

Secondly, it uses the physical characteristics of the produced foams which were identified in Chapter 4, and the adsorption characteristics found in Chapter 5, in combination to determine which adsorbent support could be considered the best for a respiratory protection application. In order to do this, the material which offers the least pressure drop for a given value of adsorption uptake is found by considering both sets of data simultaneously.

These two comparisons and discussions are thus used to find the best material out of the various samples produced and tested to recommend for further work, as well as guide the continual improvement of the materials.

6.2 Analysis and discussion of the heat treatment process

As was found in the previous Chapter, by thermally treating the foams the thickness of the bubble skin between the bulk gas phase and the adsorbent within the foam is reduced. This allows for more adsorbent to be accessible and for improved mass transfer between the adsorbent and the gas phase. This is supported by the adsorption breakthrough testing where heat treated foams showed significantly increased Thomas rate constants compared to non-heat treated foams as discussed in sections 5.3.4 and 5.3.5. The effect of the heat treatment process on skin thickness and how this could be controlled were not immediately clear however without knowledge of the chemical processes which are occurring inside the polymer. As a result, skin thickness, adsorption behaviour, heat treatment conditions and physical foam appearance must all be considered in order to determine what comprises a good heat treatment process for the foam materials.

In order to determine the bubble skin thickness, SEM images were used for analysis of heat treated foams for which adsorption breakthrough data, or isotherm data was available, as well as for comparable non-heat treated foams where available using the techniques described in section 4.2.1.1. These images focussed on capturing the cross section of the foam struts to clearly show the bubble skin between the adsorbent and the void space of the foam. Using ImageJ and the scale of the SEM image, the width of the bubble skin was then measured directly for all the considered samples, resulting in Table 35. Skin thickness data for sample 88A was missing due to sample fragility making it impossible to acquire suitable SEM images for measurement and for sample 88 as a clear skin cross section could not be identified.

It is known from the literature that the thermal degradation pathway of polyurethane changes depending on if the polyurethane is exposed to air or nitrogen during the heating process. As can be seen in Figure 111, it has been reported in the literature that the mass loss of polyurethane changes when heated in nitrogen when compared to heated in air, and with a significant mass residue at the end of the process (approximately 20%). The TGA mass loss in the polyurethane produced in this research shows similar behaviour when heated in air (Figure 112), but with the process beginning at a lower temperature, and with negligible residue at the end of the process.

Table 35: Bubble skin thicknesses and heat treatment conditions for heat treated and non-heat treated foams considered for heat treatment process analysis.

Sample number	Skin thickness (μm)	Heat treatment conditions	Comments
77A	0.175	Heated to 200°C in a vacuum oven, then exposed to air.	Browned significantly during the reintroduction of air to the vacuum oven whilst still hot.
78A	0.115	Heated to 200°C in a vacuum oven, then exposed to air.	Smouldered and turned black when exposed to air during removal from the vacuum oven in a spontaneous and uncontrolled manner.
84	0.255	Heated to 160°C in flowing air in a normal oven for 48 hours.	Lower temperature chosen to avoid total disintegration as seen in sample 87.
84A	0.091		
86	0.437	Heated to 200°C in stagnant air in a normal oven for 3 weeks.	Slowly darkened over the time period with little change towards the end.
86A	0.125		
87	0.621	Heated to 200°C in flowing air in a normal oven for 1 hour.	Burnt from the inside out, leaving a white powder structure on the inside. Disintegrated on handling.
87A	0.079		
88	No data	Heated to 200°C in flowing air in a normal oven for less than 1 hour.	Showed similar internal degradation to 87, but to a reduced extent.
88A	No data		

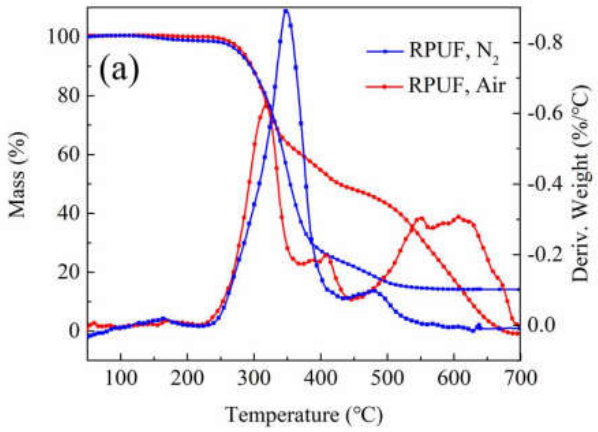

Figure 111: TGA and derivative thermogravimetry curves for rigid polyurethane foams (RPUF) as reported by Chen *et al.* (2019) (Reproduced from (Chen *et al.* 2019) under the Creative Commons license).

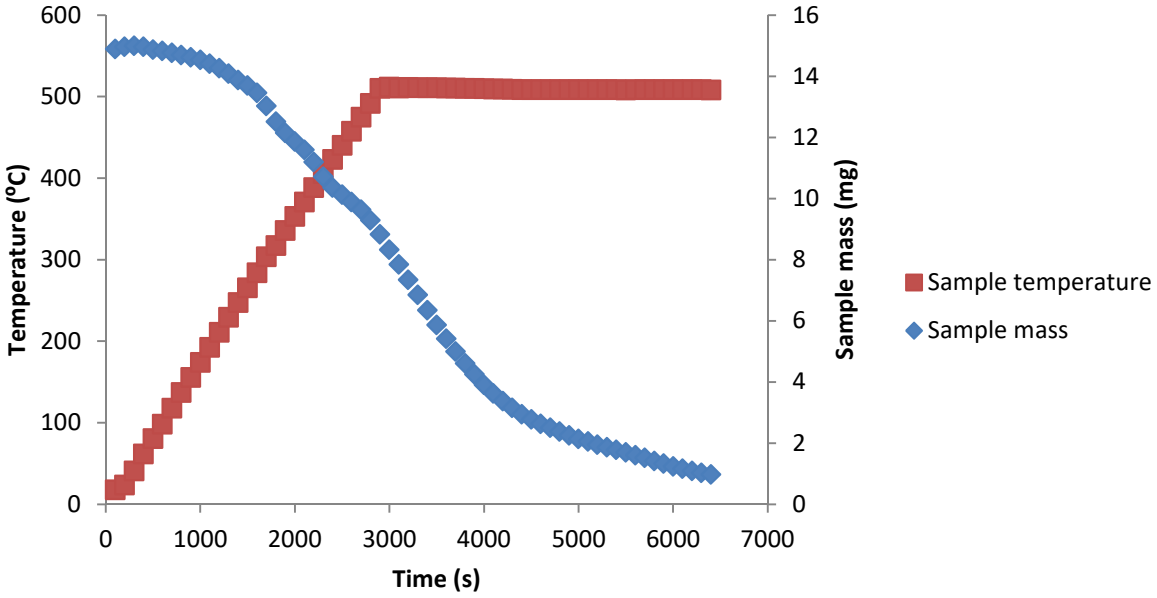

Figure 112: TGA profile for pure PU foam as produced in this work.

It was found from the recorded heat treatment conditions (Table 35) and physical examination of the foams as seen in Figure 113 to Figure 117 that the foams exposed to air showed thinner skins and darker and more charred appearance than those heated without additional airflow. This is consistent with the TGA data showing that heating in the presence of oxygen leads to greater mass loss than heating in nitrogen, and as a result it can be concluded that thinner skins are created by heating the foams in oxidising conditions.

Figure 113: Sample 77A showing brown colour after heat treatment.

Figure 114: Sample 78A showing dark black colour after heat treatment.

Figure 115: Sample 84A showing dark black colour after heat treatment.

Figure 116: Sample 86A showing brown colour after heat treatment.

Figure 117: Sample 88A showing brown outer colour after heat treatment and developing black and white internal core.

This conclusion is supported by the previous TGA work on polyurethane in section 5.2.1 which suggests that polyurethane oxidation begins at 200^{o}C as can be seen in Figure 118

where the exothermic response of the polyurethane occurs at this temperature. Adsorbent accessibility is also directly improved by heat treatment, as can be seen in isotherm data for samples 86 and 86A shown in Figure 119. The fraction of adsorbent uptake which could be accessed increased from 16.1% for sample 86 to 42.0% for sample 86A, while the higher loading in 77A showed accessibility of 81.7% calculated using the technique described in section 5.2.1. The increase in accessible adsorbent is correlated with the decrease in skin thickness as was discussed previously in section 5.3.5.

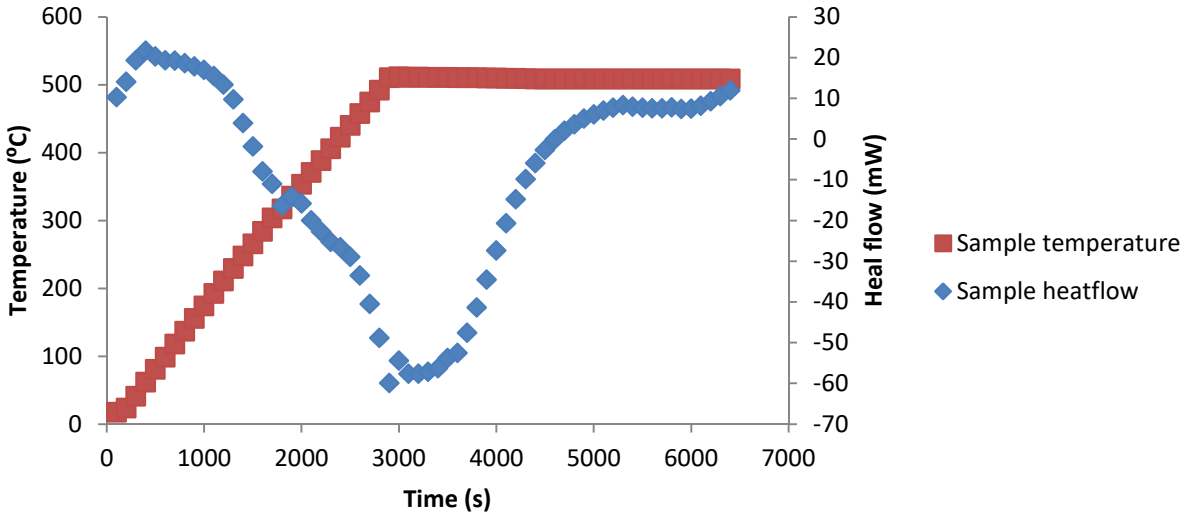

Figure 118: A TGA profile of heat flow out of a pure polyurethane sample compared to sample temperature.

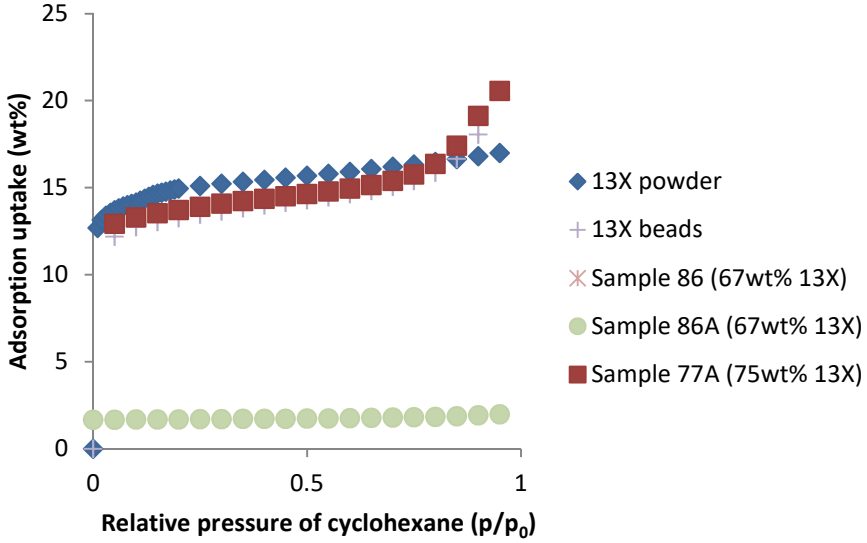

Figure 119: Cyclohexane isotherms for 13X adsorbent powder, adsorbent beads and non-heat treated and heat treated foam samples.

A trade-off exists however between adsorption properties and physical resilience. Figure 120 shows the result of the attempted heat treatment of sample 87 which was exposed to flowing air at 3 air changes per hour at 200^{o}C, which lead to the inside of the sample undergoing total combustion of the polymer fraction leaving nothing but an extremely fragile white foam inside a charred case which disintegrated upon any extended handling. Sample 88 did not have such an issue, although this was a significantly coarser sample which may explain the slower degradation, as a coarser foam will have a lower specific surface area compared to finer small bubble foams.

The temperature used for the process is too low for full oxidation to occur according to TGA analysis. However as the samples show most degradation in the centre it can be concluded that the initial oxidation that occurs is causing heat to be generated inside the sample, which due to the thermal insulation properties of polyurethane foam, is raising the temperature above the ambient temperature of the oven and driving further oxidation.

Figure 120: Sample 87 showing disintegration as a result of aggressive heat treatment.

It is clear that some degree of exposure to airflow is necessary for an effective heat treatment process. Sample 86 which was given no additional air supply showed thicker skins, despite using the 200^{o}C temperature which showed good performance in other samples. This was found to be more significant than temperature, as sample 84 showed the thinnest skins measured, despite being treated in the lowest temperature due to a constant exposure to flowing air. This is due to the different reaction pathways which the polyurethane can undergo depending on the presence or absence of oxygen. The TGA data for PU heated in nitrogen shows significantly less overall mass loss, and as a result thicker skins are left after treatment in stagnant air. The foam morphology also has an effect, with finer less dense foams being more prone to faster degradation and damage compared to denser, coarser materials due to a reduced specific surface area for the coarser foams.
As a result, a successful heat treatment process should use a temperature of at least 160^{o}C to allow for a controlled oxidation process to occur, as shown in the TGA profile in Figure 118, but no more than 200^{o}C to prevent total disintegration as seen in sample 87A. Rather,

the process should be controlled by regulating the duration of heating and air flowrate as the exposure to airflow has a significant effect on the extent of the process with all the samples exposed to flowing air (77A, 78A, 84A, 87A, 88A) showing significant oxidation regardless of the temperature used. Reducing the temperature slows the process, as seen in sample 84A taking 48 hours to oxidise at 160^{o}C but does not reduce the extent of oxidation. Reducing the exposure to air does limit the oxidation process as seen in sample 84A and the difference in sample colour. This process however could not be fully investigated and optimised in the time available for the research.

6.3 Foam effectiveness compared to existing support materials

It was concluded in Chapter 4 that many of the heat treated foam materials offered superior pressure drop characteristics compared to a comparison adsorbent bead material, and that this superior behaviour was due to their increased voidage when compared to the bead materials. However this then logically results in a reduced packing density of adsorbent in the foams compared to the beads. As a result it becomes important to consider if the adsorbent is being effectively utilised in both supports, otherwise any gains in pressure drop behaviour risk being eliminated by requiring a greater volume of foam than beads to achieve the same adsorption performance. In other words the question is: For a given adsorption uptake, which support offers the lower total pressure drop?

The first step is to calculate an adsorption uptake density for both the beads and foam materials being compared, to determine how much adsorbate a set volume of material can take up, and thus how much protection they can offer. This starts with the bulk density of the materials, which was measured in both cases by weighing a cylinder of each material of a known volume and dividing the resulting mass by said volume to obtain a density. The adsorption uptake per unit mass, as measured in section 5.2.3, is then used to convert these density values into values of adsorption uptake per unit volume to allow for the volume of material needed for each sample to achieve an equal adsorption uptake to be calculated. Finally, pressure drop is given in Figure 121 for the samples given in Table 36 as well as other comparable activated samples for which isotherm data was not available. Pressure drop for the foams varied compared to the beads and is given as a ratio of bead pressure drop in Table 36. Isotherm data for samples 83A, 84A and 88A was unavailable due to equipment availability constraints, and as such no values could be calculated based on these samples.

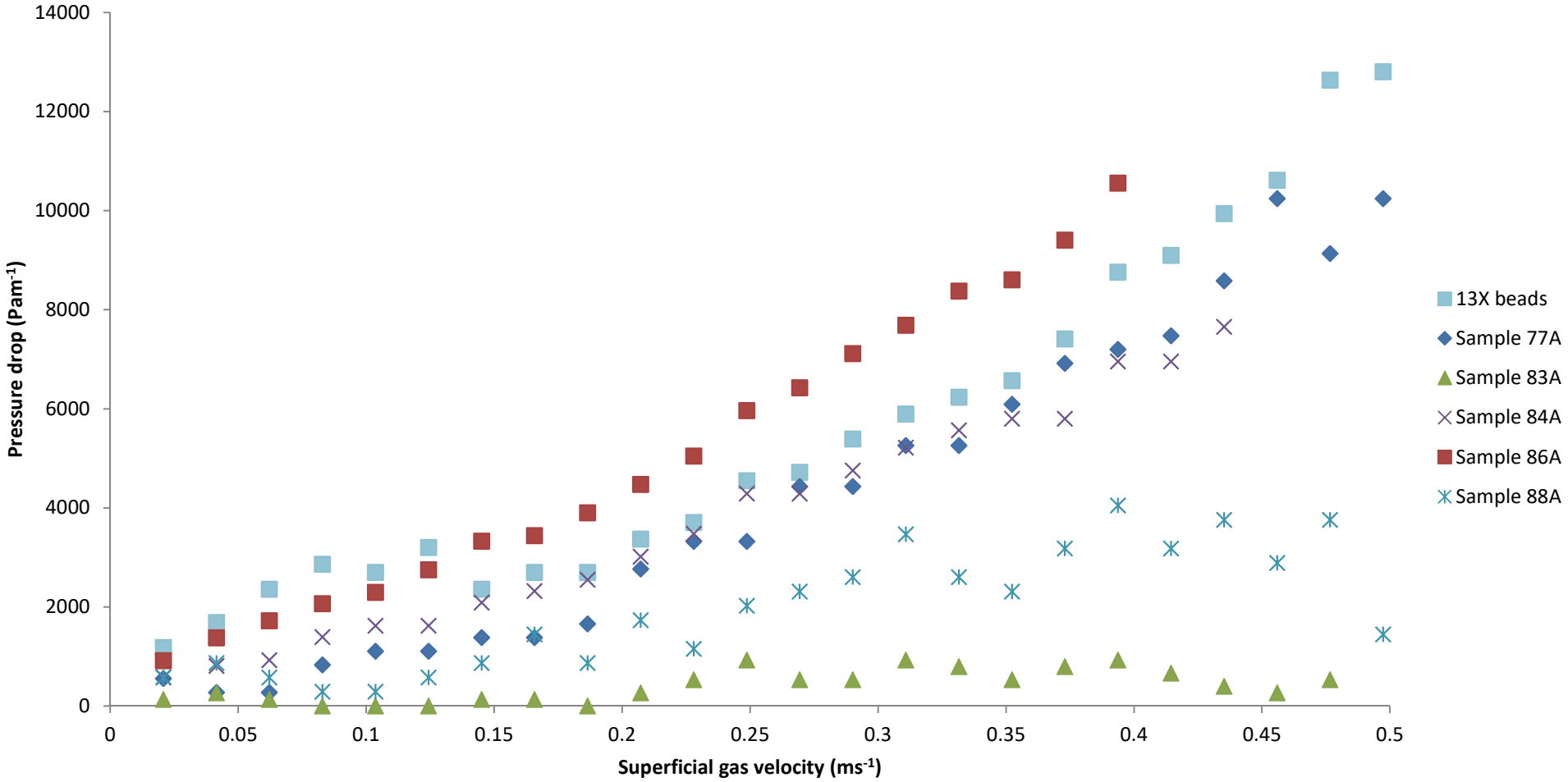

Figure 121: Pressure drop profiles for various activated foams compared to adsorbent beads.

Table 36: Density, adsorption uptake, adsorption uptake per unit volume and median pressure drop ratios of various activated foams compared to adsorbent beads.

Sample number	13X Content (wt% by formulation)	Density (kgm^{-3})	Adsorption uptake (wt%)	Adsorption uptake per volume (kgm^{-3})	Median pressure drop ratio compared to adsorbent beads
Beads	No data	680	20.6	140	1
77A	75	236	11.5	27.2	0.811
83A	75	198	No data	No data	0.0759
84A	75	208	No data	No data	0.373
86A	67	132	4.75	6.30	1.30
88A	75	592	No data	No data	0.373

As can be seen in Table 36, the beads offer significantly higher adsorbent uptake density when compared to the adsorbent foams, 6 times as much as sample 77A and far more than that for sample 86A, although 86A contains less 13X than 77A. This must be considered in combination with the pressure drop behaviour to determine if the foams offer superior overall performance or merely a less dense method of packing adsorbent. There is some variance in pressure drop behaviour of the foams. To be competitive with the beads in terms of total volume required, the foams must offer greater pressure drop reduction compared to the beads than their reduction in adsorption uptake density. In the case of sample 77A pressure drop ratios of 0.167 would be needed to compensate for the greatly increased adsorption uptake density that the beads offer.

Sample 86A showed a greater pressure drop than the beads, when combined with its extremely low adsorption uptake density makes it far inferior to the bead materials. Sample 77A falls significantly short of this requirement with a pressure drop ratio of only 0.811 but samples 83A and 88A, both having similar 13X loading to 77A, showed favourable ratios of 0.0759 and 0.373 respectively. Samples 83A and 88A underwent similar heat treatment to sample 77A, but in a controlled fashion, and in the case of sample 88A have a significantly greater density. As a result, sample 88A has the potential to be competitive

with the beads in terms of adsorption uptake density and is the most promising of the adsorbent foams analysed.

As a result it can be concluded that it is possible for the foams to be competitive with beads as an adsorbent structure, but this would require highly activated foam materials with a high loading of adsorbent and reasonable mass density. Sample 88A best fits this condition, using the addition of silicone oil in its formulation to allow for increased mass density compared to other foam materials, whilst also containing equally high loadings of 13X in the formulation as sample 77A, and reasonably low pressure drop characteristics.

Finally, the foams could offer similar mass transfer performance compared to the adsorbent beads. As can be seen in Table 37 Thomas rate constants for the foams, calculated from the breakthrough curves in Figure 122 using the technique described in section 5.3.2, are similar between the heat treated foams and the beads, with the beads offering superior mass transfer performance. Of the foams, sample 83A offered the best mass transfer performance. However for respiratory protection applications where adsorbent is only used once the adsorptive mass transfer rate is of limited importance; as long as it is sufficiently high to offer effective protection similar Thomas rate constants to the beads are acceptable.

Table 37: Thomas rate constants for activated foams compared to beads.

Sample number	Thomas rate constants ($ppm^{-1}s^{-1}$)
Beads	$-5.11x10^{-7}$
83A	$-4.236x10^{-7}$
84A	$-2.78x10^{-7}$
86A	$-4.046x10^{-7}$
88A	$-2.83x10^{-7}$

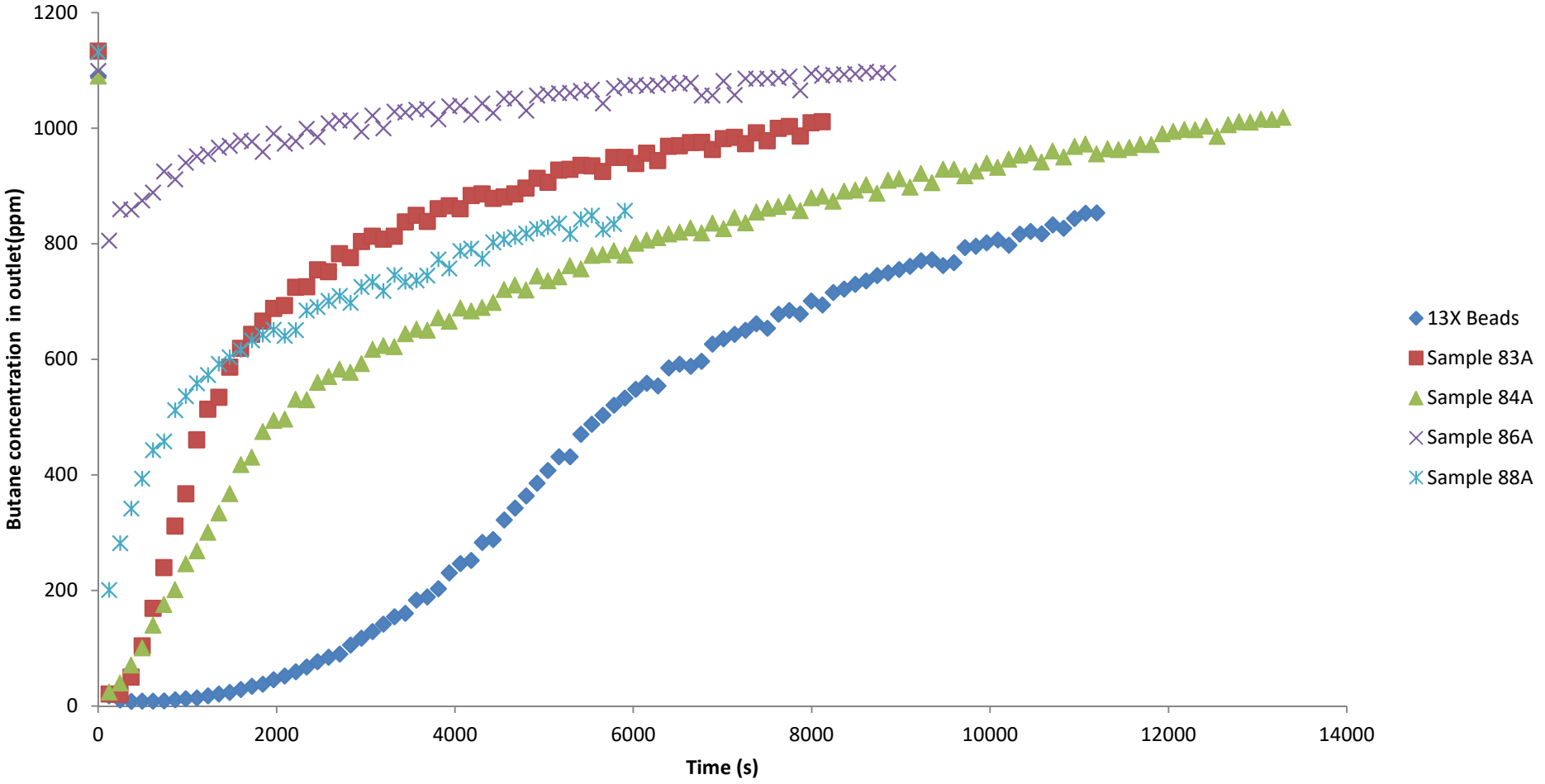

Figure 122: Breakthrough curves for heat treated samples compared to beads showing differing uptake rates.

6.4 Conclusions

It was shown in Chapter 4 that the foams can offer superior pressure drop per unit length compared to the adsorbent beads tested for foams with appropriate voidage and bubble diameter, with pressure drops of 500 to 10,500 Pam^{-1} being measured compared to 12,800 Pam^{-1} for the adsorbent beads. It was also shown in Chapter 5 that by thermally treating the foams, high accessibility of the adsorbent within the foams could be achieved resulting in adsorbent uptakes of 4.75 to 11.5 wt% compared to 20.6 wt% for the adsorbent beads.

In this Chapter, it was shown that despite the lower adsorption uptake of the foams compared to beads, it was possible for foams to be made which could offer sufficiently high adsorption uptake density to allow for lower total pressure drop for a given adsorption uptake compared to the adsorbent beads. This required an optimised foam material which had very high adsorbent loading, high bulk density and effective heat treatment which was achieved in sample 88A.

Sample 88A was a 75 wt% PU-13X formulation which used the addition of silicone oil surfactant to increase the bulk density of the material and as a result improve its adsorbent density. It underwent heat treatment at 200^{o}C in flowing air for 1 hour to improve the accessibility of the adsorbent, and was found to have a pressure drop of one-third of the adsorbent beads. When considered together, these result in a foam material which may offer a lower total pressure drop for a given value of adsorbent uptake compared to the 13X beads, the only sample to do so. As a result the formulation and processing technique used for sample 88A are recommended from this research for further development.

7 Conclusions

The objective of this research was to create a novel adsorbent support structure which could offer lower pressure drop over existing structures in respiratory protection applications. This was divided into smaller objectives in section 1.1. These objectives and how they were achieved are reviewed in this Chapter.

Objectives 1 and 2 were to identify a polymer suitable for use as a foam and select an adsorbent capable of providing respiratory protection suitable for incorporation into the polymer. The literature review identified 13X zeolite as a suitable adsorbent for respiratory protection. Two polymers were identified which were suitable for making polymeric foams, polyurethane and polyimide. 13X was found to be compatible with both polyurethane and polyimide foam chemistries. Polyurethane foams were successfully made with 75 wt% 13X by formulation, orders of magnitude higher than any previously reported foam. Polyimide foams were found to fail to foam at loadings above 67 wt% 13X. As such polyurethane foams were chosen for further development, using the formulation shown in Table 38.

Table 38: Generic formulation for PU foams containing 13X adsorbent.

Component	**Amount**
Arbitrary scaling factor	n
Desired adsorbent fraction of foam (in decimal form)	m
Monomer (PEG)	10n g
Water	n ml
Triethanolamine	6n drops
Dibutyltin dilaurate	0.05n ml
NMP	1.4*(20n*(m/(1-m)) ml
PMDI	10n g
13X	20n*(m/(1-m)) g

Objectives 3 and 4 dealt with optimisation of the foam formulation and processing to improve the adsorbent content and uptake of the foams. The most effective foam production process was found to be that seen in Table 39 and Figure 123. This formulation could be poured into moulds and made into different shapes of adsorbent foams, which was done in this research for long thin cylinders and larger flatter cake shaped samples. The presence of a polyurethane skin covering the 13X crystals in the material was found. This skin had a significantly detrimental effect on adsorption performance of the foam. The use of solvent etching to remove the polyurethane surface of the foams was found to be ineffective.

Heat treatment of the foams was found to be effective, showing skin thickness reductions of 60-90% depending on the process conditions used. This reduction was caused by oxidation of the polyurethane. Heat treatment also increased the adsorbent content of the foams to 81-92 wt% 13X (Samples 82A, 84A). Kinetic accessibility of the adsorbent (measured via Thomas rate constant) was increased by heat treatment to -4.23×10^{-7} $ppm^{-1}s^{-1}$ (sample 83A) compared to -5.11×10^{-7} $ppm^{-1}s^{-1}$ for 13X beads. Adsorption uptake was also significantly increased by heat treatment, from 16.1 wt% for sample 86 to 42.0 wt% for sample 86A. Heat treatment was found to be controlled by regulating exposure to air during the treatment process. The most effective thermal treatment conditions found were exposure to 200^{o}C in flowing air for no more than 1 hour, but significant scope for further improvement of the process remains.

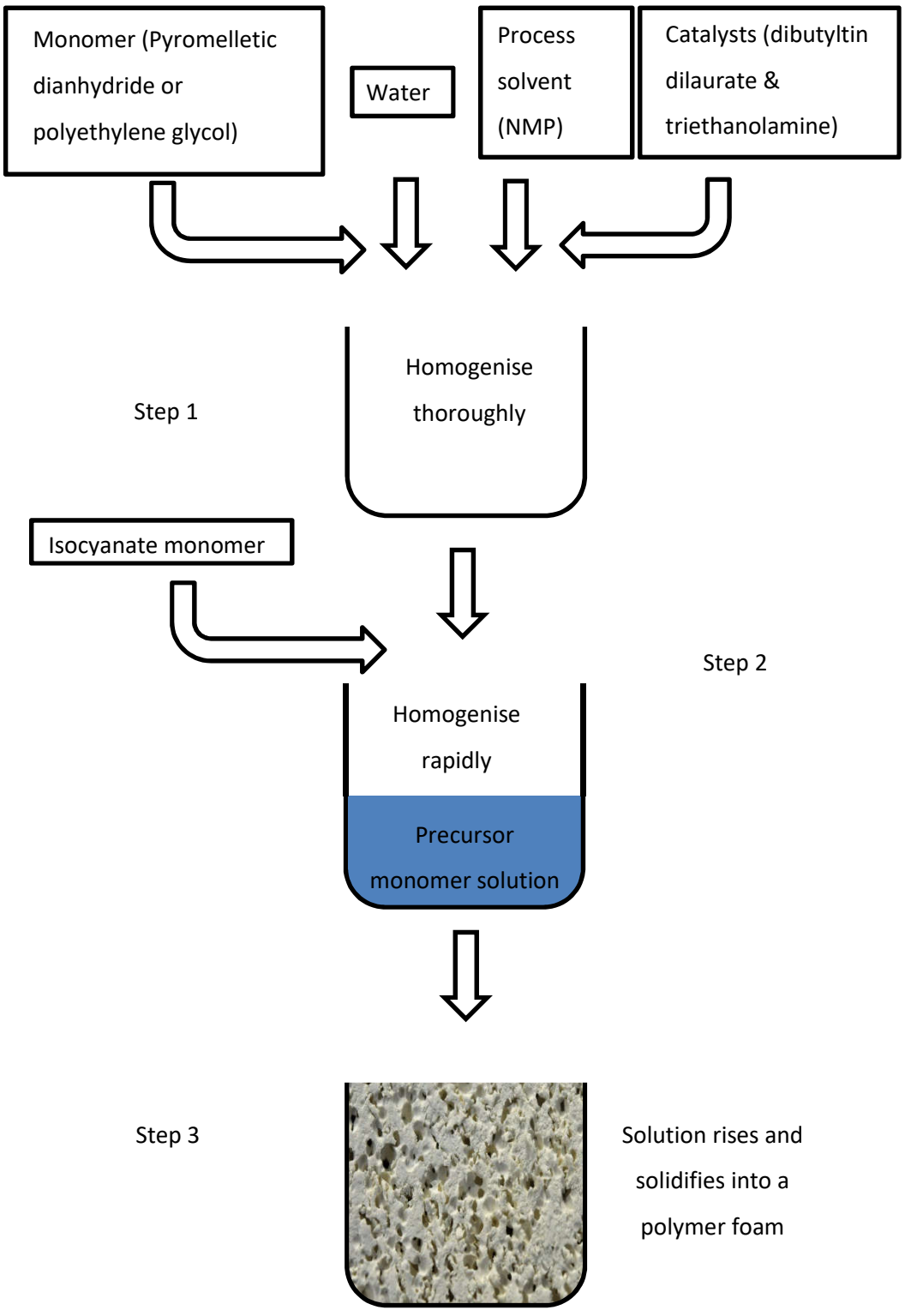

Figure 123: Flowsheet diagram of finalised production procedure as used in the research.

Table 39: Step by step production procedure for making 13X-Polymer foams.

Procedure step	**Action**
1	Pre-fill a beaker with the chosen extraction bath composition (water or a water/solvent mix)
2	Weigh the polyethylene glycol directly into the mould
3	Using a pipette, add water, dibutyltin dilaurate and triethanolamine to the mixture in the mould
4	Weigh the 13X powder into the mould
5	Add NMP as measured by measuring cylinder to the 13X powder
6	Homogenise the mixture using the homogeniser at 6,500 RPM for 60 seconds
7	Allow the mixture to cool to ambient temperature
8	Homogenise the mixture again at 6,500 RPM for 30 seconds
9	Weigh the polyisocyanate into the mixture inside the mould
10	Homogenise the mixture at 6,500 RPM for 5 seconds
11	Allow the solution to rise and set for 3 minutes or until the surface has set firm to the touch
12	Gently remove the sample from the mould using a spatula
13	Immerse the sample in the extraction bath and leave overnight
14	Remove the sample from the extraction bath and immerse in a water bath for 1 hour
15	Pat the sample dry gently with paper towel
16	Dry the sample in a vacuum oven at 80^{o}C until it reaches constant weight

Objectives 5 and 6 were to analyse the pressure drop and adsorption properties of the foam to compare them with existing adsorbent beads and to further guide foam design. A SEM technique was developed and implemented to rapidly acquire bubble and window size data from cross sectional images of produced foams (section 4.2.3). No literature model considered was found to be effective in modelling pressure drop through the PU-13X foams. A modified version of the Dietrich model for pressure drop through foams was developed (Equations (62), (63) and (64)) using new Ergun constants (298 and 17.2 in equation (62)). This model effectively predicted pressure drop through the PU-13X foams, and is likely applicable only to similar foams (polymeric foams with high powder/crystal content).

$$\frac{\Delta P}{\Delta L} = 298\frac{\mu}{\varepsilon d_h^2}u + 17.2\frac{\rho}{\varepsilon^2 d_h}u^2 \quad (62)$$

$$d_h = 4\frac{\varepsilon}{S_v} \quad (63)$$

$$S_v = 2.87\frac{1}{d_{bubble}}(1-\varepsilon)^{0.25} \quad (64)$$

Voidage was found to be the dominant physical property governing pressure drop through the foams. Heat treated foam samples displayed high voidages (0.854-0.953) compared to the 13X beads (typical voidage 0.45) resulting in superior pressure drop behaviour in the heat treated foams. 13X beads were found to offer higher overall adsorption performance as a result of their considerably higher adsorbent uptake density. The 13X beads had superior adsorbent uptake density due to their greatly increased physical density compared to the PU-13X foams (680 kgm^{-3} compared to 197-208 kgm^{-3} for heat treated foams). Adding silicone oil to the PU formulation was found to greatly improve the physical density of PU-13X foams (592 kgm^{-3} for sample 88A). Density improved samples were found to have superior pressure drop characteristics and comparable uptake kinetics to 13X beads, and have improved physical resilience. The most effective adsorbent foam made during the research was sample 88A, the formulation of which is shown in Table 40. This material is novel, showing extremely high mass fractions of 13X within a polyurethane foam, which can be accessed by adsorbate.

Table 40: Experimental formulation and heat treatment conditions for sample 88A.

Component	**Amount**
Polyethylene glycol	5g
Water	0.5 ml
Triethanolamine	3 drops
Dibutyltin dilaurate	0.025ml
NMP	42 ml
PMDI	5.7g
13X	30g
Silicone oil	2g
Heat treatment	200^{o}C in flowing air for 1 hour

Further improvement is necessary to make the PU-13X foams more suitable for respiratory protection. Heat treated foams are fragile (Figure 124) and unsuitable for rugged applications. Optimising the trade-off between low pressure drop through the foams and their adsorbent uptake density is also needed. Surface tension in the precursor foam solutions was found to control the foam porosity, density and physical strength. Adding surfactants to the formulation was found to be capable of modifying this density. This knowledge, and the knowledge found on the heat treatment process, is both novel and necessary to further develop the PU-13X foams to be more successful than the breakthroughs already achieved in this work.

Figure 124: Sample 88 after heat treatment.

7.1 Further work

During the course of the research, various areas of potential interest were identified which were not pursued due to time or equipment limitations. These areas are highlighted in this section along with brief discussion into what further work could be possible.

7.1.1 Mouldable adsorbent foams

As was mentioned in Chapter 2, respiratory protection devices can take a variety of forms depending on the user needs. This as a result changes the shape of the adsorbent depending on the respirator, with the example seen in Figure 1 having the shape of an oval cylinder.

In the course of this work, foams were made using moulds in the form of small and large diameter cylindrical forms (Figure 125). These are simple shapes to make foam inside and do not explore the possibility for using the adsorbent foams in unusual morphologies.

Figure 125: PU-13X foams made in two different forms of cylindrical moulds as part of this research.

Unlike the existing adsorbent beads, which require a container to give them shape due to their free flowing nature, it is possible for the adsorbent foams to be used to fill moulds of a variety of shapes as the mixture expands during the foaming process. This offers significant potential for the foam adsorbents in respiratory protection in not being limited to the typical cylindrical packed bed morphology.

However further investigation will be necessary into both how this affects the distribution of adsorbent within the resulting structures as a result of mixing and pouring, as well as the air flow behaviour of the resulting shapes and their pressure drops to determine the effects of the adsorbent shape on their effectiveness as adsorbents.

7.1.2 Polyimide foams as adsorbent supports

It was found in section 6.2 that whilst the heat treatment process for PU-13X foams was an effective and necessary technique for improving the adsorption properties of the foams, it left the resulting materials extremely fragile due to the resulting weakening of the polymer supporting the 13X in the foam structure (Figure 126).

Figure 126: Sample 87 showing disintegration due to fragility.

As a result of this, alternative polymers which can offer and retain higher degrees of strength after the heat treatment process are of particular interest for developing the polymer adsorbent foams into a practical form for respiratory protection applications.

Polyimide is a polymer known for its excellent physical properties (Weiser *et al.* 2000) and its ability to be made into polymeric foams is already previously described in this work. However investigation into these foams was discontinued due to encountering an upper adsorbent content limit of 13X powder of 67 wt% by formulation which was deemed to be too low for a practical adsorbent.

As PI is significantly more thermally resilient than PU (Weiser *et al.* 2000), neither a heat treatment process, nor a TGA profile for the analysis of the materials could be developed in the time available. In particular, if necessary, the heat treatment process will need

equipment capable of temperatures in the region of 260^{o}C or higher (Weiser *et al.* 2000), as well as providing an air flow, in order to develop a successful process.

A TGA profile is possible on the apparatus as used in the research, via a similar development process as described in section 5.2.1, given sufficient equipment time and will guide the choice of heat treatment equipment, as well as provide useful information on true 13X mass fractions in such materials.

7.1.3 Surface removal techniques

During the research it was found that the polymer bubble surface between the adsorbent and the gas phase had a significant detrimental effect upon both the kinetic and equilibrium performance of the foams as adsorbents. Techniques for the removal of this surface are therefore necessary. However those developed during the research are by no means optimised and leave room for improvement.

The temperature which is required for heat treatment is reasonably well known from TGA investigation to be within 160-200^{o}C for an effective process, but the combination of airflow rates and exposure time to the temperature were not optimised in any way for PU-13X foams.

Further work in the area can focus on the effects of various heat treatment conditions on the skin thickness of the foams, which can be analysed via SEM imaging, and should focus on conditions that cause uniform foam degradation as opposed to overly degrading the inside, as well as finding a minimum tolerable bubble skin thickness for acceptable physical resilience, relating skin thickness to crush strength via further physical investigation.

7.1.4 Polymer supports with intrinsic adsorbent uptake

As was found in section 5.2, the PU fraction of the PU-13X foams was found to be inert in isotherm testing. As a result, there is potential in considering foams where the polymer itself has some intrinsic adsorption properties.

This is possible by the investigation into polymers of intrinsic microporosity (PIMs). Polymers of intrinsic microporosity are polymers which due to the structure of the monomer molecules chosen causing poor packing when polymerising (Figure 127) have inherent void space within the polymer material (McKeown 2012). This void space can give

the polymers the potential for adsorption behaviour which other polymers such as polyurethane and polyimide may not have.

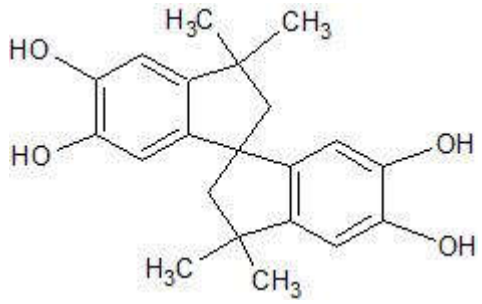

Figure 127: 3,3,3′,3′-Tetramethyl-1,1′-spirobiindane-5,5′,6,6′-tetraol, a monomer for PIMs showing the typical structure for poor molecule packing in the central stacked pentagons.

Monomer precursors which use the urethane chemistry reacting polyol and isocyanate groups to form a polyurethane based PIM have been reported in the literature (McKeown 2012). As a result, a foam version of such materials may be possible by using the isocyanate-water reaction to create CO_2 as a blowing gas, as was done in this research, which can then have a 13X adsorbent fraction added to produce an improved adsorbent activity polymer-adsorbent foam material.

7.1.5 Metal organic frameworks

This work focused on the incorporation of the zeolite 13X into a polyurethane foam support, with 13X being chosen as a stable commercially available adsorbent with wide applicability against respiratory hazards. However there are new adsorbents in the form of metal-organic frameworks (MOFs) being developed which offer the potential of greater adsorbent uptake and selectivity towards respiratory hazards.

A metal organic framework comprises of metal ions which are bound into a structure by the use of linking organic compounds, giving rise to a three dimensional structured material which can adsorb molecules within the void space of the compound (Figure 128). The selectivity of the MOF, and the capacity for adsorbent uptake can be varied widely depending upon the choice of metal ions and binding links and so offer great potential for tailored adsorbents for respiratory protection.

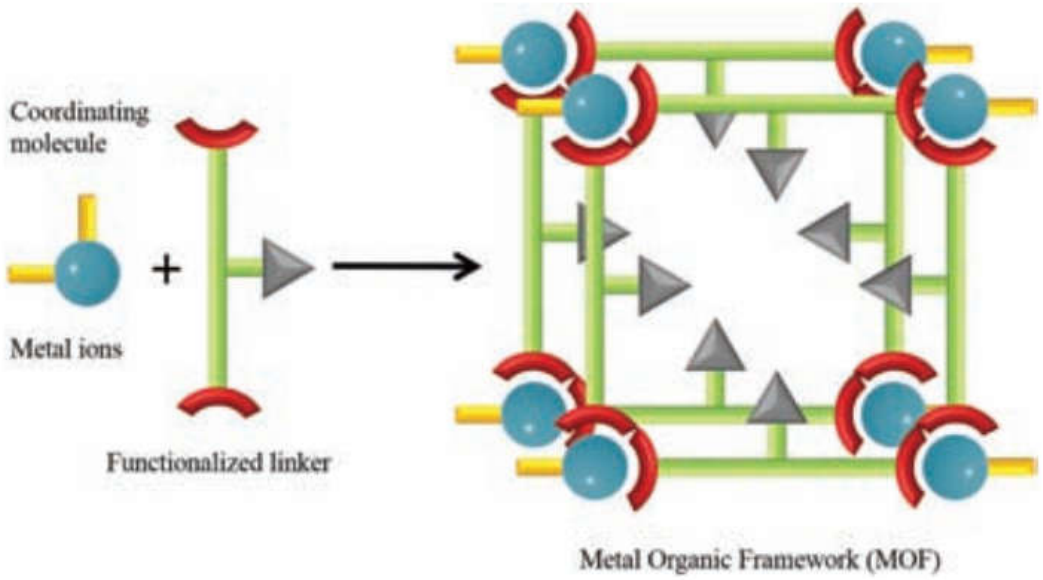

Figure 128: Example of a MOF showing void space available for adsorption (Reproduced from Valentin Valtchev (2018)).

However there exists some difficulty in simply incorporating MOFs into the foaming chemistry as developed in this work. In addition to the great expense of currently producing MOFs in quantity, the materials are well known for their instability when exposed to heat and humidity (Parvulescu *et al.* 2016). Not only is the respiratory protection environment a humid one, the foam chemistry used in this work involves exposure both to elevated temperatures and moisture as part of the chemical blowing reaction used to form the bubbles. Various MOFs have been reported with improved chemical and thermal stability, including MIL-100, MIL-101 and UiO-66 (Parvulescu *et al.* 2016) but significant work would need to be done on testing if a particular MOF can offer both useful adsorbent properties and survive the foaming process.

8 References

Abdel Hakim, A. A., M. Nassar, A. Emam and M. Sultan (2011). "Preparation and characterization of rigid polyurethane foam prepared from sugar-cane bagasse polyol." Materials Chemistry and Physics **129**(1–2): 301-307.

Abouelnasr, D., K. F. Loughlin and A. Al Mousa (2017). "Saturation loadings on 13X (faujasite) zeolite above and below the critical conditions. Part III: Inorganic monatomic and diatomic species data evaluation and modeling." Adsorption **23**(7): 945-961.

Aik Chong, L. and G. Jia (2001). "Adsorption of sulfur dioxide on activated carbon from oil palm waste." Journal of Environmental Engineering **127**(10): 895.

Alvéotec (2012). Aluminium Foam, Wikimedia Commons.

Amarsanaa, A., W. S. Shin, J.-H. Choi and S.-J. Choi (2006). "Biofiltration of gaseous toluene using adsorbent containing polyurethane foam media " Environ Eng Res **11**(1): 1-13.

Anna, D. H. (2011). Occupational Environment - Its Evaluation, Control, and Management (3rd Edition), American Industrial Hygiene Association (AIHA)**:** 4.

Ashida, K. and K. Iwasaki (1995). 2 - Thermosetting foams A2 - Landrock, Arthur H. Handbook of Plastic Foams. Park Ridge, NJ, William Andrew Publishing**:** 11-220.

Awadallah-F, A., F. Hillman, S. A. Al-Muhtaseb and H.-K. Jeong (2019). "On the nanogate-opening pressures of copper-doped zeolitic imidazolate framework ZIF-8 for the adsorption of propane, propylene, isobutane, and n-butane." Journal of Materials Science **54**(7): 5513-5527.

Balanay, J. A. G., A. A. Bartolucci and C. T. Lungu (2013). "Adsorption Characteristics of Activated Carbon Fibers (ACFs) for Toluene: Application in Respiratory Protection." Journal of Occupational and Environmental Hygiene **11**(3): 133-143.

Barg, S., C. Soltmann, A. Schwab, D. Koch, W. Schwieger and G. Grathwohl (2011). "Novel open cell aluminum foams and their use as reactive support for zeolite crystallization." Journal of Porous Materials **18**(1): 89-98.

Beer, M., R. Rybár and M. Kaľavský (2019). "Experimental heat transfer analysis of open cell hollow ligament metal foam at low Reynolds number." Measurement **133**: 214-221.

Belarbi, H., L. Boudjema, C. Shepherd, N. Ramsahye, G. Toquer, J.-S. Chang and P. Trens (2017). "Adsorption and separation of hydrocarbons by the metal organic framework MIL-101(Cr)." Colloids and Surfaces A: Physicochemical and Engineering Aspects **520**: 46-52.

Benyahia, F. and K. E. O'Neill (2005). "Enhanced Voidage Correlations for Packed Beds of Various Particle Shapes and Sizes." Particulate Science and Technology **23**(2): 169-177.

Birdi, K. S. (2009). Surface and Colloid Chemistry : Principles and Applications. Baton Rouge, UNITED STATES, Taylor & Francis Group.

Brandani, S., E. Mangano and L. Sarkisov (2016). "Net, excess and absolute adsorption and adsorption of helium." Adsorption **22**(2): 261-276.

Breck, D. W. (1977). Zeolite Molecular Sieves - Structure, Chemistry, and Use, John Wiley & Sons.

British Standards Institution (1999). BS EN 1827:1999+A1:2009 - Respiratory protective devices. Half masks without inhalation valves and with separable filters to protect against gases or gases and particles or particles only. Requirements, testing, marking.

British Standards Institution (2001). BS EN 13274-3:2001 - Respiratory protective devices. Methods of test. Determination of breathing resistance. Atemschutzgeraete. Pruefverfahren. Bestimmung des Atemwiderstandes.

British Standards Institution (2004). BS EN 403:2004 - Respiratory protective devices for self-rescue. Filtering devices with hood for escape from fire. Requirements, testing, marking, British Standards Institute.

British Standards Institution (2004). BS EN 14387:2004+A1:2008
Respiratory protective devices. Gas filter(s) and combined filter(s). Requirements, testing, marking., British Standards Institute.

British Standards Institution (2006). BS 8468-2:2006 - Respiratory protective devices for use against chemical, biological, radiological and nuclear (CBRN) agents. Negative pressure, air purifying devices with full face mask. Specification, British Standards Institute.

Cabello, B. and J. Mancebo (2006). "Work of breathing." Intensive Care Medicine **32**(9): 1311-1314.

Caretti, D. M., K. Coyne, A. Johnson, W. Scott and F. Koh (2006). "Performance when Breathing Through Different Respirator Inhalation and Exhalation Resistances During Hard Work." Journal of Occupational and Environmental Hygiene **3**(4): 214-224.

Chen, L.-H., X.-Y. Li, J. C. Rooke, Y.-H. Zhang, X.-Y. Yang, Y. Tang, F.-S. Xiao and B.-L. Su (2012). "Hierarchically structured zeolites: synthesis, mass transport properties and applications." Journal of Materials Chemistry **22**(34): 17381-17403.

Chen, L., S. Yuan, J.-F. Qian, W. Fan, M.-Y. He, Q. Chen and Z.-H. Zhang (2016). "Effective Adsorption Separation of n-Hexane/2-Methylpentane in Facilely Synthesized Zeolitic Imidazolate Frameworks ZIF-8 and ZIF-69." Industrial & Engineering Chemistry Research **55**(40): 10751-10757.

Chen, X., J. Li and M. Gao (2019). "Thermal Degradation and Flame Retardant Mechanism of the Rigid Polyurethane Foam Including Functionalized Graphene Oxide." Polymers **11**(1): 78.

Chhabra, R. and M. G. Basavaraj (2019). Coulson and Richardson's Chemical Engineering, Volume 2A - Particulate Systems and Particle Technology (6th Edition), Elsevier**:** 339.

Chu, K. H. (2010). "Fixed bed sorption: Setting the record straight on the Bohart–Adams and Thomas models." Journal of Hazardous Materials **177**(1): 1006-1012.

Code of Federal Regulations (2004). Breathing resistance test; minimum requirements., Code of Federal Regulations.

Desai, R., M. Hussain and D. M. Ruthven (1992). "Adsorption on activated alumina. II — kinetic behaviour." The Canadian Journal of Chemical Engineering **70**(4): 707-715.

Dietrich, B. (2012). "Pressure drop correlation for ceramic and metal sponges." Chemical Engineering Science **74**: 192-199.

Dietrich, B., W. Schabel, M. Kind and H. Martin (2009). "Pressure drop measurements of ceramic sponges—Determining the hydraulic diameter." Chemical Engineering Science **64**(16): 3633-3640.

Drobny, J. G. (2007). 9 - Thermoplastic Polyurethane Elastomers. Handbook of Thermoplastic Elastomers. Norwich, NY, William Andrew Publishing**:** 215-234.

Ebnesajjad, S. (2011). Surface Preparation of Thermoplastics, Thermosets, and Elastomers-7, Elsevier Inc.

Ergun, S. (1952). "Fluid Flow in Packed Columns." Chemical Engineering Progress **48**(2): 89-94.

Fellner, P., J. Jurišová, V. Khandl, A. Sýkorová and J. Thonstad (2006). "Adsorption of SO2 on alumina." Chemical Papers **60**(4): 311-314.

Gaillard, M., V. Montouillout, F. Maugé and C. Fernandez (2004). An infrared and Solid-State NMR study of the H2S adsorption on basic zeolite. Studies in Surface Science and Catalysis. E. van Steen, M. Claeys and L. H. Callanan, Elsevier. **154:** 1679-1685.

Gao, C., J. Wu, Q. Shi, H. Ying and J. Dong (2017). "Adsorption breakthrough behavior of 1-butanol from an ABE model solution with high-silica zeolite: Comparison with zeolitic imidazolate frameworks (ZIF-8)." Microporous and Mesoporous Materials **243**: 119-129.

García-Moreno, F. (2016). "Commercial Applications of Metal Foams: Their Properties and Production." Materials **9**(2): 85.

Gooch, J. W. (2007). Polyimide. Encyclopedic Dictionary of Polymers. J. W. Gooch. New York, NY, Springer New York**:** 753-753.

Große, J., B. Dietrich, H. Martin, M. Kind, J. Vicente and E. H. Hardy (2008). "Volume Image Analysis of Ceramic Sponges." Chemical Engineering & Technology **31**(2): 307-314.

Guillen, G. R., Y. Pan, M. Li and E. M. V. Hoek (2011). "Preparation and Characterization of Membranes Formed by Nonsolvent Induced Phase Separation: A Review." Industrial & Engineering Chemistry Research **50**(7): 3798-3817.

Halim, A. A., H. A. Aziz, M. A. M. Johari and K. S. Ariffin (2010). "Comparison study of ammonia and COD adsorption on zeolite, activated carbon and composite materials in landfill leachate treatment." Desalination **262**(1): 31-35.

Hamon, L., C. Serre, T. Devic, T. Loiseau, F. Millange, G. Férey and G. D. Weireld (2009). "Comparative Study of Hydrogen Sulfide Adsorption in the MIL-53(Al, Cr, Fe), MIL-47(V), MIL-100(Cr), and MIL-101(Cr) Metal−Organic Frameworks at Room Temperature." Journal of the American Chemical Society **131**(25): 8775-8777.

Hansen, F. K. and G. Rødsrud (1991). "Surface tension by pendant drop: I. A fast standard instrument using computer image analysis." Journal of Colloid and Interface Science **141**(1): 1-9.

Hansen, L. D. and V. W. McCarlie (2004). "From Foam Rubber to Volcanoes: The Physical Chemistry of Foam Formation." Journal of Chemical Education **81**(11): 1581.

Hsing, H.-h. and W. H. Wade (1974). "Weak interaction of cyclohexane with alumina." Journal of Colloid and Interface Science **47**(2): 490-498.

Inayat, A., H. Freund, A. Schwab, T. Zeiser and W. Schwieger (2011). "Predicting the Specific Surface Area and Pressure Drop of Reticulated Ceramic Foams Used as Catalyst Support." Advanced Engineering Materials **13**(11): 990-995.

Inayat, A., H. Freund, T. Zeiser and W. Schwieger (2011). "Determining the specific surface area of ceramic foams: The tetrakaidecahedra model revisited." Chemical Engineering Science **66**(6): 1179-1188.

Inayat, A., J. Schwerdtfeger, H. Freund, C. Körner, R. F. Singer and W. Schwieger (2011). "Periodic open-cell foams: Pressure drop measurements and modeling of an ideal tetrakaidecahedra packing." Chemical Engineering Science **66**(12): 2758-2763.

Janvier, F., L. Tuduri, D. Cossement, D. Drolet and J. Lara (2016). "Systematic evaluation of the adsorption of organic vapors onto a miniaturized cartridge device using breakthrough tests in parallel experiment with a full size respirator cartridge." Adsorption Science & Technology **34**(4-5): 287-306.

Jiang, H.-L. and Q. Xu (2011). "Porous metal–organic frameworks as platforms for functional applications." Chemical Communications **47**(12): 3351-3370.

Kajiwara, T., M. Higuchi, D. Watanabe, H. Higashimura, T. Yamada and H. Kitagawa (2014). "A Systematic Study on the Stability of Porous Coordination Polymers against Ammonia." Chemistry – A European Journal **20**(47): 15611-15617.

Kim, K.-M., H.-T. Oh, S.-J. Lim, K. Ho, Y. Park and C.-H. Lee (2016). "Adsorption Equilibria of Water Vapor on Zeolite 3A, Zeolite 13X, and Dealuminated Y Zeolite." Journal of Chemical & Engineering Data **61**(4): 1547-1554.

Kishan, C. K. (1997). Polymeric Foams: An Overview. Polymeric Foams, American Chemical Society. **669:** 1-7.

Klint, D. and J.-O. Bovin (1999). "Effects of additives and heat treatment on the pore size distribution in pelletized zeolite Y." Materials Research Bulletin **34**(5): 721-731.

Knox, J. C., A. D. Ebner, M. D. LeVan, R. F. Coker and J. A. Ritter (2016). "Limitations of Breakthrough Curve Analysis in Fixed-Bed Adsorption." Industrial & Engineering Chemistry Research **55**(16): 4734-4748.

Koerner, C. (2008). Integral Foam Molding of Light Metals Technology, Foam Physics and Foam Simulation. Berlin, Heidelberg, Berlin, Heidelberg : Springer-Verlag Berlin Heidelberg.

Lacroix, M., P. Nguyen, D. Schweich, C. Pham Huu, S. Savin-Poncet and D. Edouard (2007). "Pressure drop measurements and modeling on SiC foams." Chemical Engineering Science **62**(12): 3259-3267.

Lad, J. B. and Y. T. Makkawi (2014). "Adsorption of dimethyl ether (DME) on zeolite molecular sieves." Chemical Engineering Journal **256**: 335-346.

Lee, Y.-W., J.-W. Park, J.-H. Choung and D.-K. Choi (2002). "Adsorption Characteristics of SO2 on Activated Carbon Prepared from Coconut Shell with Potassium Hydroxide Activation." Environmental Science & Technology **36**(5): 1086-1092.

Lee, Y. J., J. S. Lee, Y. S. Park and K. B. Yoon (2001). "Synthesis of Large Monolithic Zeolite Foams with Variable Macropore Architectures." Advanced Materials **13**(16): 1259-1263.

Li, F., Z. Kang, X. Huang, X.-G. Wang and G.-J. Zhang (2014). "Preparation of zirconium carbide foam by direct foaming method." Journal of the European Ceramic Society **34**(15): 3513-3520.

Li, Y. Y., S. P. Perera, B. D. Crittenden and J. Bridgwater (2001). "The effect of the binder on the manufacture of a 5A zeolite monolith." Powder Technology **116**(1): 85-96.

Liu, E., B. Sarkar, Z. Chen and R. Naidu (2016). "Decontamination of chlorine gas by organic amine modified copper-exchanged zeolite." Microporous and Mesoporous Materials **225**: 450-455.

Liu, X.-Y., M.-S. Zhan, K. Wang, Y. Li and Y.-F. Bai (2011). "Preparation and performance of a novel polyimide foam." Polymers for Advanced Technologies **23**(3): 677-685.

Lozano-Castello, D., W. Zhu, A. Linares-Solano, F. Kapteijn and J. A. Moulijn (2006). "Micropore accessibility of large mordenite crystals." Microporous and Mesoporous Materials **92**(1): 145-153.

Ma, J.-J., M.-S. Zhan and K. Wang (2013). "Facile fabrication of polyimide foam sheets with millimeter thickness: Processing, morphology, and properties." Journal of Applied Polymer Science **131**(4): n/a-n/a.

Macdonald, I. F., M. S. El-Sayed, K. Mow and F. A. L. Dullien (1979). "Flow through Porous Media-the Ergun Equation Revisited." Industrial & Engineering Chemistry Fundamentals **18**(3): 199-208.

Mansdorf, S. Z. (2019). Handbook of Occupational Safety and Health (3rd Edition), John Wiley & Sons**:** 495-530.

Marcu, I. C. and I. Săndulescu (2004). "Study of sulfur dioxide adsorption on Y zeolite." Journal of the Serbian Chemical Society **69**(7): 563-569.

Masson, S., M. Gineys, S. Delpeux-Ouldriane, L. Reinert, S. Guittonneau, F. Béguin and L. Duclaux (2016). "Single, binary, and mixture adsorption of nine organic contaminants onto a microporous and a microporous/mesoporous activated carbon cloth." Microporous and Mesoporous Materials **234**: 24-34.

McCusker, L. B. and C. Baerlocher (2001). Chapter 3 Zeolite structures. Studies in Surface Science and Catalysis. H. v. Bekkum, E. M. Flanigen, P. A. Jacobs and J. C. Jansen, Elsevier. **Volume 137:** 37-67.

McKeen, L. W. (2012). 7.1 Polyamide - Imide. Permeability Properties of Plastics and Elastomers (3rd Edition), Elsevier.

McKeown, N. B. (2012). "Polymers of Intrinsic Microporosity." International Scholarly Research Network, Materials Science **2012**.

Mills, D. (2004). Chapter 7 - Gas—solid separation devices. Pneumatic Conveying Design Guide (Second Edition). Oxford, Butterworth-Heinemann**:** 139-151.

Ministry of Defence. (2012, 24/12/2019). "Soldier wearing General Service Respirator." 2019, from http://www.defenceimagery.mod.uk/fotoweb/Preview.fwx?&position=53&archiveType=ImageFolder&archiveId=5042&albumId=5042&sorting=ModifiedTimeAsc&search=(IPTC020%20contains(CBRN))&fileId=EFCC51FEE65DA414D18085DA188CAB45524FFC4F7A63A403C47E17A8BEF1E554B796D6EA4FD91784A04B36049843E1FB56B129047A099FD2448D5AA2FD3EBB84D49852E5EF22F9F166026D03B78B6C1CC74CF4A618947B1AEAD3F8D97DC9CC83B211322903123F77E2009772D3AB5563F3A2AB6EF115B554A86D550BB8EAD35BD9E618B09F6332A3E07AEC904DCCD0D0A21E12F7624F41ADE8677B97447C7F3355DDB2D421DE50AF.

Moreno-Castilla, C., M. A. Fontecha-Cámara, M. A. Álvarez-Merino, M. V. López-Ramón and F. Carrasco-Marín (2011). "Activated carbon cloth as adsorbent and oxidation catalyst for the removal of amitrole from aqueous solution." Adsorption **17**(3): 413-419.

Mota, M., J. A. Teixeira, W. R. Bowen and A. Yelshin (2001). "Binary spherical particle mixed beds: Porosity and permeability relationship measurement." Trans. Filtr. Soc. **1**(4): 101-106.

National Institute for Occupational Safety and Health (2008). Determination of ammonia service life test, powered air-purifying respirators with cartridges standard testing procedure (STP), National Personal Protective Technology Laboratory.

Nieto-Delgado, C., D. Partida-Gutierrez and J. R. Rangel-Mendez (2019). "Preparation of activated carbon cloths from renewable natural fabrics and their performance during the adsorption of model organic and inorganic pollutants in water." Journal of Cleaner Production **213**: 650-658.

Nikolina, V. Y., I. E. Neimark and M. A. Piontkovskaya (1960). "Molecular sieves - Preparation, properties and applications." Russian Chemical Reviews **29**(9): 509.

Ning, P., J. Qiu, X. Wang, W. Liu and W. Chen (2013). "Metal loaded zeolite adsorbents for hydrogen cyanide removal." Journal of Environmental Sciences **25**(4): 808-814.

Pan, L.-Y., M.-S. Zhan and K. Wang (2010). "Preparation and characterization of high-temperature resistance polyimide foams." Polymer Engineering & Science **50**(6): 1261-1267.

Park, S.-J. and B.-J. Kim (2005). "Ammonia removal of activated carbon fibers produced by oxyfluorination." Journal of Colloid and Interface Science **291**(2): 597-599.

Parvulescu, V. I. and E. Kemnitz (2016). 2.2 Stability Issues. New Materials for Catalytic Applications, Elsevier.

Pavlova, I., R. Ilibaev, O. Travkina and B. Kutepov (2013). "Exchange forms of binder-free granulated zeolites A and X: Synthesis and properties." Petroleum Chemistry **53**(2): 102-109.

Pietrowski, P., I. Ludwiczak and J. Tyczkowski (2012). "Activated Carbons Modified by Ar and CO2 Plasmas - Acetone and Cyclohexane Adsorption." Materials Science-Medziagotyra **18**(2): 158-162.

Pinto, M. L., J. Pires, A. P. Carvalho, J. C. M. Bordado and M. B. De Carvalho (2004). "Synthesis and characterization of polyurethane foam matrices for the support of granular adsorbent materials." Journal of Applied Polymer Science **92**(3): 2045-2053.

Pinto, M. L., J. Pires, A. P. Carvalho, M. B. de Carvalho and J. C. Bordado (2005). "Characterization of adsorbent materials supported on polyurethane foams by nitrogen and toluene adsorption." Microporous and Mesoporous Materials **80**(1–3): 253-262.

Qiu, S. and T. Ben (2016). 5.2 Design and Synthesis of PIMs. Porous Polymers - Design, Synthesis and Applications, Royal Society of Chemistry.

Rajhans, G. S. and B. P. Pathak (2002). 1 - Respiratory Hazards and Evaluation. Practical Guide to Respirator Usage in Industry (Second edition). Woburn, Butterworth-Heinemann**:** 1-45.

Rajhans, G. S. and B. P. Pathak (2002). 2 - Respirator Types, Uses, and Limitations. Practical Guide to Respirator Usage in Industry (Second edition). Woburn, Butterworth-Heinemann**:** 47-75.

Recepoğlu, Y. K., N. Kabay, I. Y. Ipek, M. Arda, M. Yüksel, K. Yoshizuka and S. Nishihama (2018). "Packed bed column dynamic study for boron removal from geothermal brine by a chelating fiber and breakthrough curve analysis by using mathematical models." Desalination **437**: 1-6.

Réti, F., I. Bertóti, G. Mink and T. Székely (1987). "Surface reactions of chlorine with /gg-alumina." Reactivity of Solids **3**(4): 329-336.

Rezaei, F., A. Mosca, P. Webley, J. Hedlund and P. Xiao (2010). "Comparison of Traditional and Structured Adsorbents for CO2 Separation by Vacuum-Swing Adsorption." Industrial & Engineering Chemistry Research **49**(10): 4832-4841.

Rezaei, F. and P. Webley (2009). "Optimum structured adsorbents for gas separation processes." Chemical Engineering Science **64**(24): 5182-5191.

Rezaei, F. and P. Webley (2010). "Structured adsorbents in gas separation processes." Separation and Purification Technology **70**(3): 243-256.

Richardson, J. F., J. H. Harker and J. R. Backhurst (2002). Chapter 17 - Adsorption. Chemical Engineering (Fifth Edition). Oxford, Butterworth-Heinemann**:** 970-1052.

Richardson, J. T., Y. Peng and D. Remue (2000). "Properties of ceramic foam catalyst supports: pressure drop." Applied Catalysis A: General **204**(1): 19-32.

Riley, H. T. (1855). Pliny the Elder, Naturalis Historia. London, H. G. Bohn.

Rouquerol, J., F. Rouquerol, P. Llewellyn, G. Maurin and K. S. W. Sing (2013). Adsorption by Powders and Porous Solids: Principles, Methodology and Applications, Academic Press.

Rousseau, R. W. (1987). Handbook of separation process technology. New York Chichester, John Wiley & Sons.

Saeidi, N. and M. Lotfollahi (2015). "A procedure to form powder activated carbon into activated carbon monolith." The International Journal of Advanced Manufacturing Technology **81**(5): 1281-1288.

Saha, D. and S. Deng (2010). "Characteristics of Ammonia Adsorption on Activated Alumina." Journal of Chemical & Engineering Data **55**(12): 5587-5593.

Saini, V. K. and J. Pires (2011). "Synthesis of Foam-Shaped Nanoporous Zeolite Material: A Simple Template-Based Method." Journal of Chemical Education **89**(2): 276-279.

Schaschke, C. (2014). Dictionary of Chemical Engineering, Oxford University Press.

Shiko, E., K. J. Edler, J. P. Lowe and S. P. Rigby (2013). "Probing hysteresis during sorption of cyclohexane within mesoporous silica using NMR cryoporometry and relaxometry." Journal of Colloid and Interface Science **398**: 168-175.

Sigot, L., G. Ducom, B. Benadda and C. Labouré (2016). "Comparison of adsorbents for H2S and D4 removal for biogas conversion in a solid oxide fuel cell." Environmental Technology **37**(1): 86-95.

Sigot, L., G. Ducom and P. Germain (2016). "Adsorption of hydrogen sulfide (H2S) on zeolite (Z): Retention mechanism." Chemical Engineering Journal **287**: 47-53.

Sing, K. S. W. (1985). "Reporting physisorption data for gas/solid systems with special reference to the determination of surface area and porosity (Recommendations 1984)." Pure and Applied Chemistry **57**(4): 603-619.

Song, X.-D., S. Wang, C. Hao and J.-S. Qiu (2014). "Investigation of SO2 gas adsorption in metal–organic frameworks by molecular simulation." Inorganic Chemistry Communications **46**: 277-281.

Srinivasan, A. and M. W. Grutzeck (1999). "The Adsorption of SO2 by Zeolites Synthesized from Fly Ash." Environmental Science & Technology **33**(9): 1464-1469.

Sun, W., L.-C. Lin, X. Peng and B. Smit (2014). "Computational screening of porous metal-organic frameworks and zeolites for the removal of SO2 and NOx from flue gases." AIChE Journal **60**(6): 2314-2323.

Surface Measurement Systems (2014). DVS Advantage Automated multi-vapor gravimetric sorption analyzer for advanced research applications. SurfaceMeasurementSystems.com, Surface Measurement Systems**:** 6.

Świątkowski, A. (1999). Industrial carbon adsorbents. Studies in Surface Science and Catalysis. A. Dąbrowski, Elsevier. **120:** 69-94.

Tehrani, R. M. A. and A. A. Salari (2005). "The study of dehumidifying of carbon monoxide and ammonia adsorption by Iranian natural clinoptilolite zeolite." Applied Surface Science **252**(3): 866-870.

Thomas, W. J. and B. Crittenden (1998). 2 - Adsorbents. Adsorption Technology & Design. W. J. Thomas and B. Crittenden. Oxford, Butterworth-Heinemann**:** 8-30.

Thomas, W. J. and B. Crittenden (1998). 4 - Rates of adsorption of gases and vapours by porous media. Adsorption Technology & Design. W. J. Thomas and B. Crittenden. Oxford, Butterworth-Heinemann**:** 66-95.

Thomas, W. J. and B. Crittenden (1998). 5 - Processes and cycles. Adsorption Technology & Design. Oxford, Butterworth-Heinemann**:** 96-134.

Turk, A., E. Sakalis, J. Lessuck, H. Karamitsos and O. Rago (1989). "Ammonia injection enhances capacity of activated carbon for hydrogen sulfide and methyl mercaptan." Environmental Science & Technology **23**(10): 1242-1245.

Valentin Valtchev, S. M. (2018). Zeolites and Metal-Organic Frameworks - From lab to industry. Amsterdam, Atlantis Press, Amsterdam University Press.

Weiser, E. S., T. F. Johnson, T. L. St Clair, Y. Echigo, H. Kaneshiro and B. W. Grimsley (2000). "Polyimide Foams for Aerospace Vehicles." High Performance Polymers **12**(1): 1-12.

Whittaker, P. B., X. Wang, W. Zimmermann, K. Regenauer-Lieb and H. T. Chua (2014). "Predicting the Integral Heat of Adsorption for Gas Physisorption on Microporous and Mesoporous Adsorbents." The Journal of Physical Chemistry C **118**(16): 8350-8358.

Yang, R. T. (2003). Activated Carbons. Adsorbents: Fundamentals and Applications, John Wiley & Sons, Inc.**:** 79-130.

Yang, R. T. (2003). Sorbent Selection: Equilibrium Isotherms, Diffusion, Cyclic Processes, and Sorbent Selection Criteria. Adsorbents: Fundamentals and Applications, John Wiley & Sons, Inc.**:** 17-53.

Yetgin, S., H. Unal and A. Mimaroglu (2014). "Influence of foam agent content and talc filler on the microcellular and mechanical properties of injection molded polypropylene and talc filled polypropylene composite foams." Journal of Cellular Plastics **50**(6): 563-576.

Zabiegaj, D., E. Santini, M. Ferrari, L. Liggieri and F. Ravera (2015). "Carbon based porous materials from particle stabilized wet foams." Colloids and Surfaces A: Physicochemical and Engineering Aspects **473**(0): 24-31.

Zhao, Z., X. Li and Z. Li (2011). "Adsorption equilibrium and kinetics of p-xylene on chromium-based metal organic framework MIL-101." Chemical Engineering Journal **173**(1): 150-157.

9 Appendix: List of sample compositions and conditions mentioned in this research

The following samples used specific formulations, shown below.

Sample number	13X Mass fraction by formulation	Polymer	Additional information
0	0 wt%	PI	Pure polyimide
1	20 wt%	PI	-
2	0 wt%	PI	Pure polyimide
13	30 wt%	PI	-
14	38 wt%	PI	-
16	44 wt%	PI	Collapsed
17	50 wt%	PI	Silicone oil added
19	67 wt%	PI	-
27	67 wt%	PI	NMP solvent introduced
32	67 wt%	PI	-
33	67 wt%	PU	Silicone oil included
36	67 wt%	PU	Silicone oil removed from formulation

Formulation used for sample 0

Component	**Amount**
PMDA	21.8g
Water	0.7g
Methanol	1.2g
Triethanolamine	0.01g
Dibutyltin dilaurate	0.01g
DMF	As sufficient to dissolve PMDA
PMDI	26.2g
Reaction Conditions	Ambient temperature

Formulation used for sample 1

Component	**Amount**
PMDA	21.9g
Water	1g
Methanol	1g
Triethanolamine	0.01g
Dibutyltin dilaurate	0.01g
DMF	47 ml
PMDI	28.5g
13X zeolite powder	10g
Reaction Conditions	80^{o}C

Formulation used for sample 2

Component	**Amount**
PMDA	21.9g
Water	1g
Methanol	1g
Triethanolamine	0.01g
Dibutyltin dilaurate	0.01g
DMF	47 ml
PMDI	28.5g
Reaction Conditions	30^{o}C

Formulation used for sample 13

Component	**Amount**
PMDA	11g
Water	1 ml
Methanol	0.5 ml
Triethanolamine	6 drops
Dibutyltin dilaurate	0.05 ml
DMF	24 ml
PMDI	14.3g
13X	10g
Reaction Conditions	50^{o}C

Formulation used for sample 16

Component	**Amount**
PMDA	11g
Water	1 ml
Methanol	0.5 ml
Triethanolamine	6 drops
Dibutyltin dilaurate	0.05 ml
DMF	24 ml
PMDI	14.3g
13X	17.3g
Reaction Conditions	50^{o}C

Formulation used for sample 19

Component	**Amount**
PMDA	5g
Water	0.5 ml
Methanol	0.25 ml
Triethanolamine	3 drops
Dibutyltin dilaurate	0.025 ml
DMF	30 ml
PMDI	5g
Silicone oil	2 ml
13X	20g
Reaction Conditions	50^{o}C

Formulation used for sample 27

Component	**Amount**
PMDA	5g
Water	0.5 ml
Methanol	0.25 ml
Triethanolamine	3 drops
Dibutyltin dilaurate	0.025 ml
NMP	30 ml
PMDI	5g
Silicone oil	2 ml
13X	20g
Reaction Conditions	50^{o}C

Formulation for sample 33, a 67wt% PU-13X foam.

Component	**Amount**
Polyethylene glycol	5g
Water	0.5 ml
Triethanolamine	3 drops
Dibutyltin dilaurate	0.025ml
NMP	28 ml
PMDI	5g
13X	20g
Silicone oil	2g
Reaction Conditions	30^{o}C

Experimental formulation for sample 36, a 67wt% PU-13X foam without additional surfactant

Component	**Amount**
Polyethylene glycol	5g
Water	0.5 ml
Triethanolamine	3 drops
Dibutyltin dilaurate	0.025ml
NMP	28 ml
PMDI	5g
13X	20g
Reaction Conditions	30^{o}C

The following samples used the generic PU-13X foam formulation, given below, except where noted.

Sample number	13X Mass fraction by formulation	Polymer	Additional information
45	67 wt%	PU	-
48	67 wt%	PU	-
49	75 wt%	PU	-
54	80 wt%	PU	Failed to foam
59	75 wt%	PU	50:50 NMP:Water solvent extraction stage introduced
62	60 wt%	PU	-
63	70 wt%	PU	-
65	75 wt%	PU	-
67	50 wt%	PU	-
68	60 wt%	PU	-
70	70 wt%	PU	Pre-drying of 13X powder introduced to improve weighing
72	75 wt%	PU	Silicone oil added
73	67 wt%	PU	Reaction performed in ice bath at 0^{o}C
74/A	72 wt%	PU	Treated at 200^{o}C in flowing air.
77/A	75 wt%	PU	Tin catalyst omitted. Treated at 200^{o}C in vacuum oven, then exposed to air.
78/A	75 wt%	PU	Treated at 200^{o}C in vacuum oven, then exposed to air.
80	0 wt%	PU	Pure polyurethane
82/A	75 w%	PU	Repeatability study. Treated at 160^{o}C in flowing air for 48 hours.
83/A	75 wt%	PU	Repeatability study. Treated at 160^{o}C in flowing air for 48 hours.
84/A	75 wt%	PU	Repeatability study. Treated at 160^{o}C in flowing air for 48 hours.
85	60 wt%	PU	-

86/A	67 wt%	PU	Treated at 200^{o}C in stagnant air for 3 weeks.
87/A	70 wt%	PU	Treated at 200^{o}C in flowing air for 1 hour.
88/A	75 wt%	PU	Silicone oil added. 200^{o}C in flowing air for less than 1 hour.

Notes: The letter A after a sample denotes a sample which has undergone subsequent heat treatment.

Generic formulation for PU-13X foams

Component	**Amount**
Arbitrary scaling factor	n
Desired adsorbent fraction of foam (in decimal form)	m
PEG	10n g
Water	n ml
Triethanolamine	6n drops
Dibutyltin dilaurate	0.05n ml
NMP	1.4*(20n*(m/(1-m)) ml
PMDI	10n g
13X	20n*(m/(1-m)) g
Reaction conditions	30^{o}C

Experimental formulation for sample 72.

Component	**Amount**
Polyethylene glycol	3.3g
Water	0.33 ml
Triethanolamine	2 drops
Dibutyltin dilaurate	0.0165ml
NMP	19 ml
PMDI	3.3g
13X	13.4g
Silicone oil	1.3g
Reaction conditions	30^{o}C

Experimental formulation for sample 88.

Component	**Amount**
Polyethylene glycol	5g
Water	0.5 ml
Triethanolamine	3 drops
Dibutyltin dilaurate	0.025ml
NMP	42 ml
PMDI	5.7g
13X	30g
Silicone oil	2g
Reaction conditions	30^{o}C